

For Reference

NOT TO BE TAKEN FROM THIS ROOM

Ex libris
UNIVERSITATIS
ALBERTAEENSIS





Digitized by the Internet Archive
in 2019 with funding from
University of Alberta Libraries

<https://archive.org/details/Venkateswarlu1979>

THE UNIVERSITY OF ALBERTA

RELEASE FORM

NAME OF AUTHOR: Kasichainula Venkateswarlu

TITLE OF THESIS: An Analysis of the Laminar Separated Flow
Field Near the Midchord of an Airfoil

DEGREE FOR WHICH THESIS WAS PRESENTED: Doctor of Philosophy

YEAR THIS DEGREE GRANTED: 1979

Permission is hereby granted to THE UNIVERSITY OF ALBERTA LIBRARY to reproduce single copies of this thesis and to lend or sell such copies for private, scholarly or scientific research purposes only.

The author reserves other publication rights, and neither the thesis nor extensive extracts from it may be printed or otherwise reproduced without the author's written permission.

THE UNIVERSITY OF ALBERTA

AN ANALYSIS OF THE LAMINAR SEPARATED FLOW FIELD
NEAR THE MIDCHORD OF AN AIRFOIL

by



KASICHAINULA VENKATESWARLU

A THESIS

SUBMITTED TO THE FACULTY OF GRADUATE STUDIES AND RESEARCH
IN PARTIAL FULFILLMENT OF THE REQUIREMENTS FOR THE DEGREE
OF DOCTOR OF PHILOSOPHY

DEPARTMENT OF MECHANICAL ENGINEERING

EDMONTON, ALBERTA

SPRING, 1979

THE UNIVERSITY OF ALBERTA
FACULTY OF GRADUATE STUDIES AND RESEARCH

The undersigned certify that they have read, and recommend to the Faculty of Graduate Studies and Research, for acceptance, a thesis entitled "An Analysis of the Laminar Separated Flow Field Near the Midchord of an Airfoil," submitted by Kasichainula Venkateswarlu in partial fulfilment of the requirements for the degree of Doctor of Philosophy.

ABSTRACT

Formation of laminar separation bubbles as a mechanism of transition from laminar to turbulent boundary layer flow is a characteristic of many laminar wing sections when operating at a Reynolds number of less than 2×10^6 . In the case where the separation bubble occurs near the midchord, the separated flow field has an appreciable effect on the turbulent boundary layer development and consequently affects the drag of the wing section. An analysis of the laminar separated flow field is therefore needed to predict the complete development of the boundary layers on such a wing section. Experimentally determined characteristics of the separated flow are essential in developing an adequate theory to analyze the separated flow region. This thesis describes some of the characteristics of the laminar separated flow field and the development of the necessary analytical tools to predict the boundary layer characteristics in the case when a laminar separation bubble exists as a mechanism for transition.

A wind tunnel study was made of the boundary layer in the vicinity of the bubble near the midchord of an NACA 66₃-018 airfoil section. The investigation covered the study of the mean and turbulent characteristics of the flow. The present experiments corroborated the observations of other

investigators; but also revealed some interesting new results. Based on the present experimental data, a two-layer eddy viscosity model was developed for prediction of the boundary layer in the redeveloping region downstream of reattachment.

A numerical method for analysis of the laminar separated flow field was developed, utilizing existing experimental evidence together with data obtained in this investigation. A numerical method was also developed for analysis of the upstream laminar boundary layer to provide initial conditions for the separated flow region. These numerical methods of analysis consist of finite difference iterative solutions to the steady boundary layer equations. The present method of analysis of the laminar separated flow field gives results having a qualitative behavior similar to that observed in numerous experiments; and they are also in reasonable quantitative agreement with available experimental data.

A procedure for predicting the complete development of the boundary layers in the presence of a separated flow was constructed and tested. It was found to be effective in determining the effects of separated flow on the boundary layer characteristics and thus the lift-drag characteristics of an airfoil section.

ACKNOWLEDGEMENTS

The author wishes to express his immense gratitude to Dr. D. J. Marsden for suggesting the problem and for his guidance and supervision of this thesis. It has been a great pleasure working with him.

The continued financial support to the author by the University of Alberta in the form of Graduate Teaching Assistantship is gratefully acknowledged. The present work was financially supported by NRC under the operating grant A2938.

The author especially acknowledges the guidance provided by Dr. D. J. Wilson in using the x-wire apparatus and in making the turbulence measurements.

The staff of the Mechanical Engineering Shop is acknowledged for preparing the wing model and the traversing mechanism. Thanks are extended to Tony Dyke for his assistance in programming the data acquisition system. Tony is also thanked for keeping stimulating atmosphere in the laboratory. Thanks are also due to Tom Villett for his technical assistance in running the experimental tests.

Fellow graduate students are thanked for providing the stimulating atmosphere in which this work was conducted. The author also wishes to thank Mrs. Evelyn Brady and Mrs. Marilyn Wahl for producing an excellently typed thesis.

My parents, with their unfaltering faith in me, gave me the confidence to undertake a Doctoral research. Special thanks go to my mother for her patience and understanding while I was away from home. I want this thesis to remind me always of the fond memories of my father.

TABLE OF CONTENTS

CHAPTER		PAGE
I	INTRODUCTION	1
II	CALCULATION OF THE LAMINAR BOUNDARY LAYER . .	11
	2.1 Introduction	11
	2.2 Governing Equations	12
	2.3 Method of Solution	16
	2.4 Finite-Difference Formulation	18
	2.5 Satisfaction of Asymptotic Boundary Conditions	20
	2.6 Numerical Solution	25
	2.7 Errors in the Method of Solution	27
	2.8 The Laminar Separation	28
	2.9 Calculations and Discussion of Results .	30
III	APPARATUS AND EXPERIMENTAL METHODS	35
	3.1 Model Airfoil	35
	3.2 Wind Tunnel and Auxiliaries	36
	3.3 Wind Tunnel Wall Corrections	39
	3.4 Data Acquisition	40
	3.5 Surface Pressure Measurements	41
	3.6 Mean Velocity Measurements	41
	3.7 Turbulence Measurements	43
	3.8 Probe Traversing Mechanism	44
	3.9 Hot Film and X-Wire Anemometers	46
	3.10 Error Analysis	53

CHAPTER		PAGE
IV	MEAN FLOW CHARACTERISTICS	48
	4.1 Introduction	48
	4.2 Test Program	59
	4.3 Results and Discussions	60
	4.4 Applicability of Experimental Methods .	98
	4.5 Conclusions	103
V	TURBULENCE CHARACTERISTICS	105
	5.1 Introduction	105
	5.2 Behavior of Turbulence Velocity Field in an Adverse Pressure Gradient	106
	5.3 Intermittency Correction	108
	5.4 Test Program	112
	5.5 Results and Discussion	113
	5.6 Eddy Viscosity Model	131
	5.7 Conclusions	137
VI	ANALYSIS OF LAMINAR SEPARATED FLOW FIELD . .	139
	6.1 Introduction	139
	6.2 Physical Structure of Separated Flow Field	142
	6.3 Method of Analysis	146
	6.4 Formulation of Governing Equations . .	149
	6.5 Viscous-Inviscid Interaction	163
	6.6 Method of Solution	164
	6.7 Numerical Procedure	166
	6.8 Results and Discussion	172
	6.9 Conclusions	177

CHAPTER	PAGE
VII	PREDICTION OF BOUNDARY LAYER DEVELOPMENT IN THE PRESENCE OF SEPARATED FLOW 178
7.1	Introduction 178
7.2	Effects of Viscous Flow 179
7.3	Method of Analysis 181
7.4	Calculations and Discussion of Results . 184
7.5	Conclusions 194
VIII	CONCLUSIONS 196
	REFERENCES 200
APPENDIX 1:	SYSTEM OF FIRST-ORDER EQUATIONS FOR INTEGRATING LAMINAR BOUNDARY LAYER EQUATIONS 205
2:	EVALUATION OF DERIVATIVES OF ϵ_i^* (EQUATION (6.37)) 208
3:	SYSTEMS OF FIRST-ORDER EQUATIONS FOR INTEGRATING THE DIFFERENTIAL EQUATIONS OF LAMINAR SEPARATED FLOW FIELD 210

LIST OF TABLES

TABLE		PAGE
I	COMPARISON OF PROFILES OF MODEL AIRFOIL AND NACA 66 ₃ -018 AIRFOIL [*]	37
II	POSITIONS FOR LAMINAR SEPARATION, TRANSITION, REATTACHMENT AND EQUILIBRIUM FLOW	77
III	COMPARISON OF EXPERIMENTAL AND COMPUTED BOUNDARY LAYER PARAMETERS NEAR SEPARATION	102

LIST OF FIGURES

FIGURE		PAGE
1	NOTATION AND COORDINATE SYSTEM	13
2	FINITE DIFFERENCE MARCHING SCHEME	17
3	VELOCITY DISTRIBUTION IN A BOUNDARY LAYER WITH ADVERSE PRESSURE GRADIENT, $\frac{dp}{ds} > 0$	29
4	COMPARISON OF CALCULATED AND MEASURED VELOCITY PROFILES ON THE ELLIPTIC CYLINDER STUDIED EXPERIMENTALLY BY SCHUBAUER	33
5	VIEW OF THE MODEL IN THE WIND TUNNEL	33
6	PROBE TRAVERSING APPARATUS	33
7	X-WIRE CONFIGURATION	49
8	SETUP FOR MEASURING TURBULENCE	49
9	COMPARISON OF X-WIRE AND HOT FILM MEAN VELOCITY MEASUREMENTS	55
10	COMPARISON OF X-WIRE AND HOT FILM STREAMWISE TURBULENCE INTENSITY MEASUREMENTS	57
11	PRESSURE DISTRIBUTION, NACA 66 ₃ -018, $\alpha = 0^\circ$.	61
12	PRESSURE DISTRIBUTION, NACA 66 ₃ -018, $\alpha = 2^\circ$.	62
13	VELOCITY PROFILES, $Re = 0.8 \times 10^6$, $\alpha = 0^\circ$. .	65
14	VELOCITY PROFILES, $Re = 0.8 \times 10^6$, $\alpha = 2^\circ$. .	67
15	VELOCITY PROFILES, $Re = 1.2 \times 10^6$, $\alpha = 0^\circ$. .	69
16	VELOCITY PROFILES, $Re = 1.2 \times 10^6$, $\alpha = 2^\circ$. .	71
17	VELOCITY PROFILES, $Re = 1.6 \times 10^6$, $\alpha = 0^\circ$. .	73
18	VELOCITY PROFILES, $Re = 1.6 \times 10^6$, $\alpha = 2^\circ$. .	74

FIGURE		PAGE
19	VELOCITY PROFILES, $Re = 2.0 \times 10^6$, $\alpha = 0^\circ$. .	75
20	VELOCITY CONTOURS, $Re = 0.8 \times 10^6$, $\alpha = 0^\circ$. .	79
21	VELOCITY CONTOURS, $Re = 0.8 \times 10^6$, $\alpha = 2^\circ$. .	80
22	VELOCITY CONTOURS, $Re = 1.2 \times 10^6$, $\alpha = 0^\circ$. .	81
23	VELOCITY CONTOURS, $Re = 1.2 \times 10^6$, $\alpha = 2^\circ$. .	82
24	VELOCITY CONTOURS, $Re = 1.6 \times 10^6$, $\alpha = 0^\circ$. .	83
25	VELOCITY CONTOURS, $Re = 1.6 \times 10^6$, $\alpha = 2^\circ$. .	84
26	VELOCITY CONTOURS, $Re = 2.0 \times 10^6$, $\alpha = 0^\circ$. .	85
27	CLAUSER CHART FOR EXPERIMENTAL DETERMINATION OF TURBULENT SKIN-FRICTION COEFFICIENT, $Re =$ 0.8×10^6	89
28	CLAUSER CHART FOR EXPERIMENTAL DETERMINATION OF TURBULENT SKIN-FRICTION COEFFICIENT, $Re =$ 1.2×10^6	90
29	CLAUSER CHART FOR EXPERIMENTAL DETERMINATION OF TURBULENT SKIN-FRICTION COEFFICIENT, $Re =$ 1.6×10^6	91
30	CLAUSER CHART FOR EXPERIMENTAL DETERMINATION OF TURBULENT SKIN-FRICTION COEFFICIENT, $Re =$ 2.0×10^6	92
31	VELOCITY DEFECT PROFILES, $Re = 0.8 \times 10^6$. .	93
32	VELOCITY DEFECT PROFILES, $Re = 1.2 \times 10^6$. .	94
33	VELOCITY DEFECT PROFILES, $Re = 1.6 \times 10^6$. .	95
34	VELOCITY DEFECT PROFILES, $Re = 2.0 \times 10^6$. .	96
35	VELOCITY PROFILES UPSTREAM OF SEPARATION POINT	100

FIGURE		PAGE
36	VELOCITY PROFILES AT SEPARATION POINT	101
37	TURBULENCE INTENSITY OF STREAMWISE VELOCITY, Re = 0.8×10^6 , $\alpha = 0^\circ$	114
38	TURBULENCE INTENSITY OF STREAMWISE VELOCITY, Re = 0.8×10^6 , $\alpha = 2^\circ$	115
39	TURBULENCE INTENSITY OF NORMAL VELOCITY, Re = 0.8×10^6 , $\alpha = 0^\circ$	118
40	TURBULENCE INTENSITY OF NORMAL VELOCITY, Re = 0.8×10^6 , $\alpha = 2^\circ$	119
41	REYNOLDS SHEAR STRESS DISTRIBUTION, Re = 0.8×10^6 , $\alpha = 0^\circ$	122
42	REYNOLDS SHEAR STRESS DISTRIBUTION, Re = 0.8×10^6 , $\alpha = 2^\circ$	123
43	EDDY VISCOSITY DISTRIBUTION Re = 0.8×10^6 , $\alpha = 0^\circ$	129
44	EDDY VISCOSITY DISTRIBUTION Re = 0.8×10^6 , $\alpha = 2^\circ$	130
45	INNER LAYER EDDY VISCOSITY DISTRIBUTION, Re = 0.8×10^6 - EQUATION (5.26); 0 PRESENT MEASUREMENTS	136
46	COMPOSITE PICTURE OF LAMINAR SEPARATED FLOWFIELD	143
47	SCHEME OF COORDINATES	152
48	COORELATION OF BUBBLE LENGTH	157
49	CORRELATION OF SHEAR LAYER PARAMETERS AT TRANSITION	157

FIGURE		PAGE
50	STREAMWISE VELOCITY DISTRIBUTION, NACA 66 ₃ -018, $Re = 0.8 \times 10^6$, $\alpha = 2^\circ$	173
51	PRESSURE DISTRIBUTION	175
52	VARIATION OF SHAPE FACTOR H, NACA 66 ₃ -018, $Re = 0.8 \times 10^6$, $\alpha = 2^\circ$	175
53	STREAMWISE VELOCITY DISTRIBUTION, NACA 66 ₃ -018, $Re = 1.7 \times 10^6$, $\alpha = 0^\circ$	176
54	PRESSURE DISTRIBUTION ON AN AIRFOIL SECTION IN VISCOUS FLOW (DOTTED LINE) AND INVISCID FLOW (FULL LINE)	179
55	FLOW CHART OF VISCOUS FLOW PROCEDURE	182
56	PRESSURE DISTRIBUTION, FX 66 - S - 196 V1, $Re = 0.5 \times 10^6$, $\alpha = 0^\circ$	186
57	LAMINAR SEPARATION, TRANSITION AND REATTACHMENT	188
58	LAMINAR SEPARATION, TRANSITION AND REATTACHMENT	189
59	LAMINAR SEPARATION, TRANSITION AND REATTACHMENT	190
60	LAMINAR SEPARATION, TRANSITION AND REATTACHMENT	191
61	PROFILE DRAG POLAR, FX 66 - S - 196 V1, $Re = 0.5 \times 10^6$	192
62	PROFILE DRAG POLAR, FX 66 - S - 196 V1, $Re = 1.5 \times 10^6$	193

LIST OF SYMBOLS

C	Airfoil chord
C_D	Drag coefficient, Equation (7.1)
C_f	Skin friction coefficient
C_L	Lift coefficient
C_p	Pressure coefficient, Equation (4.1)
f	Dimensionless stream function
H	Shape factor, $\frac{\delta^*}{\theta}$
K_1	Von Kármán's mixing-length constant (= 0.40)
l	Mixing length, Equation (5.22)
L_b	Length of the bubble as a percent of chord
p	Static pressure
P_∞	Free stream total pressure
q	Local free stream dynamic pressure, $\frac{1}{2} \rho U^2$
Re	Reynolds number based on model chord, $\frac{U_\infty C}{\nu}$
RL	Shear layer in the bubble region
Ry	Reynolds number based on y , $\frac{Uy}{\nu}$
$R\delta^*$	Reynolds number based on displacement thickness, $\frac{U\delta^*}{C}$
$R\theta$	Reynolds number based on momentum thickness, $\frac{U\theta}{\nu}$
s	Distance from leading edge along the airfoil surface
SL	Shear layer in the free shear layer region
u, \bar{u}	s component of mean velocity inside the boundary layer

u'	Fluctuating portion of the velocity
u_*	Friction velocity, $\sqrt{\frac{\tau_w}{\rho}}$
U	Mean velocity at the edge of the boundary layer
U_∞	Free stream velocity
v, \bar{v}	y component of mean velocity inside the boundary layer
v'	Fluctuating portion of the velocity
V^*	Mean velocity inside the boundary layer, Equation (6.5)
x	Wall shear, f_w''
y	Distance normal to the airfoil surface

Greek Symbols

α	Angle of attack, deg
β	Pressure gradient parameter
γ	Intermittency factor
δ	Boundary layer thickness
δ^*	Displacement thickness
Δ	Defect thickness, Equation (4.5)
Δ^*	Dimensionless displacement thickness, Equation (5.19)
ϵ	Eddy Viscosity
η	Transformed y coordinate Equation (2.7)
θ	Momentum thickness
μ	Dynamic viscosity
ν	Kinematic viscosity
ξ	Transformed y coordinate, Equation (6.4)

ρ	Mass density
τ	Shear stress
ψ	Stream function
ϕ	Bubble shape, line of zero velocity

Subscripts

e	Boundary layer edge
ex	Derivative with respect to f_w'' at the boundary layer edge
e β	Derivative with respect to β at the boundary layer edge
i	Inner
J	Index of η -grid
JJ	Index of s^* -steps
o	Outer
r	reattachment
s	Separation
t	Turbulent
te	Trailing edge
tr	Transition to fully turbulent flow
w	Wall
x	Derivative with respect to wall shear f_w''
∞	Free stream conditions
ℓ	Laminar
ϕ	At the line of zero velocity
ϕx	Derivative with respect to f_w'' at the line of zero velocity

$\phi\beta$ Derivative with respect to β at the line of zero velocity

Superscripts

$n,$ ' Order of the derivative

$*$ Dimensionless

CHAPTER I

INTRODUCTION

Separation of laminar boundary layer from a surface is a common phenomena in engineering practice. Observations at low speeds have shown that the separated laminar boundary layer often reattaches to the surface at some distance downstream as a turbulent boundary layer. The region underneath the separated flow between the limits of separation and reattachment is commonly referred to as a laminar separation bubble. As the flow progresses downstream of reattachment the reattached turbulent boundary layer gradually assumes the characteristics of an undisturbed boundary layer, that is, the boundary layer becomes oblivious to the upstream separation. The entire flow region between the limits of laminar separation and undisturbed turbulent flow is designated as laminar separated flow field.

The aerodynamic characteristics of most laminar wing sections operating at low Reynolds numbers, typically less than 2×10^6 , are seen to be associated with the behavior of the laminar boundary layer separation resulting in the formation of laminar separated flow field. The phenomena of bubble separation plays an important part in determining the behavior of the boundary layer on the surface, and consequently the drag and stalling characteristics of airfoils.

There is strong interaction between the viscous separation region near the wall and the inviscid outer region, and consequently there is a change in the interface boundary conditions. This implies that the presence of the bubble alters the pressure distribution that would otherwise be imposed on the bubble. Thus the real issue is not whether separation occurred but the nature of the flow field to which it gives rise. It is obviously desirable to design airfoil sections with pressure distributions which completely eliminate laminar separation or at least shift the onset of separation to higher angles of attack. However, in practice this kind of designing is restricted by the desired airfoil performance. The laminar separation bubbles are therefore characteristic of laminar wing section (perhaps all wing sections) when operating at a Reynolds number of less than 2×10^6 . There is therefore a need for method of analysis of the laminar separated flow field while developing reliable methods of analysis and design of airfoil sections.

It has been observed that bubbles on airfoils can form into either of two types, leading edge bubbles and mid-chord bubbles, depending on whether they occur near the leading edge or at distances well away from the leading edge along the surface. The leading edge bubbles are usually referred to as being either short or long. For the short bubble the length of the turbulent separated shear layer is of the same order as the laminar region, and the total length

of the bubble is never more than a few percent of the chord. The short leading edge bubble generally produces a relatively small effect on the pressure distribution and the resulting effects on the lift and drag of the wing are usually negligible. However, with an increase of angle of attack or a decrease of Reynolds number, the separated shear layer may fail to reattach and the short bubble may burst to form either a long bubble or an unattached free shear layer. Typically a long bubble has a turbulent separated shear layer extending over much of the wing chord, and the interaction with the external stream is profound. When a short bubble on a wing bursts to become a long bubble there is a significant reduction of lift and an equally significant increase in drag. The process of bubble bursting therefore can play an important part in determining the development and severity of the stall of a wing. From an analysis of the available experimental results on leading edge bubbles, Owen and Klanfer [1] suggested a criterion for the formation of either short or long bubbles depending on whether the displacement thickness Reynolds number at separation is greater or less than 400-500.

While leading edge bubbles form at high angles of attack, midchord bubbles form only at small angle of attack. For the midchord bubble the length of the turbulent separated shear layer is much smaller than the laminar region, and the total length of the bubble is about five to fifteen percent

of the chord. The length of the bubble becomes slightly shorter either with an increase in Reynolds number or angle of attack. The presence of the midchord bubble produces a small but characteristic effect on the pressure distribution, and the resulting effect on the lift is usually small. However, the midchord bubble has an influence on the turbulent boundary layer development downstream of flow reattachment point, and the resulting effects on the drag are not negligible.

There have been numerous experimental studies on laminar separation bubbles, and much of this work has been surveyed by Tani [2], and Ward [3]. A comprehensive survey of the literature on experimental and analytical results involving bubble separations is presented here.

Bursnall and Loftin [4] made an experimental investigation of a localized region of laminar separation occurring near the midchord of an NACA 66₃-018 airfoil at zero angle of attack. Analysis of their results indicated that after transition occurs in the separated shear layer the resulting turbulence spreads at a relatively constant angle. The value of the shape factor H was seen to decrease from a value of approximately 2.6 to a value of 1.2 to 1.3 within a very short distance after reattachment. Results of their calculations suggested that the usual methods of predicting turbulent boundary layer growth do not give satisfactory results when applied to the region downstream of reattachment. However,

Bursnall and Loftin could not indicate at what position downstream of reattachment the conventional methods will begin to yield satisfactory results.

In an effort to provide some insight into the conditions which control the occurrence and extent of a bubble, Gault [5] made an extensive investigation of regions of separated flow forming on an NACA 66₃-018 airfoil, and on a 10.5 percent thick symmetric airfoil. The investigation included the study of both leading edge and midchord bubbles. At the angle of attack corresponding to maximum lift, the short bubble near the leading edge was seen to burst to form an unattached free shear layer leading to an abrupt stall. The experimental results indicated a critical Reynolds number above which only short leading edge bubbles are formed; this critical value, consistent with the Owen-Klanfer criterion, is of the order of 500, based on the boundary layer displacement thickness at separation. The regions of separated flow near the midchord were not observed for angles of attack greater than 2°. Gault suggested that the extent of separated laminar flow along a bubble is dependent on boundary layer thickness at separation, and on some measure of the local Reynolds number of the laminar boundary layer flow.

The analysis of the wide variety of data collected by Crabtree [6] confirmed the existence of a critical Reynolds number ($R\delta^*_s$) of about 450-500 separating the short and long bubble regimes. However, experiments have shown [3] that

this critical Reynolds number criterion is not sufficient, although a necessary condition, to determine the bursting condition. For that reason Crabtree proposed an additional parameter $\sigma \left(= \frac{C_{p_r} - C_{p_s}}{1 - C_{p_s}} \right)$, based on the pressure rise over the bubble, to determine short bubble bursting. He suggested that there is a maximum value of this parameter that a short bubble can sustain, bursting occurring either through the Reynolds number $R\delta^*_s$ falling to 450 - 500, or σ rising to a critical value of about 0.35.

In order to describe the principal processes by which transition can occur in the separated shear layer, Lochtenberg [7] conducted experimental investigation of separation bubbles induced by flow over a step. From an analysis of his results he suggested that if the parameter $[\delta^*_s h U_\infty^2 / \nu^2]$ (where h is step height) is less than 4.2×10^6 then transition in the shear layer occurs due to the wave mechanism consisting of the amplification, distortion, and breaking up of the Tollmien-Schlichting waves. When that parameter is greater than the critical value the transition occurs due to burst mechanism consisting of the appearance, growth, and coalescence of spots of turbulence. Lochtenberg proposed that a short bubble is the result of a burst type transition in the separated layer, and a long bubble is caused by the longer Tollmien - Schlichting wave amplification type transition mechanism.

Gaster [8] carried out experiments over a wide range of Reynolds numbers and in a variety of pressure distributions, in an effort to find out some criteria for predicting which form of bubble is most likely to arise in any given circumstances. The model used in the investigation consisted of a flat plate with a small auxiliary airfoil mounted inverted above its surface. The pressure distribution obtained on the plate was similar to the suction peak around the nose of a thin airfoil at incidence. He proposed that the structure of the bubble depends on the two parameters $R\theta_s$ and $\frac{\theta_s^2}{\nu} \frac{dU}{ds}$. The type of burst seems to depend on the shape of the trajectories in the $\frac{\theta_s^2}{\nu} \frac{dU}{ds} - R\theta_s$ plane. However, as the trajectories can cross it is clear that the path and thus the subsequent behavior of the bubble is not solely a function of $R\theta_s$ and $\frac{\theta_s^2}{\nu} \frac{dU}{ds}$. The upstream flow must have a controlling influence but it was not at all clear what parameters are important.

The first semi empirical theory for the growth and bursting of laminar separation bubbles was put forward by Horton [9]. Considering the behavior of momentum integral and kinetic energy integral equations for turbulent flow at the point of reattachment, Horton suggested a criterion for reattachment which is of the form $\left[\frac{\theta}{\nu} \frac{dU}{ds} \right]_r = -0.0082$. He analyzed some of the available experimental data on bubbles

and obtained a correlation between the nondimensional length of separated flow $\bar{L}_b \left\{ = \frac{L_b}{\theta_s} \right\}$ and $R\theta_s$ such that $\bar{L}_b = 4 \times 10^4 / R\theta_s$.

He expressed the nondimensional bubble length at bursting

$$\bar{L}_{bu} = \frac{L_{bu}}{\theta_s} \text{ in the form } \bar{L}_{bu} = 6 \times 10^4 / R\theta_s.$$

Because of the extremely complex nature of the laminar separated flow field there has not been much analytical treatment of this subject. Briley and McDonald [10] present a numerical analysis of the separation bubbles which occur near midchord on relatively thick airfoils at zero angle of attack. The results of that analysis are in reasonable agreement with flow measurement except near reattachment. Rapid flow variations just downstream of reattachment could not be predicted by their method. The calculations were found to be sensitive to freestream turbulence level even when the turbulence level is relatively low. Briley and McDonald verified the validity of the boundary layer approximation for analysis of the bubble region by direct comparison with a solution using the complete Navier - Stokes equations.

Crimi and Reeves [11] devised an integral procedure for analyzing the leading edge separation bubbles which accounts for viscous-inviscid interaction and transition to turbulent flow. The results of the analysis between separation and reattachment are in good agreement with the flow measurements reported by Gault [5]. However, it is not clear from their calculations whether such an integral formulation

would be effective for analysis of the redeveloping flow just downstream of reattachment.

While the presence of a laminar separation bubble will certainly affect the lift, and especially the drag of an airfoil no methods of analysis are available at the present time to adequately predict such effects. Laminar separation can be predicted to good accuracy by existing methods. However, the position of reattachment of the turbulent boundary layer and its characteristics downstream of reattachment are not so well known. There is therefore a need for a method of analysis of the details of the laminar separated flow field including the redevelopment region downstream of reattachment, and incorporation of this analysis into the determination of the flow around an airfoil. The flow field generated by a midchord bubble is considered in this thesis. A differential method for analysis of the separated flow field was required for a satisfactory solution in this case.

Both qualitative and quantitative experimental evidence about the processes involved in a separated flow field was required to form the basis for an analytical approach. However, such information was scant even though the physical behavior of the separation bubble has been the subject of numerous investigations. Especially, there was no information available about the structure and characteristics of the mean and turbulent velocity fields just downstream of reattachment. Experiments were therefore needed

to furnish new data where information was not already available. Such experiments were conducted in the present study.

The ultimate objective of this thesis was to develop a calculation method which includes the analysis of laminar separated flow field while determining the boundary layer over an airfoil section. First, an efficient finite difference method of analysis of the laminar boundary layer was developed. The necessary experiments conducted to furnish information about the structure and characteristics of the mean and turbulent velocity fields are described. Then, in view of these experimental results and other available reference data, the necessary analytical tools to predict the separated flow field were developed. Finally, a procedure which includes the analysis of the separated flow field in determining the boundary layer development on an airfoil surface was proposed and tested.

CHAPTER II

CALCULATION OF THE LAMINAR BOUNDARY LAYER

2.1 Introduction

The accurate prediction of the development of laminar boundary layers is a primary task in many design procedures. The calculation method described here was developed primarily to provide initial conditions for the prediction of the laminar separated flow field. This method is also applied in Chapter VII for the viscous flow analysis in the design of an airfoil.

Even though there are many methods for calculating "a" laminar boundary layer, a finite difference method was chosen because it provides a detailed solution for the boundary layer velocity profiles over the airfoil surface. As will be discussed in Chapter VI such velocity profiles calculated from the upstream laminar boundary layer are necessary for the analysis of the separated flow field. The finite difference procedure used in the calculations is based on the ideas originated by Hartree and Womersley [12] and later developed by Smith and Clutter [13].

The present method of solution consists of approximating the partial differential equation of the boundary layer by an ordinary differential equation using finite differences for the streamwise partial derivatives. The

resulting ordinary differential equation is integrated by choosing a proper value of wall shear such that the boundary conditions are satisfied. The numerical procedure developed here for choosing a proper value of wall shear and integrating the equation out to the edge of the boundary layer is different from those used in previous finite difference methods. Using computed variables at the edge of the boundary layer, the guessed wall shear is adjusted iteratively, so that the mean square error between the computed variables and the asymptotic values is minimized. The edge of the boundary layer is approached in steps so that the variables are kept within prescribed limits while integrating in a direction normal to the boundary.

A simple method of solution based on finite-differences and least-squares convergence criterion is proposed for solving the two-dimensional incompressible steady laminar boundary layer. The method appears to be simple and accurate. The convergence rate to a solution is rapid and convergence seems to be insensitive to the initial guesses of the wall conditions. A description of the method is given, and two examples are worked out. Results of calculations are presented and compared with reference data.

2.2 Governing Equations

Two-dimensional, steady flow of an incompressible fluid over an airfoil is considered. The basic notation and scheme of coordinates is illustrated in Figure (1). Prandtl's

laminar boundary layer equations for this case are given by [14]

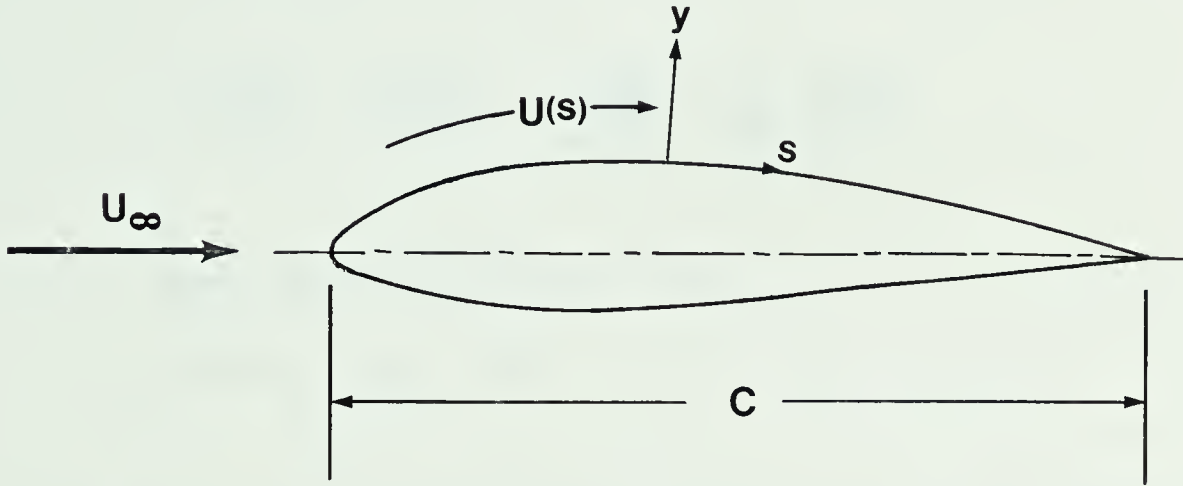


FIGURE 1--NOTATION AND COORDINATE SYSTEM

$$\frac{\partial u}{\partial s} + \frac{\partial v}{\partial y} = 0 \quad (2.1)$$

$$u \frac{\partial u}{\partial s} + v \frac{\partial u}{\partial y} = U \frac{dU}{ds} + v \frac{\partial^2 u}{\partial y^2} \quad (2.2)$$

with the boundary conditions

$$\begin{aligned} y = 0: \quad u &= 0; \quad v = 0 \\ y \rightarrow \infty: \quad u &\rightarrow U(s) \end{aligned} \quad (2.3)$$

It is often convenient to rewrite these equations in dimensionless form by referring all distances to the chord length C , and all velocities to the free stream velocity U_∞ .

Equations (2.1), (2.2) and (2.3) are written in dimensionless form as

$$\frac{\partial u^*}{\partial s^*} + \frac{\partial v^*}{\partial y^*} = 0 \quad (2.4)$$

$$u^* \frac{\partial u^*}{\partial s^*} + v^* \frac{\partial u^*}{\partial y^*} = U^* \frac{dU^*}{ds^*} + \frac{1}{Re} \frac{\partial^2 u^*}{\partial y^{*2}} \quad (2.5)$$

$$y^* = 0: \quad u^* = 0, \quad v^* = 0$$

$$y^* \rightarrow \infty \quad u^* \rightarrow U^* \quad (2.6)$$

where the star denotes dimensionless variable and Re denotes the Reynolds number based on the airfoil chord.

In these equations there are two dependent variables u^* and v^* which are functions of the independent variables s^* and y^* . A direct solution of these equations is rather difficult. However, a far more convenient form is obtained by introducing a coordinate transformation in Equations (2.4) and (2.5). The resulting equation is a third order nonlinear partial differential equation which is more amenable to a numerical solution because the dependent variables have been reduced from two to one. The two transformation variables introduced are, a dimensionless height η and a dimensionless stream function f defined as:

$$\eta = y^* \sqrt{\frac{U^*}{s^*} Re}, \quad \psi^* = \sqrt{\frac{U^* s^*}{Re}} f(s^*, \eta) \quad (2.7)$$

where ψ^* is a stream function (dimensionless with respect to the product $U_\infty C$) defined by the relations

$$\begin{aligned} u^* &= \frac{\partial \psi^*}{\partial y^*} \\ v^* &= - \frac{\partial \psi^*}{\partial s^*} \end{aligned} \quad (2.8)$$

Since the stream function ψ^* satisfies the continuity equation, Equations (2.4) and (2.5) can be combined into a single equation in terms of the stream function using the relations (2.8). The resulting equation is

$$\frac{\partial \psi^*}{\partial y^*} \frac{\partial^2 \psi^*}{\partial s^{*2} \partial y^*} - \frac{\partial \psi^*}{\partial s^*} \frac{\partial^2 \psi^*}{\partial y^{*2}} = U^* \frac{dU^*}{ds^*} + \frac{1}{Re} \frac{\partial^3 \psi^*}{\partial s^{*3}} \quad (2.9)$$

together with the boundary conditions

$$y^* = 0: \quad \frac{\partial \psi^*}{\partial y^*} = 0, \quad \frac{\partial \psi^*}{\partial s^*} = 0 \quad (2.10)$$

$$y^* \rightarrow \infty: \quad \frac{\partial \psi^*}{\partial y^*} \rightarrow U^*$$

with the notation $f' = \frac{\partial f}{\partial \eta}$, etc., the following equation is obtained upon introducing the transformation variables (2.7) in Equation (2.9):

$$f''' + \frac{1+\beta}{2} f f'' + \beta (1-f'^2) = s^* \left[f' \frac{\partial f'}{\partial s^*} - f'' \frac{\partial f}{\partial s^*} \right] \quad (2.11)$$

with the boundary conditions

$$\eta = 0: \quad f = 0, \quad f' = 0$$

(2.12)

$$\eta \rightarrow \infty: \quad f' \rightarrow 1$$

The term β is a pressure gradient parameter defined as

$$\beta = \frac{s^*}{U^*} \frac{dU^*}{ds^*}.$$

2.3 Method of Solution

There are two phases of the method of obtaining a solution. The first phase consists of approximating the partial differential equation of the boundary layer by an ordinary differential equation. This is achieved by replacing the streamwise partial derivatives by implicit finite differences while retaining the derivatives in a direction normal to the surface. This method is of the downstream marching type which takes advantage of parabolic behavior of the Equation (2.11). Smith and Clutter [13] found that three-point and four-point differences are both accurate and stable. The three-point form is used in the present calculations. When only one upstream solution is known, the three-point form is replaced by a two-point form.

The finite difference marching scheme is shown in Figure (2). The (s^*, η) plane is divided into small rectangular grids bounded by lines s^*_{JJ} , s^*_{JJ-1} , s^*_{JJ-2} etc., and by

lines η_J , η_{J+1} , η_{J+2} etc. It is assumed

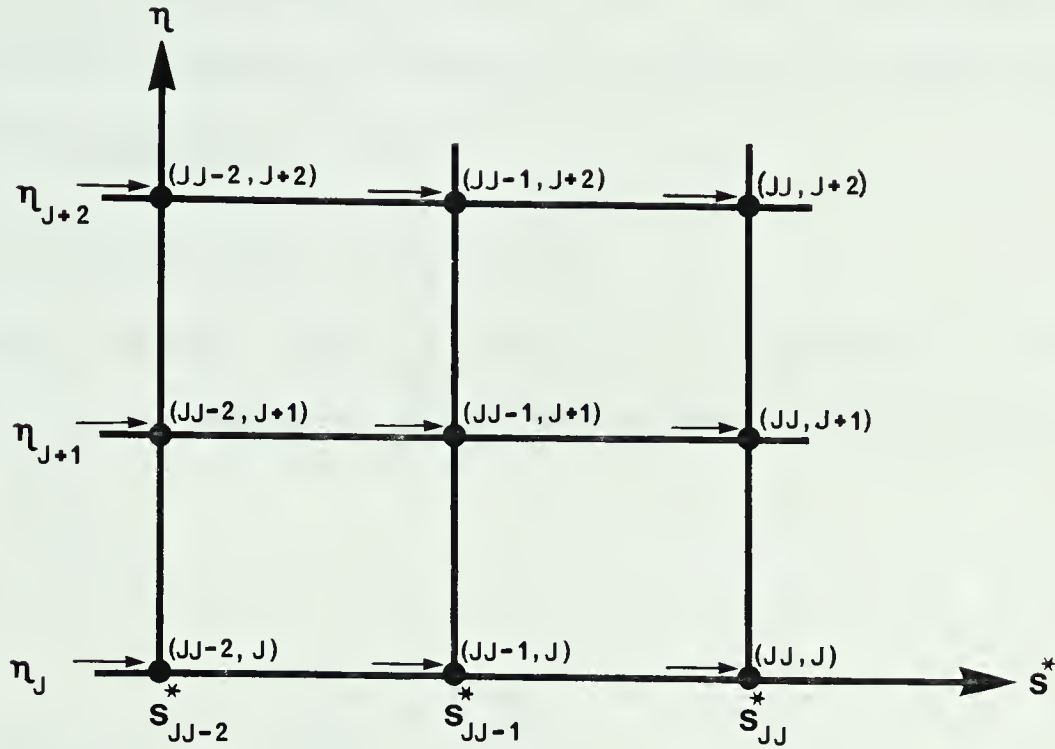


FIGURE 2--FINITE DIFFERENCE MARCHING SCHEME

that the variable quantities f and f' at the $JJ-1$ and $JJ-2$ stations are known. Then the problem is to find the solution $f(\eta)$ at the new station JJ .

The second phase is the numerical solution of the resulting ordinary differential equation in η direction. Given the free stream velocity distribution $U(s)$, the method of solution involves choosing a proper value of f''_w and integrating the approximated ordinary differential equation such that the outer boundary condition is satisfied.

In order to compute a solution of Equation (2.11), it is necessary to prescribe the velocity profile at the first starting s^* station. In most cases the nature of the flow at starting station can be characterized by a member of

the Falkner-Skan family of laminar wedge flows including the flat plate and stagnation point flow. The calculation of these similar solutions requires a relatively simple specialization of Equation (2.11).

2.4 Finite-Difference Formulation

The general form of the finite difference Lagrangian formulas for two-points and three-points can be written as follows [13]:

two-point form

$$\left. \frac{\partial f^{(n)}}{\partial s^*} \right|_{JJ} = \frac{f_{JJ}^{(n)} - f_{JJ-1}^{(n)}}{s_{JJ}^* - s_{JJ-1}^*} \quad (2.13)$$

three-point form

$$\begin{aligned} \left. \frac{\partial f^{(n)}}{\partial s^*} \right|_{JJ} &= \left[\frac{1}{s_{JJ}^* - s_{JJ-1}^*} + \frac{1}{s_{JJ}^* - s_{JJ-2}^*} \right] f_{JJ}^{(n)} \\ &\quad - \left[\frac{s_{JJ}^* - s_{JJ-2}^*}{(s_{JJ}^* - s_{JJ-1}^*)(s_{JJ-1}^* - s_{JJ-2}^*)} \right] f_{JJ-1}^{(n)} \\ &\quad + \left[\frac{s_{JJ}^* - s_{JJ-1}^*}{(s_{JJ}^* - s_{JJ-2}^*)(s_{JJ-1}^* - s_{JJ-2}^*)} \right] f_{JJ-2}^{(n)} \end{aligned} \quad (2.14)$$

where n indicates the order of the derivative.

Let

$$A_{11} = \frac{s_{JJ}^*}{s_{JJ}^* - s_{JJ-1}^*} \quad (2.15a)$$

$$A_{22} = \frac{s_{JJ}^*}{s_{JJ}^* - s_{JJ-1}^*} + \frac{s_{JJ}^*}{s_{JJ}^* - s_{JJ-2}^*} \quad (2.15b)$$

$$A_{33} = \frac{s_{JJ}^* (s_{JJ}^* - s_{JJ-2}^*)}{(s_{JJ}^* - s_{JJ-1}^*) (s_{JJ-1}^* - s_{JJ-2}^*)} \quad (2.15c)$$

and
$$A_{44} = \frac{s_{JJ}^* (s_{JJ}^* - s_{JJ-1}^*)}{(s_{JJ}^* - s_{JJ-2}^*) (s_{JJ-1}^* - s_{JJ-2}^*)} \quad (2.15d)$$

Replacing the streamwise derivatives in Equation (2.11) by two-point finite difference formula at $s^* = s_{JJ}^*$, we get

$$\begin{aligned} f''' + \frac{1+\beta}{2} f f'' + \beta (1-f'^2) \\ = A_{11} f' \left[f' - f'_{JJ-1} \right] - A_{11} f'' \left[f - f_{JJ-1} \right] \end{aligned} \quad (2.16)$$

Replacing the streamwise derivatives in Equation (2.11) by three-point finite difference formula at $s^* = s_{JJ}^*$, we get

$$\begin{aligned} f''' + \frac{1+\beta}{2} f f'' + \beta (1-f'^2) \\ = f' \left[A_{22} f' - A_{33} f'_{JJ-1} + A_{44} f'_{JJ-2} \right] \\ - f'' \left[A_{22} f - A_{33} f_{JJ-1} + A_{44} f_{JJ-2} \right] \end{aligned} \quad (2.17)$$

Equations (2.16) and (2.17) are ordinary differential equations in η with the known variable quantities f and f' at the upstream stations.

2.5 Satisfaction of Asymptotic Boundary Conditions

The satisfaction of asymptotic boundary conditions is a problem while solving Equation (2.11) with the boundary conditions (2.12). One must find the correct value of the unknown wall shear f''_w which makes f' approach unity at infinity. Since the ordinary differential equation must be solved by an initial-value method, a "shooting technique" is normally used. Smith and Clutter [13] proposed a shooting method which selects a range of values of f''_w and integrates the ordinary differential equation directly out to a suitably large value of η until three of the values of f' remain close to unity at that value of η . Then, a three-point interpolation procedure is used to determine the solution that satisfies the outer boundary condition. While an attempt was made to adapt this procedure in the present calculations, it was realized that this is a tedious trial and error procedure. The obvious solution to this problem is to seek an iterative procedure that chooses a proper value of f''_w which satisfies the outer boundary condition to a prescribed degree of accuracy. During the search for such an iterative procedure, the method developed by Nachtsheim and Swigert [15], which is based on a least-squares convergence criterion,

was found attractive. Corrections to the initial guesses are obtained from the original differential equation and from an additional equation which is derived by differentiating the terms of the original differential equation with respect to the initial condition f''_w . However, their study was restricted to similar flows. The present numerical technique was developed to adapt their idea to the solution of approximated ordinary differential equations of nonsimilar laminar flows. Since the fundamental idea has been discussed in detail by Nachtsheim and Swigert [15], only a brief summary is given here, along with a description of the modifications introduced for the application to Prandtl's laminar boundary layer equations.

In practical calculations the asymptotic boundary condition is replaced by the condition that $f' = 1$ at $\eta = \eta_e$ where η_e is the value of the independent variable at the edge of the boundary layer. Nachtsheim and Swigert illustrated the difficulties that arise when the boundary condition $f' = 1$ is applied at a finite value of η . They proposed that in order to ensure the satisfaction of the original outer boundary condition, i.e., $f' \rightarrow 1$ as $\eta \rightarrow \infty$, it is required to satisfy the conditions $f' = 1$ and $f'' = 0$ at $\eta = \eta_e$. The condition $f'' = 0$ at $\eta = \eta_e$ merely implies that the shear stress approaches zero as the edge of the boundary layer is approached. This imposition is consistent with the boundary layer theory. In order to solve Equation (2.16) or

(2.17) it is required to find a value of $f''(0)$ for which both these boundary conditions at the edge of the boundary layer are satisfied. This is equivalent of finding a solution from the equations

$$f'(\eta_e)[f''(0)] = 1 \quad (2.18)$$

and $f''(\eta_e)[f''(0)] = 0 \quad (2.19)$

Let $x = f''(0)$. A small change Δx in x changes $f'(\eta)$ and $f''(\eta)$ by the amounts $\frac{\partial f'}{\partial x}\Delta x$ and $\frac{\partial f''}{\partial x}\Delta x$, respectively.

Therefore, for a small change in wall shear the conditions at the edge of the boundary layer can be written as

$$f' + \frac{\partial f'}{\partial x}\Delta x = 1 \quad (2.20)$$

and $f'' + \frac{\partial f''}{\partial x}\Delta x = 0 \quad (2.21)$

In order to satisfy the conditions (2.18) and (2.19), it is necessary to apply corrections to a first approximation in x . As shown above, the necessary correction Δx should be chosen from the Equations (2.20) and (2.21). Here there is only one adjustable parameter Δx but there are two equations to be satisfied. Therefore, a satisfactory procedure is to seek the least squares solution of Equations (2.20) and (2.21).

Let

$$\delta_1 = f' + \frac{\partial f'}{\partial x} \Delta x - 1$$

and
$$\delta_2 = f'' + \frac{\partial f''}{\partial x} \Delta x$$

To minimize the sum of the squares of δ_1 and δ_2 , it is necessary to equate its first derivative with respect to Δx to zero. This calculation yields an expression for Δx , given by

$$\Delta x = \frac{f'_x(1 - f') - f''f''_x}{f'^2_x + f''_x} \quad (2.22)$$

where

$$f'_x = \frac{\partial f'}{\partial x}, \quad f''_x = \frac{\partial f''}{\partial x}, \text{ etc.}$$

In Equation (2.22), the partial derivatives of f with respect to x have to be evaluated at the edge of the boundary layer. This can be done by integrating an additional differential equation. The additional differential equation is obtained by differentiating the terms of the original differential equation (2.16) or (2.17), with respect to the wall shear $x = f''_w = f''(0)$. The integrals of this perturbation equation give the rate of change of the integrals of original differential equation with respect to the initial conditions. Differentiating Equations (2.16) and (2.17) respectively, with respect to x , the following perturbation equations are obtained:

when only one upstream solution is known,

$$\begin{aligned}
& f'''_x + \frac{1+\beta}{2} \left[f f''_x + f'' f_x \right] - 2\beta f' f'_x \\
& = A_{11} f'_x \left[f' - f'_{JJ-1} \right] + A_{11} f' f'_x \\
& - A_{11} f''_x \left[f - f_{JJ-1} \right] - A_{11} f'' f_x
\end{aligned} \tag{2.23}$$

when two upstream solutions are known,

$$\begin{aligned}
& f'''_x + \frac{1+\beta}{2} \left[f f''_x + f'' f_x \right] - 2\beta f' f'_x \\
& = f'_x \left[A_{22} f' - A_{33} f'_{JJ-1} + A_{44} f'_{JJ-2} \right] + A_{22} f' f'_x \\
& - f''_x \left[A_{22} f - A_{33} f_{JJ-1} + A_{44} f_{JJ-2} \right] - A_{22} f'' f_x
\end{aligned} \tag{2.24}$$

with the initial conditions

$$\eta = 0: \quad f_x = f'_x = 0, \quad f''_x = 1 \tag{2.25}$$

With the given initial guess of $x = f''(0)$, an attempt is made to integrate the original differential equation and the corresponding perturbation equation out to the edge of the boundary layer. If this can be accomplished, corrections are made for the initial guesses using Equation (2.22) and the process is repeated iteratively until the conditions (2.18) and (2.19) are satisfied to a sufficient degree of accuracy. The sum of the squares of the variations of the

computed variables from their asymptotic values, that is,

$$E = (1-f')^2 + f''^2 \quad (2.26)$$

gives an indication of how unsatisfactory the asymptotic boundary conditions are. Smaller values of the error E represents higher degree of accuracy in the computed variables. Thus, the asymptotic boundary conditions are satisfied by adjusting the wall shear f''_w so that the mean square error E between computed variables and the asymptotic values is minimized.

2.6 Numerical Solution

In order to integrate the boundary layer and perturbation differential equations, it is necessary to write them as system of first-order differential equations. This system of first-order equations for the present problem is written in Appendix 1. At each s^*_{JJ} station the unknown wall shear $f''(0)$ is found in the following manner.

The value of $f''(0)$ found at the station s^*_{JJ-1} is used as the initial guess. With this guessed value an attempt is made to integrate the differential equations out to a pre-assigned value of η_e . For the first integration the value of f'' tends to deviate radically from the correct solution at a relatively small value of η . If the value of f' becomes greater than 1, the integration is terminated. Then, at this value of $\eta < \eta_e$, the correction $\Delta f''(0)$ to $f''(0)$

is obtained by attempting to minimize the mean square error between the computed solution and the asymptotic values. The corrections are made for the initial guesses by the Newton-Raphson method. After the value of the error E is less than some prescribed minimum E_{\min} , no further corrections to the initial conditions need to be made at the chosen value of η_e . If the value of E_{\min} found at the chosen value of η_e is not small enough, it will be necessary to increase the range of integration. In this way the edge of the boundary layer is approached in steps. Since the boundary layer grows parabolically with s^* , the value of E becomes larger for the downstream stations. In order to use a single value of E_{\min} throughout the calculations, an additional convergence criterion has to be used so that the wall conditions converge to the same degree of accuracy at all stations. The additional requirement is that the free stream conditions at all stations should converge to a specified degree of accuracy. The wall shear $f''_w = f''(0)$ tends to a definite value as the error E and the free stream variables tends to satisfy the prescribed requirements. This converged wall shear is the solution for the problem.

The present calculation method was programed in double precision on the Amdahl 470 V/6 computer at the University of Alberta. Integration of the differential equations was performed by a predictor-corrector type method that uses Adams-Moulton formulas [16]. Integrations can be

performed either with a uniform grid or a variable grid in the η -direction. For most laminar flows a transformed boundary layer thickness of $\eta_e = 6$ is quite satisfactory with a uniform grid spacing $\Delta\eta = 0.025$. The calculations on a two-dimensional body are usually started from the front stagnation point. In such cases, the use of stagnation flow profile as the initial starting velocity profile is appropriate. With the present computer program such starting velocity profiles can be generated internally with a high degree of accuracy. The outer boundary conditions are required to converge to at least four decimal places at each station so that the wall shear converges to about twelve decimal places. It was found that the value of E_{\min} required in the present range of calculations is about 1×10^{-14} . It was observed that when η_e is not very large the convergence seems to be insensitive to reasonable initial guesses.

2.7 Errors in the Method of Solution

The errors introduced by the Lagrangian finite difference formulas (2.13) and (2.14), are derived by Smith and Clutter [17]. The errors are given by

$$E_2 = \frac{s_{JJ}^* - s_{JJ-1}^*}{2} \frac{\partial^2 f(n)}{\partial s^{*2}} \bigg|_{JJ} \quad (2.27)$$

and

$$E_3 = \frac{\{s_{JJ}^* - s_{JJ-1}^*\} \{s_{JJ}^* - s_{JJ-2}^*\}}{6} \frac{\partial^3 f(n)}{\partial s^{*3}} \bigg|_{JJ} \quad (2.28)$$

respectively. With the Hartree-Womersley method the most important error parameter is not the step size Δs^* , but instead, the ratio $s^*/\Delta s^*$. Smith and Clutter [13] have devoted much effort in studying the effect of variation of this parameter on the solution. They observed that sensitivity problems and error propagation are reduced if the value of $s^*/\Delta s^*$ does not exceed 25. Similar observations were also made in the present study. To have the same accuracy in the solution at all stations the step size Δs^* can usually grow parabolically because the boundary layer thickness grows parabolically with s^* .

The amount of error introduced is also dependent on the degree of accuracy with which the free stream conditions are satisfied. As stated in the previous section, the outer boundary conditions are satisfied to four decimal places. Therefore, the error introduced is in the fifth decimal place and occurs at the edge of the boundary layer. Accuracy should improve at lower values of η since about twelve-place accuracy in the wall conditions is required to obtain four-place accuracy at the edge of the boundary layer.

2.8 The Laminar Separation

Under the influence of an adverse pressure gradient, the motion within the boundary layer may be retarded to the extent that beyond a certain point along the surface the direction of the flow near the surface becomes reversed. When this occurs, the forward moving fluid in the boundary

layer detaches from the surface at that point. This phenomenon is commonly known as separation.

Specializing the boundary layer equation at the wall, it can be written that

$$\mu \left(\frac{\partial^2 u}{\partial y^2} \right)_{y=0} = \frac{dp}{ds}$$

In the region of adverse pressure gradient (decelerated flow, $\frac{dp}{ds} > 0$) it can be seen from the above equation that

$$\left(\frac{\partial^2 u}{\partial y^2} \right)_{y=0} > 0. \text{ Since, however, } \frac{\partial^2 u}{\partial y^2} < 0 \text{ at a large distance}$$

from the wall, there must exist a point for which $\frac{\partial^2 u}{\partial y^2} = 0$.

This is a point of inflexion of the velocity profile in the boundary layer, as shown in Figure (3).

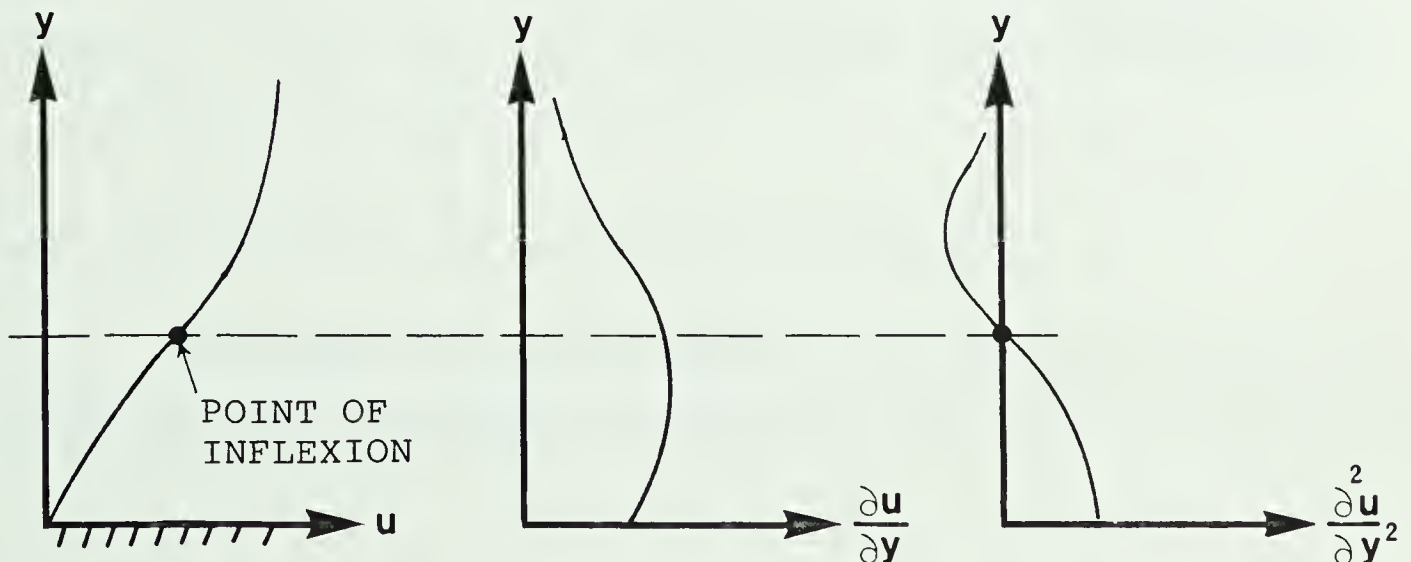


FIGURE 3--VELOCITY DISTRIBUTION IN A BOUNDARY LAYER WITH ADVERSE PRESSURE GRADIENT, $\frac{dp}{ds} > 0$

The exact separation point, that is the point where $f_w'' = 0$ cannot be calculated because singularities arise in the solution of nonlinear parabolic equations at and near this point. This singularity has been discussed by Goldstein [18]. However, the separation point may be approached by taking small steps in s . But in the present method there is a restriction on the smallest step size in s , that can be used. Because of this limitation the separation point was calculated by following the procedure proposed by Smith and Clutter [13]. When a solution is not obtained at a point near separation, a "suction" velocity, v_w , normal to the wall is applied and a solution obtained with the resulting velocity profile which now looks like a normal laminar profile. With this solution as a starting point another solution can be attempted with reduced suction and this process repeated until a solution is obtained with $v_w = 0$. Separation is assumed to occur when the local skin friction coefficient, C_f , becomes less than 5×10^{-4} .

2.9 Calculations and Discussion of Results

Solutions for both similar and nonsimilar flows are presented here in order to demonstrate the basic accuracy and

the rate of convergence of the present method.

2.9.1 Blasius Flow

Specializing the Equation (2.11) for the flow over a flat plate, the following equation is obtained:

$$f''' + \frac{1}{2}ff'' = 0 \quad (2.29)$$

with the boundary conditions

$$\begin{aligned} \eta = 0: \quad f &= 0, \quad f' = 0 \\ \eta \rightarrow \infty: \quad f' &\rightarrow 1 \end{aligned} \quad (2.30)$$

This is well known Blasius equation for which a high accuracy solution is known. The wall shear f''_w , accurate to six decimal places, for this flow is 0.332057.

Because the flow is similar, the solution should be the same at all stations and any change in solutions represents the growth in error. The error growth was studied with different $\Delta\eta$ spacing. In this case a transformed boundary layer thickness $\eta_e = 8$ was used. With a spacing $\Delta\eta = 0.02$ (400 points within the boundary layer), the value of f''_w after 25 equal length stations in s^* was 0.332048. The error in f''_w is therefore approximately 9×10^{-6} . The average number of iterations per station was about 6 and the average computer time per station was approximately 0.5 seconds. With a spacing $\Delta\eta = 0.01$, which corresponds to 800 points

within the boundary layer, the error in f_w'' , $\Delta f_w''$, did not change significantly. However, with a spacing $\Delta \eta = 0.04$, the solution was affected in the third decimal place. Therefore, this suggests that the accuracy of the method of solution depends on the integration in the η direction. It was observed that the error propagation also depends on the degree of accuracy in the solution at the initial starting station s^* .

2.9.2 Boundary Layer Measured by Schubauer

Since the purpose of the present method is to study physical flows, the accuracy of the method is also tested by comparing the calculated boundary layer with the measurements of Schubauer on an elliptic cylinder. Calculated velocity profiles by the present method are compared with those given by Hartree method [19] and with those given by Smith-Clutter method. The numerical values of pressures and pressure-gradients used in the calculations were obtained from Hartree [19], who derived them from an analysis of Schubauer's experimental data. Comparison of the calculated profiles with the measured ones are shown in Figure (4) at four stations. Very close agreement is observed between calculations and experiments. When the velocity profiles calculated by Smith and Clutter [13] at the first three stations were plotted on the same graph, they coincided with the present profiles within the plotting accuracy. The dotted line in Figure (3) represents the velocity profile calculated by Hartree [19]. The

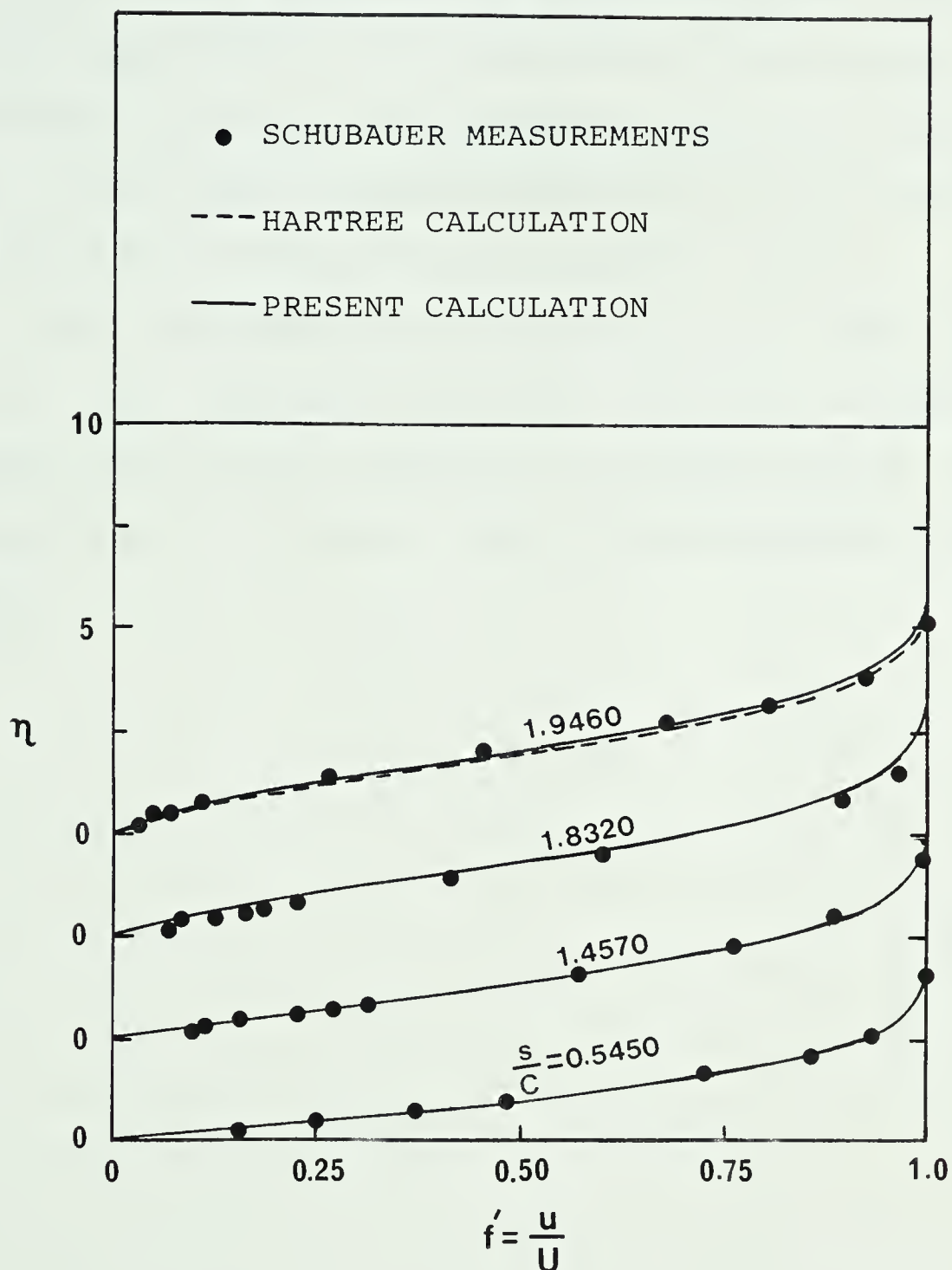


FIGURE 4--COMPARISON OF CALCULATED AND MEASURED VELOCITY PROFILES ON THE ELLIPTIC CYLINDER STUDIED EXPERIMENTALLY BY SCHUBAUER

present calculations also agree quite well with Hartree's calculation. The present calculation did not give any separation, although Schubauer observed separation at $s/c = 1.99 \pm 0.02$. Neither the Hartree-solution nor the Smith-Clutter solution gave separation of the boundary layer on Schubauer's ellipse. A transformed boundary layer thickness $\eta_e = 6$ was used in these calculations with a spacing $\Delta\eta = 0.025$ (240 points within the boundary layer).

Thus the present method appears to be simple and accurate. The convergence rate to a solution is rapid. The successful use of this technique for predicting the laminar boundary layer on an airfoil will be demonstrated in later chapters.

CHAPTER III

APPARATUS AND EXPERIMENTAL METHODS

3.1 Model Airfoil

The proposed experimental investigation was made on an NACA 66₃-018 symmetric airfoil section. This particular section was chosen because relatively large localized regions of laminar separation which could be measured easily were found to exist behind the position of minimum pressure near the midchord [4,5]. Also such a symmetric section is easy to fabricate. The model chord was chosen as one metre as it allows for a Reynolds number of 2×10^6 in the wind tunnel and also the large model section could be built more accurately.

The model was built from a series of sheets of "Styrofoam S.M." insulating material glued together. The model section profile was cut out using an electrically heated wire. Grooves were cut on the lower surface of the section for the vinyl tubing used to connect the pressure taps to the pressure transducer. The skin of the section, 0.508 mm thick aluminum sheet, was wrapped around the foam section and bonded to it. The static pressure tapings were made by drilling through the skin, perpendicular to the surface, and pulling the vinyl tubing through the skin. These tubes were cemented in place and sheared off flush with the airfoil surface. The surface was sanded and painted

until an aerodynamically smooth surface was obtained.

After completion of the model the coordinates of the profile at the mid span location were measured. It is estimated that the measurements of the coordinates were accurate to 0.1 mm. A comparison of profiles of model airfoil and NACA 66₃-018 airfoil is given in Table I. The airfoil was manufactured to an accuracy of better than 3 mm (0.3% chord).

3.2 Wind Tunnel and Auxiliaries

The experimental investigation was conducted in the closed-circuit low speed wind tunnel at the Department of Mechanical Engineering, the University of Alberta. The test section measures 1.2 m high x 2.4 m wide and 11 m long. The model airfoil completely spanned the 1.2 m dimension and it was mounted on the tunnel centre line as shown in Figure (5). The model was attached to circular end turntables, as shown in Figure (5), which formed part of the wind tunnel floor and ceiling. The end turntables enabled the model to be rotated to any desired angle of attack even when the tunnel was running. A series of boundary layer suction holes, 3.175 mm in diameter, were drilled through the end plates at 6.35 mm intervals at the junction of the model and the end plates. The purpose of these holes is to remove parts of the boundary layer which builds up on the floor and ceiling of the tunnel. If this is not done these thick boundary layers may separate under the influence of the adverse pressure gradients

TABLE I

COMPARISON OF PROFILES OF MODEL AIRFOIL
AND NACA 66₃-018 AIRFOIL*

Distance from Leading Edge as a Percent of Chord	NACA 66 ₃ -018 Section Ordinate as Percent of Chord	Model Airfoil Section Ordinate as Percent of Chord	
		Upper	Lower
0.00	0.000	0.000	0.000
0.50	1.323	1.318	1.325
0.75	1.571	1.558	1.570
1.25	1.952	1.972	1.958
3.50	2.646	2.650	2.710
5.00	3.690	3.543	4.178
7.50	4.513	4.316	4.826
10.00	5.210	4.826	5.573
15.00	6.333	6.193	6.617
20	7.188	7.112	7.158
25	7.848	7.789	8.022
30	8.346	8.298	8.507
35	8.701	8.668	8.834
40	8.918	8.992	9.060
45	8.998	9.044	9.141
50	8.942	9.025	9.063
55	8.733	8.814	8.820
60	8.323	8.397	8.347
65	7.580	7.681	7.604
70	6.597	6.495	6.591
75	5.451	5.588	5.403
80	4.206	4.343	4.115
85	2.934	3.108	2.815
90	0.714	1.920	1.651
95	0.646	0.902	0.719
100	0.000	0.000	0.000

*For both cases leading edge radius is 1.955 percent of chord



Figure 5—View of the Model in the Wind Tunnel

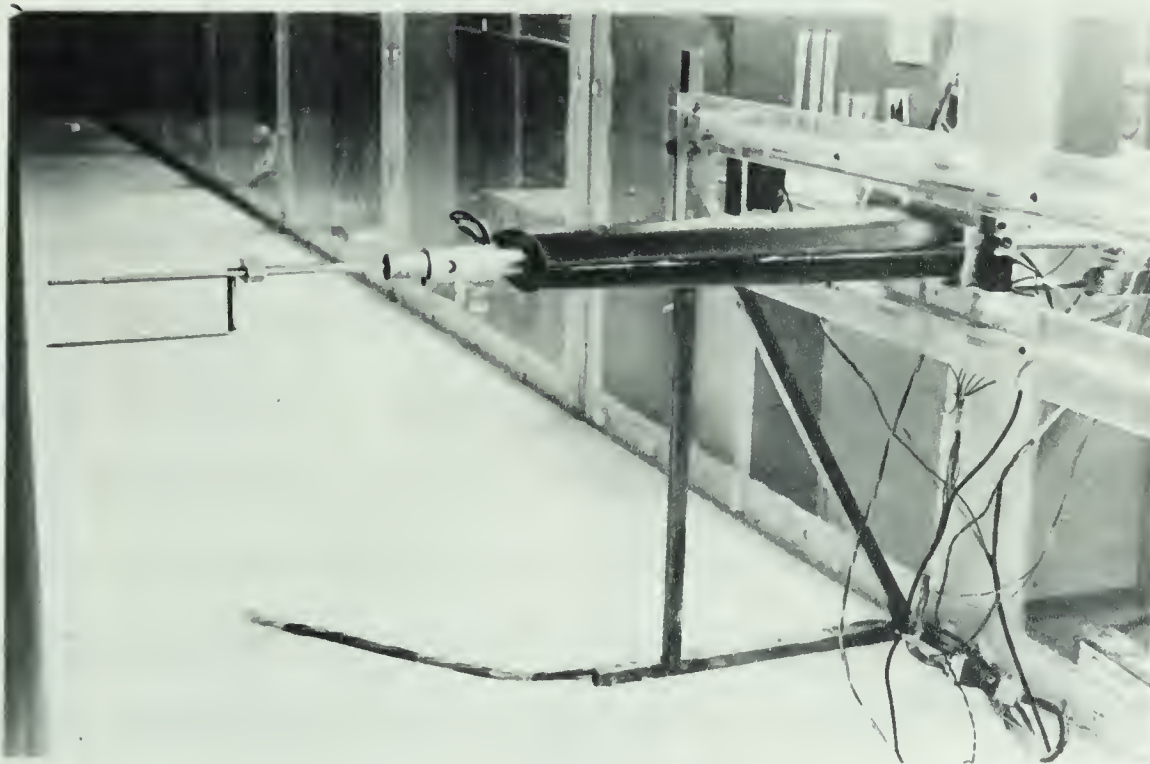


Figure 6—Probe Traversing Apparatus

generated by the airfoil section. This would result in large disturbances to the flow field which would interfere with the two-dimensional nature of the flow. The other side of the suction holes were connected via plenum chambers to a large air suction pump.

Throughout the range of present wind tunnel speeds the true rms turbulence level of the wind tunnel air stream was 0.07 to 0.20 percent of the free stream velocity. However, the free stream turbulence measured in this wind tunnel on a previous occasion, for example Reference [20], was about 0.03 percent.

3.3 Wind Tunnel Wall Corrections

Because the model and its wake occupy a certain volume within the finite tunnel stream the streamline pattern about the model is distorted compared with free-air conditions. The magnitude of the streamline displacement will mainly depend on the relative sizes of the model and tunnel working section. It is assumed that the model behaves within the tunnel as it would in free air at some dynamic pressure slightly different from the nominal tunnel dynamic pressure. Therefore the measured dynamic pressure of the free stream must be corrected for the blockage. The standard corrections have been developed over the years on a semi-empirical basis and are well documented by Garner [21].

The necessary increment $\Delta(\frac{1}{2}\rho U_\infty^2)$ which must be applied to the measured dynamic pressure is given by (for

incompressible flow)

$$\Delta(\frac{1}{2}\rho U_{\infty}^2) = \rho U_{\infty}^2 \epsilon_B$$

where ϵ_B is the blockage factor which is the sum of corresponding solid and wake blockage factors. In the present case the wake blockage is small compared to solid blockage and, therefore, is neglected. For a closed rectangular tunnel

$$\epsilon_B = \frac{\pi^2}{12} \left(\frac{c}{h}\right)^2 \left(\frac{t}{c}\right)^2 \lambda_2$$

where

h = width of the tunnel

t = maximum thickness of the model

λ_2 = parameter related to profile thickness
 = 3 for the present model

For the present configuration the necessary correction was found to be $0.033\rho U_{\infty}^2$ and, therefore, the corrected dynamic pressure is equal to $1.066(\frac{1}{2}\rho U_{\infty}^2)$.

3.4 Data Acquisition

The HP 3050B Automatic Data Acquisition System was used for this experimental investigation. This system utilizes a model 9820A programmable calculator to control a model 3490A digital multimeter and 3495A scanners for data logging and high level algebraic manipulations on up to 40 channels of test data. Pressure, temperature and velocity

can be measured with appropriate transducers connected to the different channels of the system.

3.5 Surface Pressure Measurements

The surface static pressure tapings were approximately 1 mm in diameter. There were 40 pressure taps and all of them were located on the lower surface of the airfoil at the midspan line. The taps were closely spaced in the vicinity of the separated region.

The pressure measurement technique, based on sequential connection of each pressure tapping by vinyl tubing to a "Scanivalve" and a single pressure transducer, was used. The output of the pressure transducer was connected to the data acquisition system. The switching mechanism of the scanivalve was operated by the channel selector in the data acquisition system.

All the pressure transducers were calibrated against an accurate inclined tube manometer. The linearity and sensitivity of all the transducers used were found to be good.

3.6 Mean Velocity Measurements

The mean velocity in a boundary layer could be measured by using either small pitot tubes or hot element anemometers. Pitot tubes have directional sensitivity and so one can theoretically find whether the flow is in the forward or reverse direction at any point in a steady flow.

But, this property may not hold good in a highly turbulent flow such as that treated in the present study. In order to measure the velocity at any station in a boundary layer, using a pitot tube, it is required to know the static pressure at that station. Gault [5] suggested that the probe consisting of separate static and total pressure tubes interferes with the flow and influences the measurements near the wall.

The hot element sensor is smaller in size and therefore it causes only the minimum admissible disturbance of the flow pattern. The hot element is only sensitive to the flow normal to the element and therefore, it cannot detect the flow direction. However, contour plots of lines of constant apparent velocity as measured by the anemometer do indeed reveal the general structure of the bubble. The transition from laminar to turbulent flow in the free shear layer could be determined by observing the velocity fluctuations in the boundary layer as indicated by a hot element probe. Measurements of rms values of the velocity fluctuations give the turbulence intensity distribution across the boundary layer. In view of these capabilities a hot element anemometer was chosen for this investigation.

Hot element sensors are either fine wires such as platinum or tungsten, or a thin film of metal deposited on a

ceramic substance. Hot wires have advantages in terms of small diameter and high frequency response. On the other hand hot film sensors have several other advantages in terms of stability, ruggedness, spatial resolution and rigidity that make them superior to hot wire sensors in many applications. In the present investigation hot film sensors were preferred to hot wire sensors.

The tunnel free stream velocity was measured with a pressure transducer connected to a total pressure tube in the free stream and a test section static pressure tap. The static pressure tap was located at 1.5 m upstream of the model where it was not affected by the presence of the model.

The flow data was corrected for temperature whenever it was necessary. Temperature measurements in the tunnel flow were made with the data acquisition system using a copper-constantan thermocouple. Mean velocity measurements in the boundary layer were also made with the use of the data acquisition system. Velocity measurements in the boundary layer of the separated flow field were made on a horizontal line along the chord at a position 3 cm below the wing centreline.

3.7 Turbulence Measurements

The turbulent intensities of streamwise and normal velocities $\left[\frac{\sqrt{u'^2}}{U} \text{ and } \frac{\sqrt{v'^2}}{U} \right]$ were measured using an x-wire anemometer. Due to large body size of the x-wire probe, measurements could not be made at distances any closer to the

wall than 1.5 mm. In order to study the behavior of turbulent intensities closer to the wall, the streamwise intensities were also measured with a single element hot-film probe. The output of the hot film sensor was fed to an oscilloscope so that the velocity fluctuations could be observed directly. Transition in the free shear layer was determined from these observations depending on the nature of fluctuations.

Reynolds shear stress distribution ($-\overline{u'v'}$) in the turbulent boundary layer was also measured using the x-wire anemometer.

3.8 Probe Traversing Mechanism

To carry out detailed boundary layer surveys within the separated flow it was necessary to be able to easily move the measuring probe from one station to another while the tunnel was running, and to know the coordinates of these stations to good accuracy.

The traversing apparatus is shown in Figure (6). The main boom carrying the probe is attached to a micrometer screw driven by a small electric motor. This allows the movement of the probe in a direction normal to the airfoil surface at a very slow and fine speed. The micrometer and the driving electric motor are mounted on a carriage which slides on two frictionless guides. An electric motor drives the carriage in a horizontal direction along the chord. The main boom and so the probe move with the carriage along the airfoil chord. This apparatus has a probe movement of about

60 cm along the chord and 2.5 cm normal to the surface. The coordinates of the probe position are indicated by the readings of the calibrated ten turn potentiometers fitted to the driving motors. In this way it is possible to read the position normal to the surface to within 0.025 mm and the chord wise position to within 1 mm. The distance of the probe above the surface is adjusted to the desired value with the help of a zero positioning mechanism attached to the end of the main boom. The push rod parallel to the probe holder, shown in Figure (6), is attached to a micro-switch that controls the probe drive motor. The micro-switch is switched off when the push rod just pushes against the surface. Then immediately the motion of the probe stops, thus preventing the probe touching the surface. While taking the measurements the probe is always moved only in one direction to avoid the backlash in the system.

Bare structure of the boom may create vorticies behind the boom resulting in the vibration of the probe, so a fairing was built around the main boom as shown in Figure (6) to smooth the flow. The fairing has the NACA 0025 airfoil section shape.

Apart from the micro-switch on the end of the main boom there is a manually operated switch control for the probe drive motor. The switch controls for both the motors are mounted on a small switchboard connected to the traversing unit by long lengths of flex. This allows the operator either

to sit at a desk with all the hot film gear, or to work inside the tunnel setting up to the probe. While making the measurements, the movement and precise location of the probe inside the boundary layer are controlled and measured by the automatic data acquisition system.

The effect of the airstream on the arm carrying the measuring probe was examined at different Reynolds numbers. At Reynolds numbers below 1.0×10^6 the movement of the arm away from the airfoil surface was very small, less than 0.025 mm. However, with increasing speed there was a slight tendency for the arm to lift away from the surface. A displacement of about 0.10 mm was noted at a Reynolds number of about 2.0×10^6 .

3.9 Hot Film and X-Wire Anemometers

3.9.1 Hot Film Anemometer

If it is assumed that the flow direction is normal to a sensor then the effective cooling velocity past the sensor is approximately equal to the flow velocity, u . In a flow such as that treated here, it can be assumed that the direction of streamwise velocity will be normal to the measuring hot film sensor. Then the basic bridge output signal is related to the flow approximately as

$$E^2 = a + bu^n \quad (3.1)$$

where a , b are constants depending on the fluid properties,

u is the flow velocity, and n is an exponent that varies with range and fluid.

In the present study quartz coated cylindrical hot film sensors, 0.05 mm diameter x 1.0 mm long, were used with a TSI 1054B constant temperature anemometer unit. This unit has a built in split point linearizer which linearizes the basic bridge output signal. Then the calibration curve for the sensor is given by

$$E_L = Ku \quad (3.2)$$

where E_L is the linearized output voltage, K is an experimental constant that depends on the type of sensor and range, u is the flow velocity perpendicular to the sensor. If K is determined from the calibration experiments then the streamwise velocity can be determined from Equation (3.2).

The turbulence intensity of streamwise velocity, $\sqrt{\frac{u'^2}{U}}$, can be measured using the calibration curve (3.2).

From equation (3.2) it can be written that

$$dE_L = Kdu$$

or, for small fluctuations

$$e' = Ku' \quad (3.3)$$

where e' is the fluctuation in voltage and u' the fluctuation

of velocity. The quantity $e' = dE$ is usually measured as the rms value of the fluctuating voltage, $\sqrt{e'^2}$, on an rms voltmeter. The corresponding rms value of the fluctuating component of the velocity $\sqrt{u'^2}$ can be found from Equation (3.3).

Calibration curves for the hot film probes were determined using the DISA 55D41 calibration unit. The TSI anemometer used in the present study was not temperature compensated. However, the linearized output was corrected for temperature by following the procedure recommended by manufacturers.

3.9.2 X-Wire Anemometer

Two hot wires placed at an angle of 45 degrees with respect to the mean velocity shown in Figure (7), will generate output signals proportional to the sum ($u' + v'$) and the difference ($u' - v'$) of the two fluctuating components. Based on this principle, the simplest form of x-probe consists of two separate hot wires attached to the prongs of the supports so that the two wires are in the same plane. This plane is usually referred to as the "probe plane." In the probe plane the two wires form a cross. Figure (7) shows the two-sensor orientation. With this arrangement the turbulence in two perpendicular directions and the directional correlation (Reynolds stress) can be measured. The two wires are connected to separate anemometers. Since it is very difficult to find an x-probe which has hot wires with

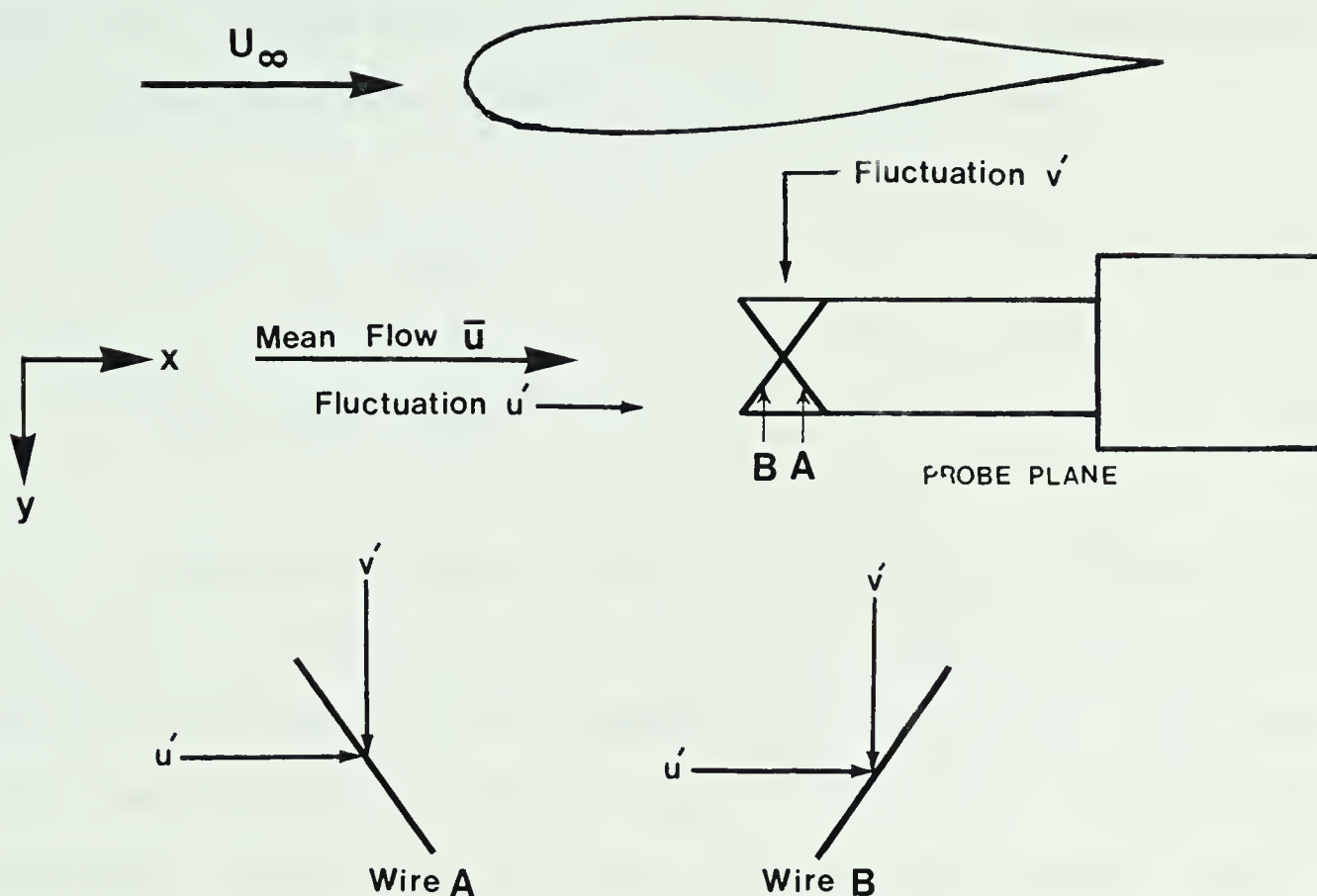


FIGURE 7--X-WIRE CONFIGURATION

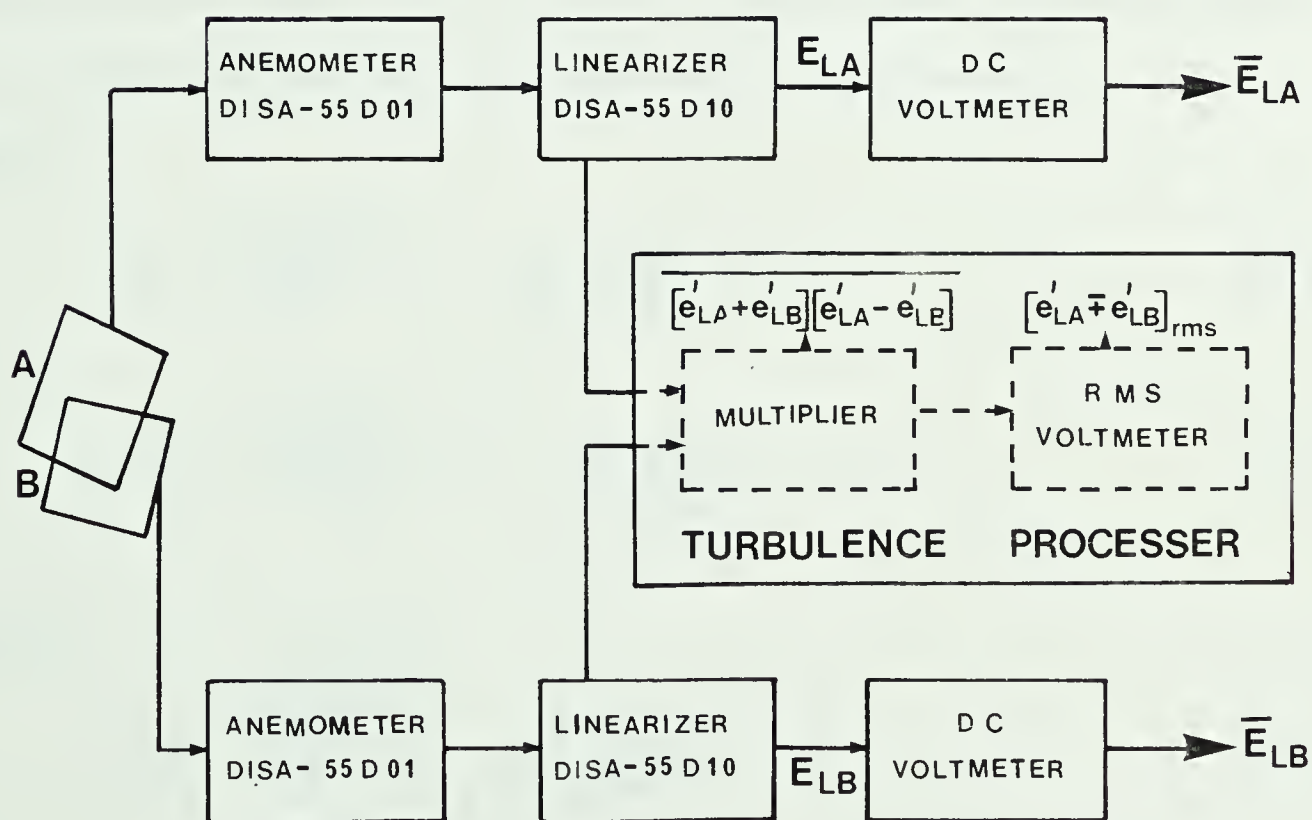


FIGURE 8--SETUP FOR MEASURING TURBULENCE

identical calibration curves, it is assumed the calibration curves for hot wires A and B of the x-probe are:

$$E_A^2 = a_A + b_A Q_A^{n_A} \quad (3.4)$$

$$E_B^2 = a_B + b_B Q_B^{n_B} \quad (3.5)$$

Since the working equations used in the present calculations have been developed and discussed in detail by Wilson [22], only a brief summary is given here. The equations were developed based on the "linearized" analysis where the higher order terms are dropped. In the present study, it is tacitly assumed that turbulence intensities are low so the usual assumptions regarding neglect of higher order terms can be made. The following equations can be written for effective cooling velocities of each sensor:

Wire A

$$\bar{Q}_A = \frac{\sqrt{1+k^2}}{\sqrt{2}} \bar{u} + \frac{(1-k^2)}{\sqrt{2} \sqrt{1+k^2}} \bar{v} + \bar{K} \quad (3.6)$$

$$Q'_A = \frac{\sqrt{1+k^2}}{\sqrt{2}} u' + \frac{(1-k^2)}{\sqrt{2} \sqrt{1+k^2}} v' + K' \quad (3.7)$$

Wire B

$$\bar{Q}_B = \frac{\sqrt{1+k^2}}{\sqrt{2}} \bar{u} - \frac{(1-k^2)}{\sqrt{2} \sqrt{1+k^2}} \bar{v} + \bar{K} \quad (3.8)$$

$$Q'_B = \frac{\sqrt{1+k^2}}{\sqrt{2}} u' - \frac{(1-k^2)}{\sqrt{2} \sqrt{1+k^2}} v' + K' \quad (3.9)$$

where

\bar{Q} = average effective cooling velocity

Q' = fluctuating component of effective cooling velocity

k = effective cooling velocity factor which depends on $1/d$ ratio of sensor
= 0.2 for wires

and \bar{K} , K' = error terms.

In general, \bar{K} and K' are functions of turbulence in three mutually perpendicular directions and the directional correlations. The presence of these terms makes data reduction difficult. In order to circumvent this problem, \bar{K} and K' are usually dropped while reducing the data and later on these terms are estimated as error terms. This will be further discussed in the next section. If \bar{K} and K' are dropped the following equations can be obtained:

$$\bar{u} = \frac{\bar{Q}_A + \bar{Q}_B}{\sqrt{2} \sqrt{1+k^2}} \quad (3.10)$$

$$\bar{v} = \frac{\{\bar{Q}_A - \bar{Q}_B\} \sqrt{1+k^2}}{\sqrt{2} (1-k^2)} \quad (3.11)$$

$$u' = \frac{Q'_A + Q'_B}{\sqrt{2} \sqrt{1-k^2}} \quad (3.12)$$

$$v' = \frac{\{Q'_A - Q'_B\} \sqrt{1+k^2}}{\sqrt{2} (1-k^2)} \quad (3.13)$$

$$\overline{u'v'} = \frac{\{Q'_A + Q'_B\} \{Q'_A - Q'_B\}}{2 (1 - k^2)} \quad (3.14)$$

Since the system is linearized due to the higher order terms that are being neglected, the linearized output voltage is related to flow as follows:

$$E_L = GQ \quad (3.15)$$

where E_L is the linearized output voltage, G is the transfer coefficient, and Q is the effective cooling velocity. The fluctuating velocities, u' and v' , are usually measured as rms fluctuations. Upon introducing the Equation (3.15) into Equations (3.10) to (3.14) the following data reduction equations are obtained for the mean and turbulence velocity fields:

$$\bar{u} = \frac{\bar{E}_{LA} + \bar{E}_{LB}}{G \sqrt{2} \sqrt{1+k^2}} \quad (3.16)$$

$$\bar{v} = \frac{\{\bar{E}_{LA} - \bar{E}_{LB}\} \sqrt{1+k^2}}{G \sqrt{2} (1-k^2)} \quad (3.17)$$

$$\sqrt{u'^2} = \frac{\{e'_{LA} + e'_{LB}\} \text{rms}}{G \sqrt{2} \sqrt{1+k^2}} \quad (3.18)$$

$$\sqrt{v'^2} = \frac{\{e'_{LA} - e'_{LB}\} \text{rms} \sqrt{1+k^2}}{G \sqrt{2} (1-k^2)} \quad (3.19)$$

$$\overline{u'v'} = \frac{\{e'_{LA} + e'_{LB}\} \{e'_{LA} - e'_{LB}\}}{G^2 2(1-k^2)} \quad (3.20)$$

The equipment needed to make these measurements is shown in Figure (8). A DISA type 55P61 x-probe was used in the present experimental investigation. A standard computer program that is available in the Department of Mechanical Engineering, University of Alberta, was used to determine the best fit curve to the calibration data. As was mentioned earlier the constants a and b in the basic response curve, Equation (3.1), depend on the fluid properties. Since the fluid properties vary with pressure and temperature, the constants a and b should be adjusted daily according to pressure and temperature variations in the laboratory. The computer program tabulates a and b for different pressure and temperatures. The transfer coefficient G is the gain of the DISA 55D10 linearizer.

3.10 Error Analysis

It was assumed that the relative turbulence intensity is small, in order to make possible a linearization of the hot wire (hot film) response to turbulence fluctuations. A distortion of the linearized hot wire response, which gives rise to errors in measurements, is therefore expected at relatively high turbulence intensities (greater than about 10%). Inaccurate angles of attack introduce error in x-wire measurements. However, in the present study the error

caused was found to be very small. Error in the velocity measurements near a surface are usually introduced owing to the surface cooling effect on the measuring probe. However, there is no satisfactory means of predicting the correction.

As will be shown in Chapter IV, there is close agreement between measured and calculated mean velocity profiles in the region of laminar separation. The maximum error in measurements would have probably occurred near turbulent reattachment because of reverse flow and high level of turbulence present near the wall. At this location the relative values of the mean velocity measured with the hot film are estimated to be accurate to within about $\pm 12\%$. The error in absolute values is probably higher.

As was mentioned in the previous section, the error terms \bar{K} and K' are functions of turbulence in three mutually perpendicular directions and the directional correlations. However, in the present investigation only u' , v' and $\overline{u'v'}$ are measured; and it is therefore not possible to evaluate these terms accurately. The accuracy of the x-wire measurements can be studied by comparing with the hot film measurements near reattachment point and equilibrium point where the discrepancies were found to be maximum and minimum, respectively.

The mean velocity profile measured by the x-wire is shown in Figure (9) for comparison with the hot film measurement. At reattachment point, the maximum discrepancy between

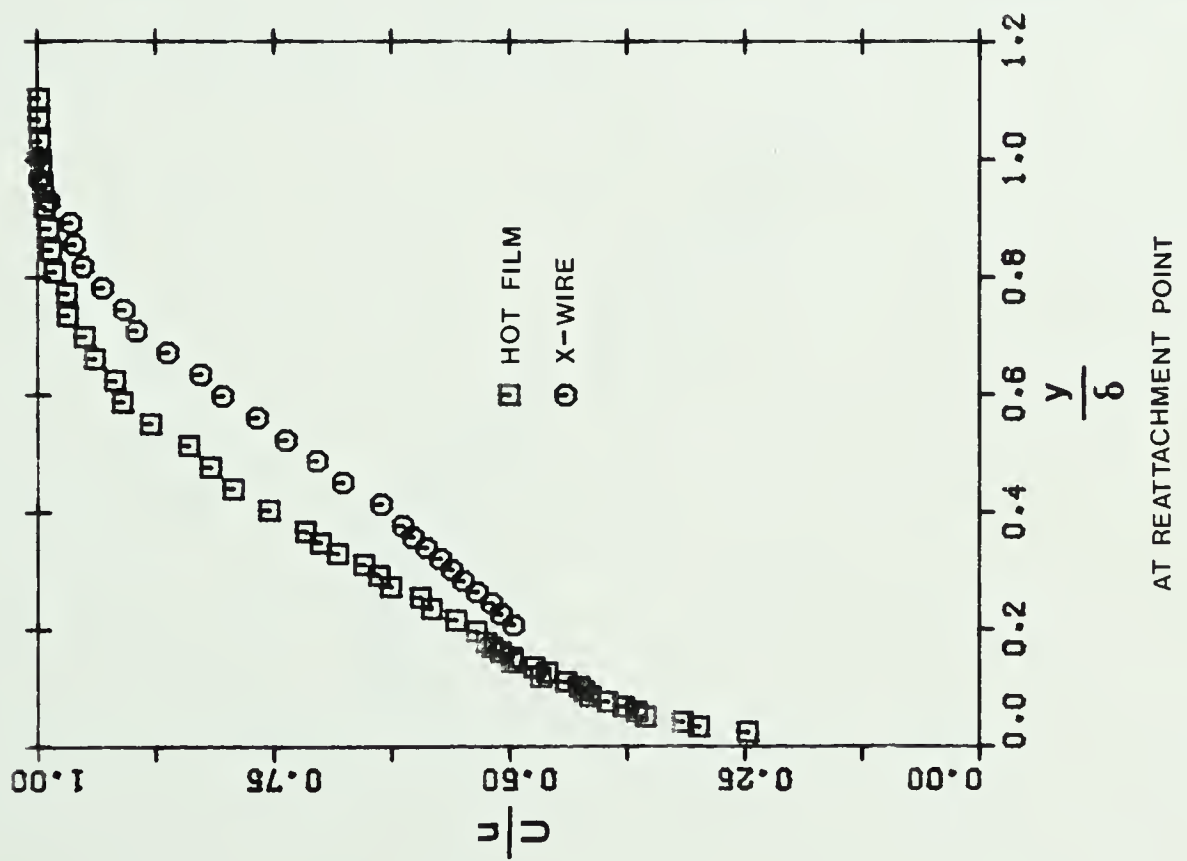
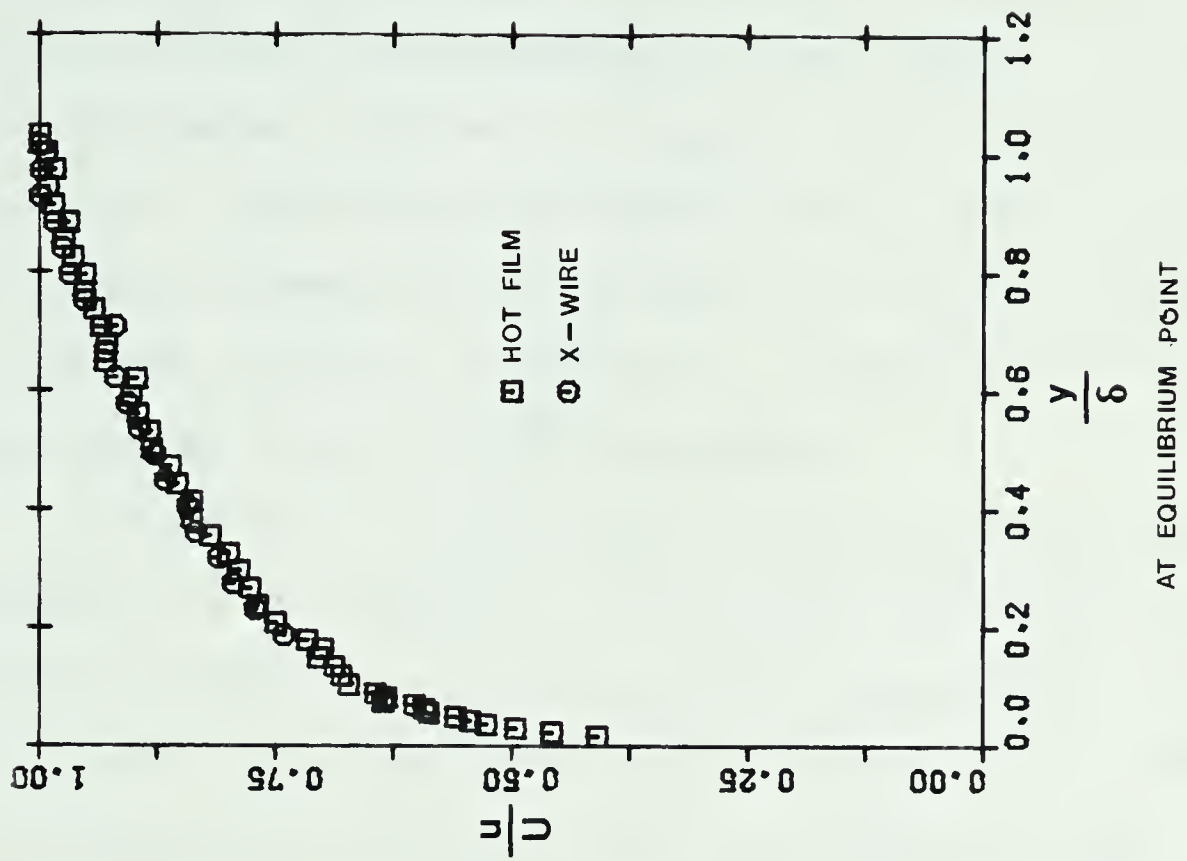


FIGURE 9--COMPARISON OF X-WIRE AND HOT FILM MEAN VELOCITY MEASUREMENTS

the two measurements is seen to be about 12% whereas at equilibrium point the discrepancy is very small. A comparison of streamwise turbulence intensity profiles is shown in Figure (10). The maximum difference between the two measurements at reattachment point is found to be about 15% occurring near the vicinity of the wall. At equilibrium point the discrepancy is about half of this value.

Errors of 10 to 20 percent in the measurement of turbulence are acceptable in a flow field that exists near turbulent reattachment. In the present measurements the maximum error is within this limit. The hot film is usually less susceptible to the errors due to reverse flow and turbulence and therefore the measurements are closer to the actual flow. The hot film measurements were adopted for the analysis of the mean velocity.

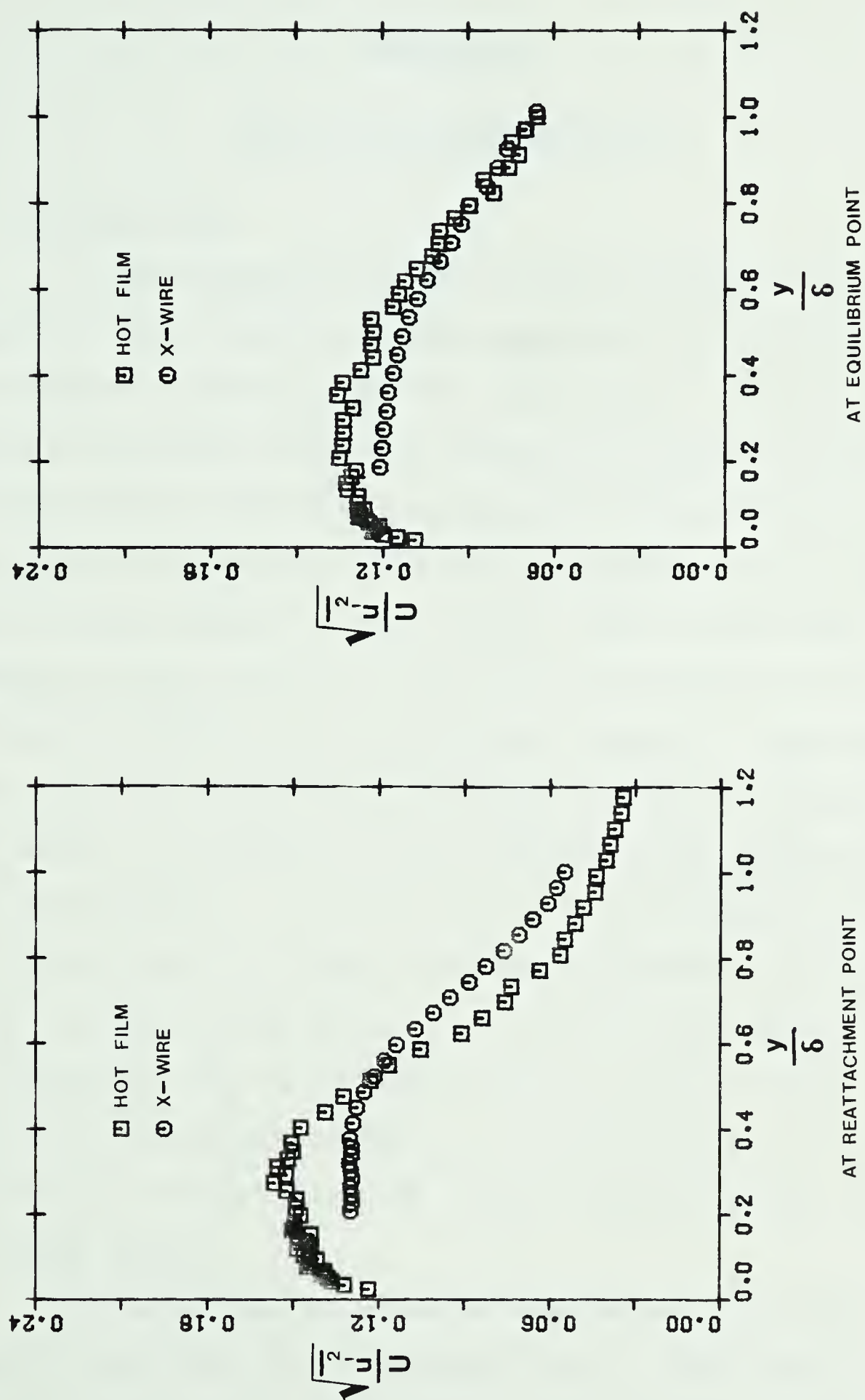


FIGURE 10--COMPARISON OF X-WIRE AND HOT FILM STREAMWISE TURBULENCE INTENSITY MEASUREMENTS

CHAPTER IV

MEAN FLOW CHARACTERISTICS

4.1 Introduction

A comprehensive survey of the literature on experimental results involving bubble separation is available from the review articles by Tani [2] and Ward [3]. It is seen from the literature that the phenomena of bubble formation and the physical behavior of the bubble are well understood. The qualitative nature of the flow processes in the separated flow is also studied to some extent. But the existing evidence is not enough to completely understand the flow processes involved for an analytical approach. Especially, there is hardly enough data available to make an interpretation about the character of the boundary layer downstream of flow reattachment. In view of this an experimental study of the laminar separated flow field was undertaken. The purpose of the present investigation was to provide new information, to supplement the available data and to provide further insight into the flow processes. An experimental study was made of the boundary layer on an NACA 66₃-018 airfoil section in a wind tunnel.

The experimental pressure distributions and mean velocity measurements are presented here. The composite physical structure of the separated flow field was described

by the contours of constant velocity. The measurements obtained have been compared with similar results from previous investigations. The present experiments corroborated the observations of other investigators in many respects; but also revealed some interesting new results. It was found that at some distance downstream of flow reattachment the turbulent velocity profiles tend to settle down to a nearly equilibrium form. However, not much attention was given to this region by other mean flow investigators. It is believed that the present study has gone further than the other investigators reported to date, especially with regard to the redeveloping turbulent flow region downstream of reattachment.

4.2 Test Program

The test program consisted of surface static pressure measurements and measurements of mean flow velocity in the boundary layer near the vicinity of the bubble. It also included the observations of velocity fluctuations in the boundary layer as indicated by a hot film anemometer. Surface flow visualization experiments were conducted on the model to determine the laminar boundary layer separation point. The investigation was made at Reynolds numbers based on airfoil chord of 0.8×10^6 , 1.2×10^6 , 1.6×10^6 and 2×10^6 , and at angles of attack of 0° and 2° , except for the Reynolds number of 2×10^6 where the measurements were only made for an angle of attack of 0° . The experimental data obtained in the present investigation described seven different laminar

separation bubbles.

Although it would have been desirable to cover a wide range of Reynolds number it was only possible to cover the range from 0.8×10^6 to 2×10^6 in this investigation. The capabilities of the wind tunnel facility limited the Reynolds number to 2×10^6 and the lower limit was imposed by an instability that appeared in the flow for Reynolds numbers less than 0.8×10^6 . A detailed investigation as to the cause of these fluctuations was not made because this was outside the objectives of the present investigation. Instead, it was decided not to make measurements at Reynolds numbers smaller than 0.8×10^6 .

4.3 Results and Discussions

4.3.1 Longitudinal Pressure Distribution

Pressure distributions along the surface on the airfoil model are presented in Figures (11) and (12). In these Figures, the surface static pressure is plotted in terms of a nondimensional pressure coefficient C_p defined as

$$C_p = 1 - \frac{P_\infty - p}{\frac{1}{2}\rho U_\infty^2} \quad (4.1)$$

The effect of Reynolds number for 0° and 2° angles of attack is illustrated in Figures (11) and (12). The measured pressure distribution has a maximum value of about -0.58 for C_p which agrees with the value of about -0.6 measured by

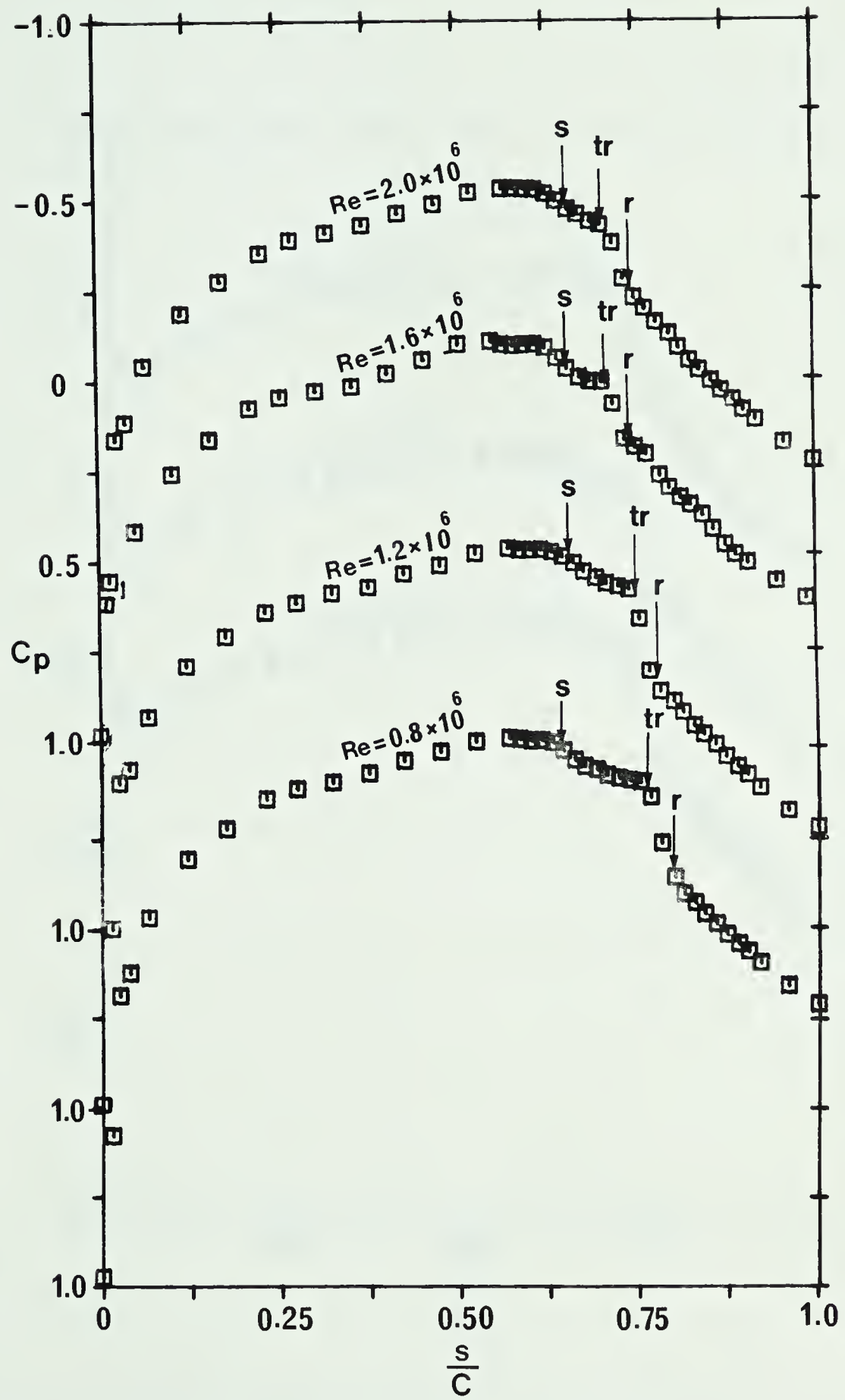


FIGURE 11--PRESSURE DISTRIBUTION, NACA 66₃-018, $\alpha = 0^\circ$

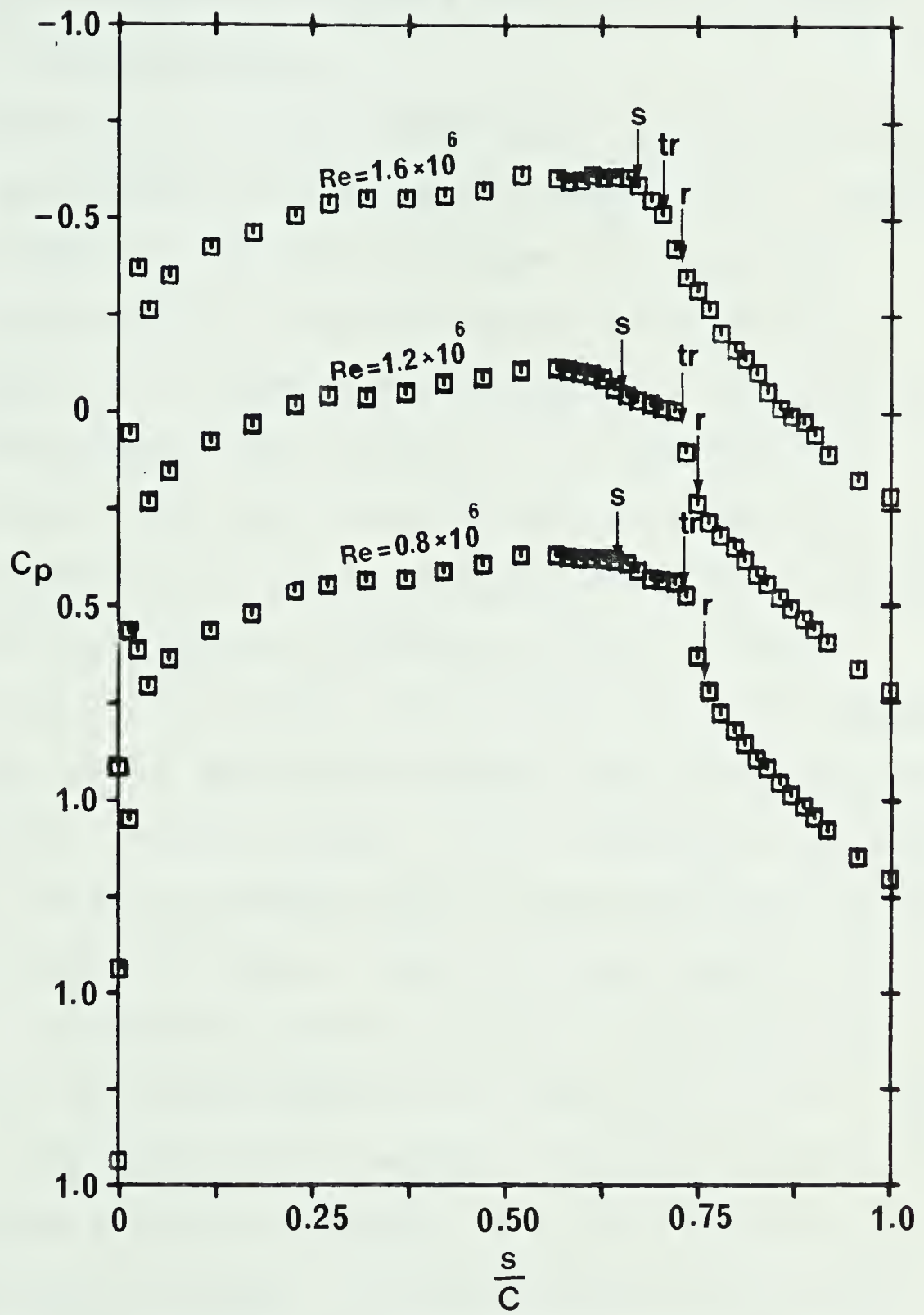


FIGURE 12--PRESSURE DISTRIBUTION, NACA 66₃-018, $\alpha = 2^\circ$

Gault [5]. This value disagrees with the value of about -0.8 obtained by Bursnall and Loftin [4]. However, the pressure distribution presented by Bursnall and Loftin was not corrected for tunnel blockage.

Figures (11) and (12) demonstrate the effects of the bubble on the surface static pressure distribution. Observation of the kinks in the data indicates that the static pressure increases by a relatively small amount in the laminar region of the bubble but increases very rapidly as the flow reattaches to the surface. It is apparent from Figures (11) and (12) that the extent of the separation region is reduced with increasing Reynolds number. A similar effect is observed with an increase in angle of attack. Careful observation of Figure (11) suggests that the pressure curve in the laminar part of the bubble tends to flatten out with decreasing Reynolds number. It is, therefore, possible to obtain a constant pressure step in the bubble with sufficiently low Reynolds number. This, perhaps, explains the observation of constant pressure region in the bubble by Gaster [8] in his measurements at low Reynolds numbers. This observation led Horton [9] to assume a constant pressure, and hence a constant external velocity, over the laminar part of the bubble in his analysis. Sufficient data are not available, however, to indicate at what Reynolds number the pressure in the laminar part of the bubble becomes constant.

4.3.2 Mean Velocity Profiles

Figures (13) to (19) show the mean velocity profiles in the boundary layer as measured by the hot film. The results are plotted in the transformed coordinates as u/U vs η . Some attention is necessary in interpreting this data as the hot film device is insensitive to flow direction. The hot film device treats the region close to the surface and the region away from the surface as a single viscous flow field. Then, the apparent mean velocity profiles as measured by a hot film present much more realistic flow phenomena as compared to those obtained from a pitot tube. The hot film measures higher mean flow magnitudes in the regions where the turbulence is high and the mean flow small.

An inspection of Figures (13) to (19) shows that the profiles have the characteristic laminar shape from the point of separation to the point of transition to turbulence. Because of the nature of the data obtained it is difficult to determine where exactly the flow reattaches to the surface. The shape of the mean velocity profiles in the immediate neighbourhood of transition is somewhat different from the characteristic laminar shape. A further inspection of Figures (13) to (19) indicates that the profiles after transition tend toward the characteristic shape of turbulent boundary layer profiles as the downstream stations are approached.

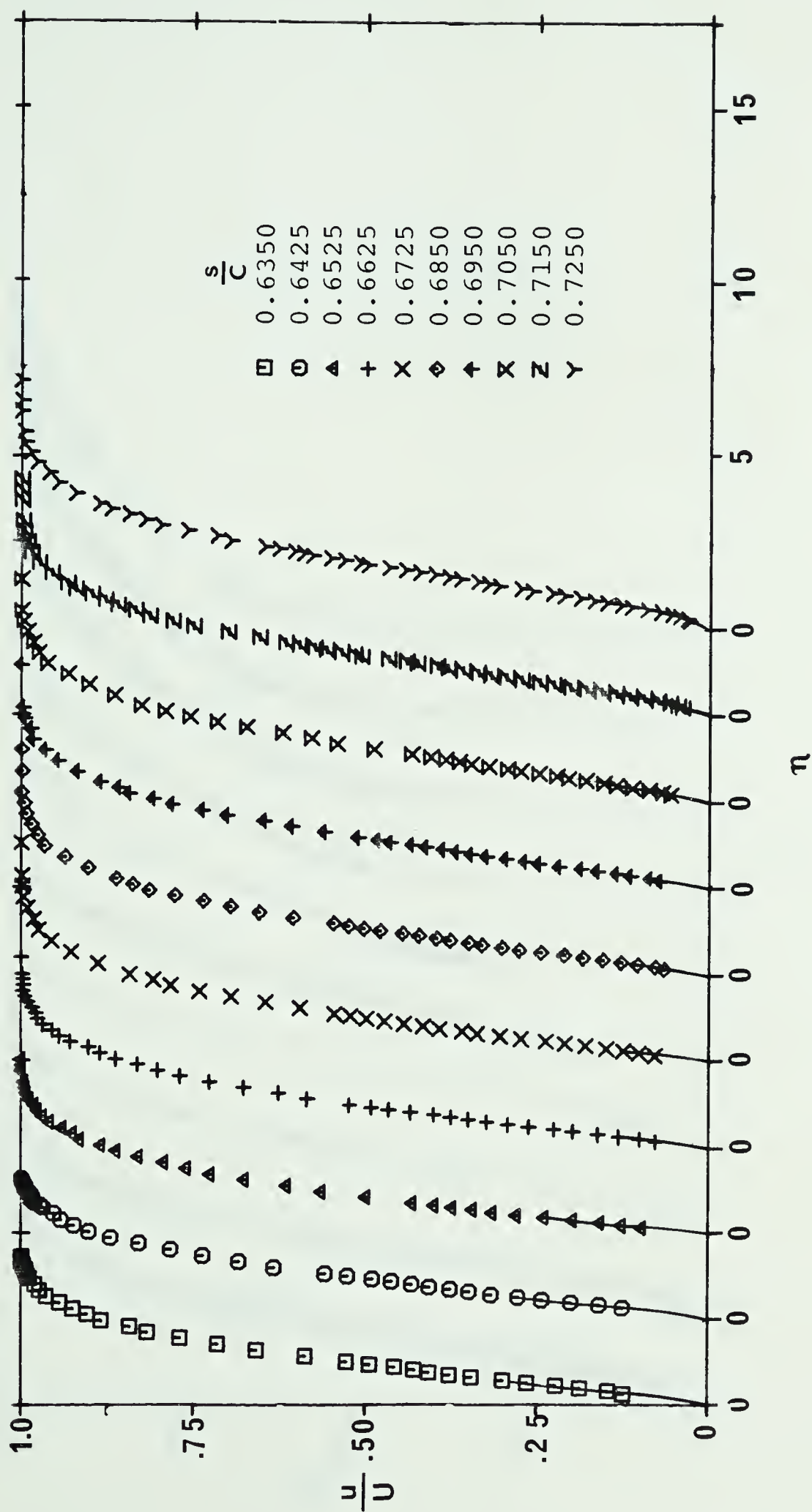


FIGURE 13--VELOCITY PROFILES, $Re = 0.8 \times 10^6$, $\alpha = 0^\circ$

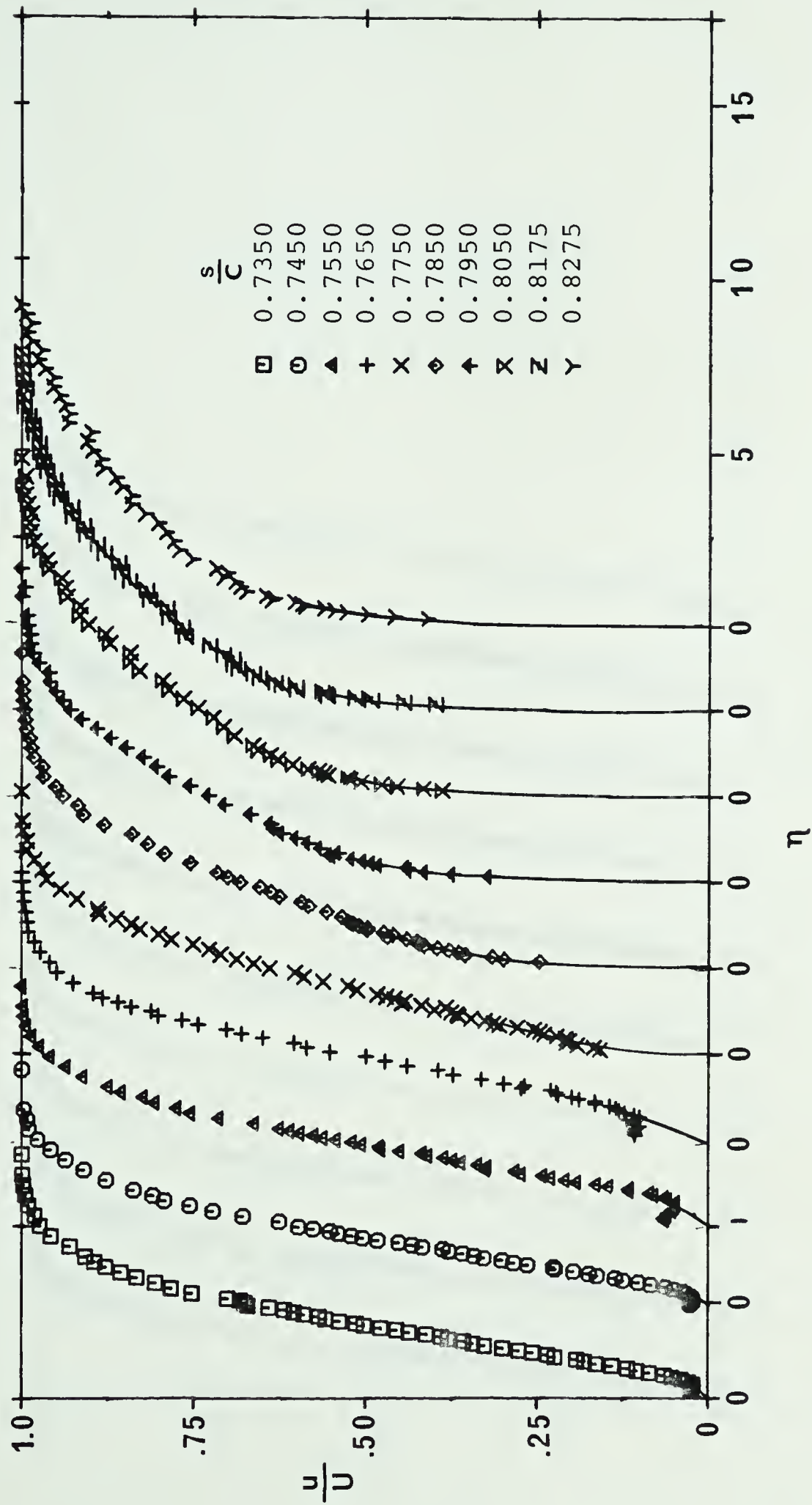


FIGURE 13--CONTINUED . . .

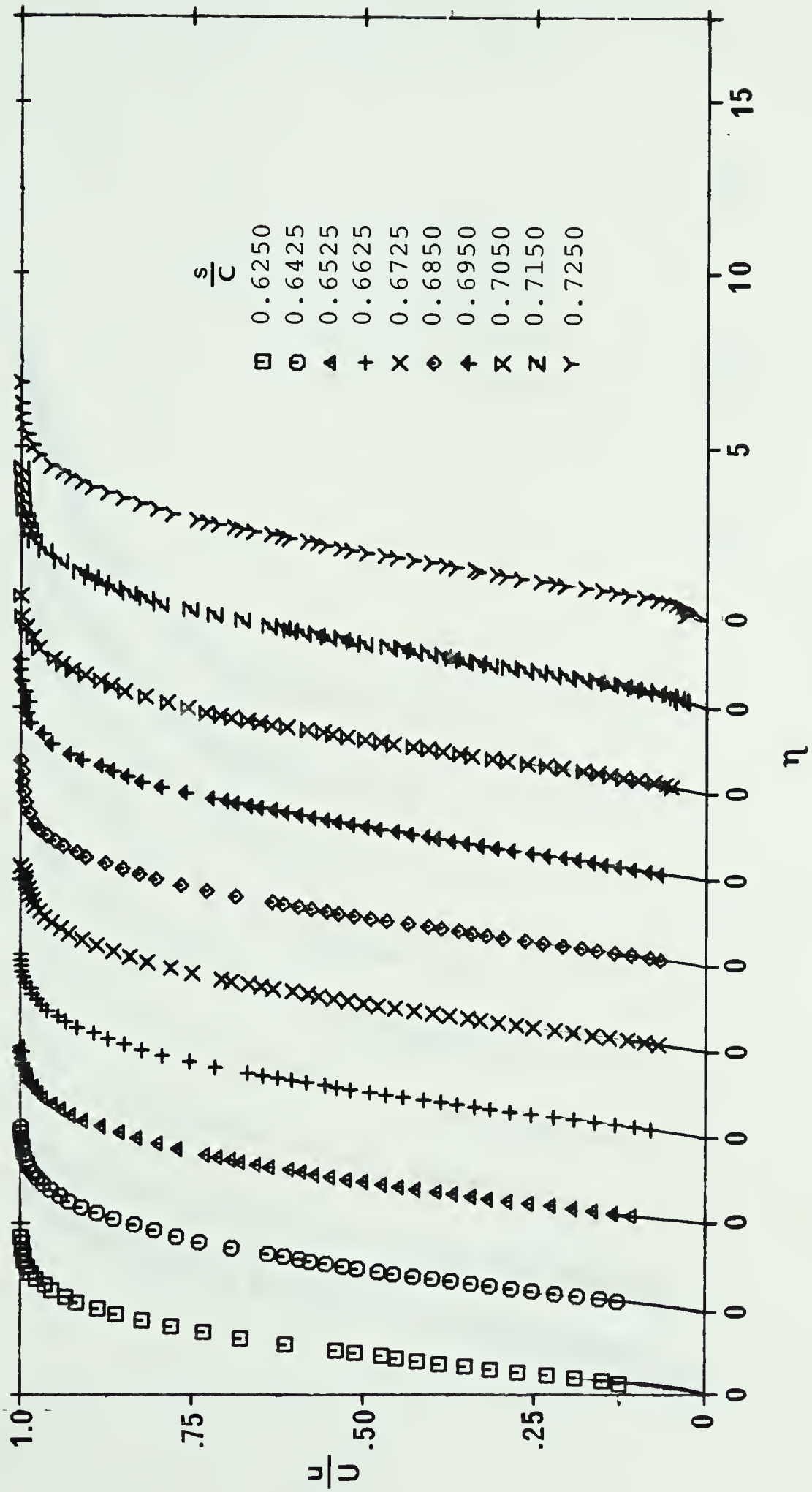


FIGURE 14--VELOCITY PROFILES, $Re = 0.8 \times 10^6$, $\alpha = 2^\circ$

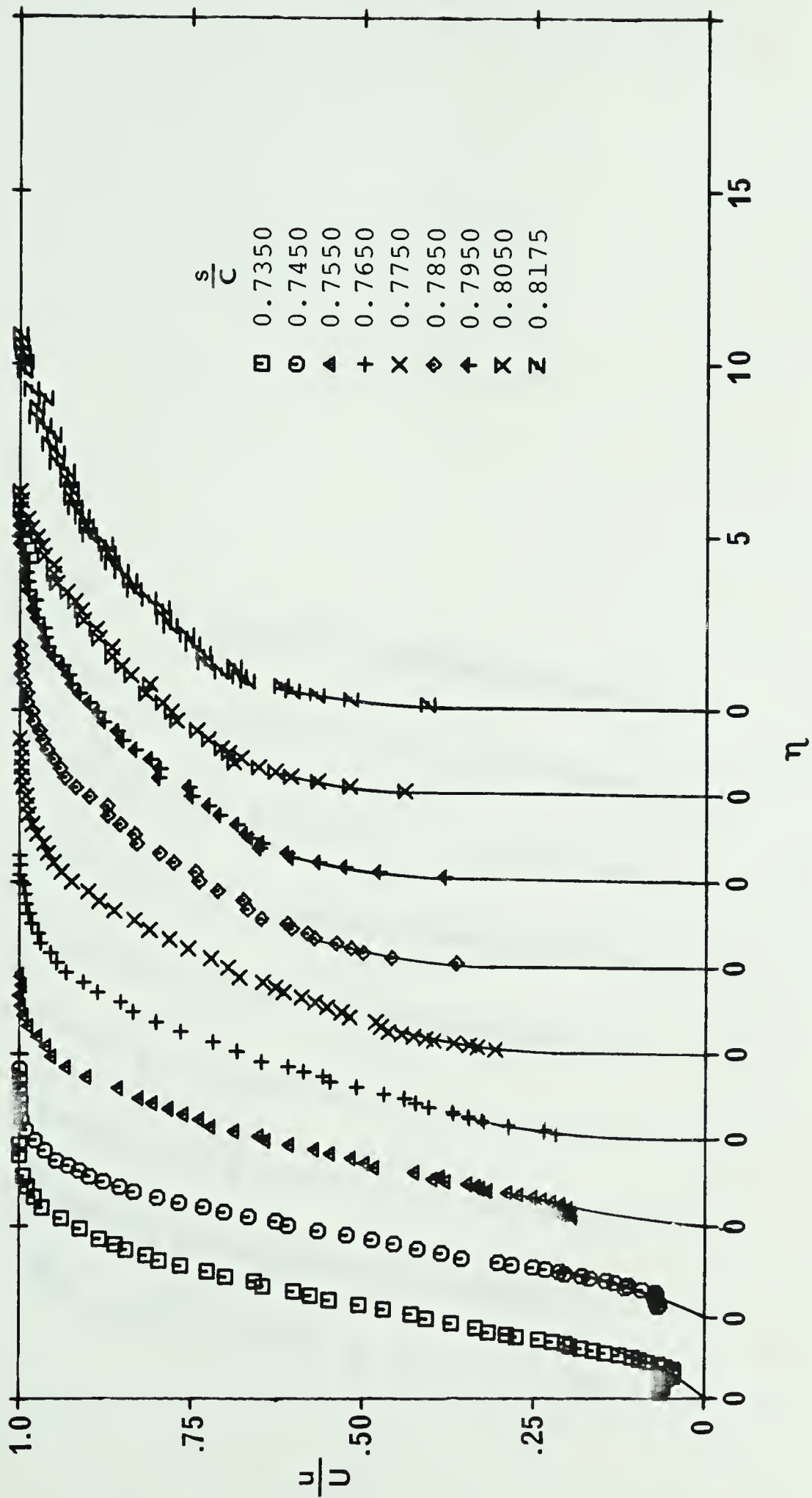


FIGURE 14--CONTINUED . . .

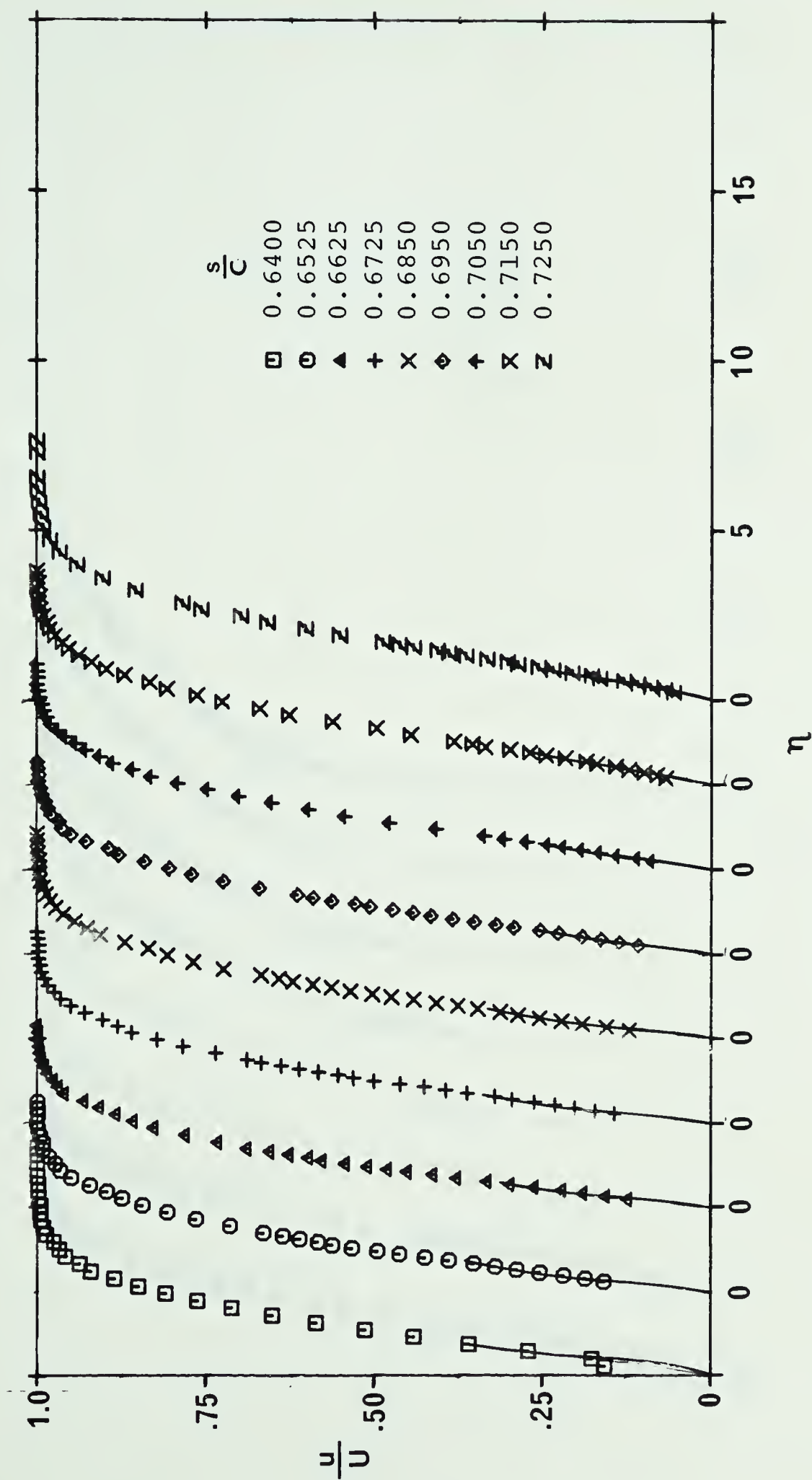


FIGURE 15--VELOCITY PROFILES, $\text{Re} = 1.2 \times 10^6$, $\alpha = 0^\circ$

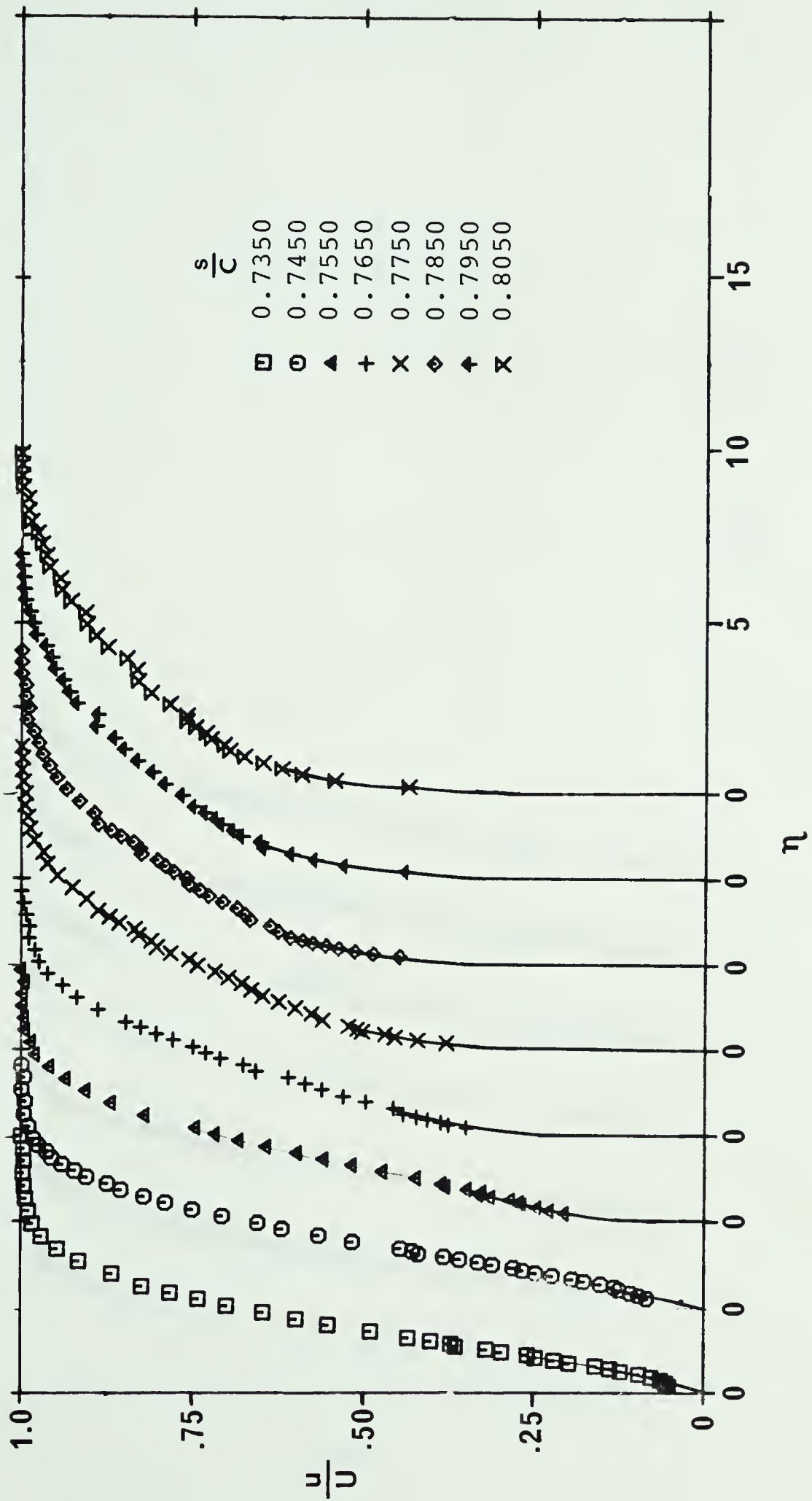


FIGURE 15--CONTINUED . . .

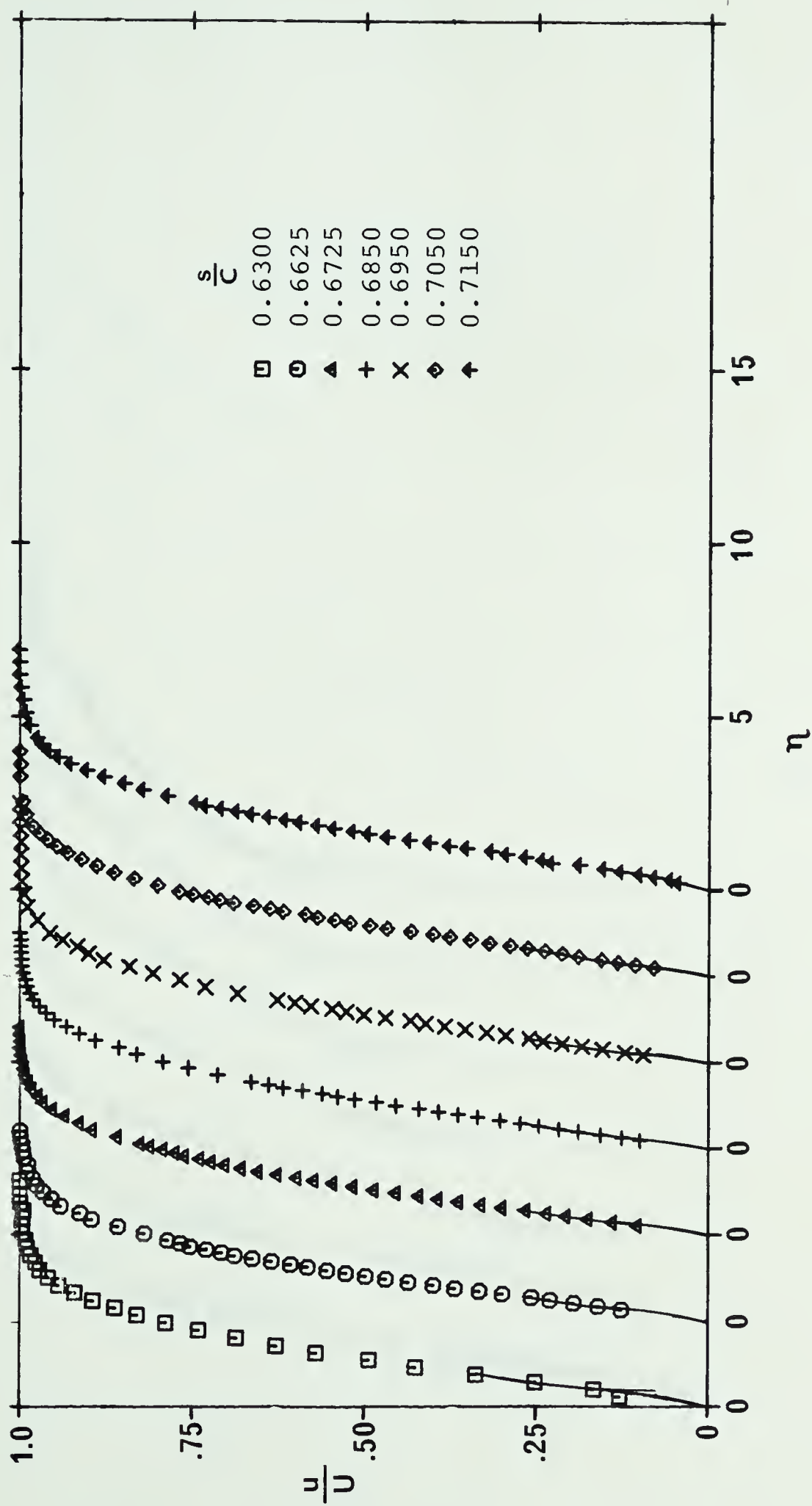


FIGURE 16--VELOCITY PROFILES, $Re = 1.2 \times 10^6$, $\alpha = 2^\circ$

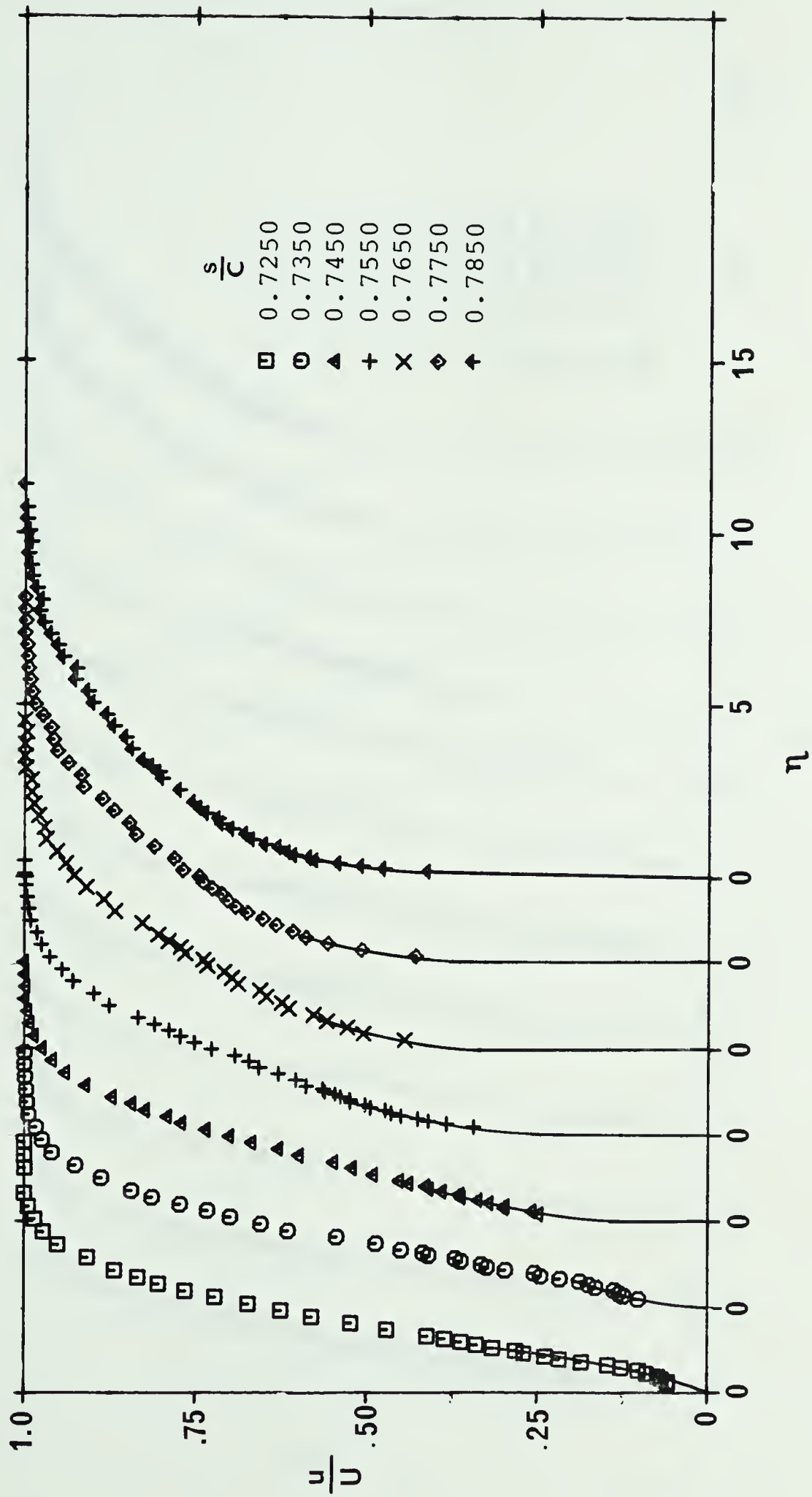


FIGURE 16--CONTINUED . . .

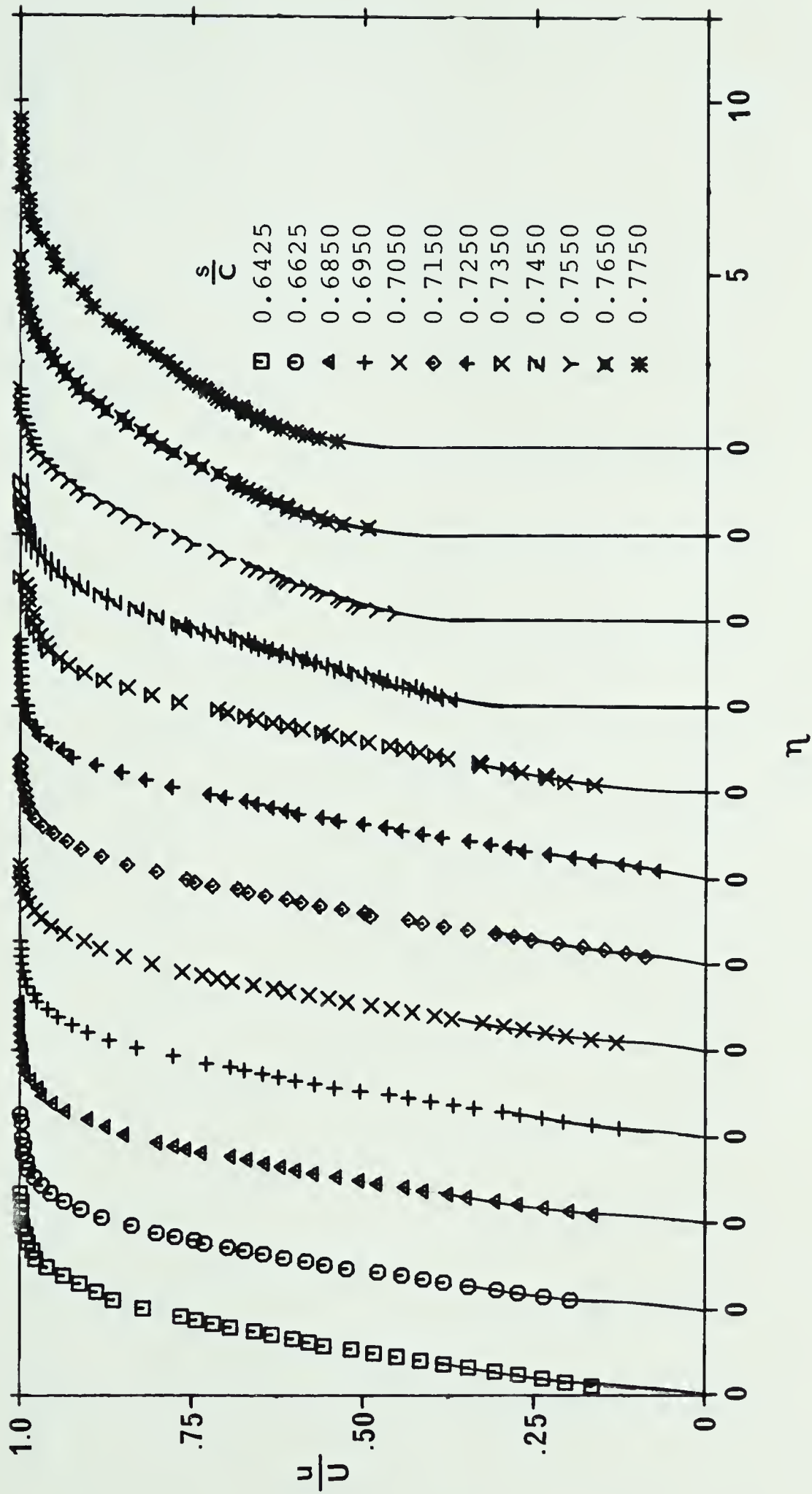


FIGURE 17--VELOCITY PROFILES, $\text{Re} = 1.6 \times 10^6$, $\alpha = 0^\circ$

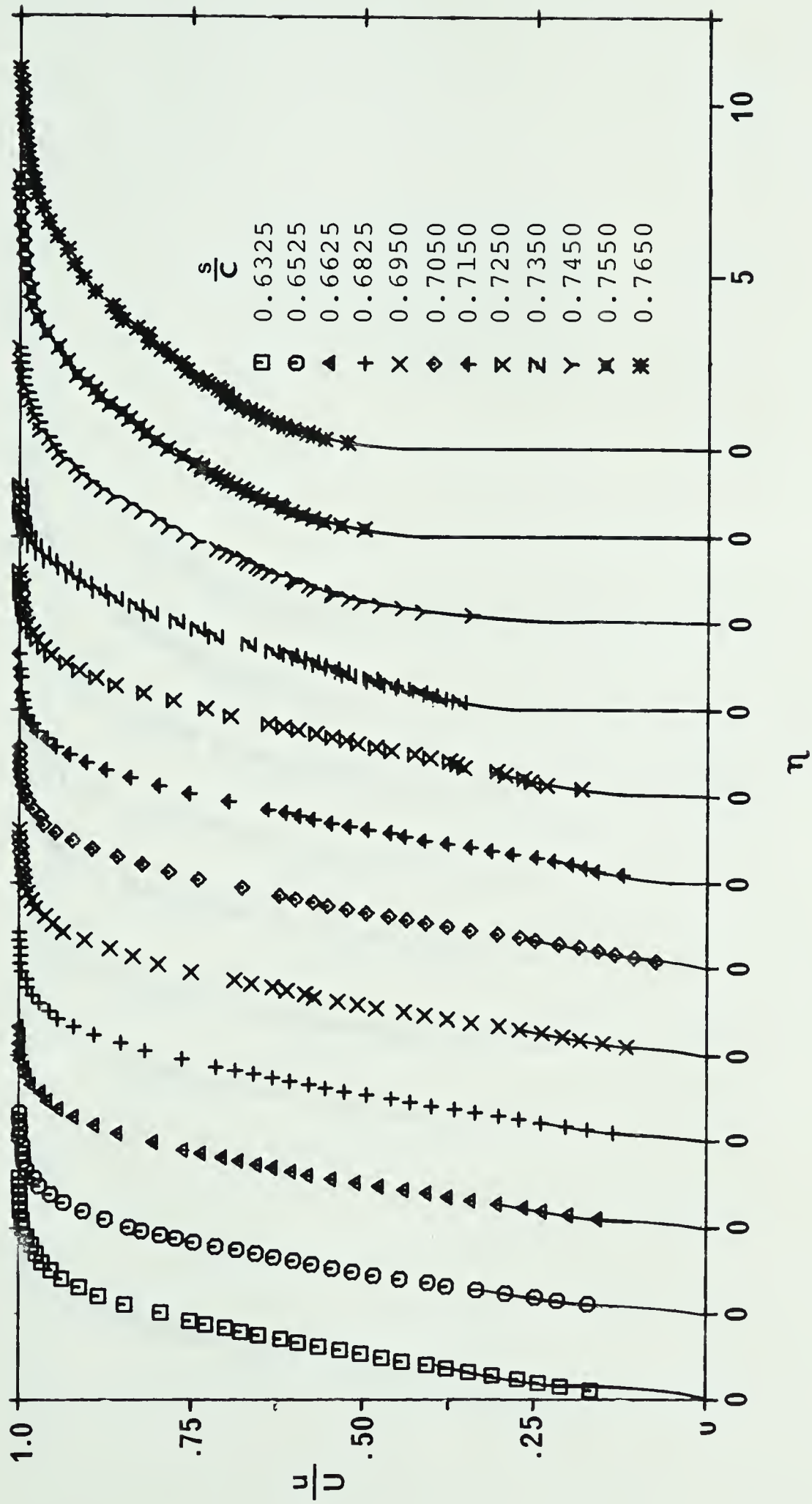


FIGURE 18--VELOCITY PROFILES, $Re = 1.6 \times 10^6$, $\alpha = 2^\circ$

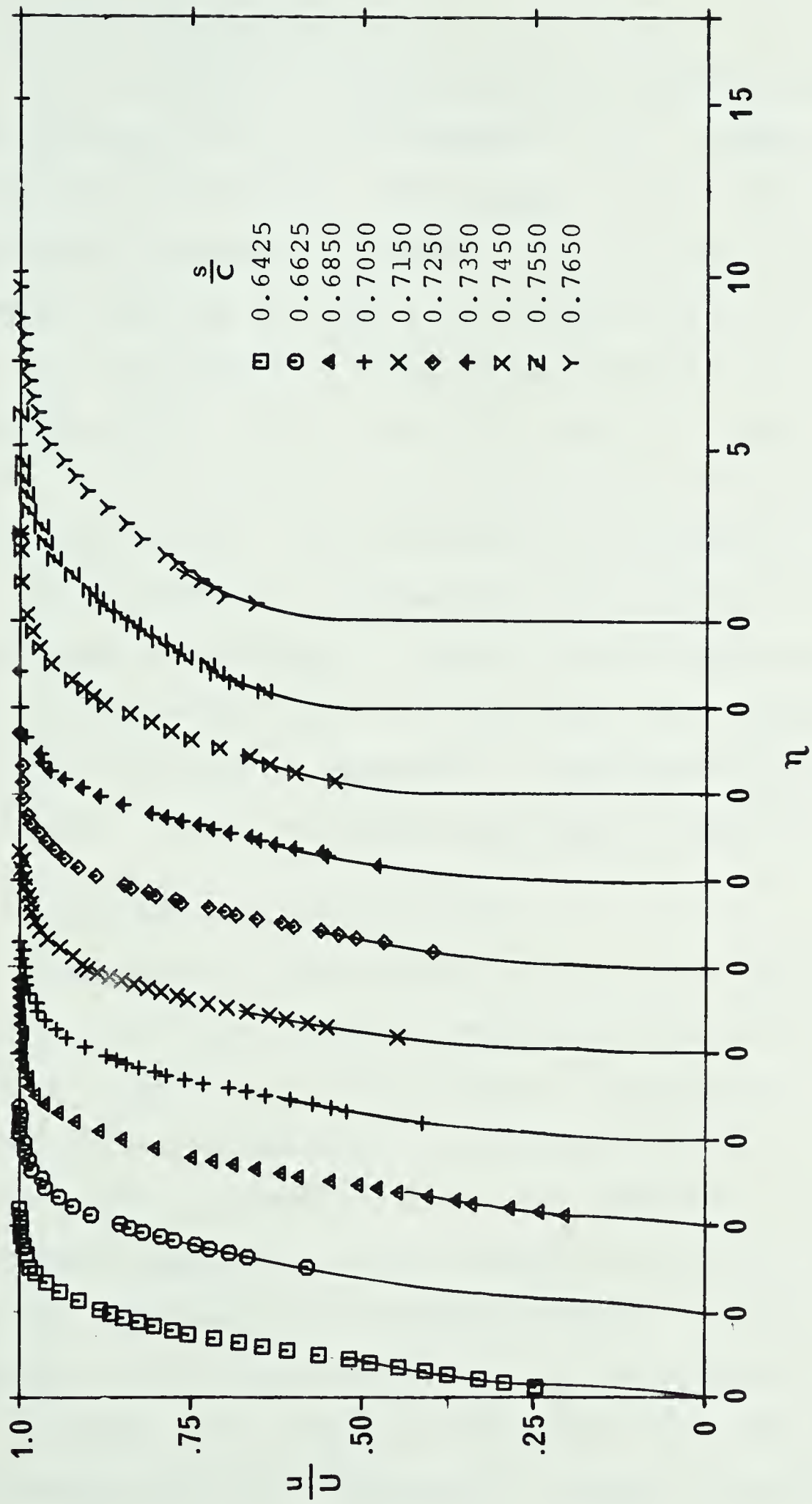


FIGURE 19--VELOCITY PROFILES, $Re = 2.0 \times 10^6$, $\alpha = 0^\circ$

4.3.3 Laminar Separation

The positions of laminar separation near midchord were determined from detailed boundary layer surveys and flow visualization experiments. The airfoil surface was lightly painted with a mixture of solvent and Kaolin and it was allowed to dry with the wind tunnel running at the desired speed. In the regions of higher skin friction the solvent evaporated quickly leaving the white deposit of Kaolin on the surface. In the region of the separated flow the surface coating remained wet. Skin friction in the laminar boundary layer near separation is approaching zero causing the evaporation process to slow down. Liquid on the surface is pushed toward the separation point and then drops down vertically indicating the point of separation. Experimentally determined positions for laminar separation are given in Table II.

4.3.4 Transition to Turbulent Flow

Experimentally determined positions of transition corresponding to each Reynolds number and angle of attack are presented in Table II. The positions of transition to fully turbulent flow were obtained from the observations of velocity fluctuations as indicated by a hot film anemometer, and these results were augmented with the pressure distribution determinations. The positions of abrupt pressure increase, shown in Figures (11) and (12), correspond to the positions at which transition from laminar to turbulent flow was completed. Oscilloscope traces were observed at a number of horizontal

TABLE II

POSITIONS FOR LAMINAR SEPARATION, TRANSITION, REATTACHMENT AND EQUILIBRIUM FLOW

Re	α°	Separation Point		Transition Point s/C	Reattachment Point s/C	Equilibrium Point s/C
		Theory	Experiment			
0.8×10^6	0°	0.64 - 0.65	0.635	0.7550	0.7800	0.8275
	2°	0.63 - 0.64	0.6250	0.7400	0.7600	0.8100
1.2×10^6	0°	0.65 - 0.66	0.6400	0.7400	0.7600	0.8050
	2°	0.635 - 0.65	0.6300	0.7325	0.7475	0.7850
1.6×10^6	0°	0.65 - 0.66	0.6425	0.7200	0.7500	0.7750
	2°	0.64 - 0.65	0.6300	0.7075	0.7375	0.7600
2.0×10^6	0°	0.65 - 0.665	0.6425	0.6950	0.7350	0.7550

and vertical positions in the separation bubble. The separated shear layer was considered to be completely turbulent at the position corresponding to the first observation of continuous random fluctuations.

An inspection of Table II indicates that the distance between the separation point and the transition point decreases as the Reynolds number increases. It is also observed that this distance decreases with increasing angles of attack.

4.3.5 Structure of the Separated Flow Field

Mean velocities measured by the hot film are shown in Figures (20) to (26), plotted as contours of constant velocity over the separated region. These velocity contours describe the composite physical structure of the separated flow field. The initial portion of the bubble is composed of the laminar shear layer detached from the surface at separation point. It is seen clearly from the Figures that the stream lines are moved away from the surface in the laminar part of the bubble. After separation the shear layer spreads slowly and almost at a constant rate. This may be because the shear stresses are all viscous and therefore small. The expanding shear layer is much less stable than an attached boundary layer and so transition will be triggered in this layer at some downstream position. Comparison of measured positions of transition with the positions of peaks in the velocity contours indicates that the flow begins to return to the surface close to the position corresponding to

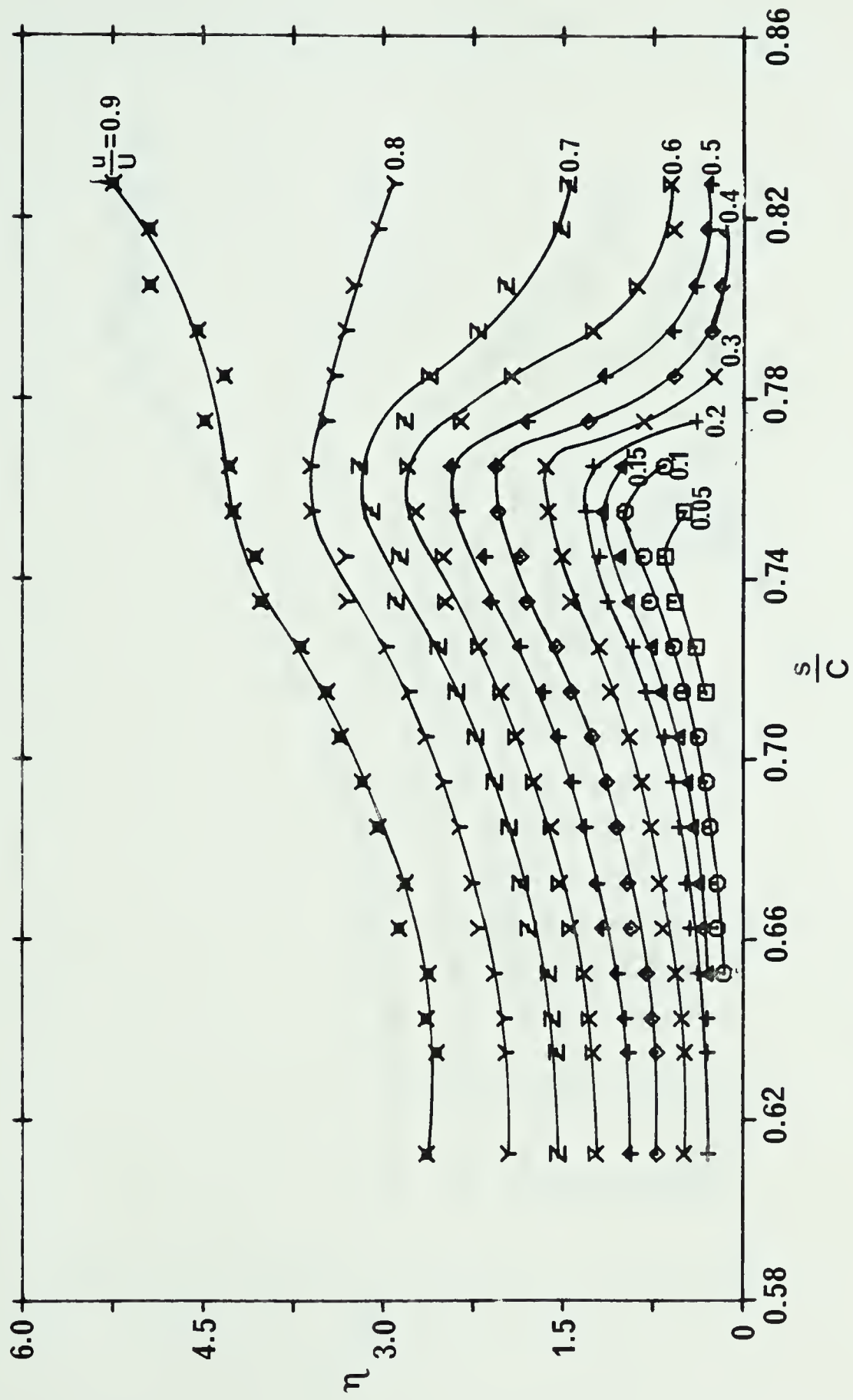


FIGURE 20---VELOCITY CONTOURS, $Re = 0.8 \times 10^6$, $\alpha = 0^\circ$

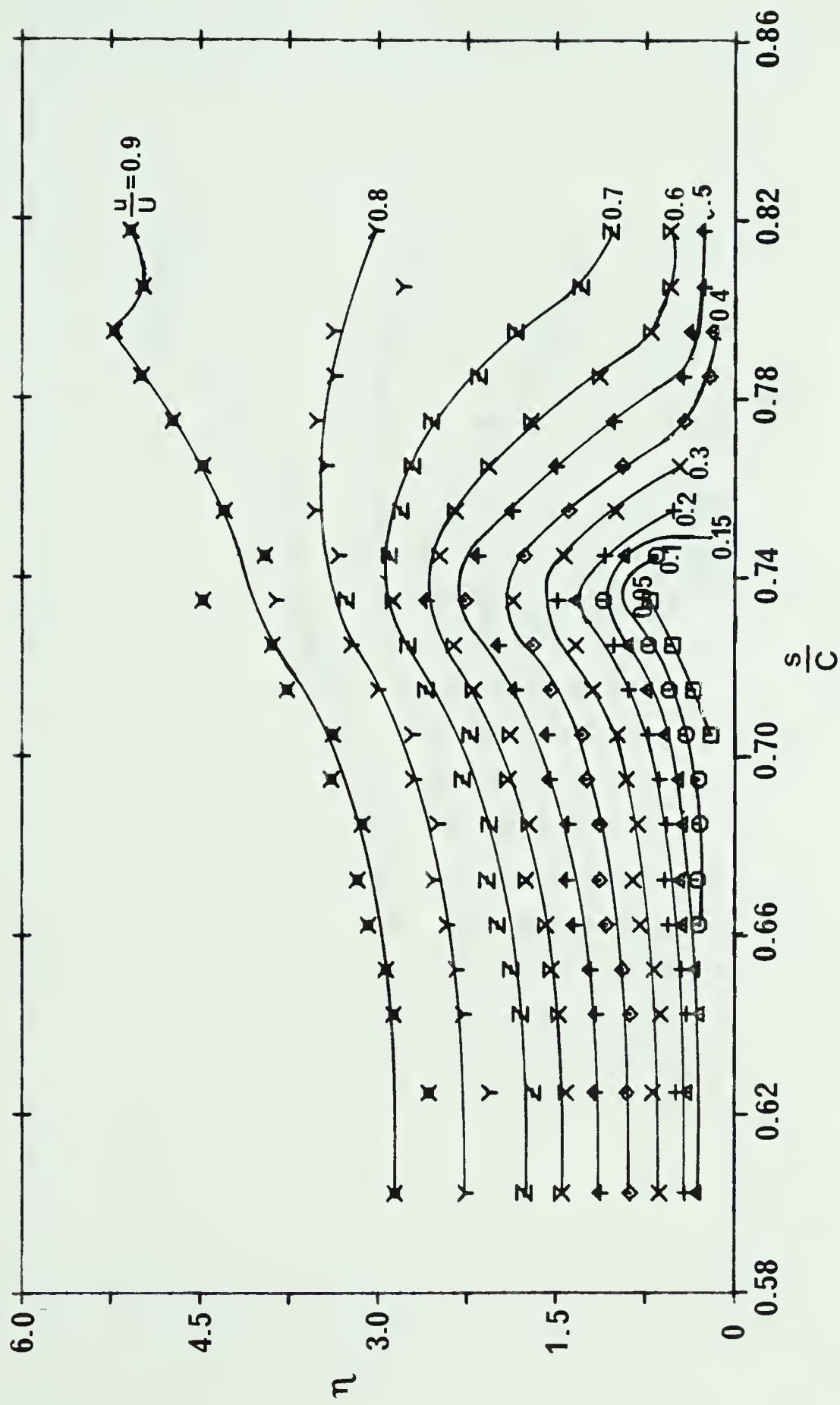


FIGURE 21--VELOCITY CONTOURS, $Re = 0.8 \times 10^6$, $\alpha = 2^\circ$

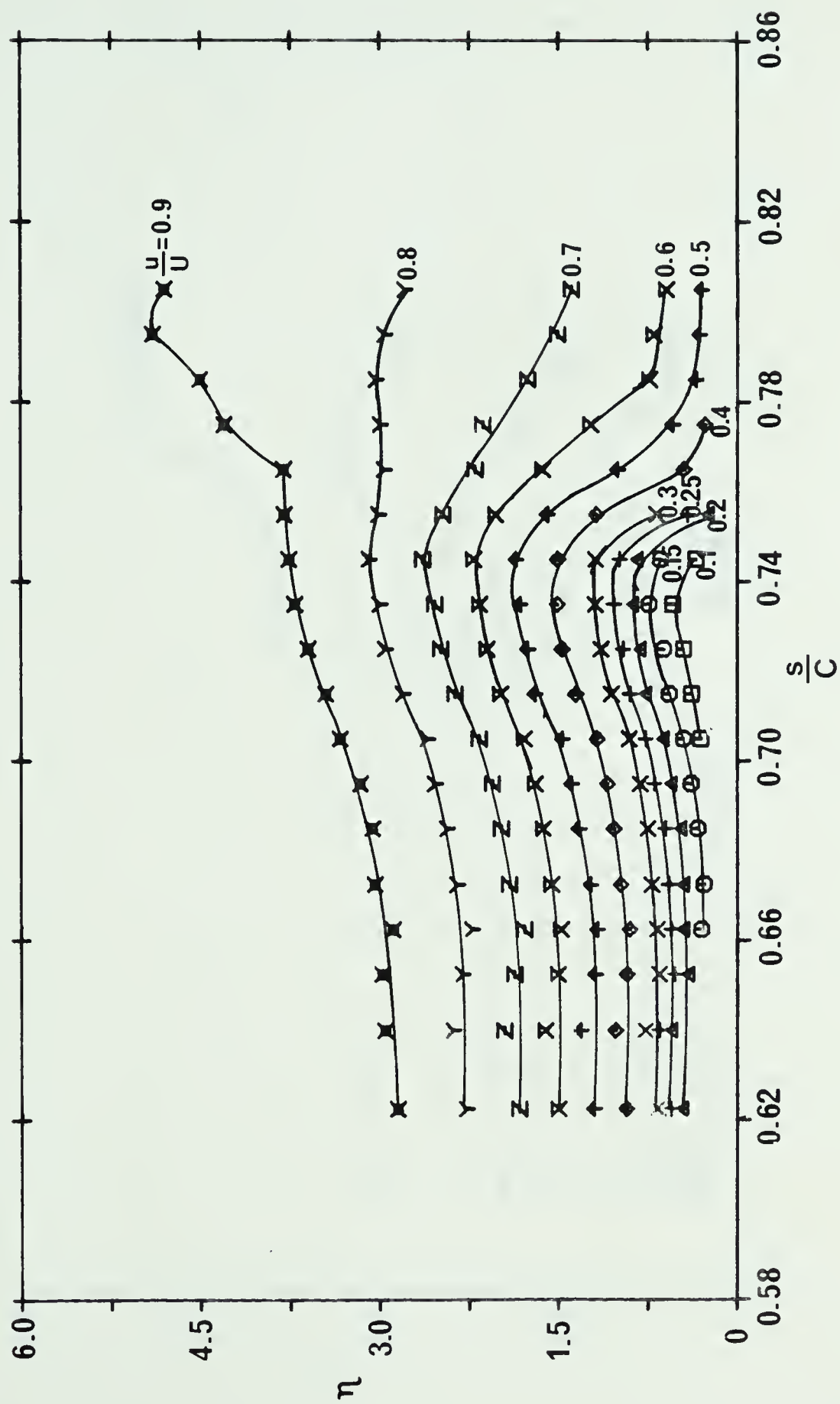


FIGURE 22--VELOCITY CONTOURS, $Re = 1.2 \times 10^6$, $\alpha = 0^\circ$

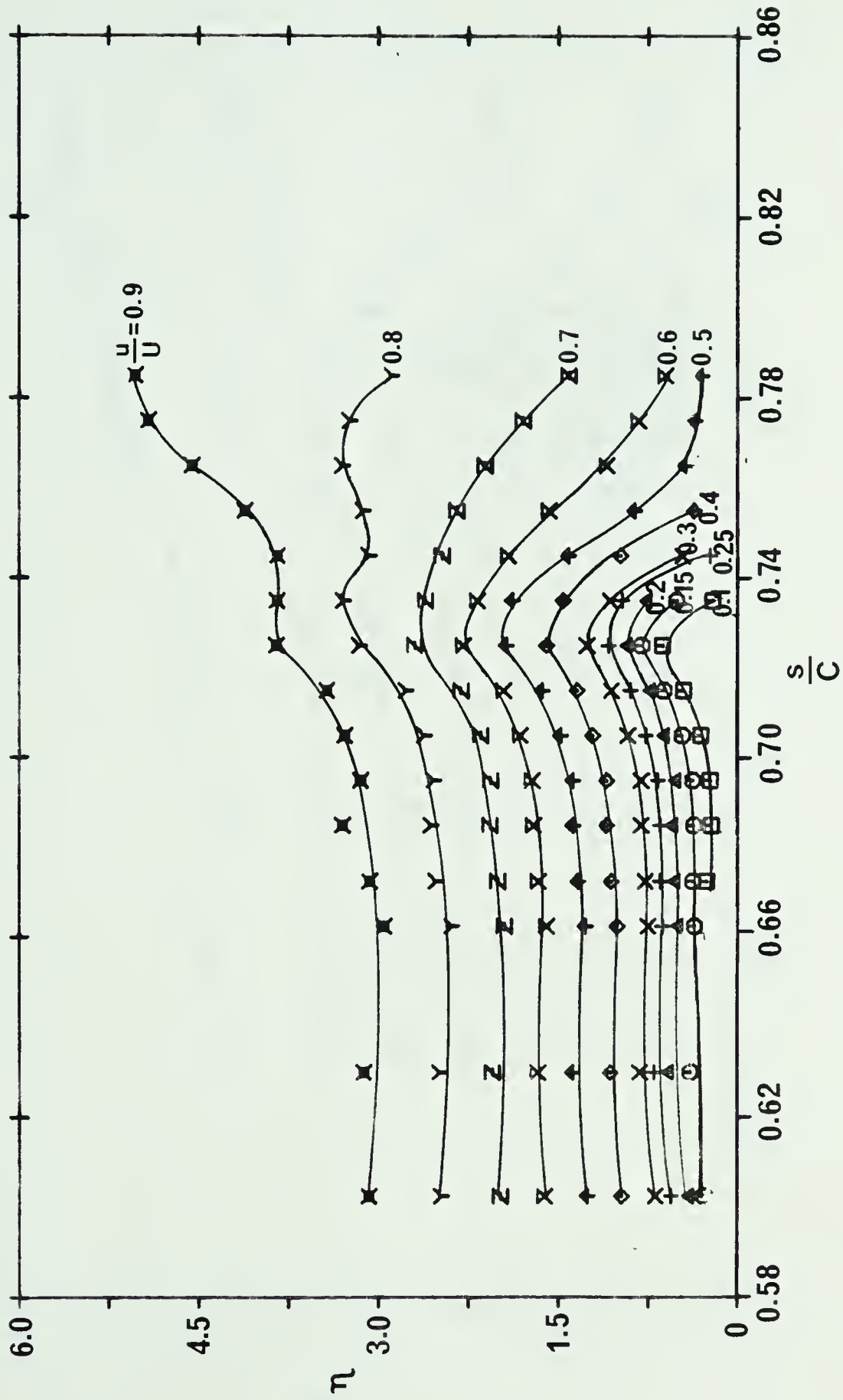


FIGURE 23---VELOCITY CONTOURS, $Re = 1.2 \times 10^6$, $\alpha = 2^\circ$

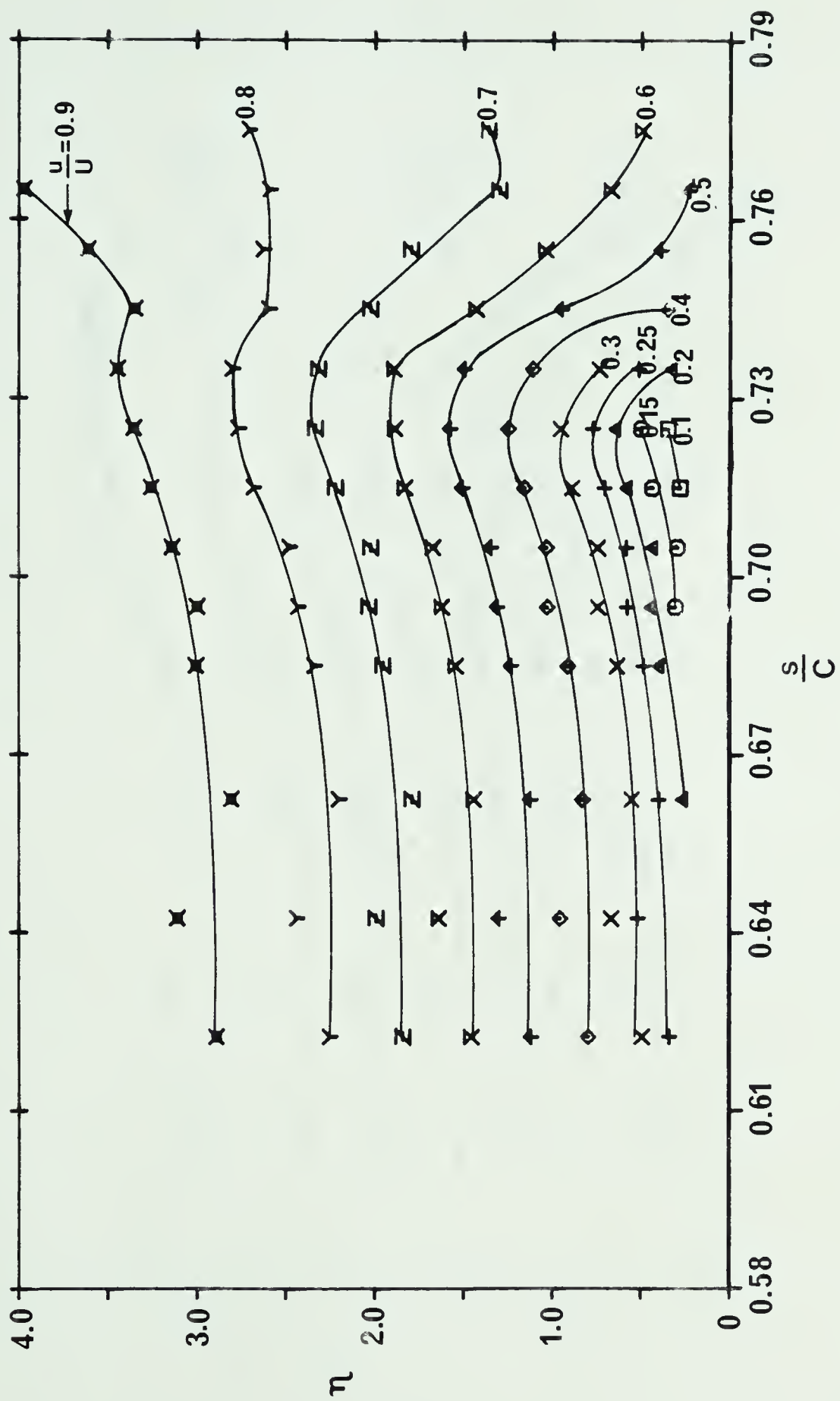


FIGURE 24--VELOCITY CONTOURS, $Re = 1.6 \times 10^6$, $\alpha = 0^\circ$

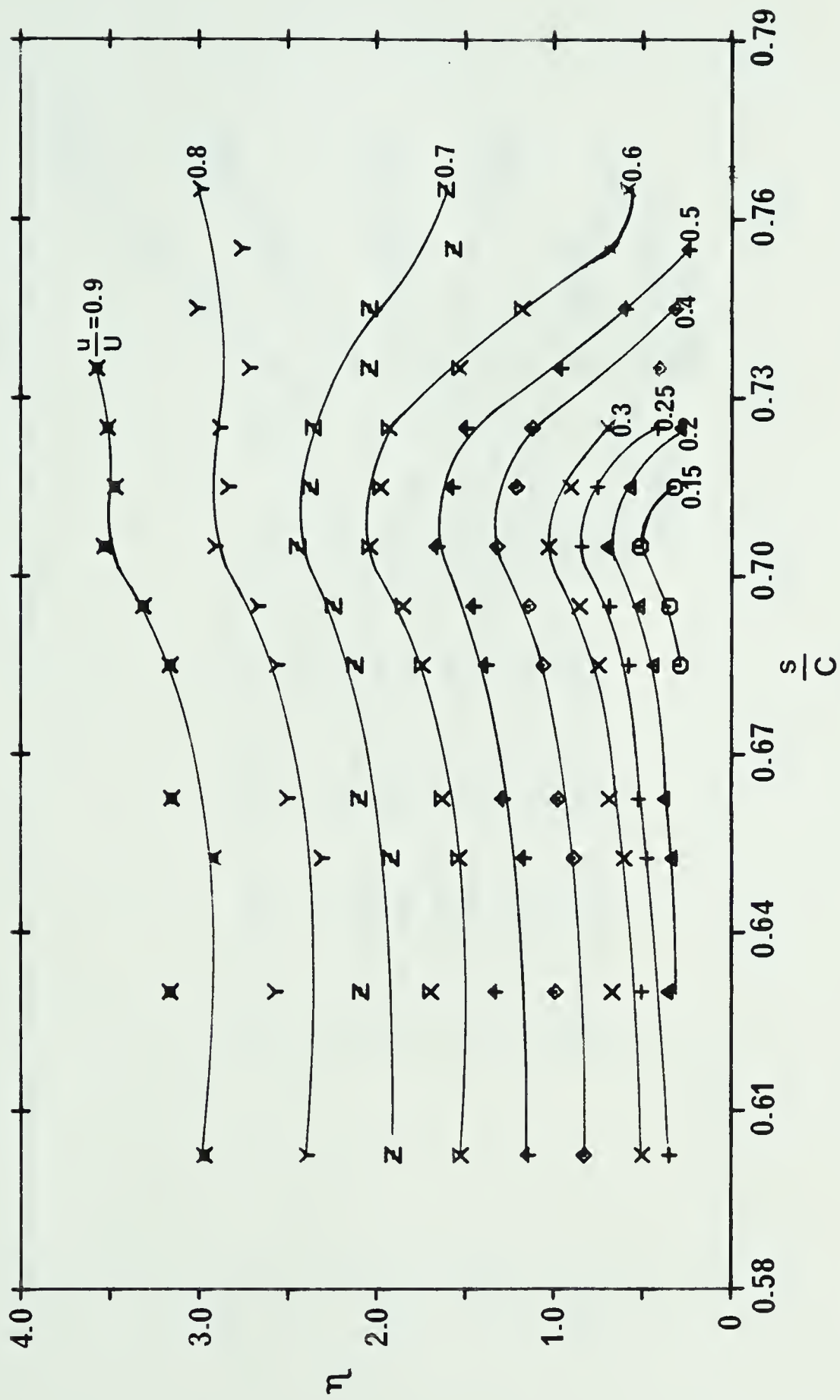


FIGURE 25--VELOCITY CONTOURS, $Re = 1.6 \times 10^6$, $\alpha = 2^\circ$

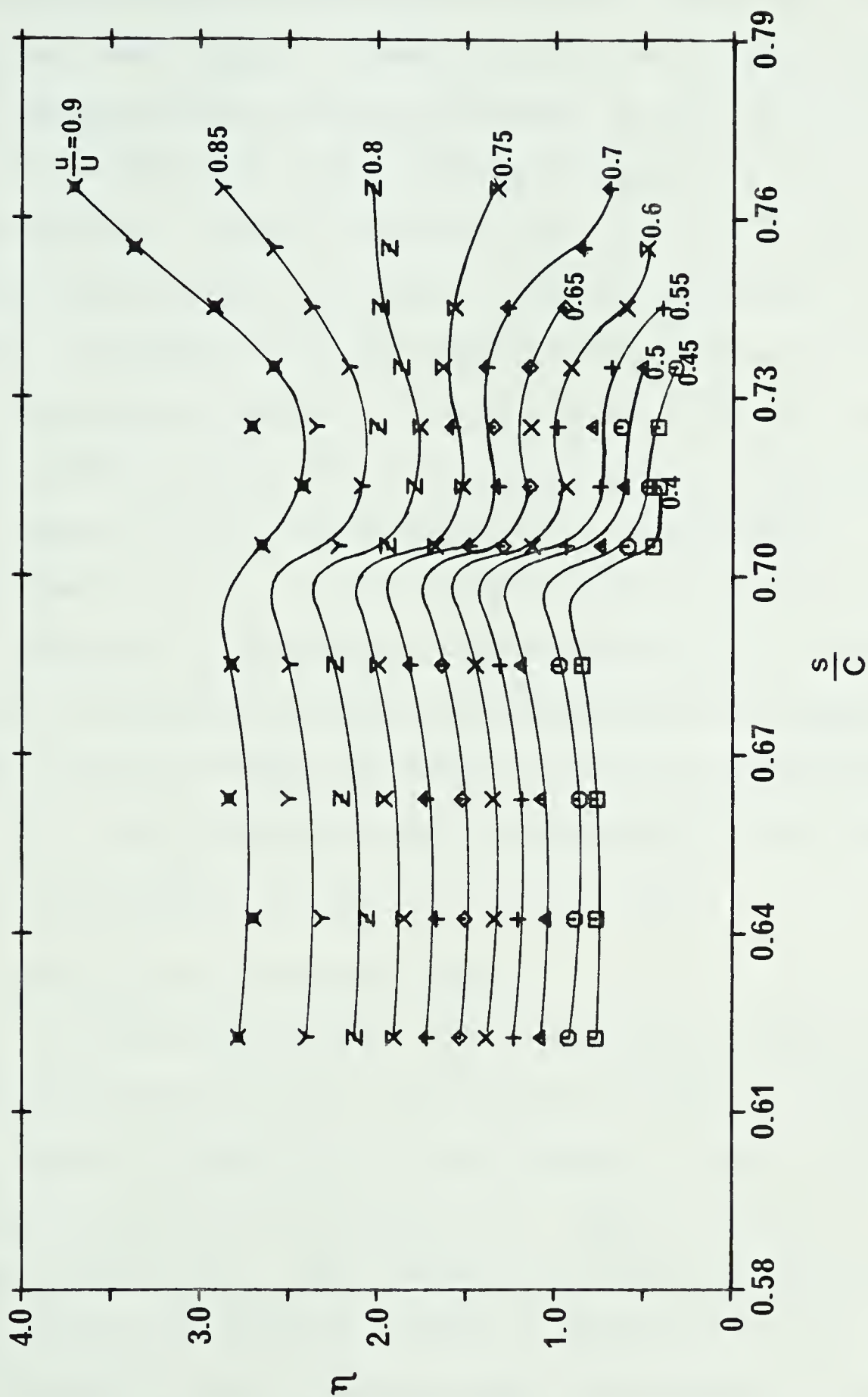


FIGURE 26--VELOCITY CONTOURS, $Re = 2.0 \times 10^6$, $\alpha = 0^\circ$

the first observation of fully developed turbulence in the separated shear layer. In other words the separated shear layer becomes fully turbulent at about the position of the peak in the velocity contours where the flow starts to return to the surface. After transition the resulting turbulence spreads and entrains the flow so that it reattaches to the surface. Although it is not apparent from Figures (20) to (26) it has been observed that the separated region consists of relatively stagnant flow just downstream of separation with a more vigorous vortex motion near reattachment. Near reattachment the flow varies rapidly and eventually becomes fully turbulent at subsequent downstream stations. Experimentally determined positions of reattachment corresponding to each Reynolds number and angle of attack are presented in Table II. These positions were determined both from the velocity contours and pressure distributions.

4.3.6 Redeveloping Boundary Layer

A prime objective of this investigation was to learn the characteristics of the redeveloping turbulent boundary layer behind the position of reattachment. The velocity profiles downstream of reattachment appear to settle down to some steady form. This behavior can best be predicted by viewing the redevelopment process as analogous to the redevelopment of the turbulent shear flow behind a leading edge obstacle. Rai [23] conducted an experimental investigation of two-dimensional turbulent "wall wake" formed behind

an obstacle. The flow separates at the exposed edge of the obstacle and reattaches downstream. The reattached shear flow redevelops toward ordinary boundary layer type flow. Rai found the existence of similarity of flow pattern in this boundary layer type flow region called "far wake region." Such a behavior is, therefore, to be expected in the present flow. It is shown here that the turbulent boundary layer tends to settle down to a nearly "equilibrium" state at some position downstream of flow reattachment. This position on the airfoil surface is referred to as the "equilibrium point."

Equilibrium boundary layers constitute a class of boundary layers in which the mainstream velocity distribution is characterized by a constant value of the parameter

$$\Phi = \frac{\delta^*}{\tau_w} \frac{dp}{ds} \quad (4.2)$$

which represents the ratio of pressure forces to shear forces in a section of the boundary layer. The parameter Φ is referred to as Clauser's equilibrium parameter. The gross properties of the boundary layer in equilibrium or self-preserving flows can be scaled with a single parameter. This implies that the velocity profiles exhibit self-similarity in these flows.

It is necessary to find the wall friction τ_w in the correlation of turbulent velocity profiles in the redeveloping

region. τ_w in this region was determined from the mean velocity profiles following the method suggested by Clauser [24], for smooth walls. There is a region outside the laminar sublayer in which the velocity distribution can be represented by the well known log law,

$$\frac{u}{u_*} = 5.6 \log_{10} \left(\frac{u_* y}{\nu} \right) + 4.9 \quad (4.3)$$

even when pressure gradients are present. This law can be rewritten in terms of the surface skin friction coefficient C_f as given below

$$\frac{u}{U} = \sqrt{C_f/2} \left[5.6 \log_{10} \left(\frac{Uy}{\nu} \sqrt{C_f/2} \right) + 4.9 \right] \quad (4.4)$$

This equation can be plotted as a universal family with C_f as a parameter as shown in Figures (27) to (30). In these figures $\frac{u}{U}$ is plotted against Ry on a semilogarithmic graph. Experimental points taken near the wall are plotted on these graphs. Skin friction coefficient C_f is determined by selecting the appropriate member of the family which fits the experimental points. The full line represents the appropriate member of the family given by Equation (4.4). It appears that the Equation (4.4) fits the experimental data quite well. It is evident from Figures (27) through (30) that the value of C_f increases as the downstream stations are approached and converge to nearly the same value.

Figures (31) to (34) show the velocity defect

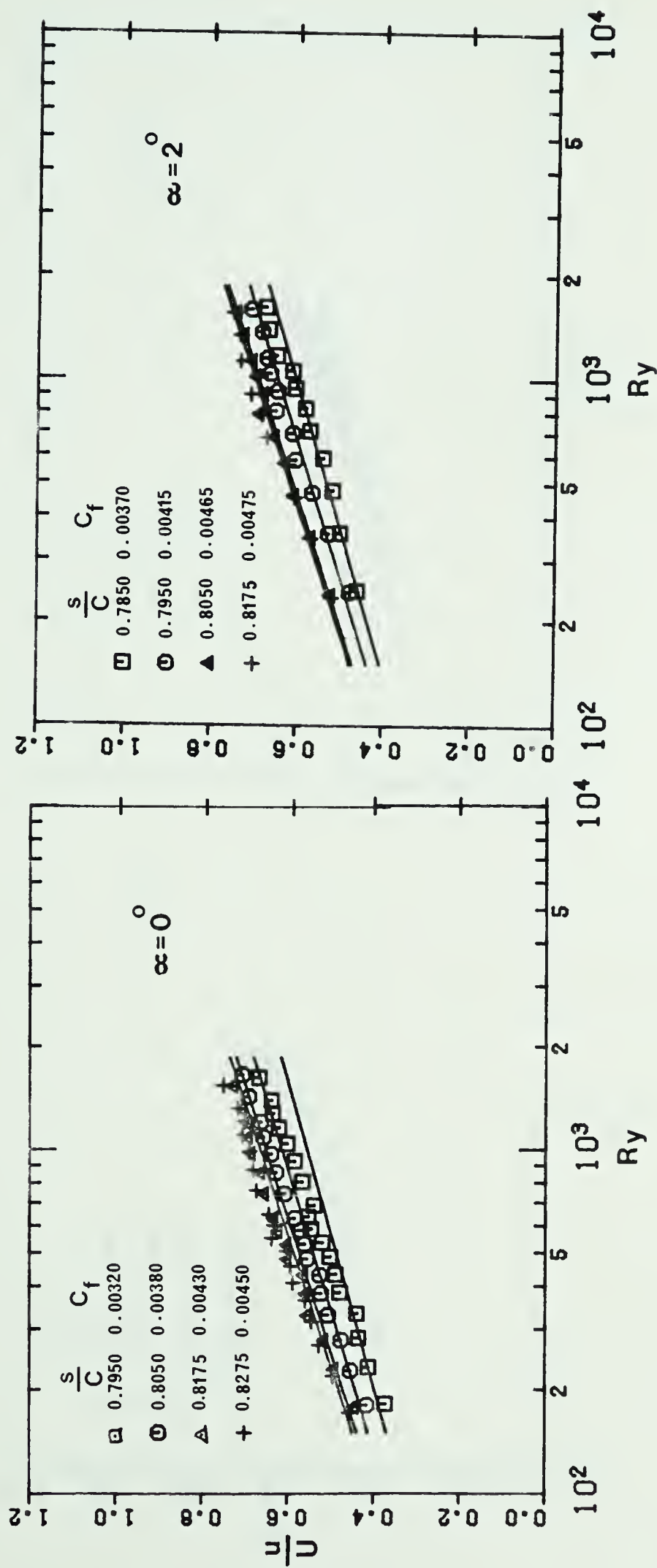


FIGURE 27--CLAUSER CHART FOR EXPERIMENTAL DETERMINATION OF TURBULENT SKIN-FRICTION COEFFICIENT, $Re = 0.8 \times 10^6$

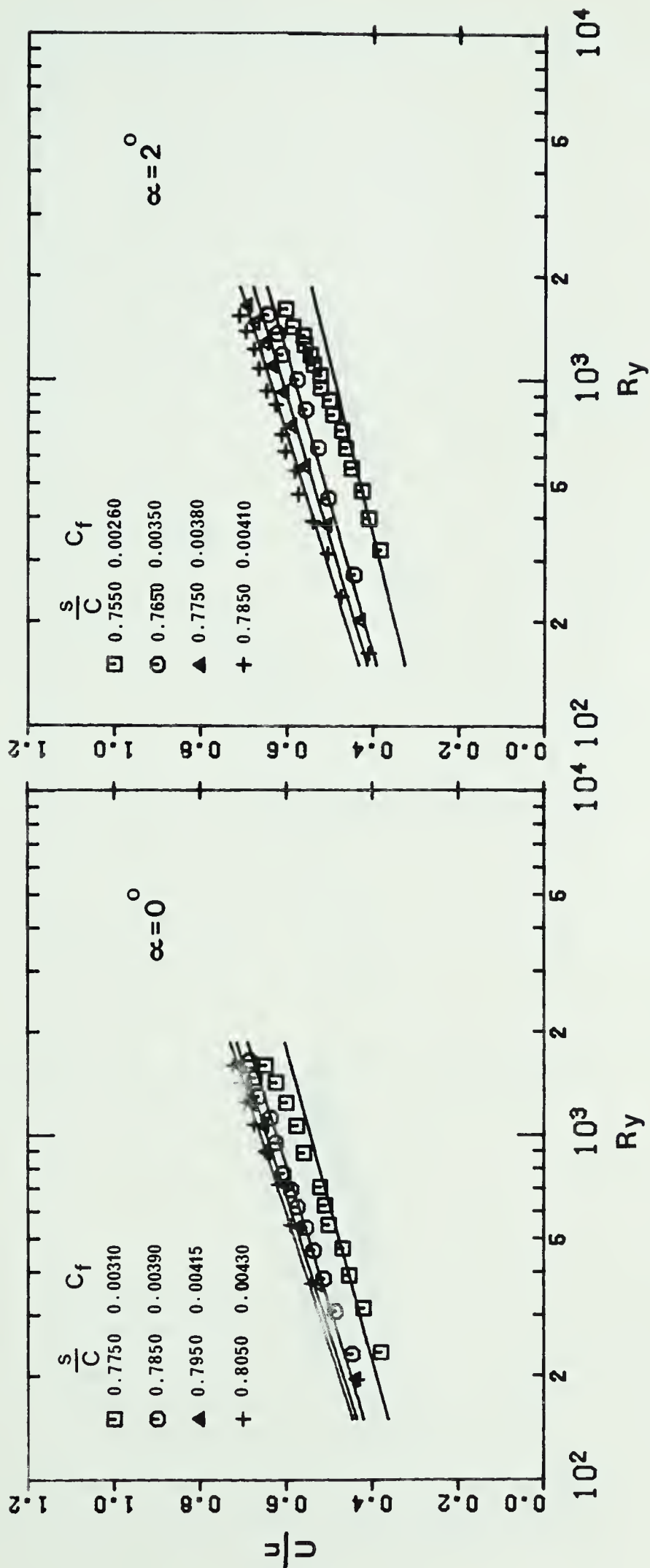


FIGURE 28--CLAUSER CHART FOR EXPERIMENTAL DETERMINATION OF TURBULENT SKIN-FRICTION COEFFICIENT, $Re = 1.2 \times 10^6$

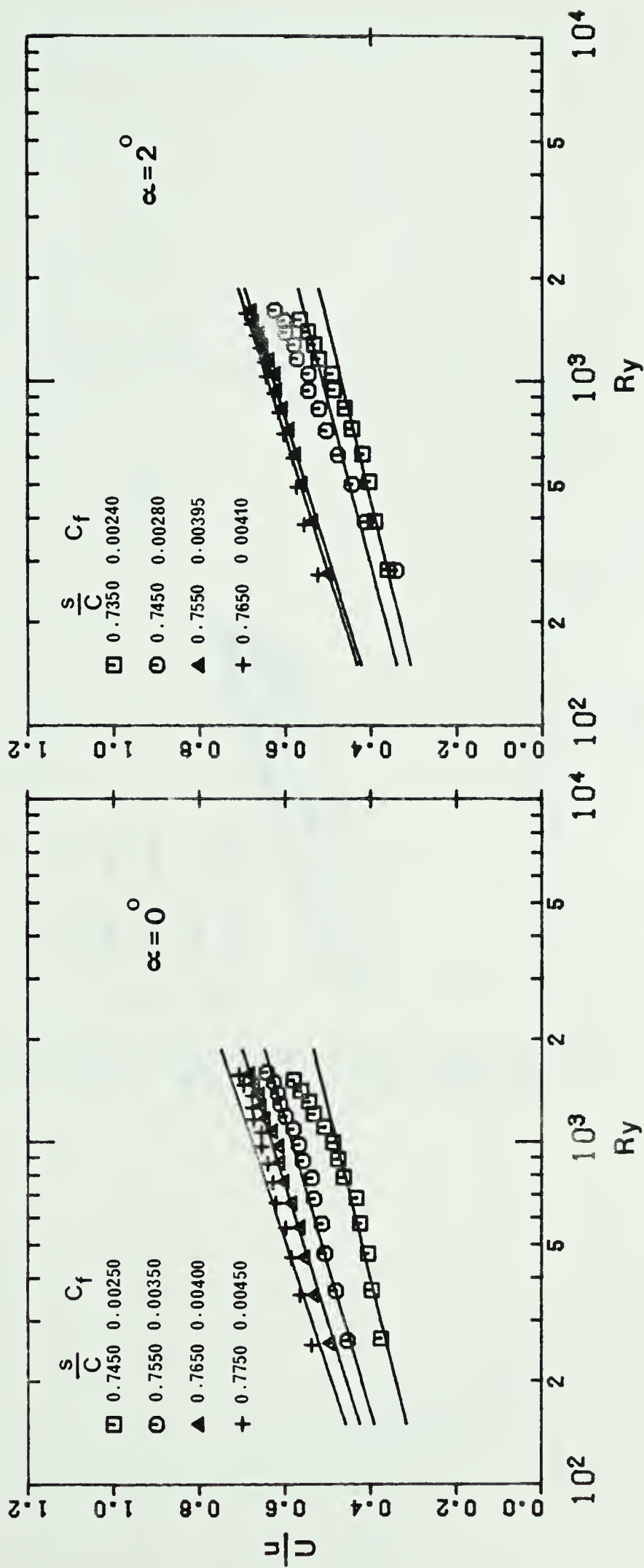


FIGURE 29--CLAUSER CHART FOR EXPERIMENTAL DETERMINATION OF TURBULENT SKIN-FRICTION COEFFICIENT, $Re = 1.6 \times 10^6$

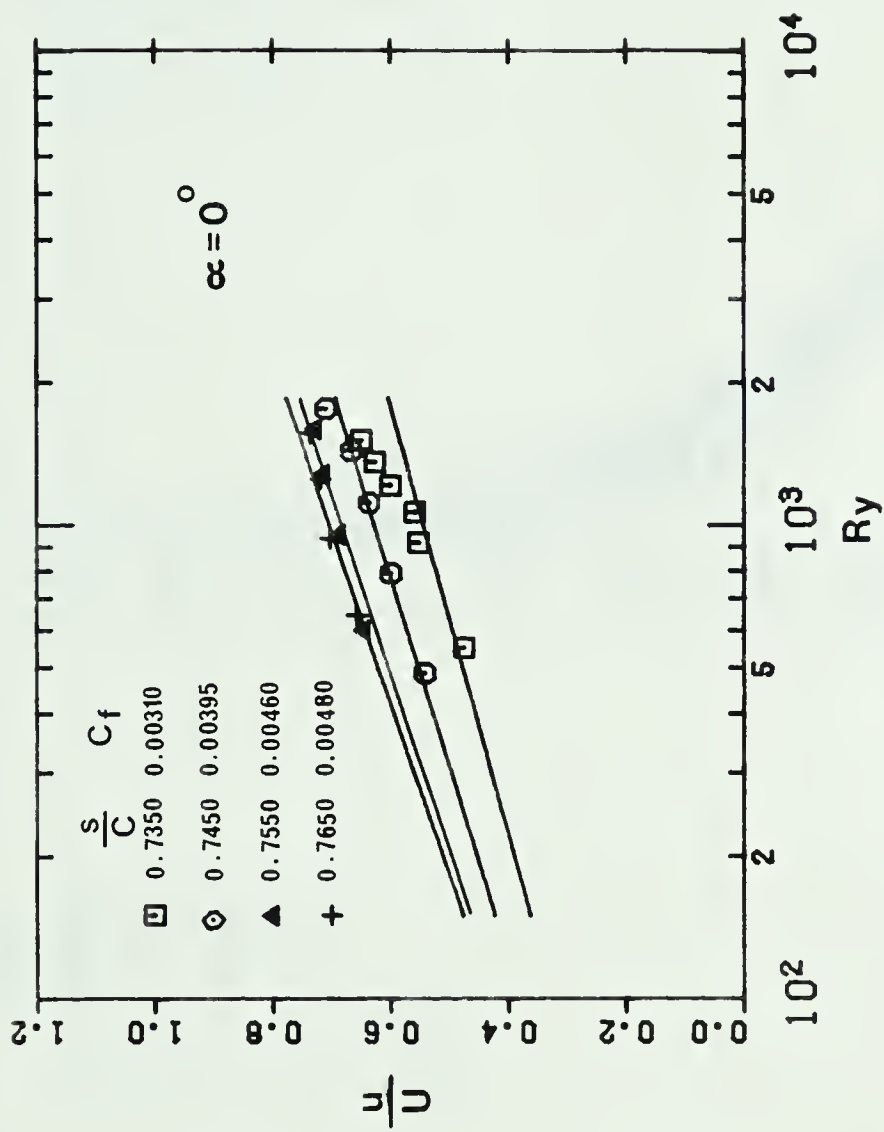


FIGURE 30--CLAUSER CHART FOR EXPERIMENTAL DETERMINATION
OF TURBULENT SKIN-FRICTION COEFFICIENT,
 $Re = 2.0 \times 10^6$

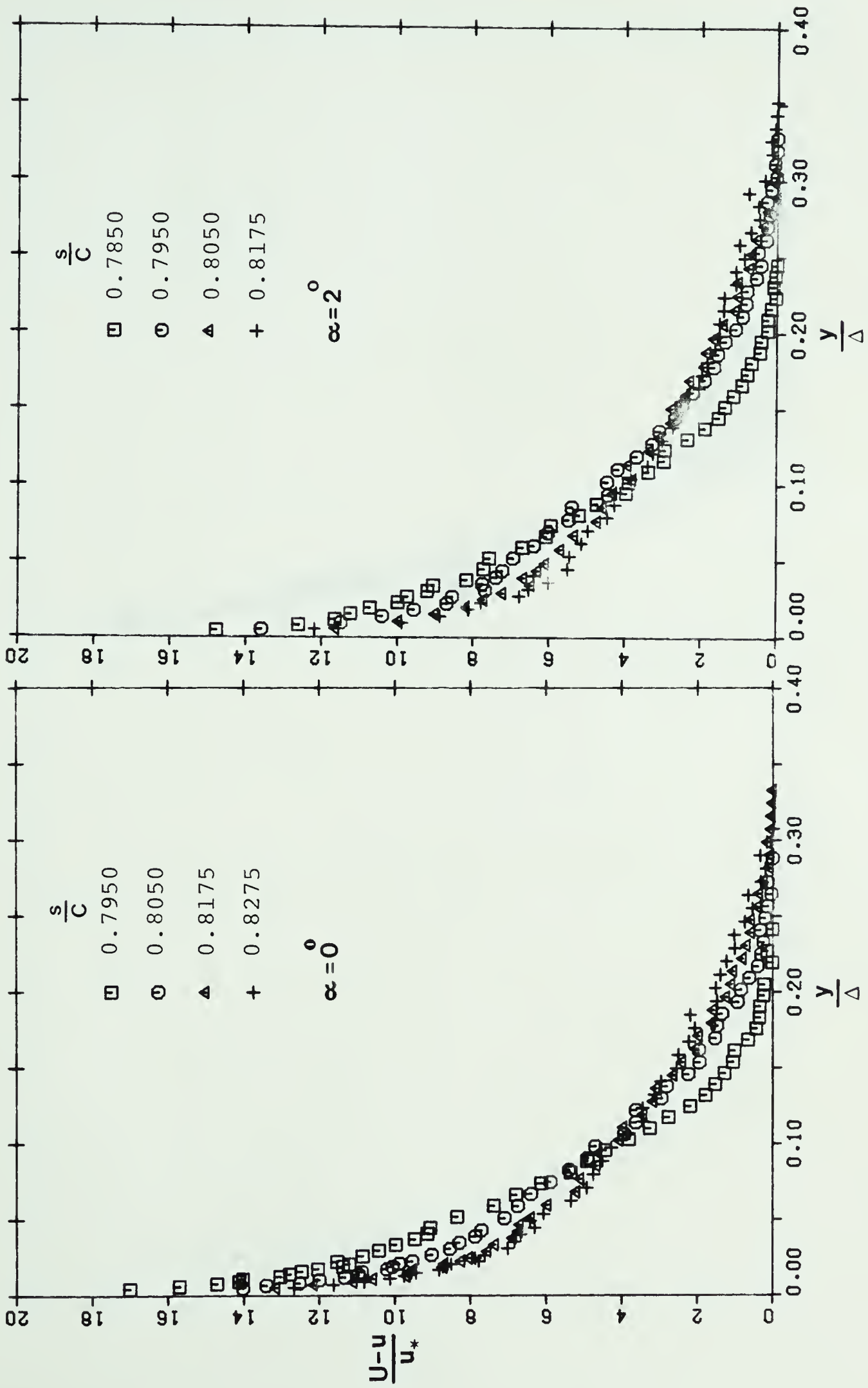


FIGURE 31--VELOCITY DEFECT PROFILES, $Re = 0.8 \times 10^6$

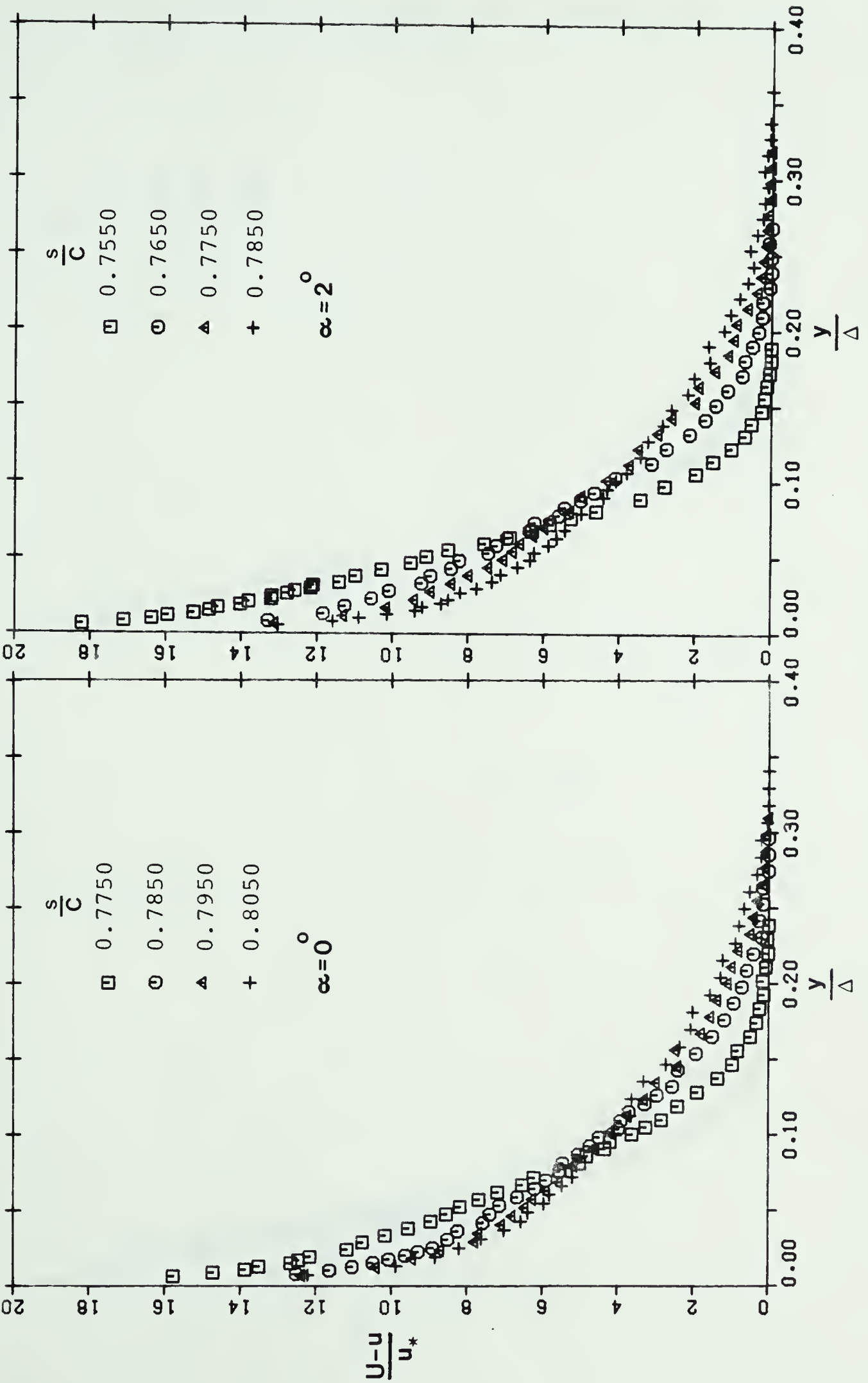


FIGURE 32--VELOCITY DEFECT PROFILES, $Re = 1.2 \times 10^6$

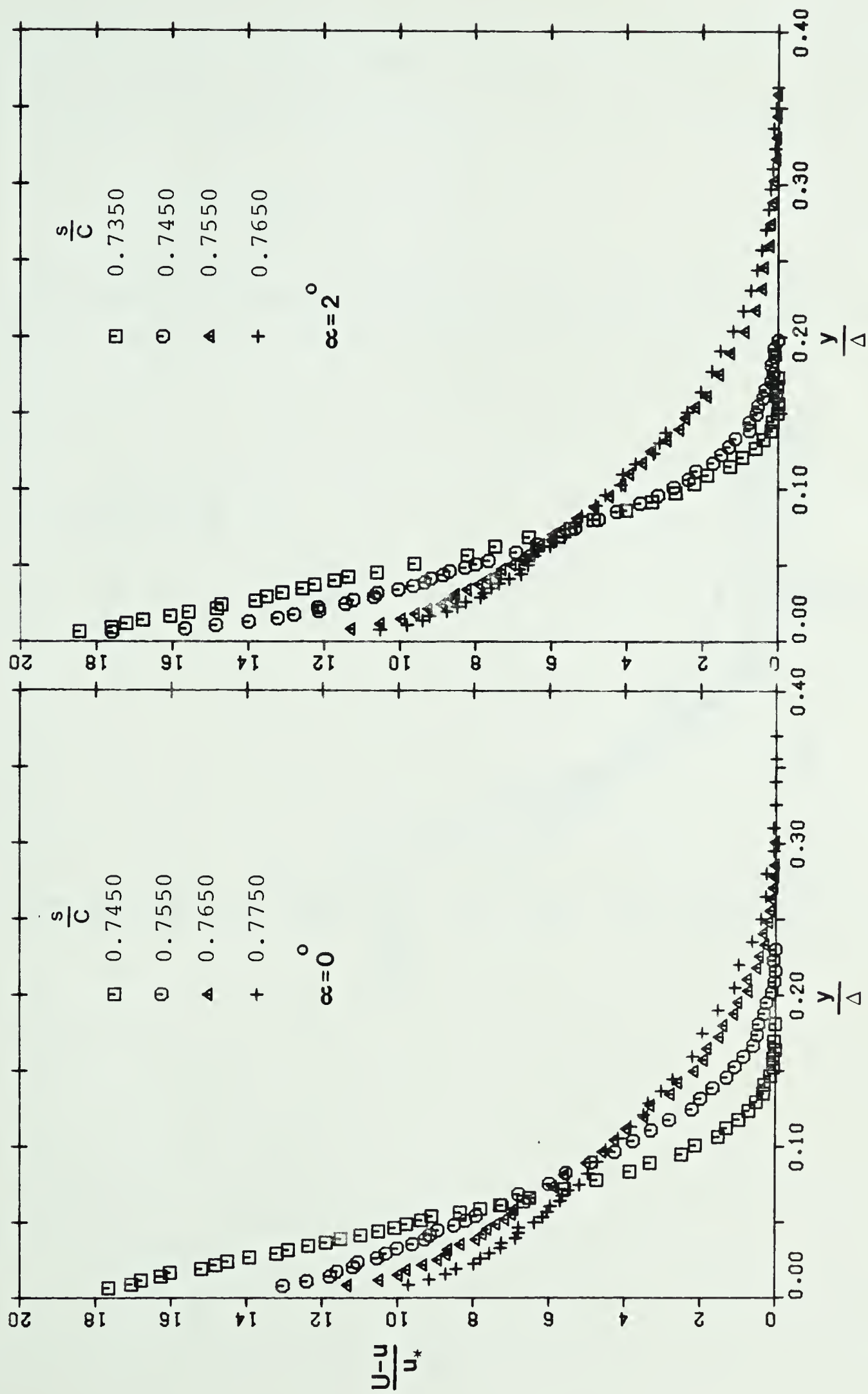


FIGURE 33--VELOCITY DEFECT PROFILES, $Re = 1.6 \times 10^6$

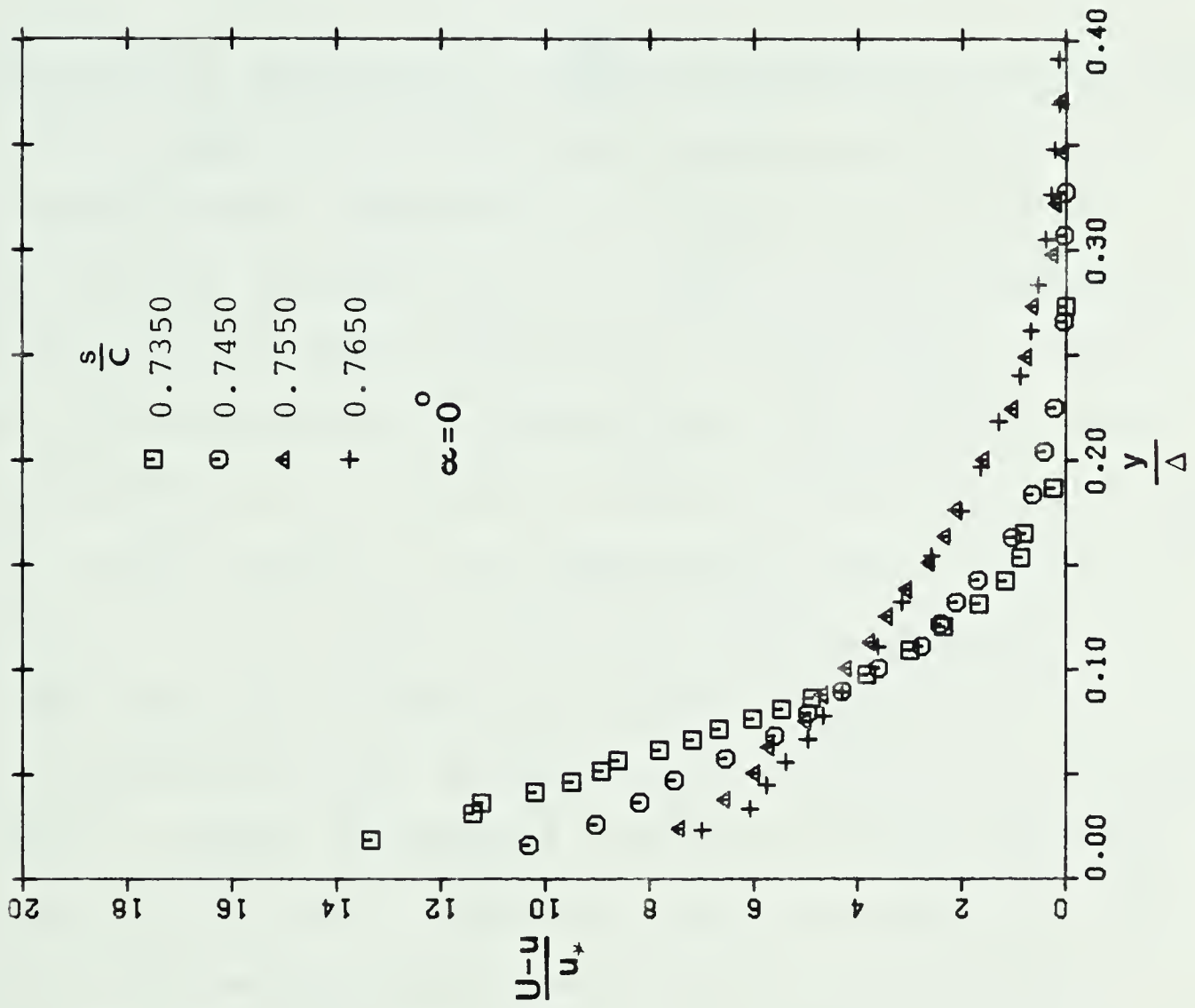


FIGURE 34--VELOCITY DEFECT PROFILES,
Re = 2.0×10^6

profiles plotted in the defect coordinates as $(U - u)/u_*$ vs y/Δ where Δ is the "Clauser defect thickness," defined by

$$\Delta = \int_0^{\infty} \frac{U-u}{u_*} dy \quad (4.5)$$

The friction velocity $u_* = \sqrt{\frac{\tau_w}{\rho}}$ was determined from the wall friction obtained from the mean velocity profiles as was described above. Observation of these figures indicate that the velocity profiles appear to reach a nearly self-preserving form at some distance downstream of reattachment. For all the seven flow cases considered here, the positions where the profiles start showing up the self-similar behavior along the airfoil surface in the redeveloping region are given in Table II. It is observed that the laminar separated flow field, that is, the distance between the separation point and the equilibrium point decreases with an increase in Reynolds number. Careful examination of Table II reveals that the extent of the region between the limits of separation and transition decreases much more rapidly with increasing Reynolds number as compared to the decrease in the extent of the region between the limits of transition and equilibrium point. It can, therefore, be interpreted that the transition to turbulence in the shear layer has a governing effect on the extent of the laminar separated flow field.

The value of the shape parameter $H = \delta^*/\theta$ was seen to decrease from a value of approximately 2.5 to a value of

1.35 within the redeveloping region after reattachment for all the flow cases considered here.

4.4 Applicability of Experimental Methods

In order to establish the applicability of experimental methods, the measurements are usually compared with known calculations and other established measurements if any. In the present study, a numerical method was developed in Chapter II to calculate the laminar boundary layer which facilitates the comparison of measurements with calculations. The measured laminar boundary layer in the present experiments is compared here with the calculations and other available data.

The position for laminar separation and velocity profiles in the vicinity of separation were calculated by the finite difference method developed in Chapter II. The laminar boundary layer on the airfoil surface was calculated using the measured pressure distribution, with smooth curves fitted through the data to facilitate evaluation of derivatives. Since the exact separation point can not be calculated by the present solution method, the separation point was estimated by following the method suggested in Chapter II; that is, by studying the retarded flow at various amounts of suction. Laminar flow separation was assumed to occur at a point where the local skin friction coefficient C_f becomes smaller than 5×10^{-4} . Comparison of the calculated positions for laminar separation with the measured ones are shown in Table II.

Agreement is probably within the experimental accuracy of the measurements. As indicated in Table II, the calculated position for separation was found to depend on the manner in which the pressure data are faired. Figures (35) and (36) compare the measured profiles and calculated profiles in the vicinity of laminar separation. Displacement thickness and momentum thickness of the measured boundary layer and calculated boundary layer are shown compared in Table III. In general, the shape, thickness and growth of the measured profiles are in good agreement with the calculated profiles.

Similar measurements in the region of separated flow near midchord on the NACA 663-018 airfoil were presented by Gault [5] and Bursnall and Loftin [4] separately. Although a direct comparison cannot be made, the data from these references together with data obtained with present investigation afford a comparison of results obtained in different wind tunnel facilities with different experimental techniques.

Gault measured the position for separation at a value of s/C equal to approximately 0.62 for a Reynolds number of 2.0×10^6 at 0° angle of attack. However, for the same Reynolds number and angle of attack in the present investigation, separation was determined to have occurred at approximately 0.64. Using an integral method with his measured pressure distribution, Gault calculated the position for separation at s/C equal to approximately 0.66. It is interesting to note that this value is in close agreement

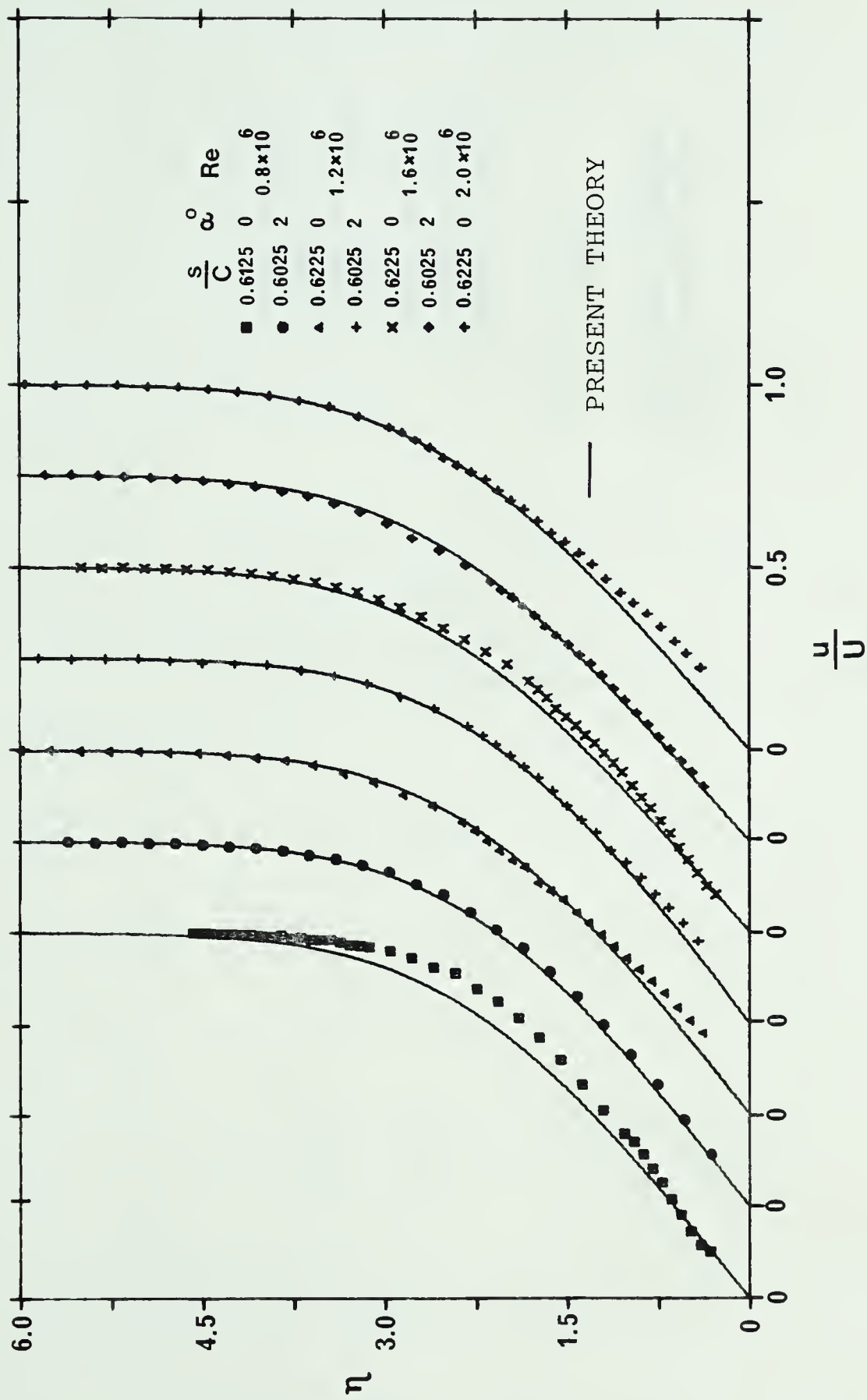


FIGURE 35--VELOCITY PROFILES UPSTREAM OF SEPARATION POINT

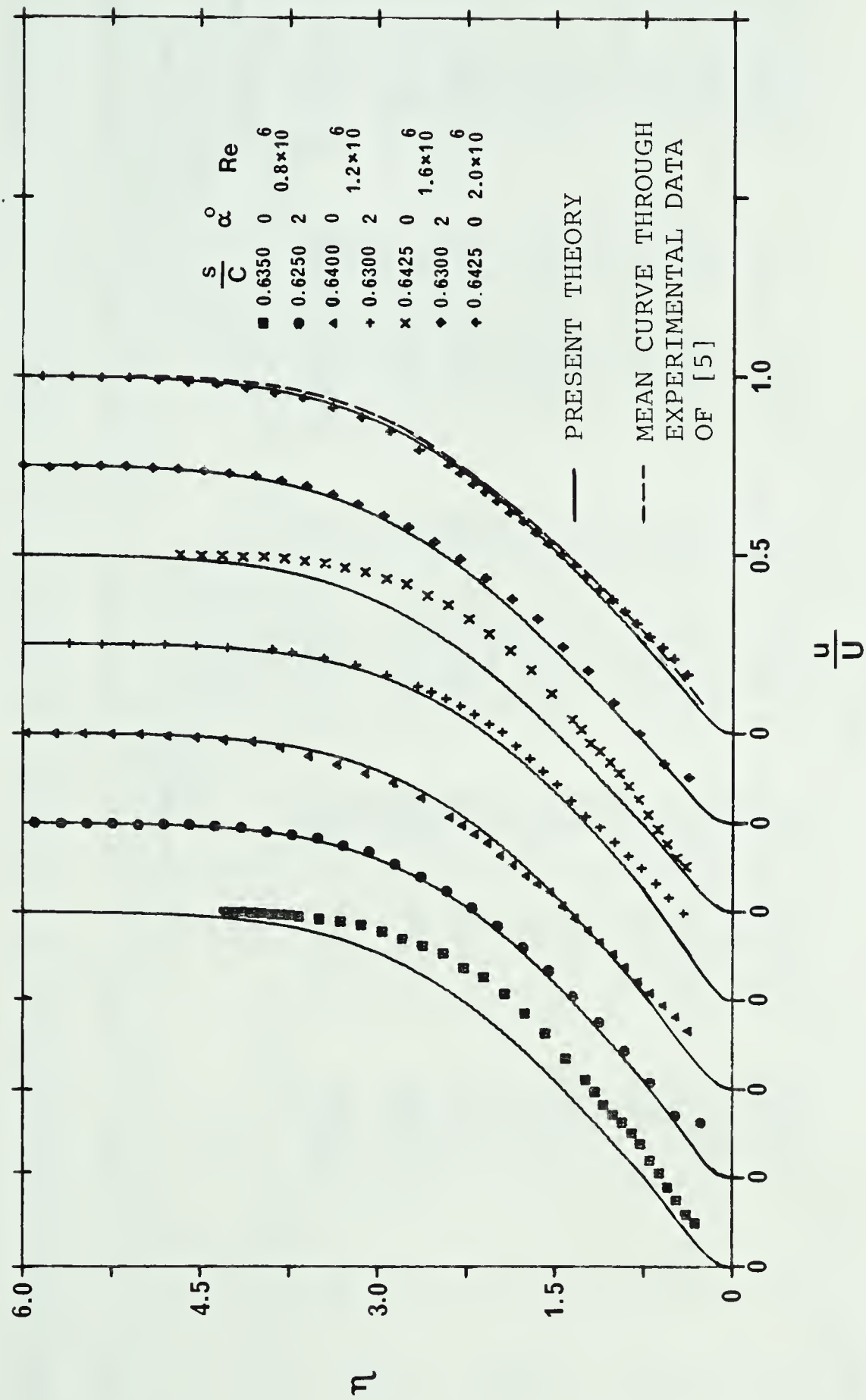


FIGURE 36--VELOCITY PROFILES AT SEPARATION POINT

TABLE III

COMPARISON OF EXPERIMENTAL AND COMPUTED BOUNDARY LAYER PARAMETERS NEAR SEPARATION

Re	α	s/C	Displacement Thickness δ^*/C		Momentum Thickness θ/C	
			Theory	Experiment	Theory	Experiment
0.8×10^6	0°	0.6125	0.1176×10^{-2}	0.1058×10^{-2}	0.4609×10^{-3}	0.4375×10^{-3}
		0.6350	0.1296×10^{-2}	0.1100×10^{-2}	0.4810×10^{-3}	0.4618×10^{-3}
	2°	0.6025	0.1201×10^{-2}	0.1071×10^{-2}	0.4678×10^{-3}	0.4605×10^{-3}
		0.6250	0.1227×10^{-2}	0.1111×10^{-2}	0.4800×10^{-3}	0.4616×10^{-3}
1.2×10^6	0°	0.6225	0.9449×10^{-3}	0.8915×10^{-3}	0.3720×10^{-3}	0.3689×10^{-3}
		0.6400	0.1132×10^{-2}	0.9892×10^{-3}	0.4220×10^{-3}	0.4082×10^{-3}
	2°	0.6025	0.9996×10^{-3}	0.9485×10^{-3}	0.3868×10^{-3}	0.3914×10^{-3}
		0.6300	0.1127×10^{-2}	0.1025×10^{-2}	0.4101×10^{-3}	0.4334×10^{-3}
1.6×10^6	0°	0.6225	0.8266×10^{-3}	0.7601×10^{-3}	0.3253×10^{-3}	0.3223×10^{-3}
		0.6425	0.9852×10^{-3}	0.8608×10^{-3}	0.3417×10^{-3}	0.3689×10^{-3}
	2°	0.6025	0.8621×10^{-3}	0.7870×10^{-3}	0.3351×10^{-3}	0.3384×10^{-3}
		0.6300	0.9266×10^{-3}	0.8835×10^{-3}	0.3486×10^{-3}	0.3676×10^{-3}
2.0×10^6	0°	0.6225	0.7222×10^{-3}	0.6728×10^{-3}	0.2885×10^{-3}	0.2907×10^{-3}
		0.6425	0.7474×10^{-3}	0.6867×10^{-3}	0.2950×10^{-3}	0.2883×10^{-3}

Displacement thickness:

$$\frac{\delta^*}{C} \sqrt{\frac{U}{(s/C)}} \frac{Re}{U_\infty} = \int_w^\infty \left(1 - \frac{u}{U}\right) d\eta$$

Momentum thickness:

$$\frac{\theta}{C} \sqrt{\frac{U}{(s/C)}} \frac{Re}{U_\infty} = \int_w^\infty \frac{u}{U} \left(1 - \frac{u}{U}\right) d\eta$$

with the present calculated value between 0.65 and 0.665. The separation profile measured by Gault is compared in Figure (36) with the present measurement. The profiles correlate even though the separation point indicated by the reference data is different from the separation point determined from the current data.

Bursnall and Loftin [4] measured the position of separation at a value of s/C equal to approximately 0.63 for a Reynolds number of 1.2×10^6 at 0° angle of attack. In the current investigation the position of separation was measured at a value of s/C equal to 0.64 which is in agreement with that obtained by Bursnall and Loftin.

These comparisons suggest that the apparatus and experimental methods adopted in the present investigation are quite satisfactory. This of course gives confidence in the degree of accuracy of the present measurements.

4.5 Conclusions

The experimental results reported here provide information, previously not available, about the character of attached redeveloping boundary layer. At some distance downstream of flow reattachment the turbulent velocity profiles tend to settle down to a nearly equilibrium form. In this vicinity the local skin friction can be determined from the measured velocity profiles, following the method suggested by Clauser.

The turbulent flow region downstream of reattachment

is also important when studying the behavior of laminar separation bubbles.

Transition to turbulent flow in the separated laminar shear layer has a governing effect on the extent of the separated flow field.

The present investigation verified the existing interpretations of the physical behavior of the laminar separation bubble.

CHAPTER V

TURBULENCE CHARACTERISTICS

5.1 Introduction

The laminar boundary layer separates from the airfoil surface, transition occurs in the separated shear layer, and the resulting turbulence spreads and entrains the flow so that it reattaches to the surface. The reattached turbulent boundary layer develops into a fully turbulent boundary layer at some distance downstream of reattachment. The turbulent boundary layer in this redeveloping region may be calculated by utilizing Boussinesq's eddy viscosity concept. In order to use this hypothesis it is necessary to have information about the eddy viscosity distribution in the redeveloping region. Since no such information was available in the literature, experimental measurements were carried out to furnish data on the actual behavior of eddy viscosity in this region. A comprehensive experimental study of the turbulence velocity field in the separated, reattached, and redeveloped regions is described here.

The experimental results presented here, describe the behavior of some of the turbulence characteristics that have not hitherto been available. The measurements in the present experiments include turbulence intensities of streamwise and normal velocities, and Reynolds shear stress. The shear

stress data were used to examine the distribution of eddy viscosity in a boundary layer, based on Boussinesq's eddy viscosity concept. It was found that the nondimensional eddy viscosity, defined as $\epsilon/\delta*U$, is constant across outer portion of boundary layer throughout the flow region of interest. It appeared that the turbulence velocity field tends to attain self-preservation at some distance downstream of reattachment. Based on the experimental evidence a two-layer eddy viscosity model is proposed for the flow in the redeveloping region.

A wide range of Reynolds number is needed to study the effect of Reynolds number on the turbulence structure of the laminar separated flow field, but only a limited range could be covered, due to the limitations on the equipment available. Consequently, a possible limitation of the present investigation is the lack of information about the effects of Reynolds number on the turbulence velocity field. However, because the turbulent stresses predominate except very near the wall it may be expected that the nondimensional turbulence distributions would be relatively insensitive to Reynolds number variations in low speed flows such as that treated in the present study.

5.2 Behavior of Turbulence Velocity Field in an Adverse Pressure Gradient

Observations have indicated that in a region of adverse pressure gradient the Reynolds shear stress attains

its maximum value at distances well away from the wall. Consequently there is a high level of turbulence at points away from the wall.

The effects of adverse pressure gradient on turbulence can best be understood by examining the "Production" terms in the turbulent energy equation (Cebeci and Smith [25], Chapter 2). For two-dimensional turbulent flows the combined production of turbulence is

$$PR = \underbrace{-\overline{u'v'}}_{(1)} \frac{\partial u}{\partial y} - \underbrace{\overline{u'^2}}_{(2)} \frac{\partial u}{\partial s} - \underbrace{\overline{v'^2}}_{(3)} \frac{\partial v}{\partial y} \quad (5.1)$$

From this equation it can be seen that the term (1) is always positive and the term (3) is always negative. Since $\overline{u'^2}$ is always positive, increase or decrease in PR is, therefore, determined by the gradient $\frac{\partial u}{\partial s}$. In a flow with a velocity that decreases in the flow direction, s , (retarded flow in space), the gradient $\frac{\partial u}{\partial s}$ is negative. Then the term (2) becomes positive and it promotes an increase in the turbulence. Thus, in a flow with an adverse pressure gradient the tendency is toward an increase in turbulence. Similarly, in a flow with favourable pressure gradient there is a tendency for a relative turbulence intensity to decrease.

Although the behavior of turbulent flow in the inner and the outer regions is quite different, those regions are strongly coupled by the shear stress profile and the general diffusivity of the turbulence. Within the inner region the

energy exchange processes are in a state of near equilibrium and for that reason the flow in the inner region is governed essentially by the local conditions. On the other hand, in the outer region the dominant terms are those due to convection and those due to dissipation (Cebeci and Smith [25], Chapter 4). The turbulence obtains its energy mainly by diffusion from the inner region. A consequence of this is that, in the outer region, the turbulent flow phenomena depend not only on the local conditions but also on the whole history of events in the flow upstream of the point in question. The large and long eddies in this region make quick recovery from any upstream generated disturbance difficult. In other words, the flow in the outer region has a long memory. In contrast, the inner region must have a short memory, since the eddies are very small in this region. Therefore, in a region with continued pressure rise, a high level of upstream generated turbulence at distances well away from the wall persists for downstream development.

The foregoing is simply a description of the behavior of turbulence velocity field in an adverse pressure gradient. The present experimental results are discussed in the light of these observations.

5.3 Intermittency Correction

As the outer boundary of a fully developed turbulent boundary layer is approached, the turbulence fluctuates with time so that the flow alternates between a turbulent and a

substantially irrotational state. Intermittency is the name given to the on-and-off character of the turbulence. Intermittency factor γ is defined as the ratio of time turbulent to total time at any point, so that it measures the probability of finding turbulent flow at any instant at the point considered. Since a stationary detector in the flow responds to alternate turbulent and nonturbulent flow, the measured quantities may have to be corrected for the effect of intermittency.

Consider a flow quantity Q measured by a stationary detector in the flow. Then

$$\bar{Q} = \bar{Q}_{\text{turbulent}} \times \gamma + \bar{Q}_{\text{potential}} (1-\gamma) \quad (5.2)$$

where the bars represent mean quantities. If τ_t represents the turbulent shear stress measured, then from Equation (5.2) the actual shear stress in the turbulent fluid is given approximately by

$$\tau_{ta} = \frac{\tau_t}{\gamma} = \frac{-\rho \overline{u'v'}}{\gamma} \quad (5.3)$$

The actual velocity in the boundary layer may be determined from the relation given by Equation (5.2). If u is the mean velocity measured by a hot film, then the actual velocity u_t is given approximately by

$$u_t = [u - U(1-\gamma)]/\gamma \quad (5.4)$$

assuming as did Corrsin and Kistler [26] that for practical purposes $U = U_{\text{potential}}$, the local potential velocity.

The experimental distribution of the intermittency factor γ in a direction normal to the surface can be represented by the expression given by Fiedler and Head [27],

$$\gamma(y) = \frac{1}{\sigma \sqrt{2\pi}} \int_y^{\infty} \exp \left[- \left(\frac{y-\bar{y}}{\sqrt{2}\sigma} \right)^2 \right] dy \quad (5.5)$$

where \bar{y} = the value of y for which $\gamma = 0.5$

$$\sigma = \text{the standard deviation} = \left[\overline{(y-\bar{y})^2} \right]^{\frac{1}{2}}$$

Equation (5.5) may be rewritten as

$$\gamma(y) = \frac{1}{\sqrt{\pi}} \left[\int_{\Omega=0}^{\infty} \bar{e}^{\Omega^2} d\Omega - \int_{\Omega=0}^{\Omega=\frac{y-\bar{y}}{\sqrt{2}\sigma}} \bar{e}^{\Omega^2} d\Omega \right] \quad (5.6)$$

where

$$\Omega = \frac{y-\bar{y}}{\sqrt{2}\sigma}$$

Therefore, the intermittency distribution can be described by an error function of the form (from Equation (5.6))

$$\gamma(y) = \frac{1}{2} \left[1 - \operatorname{erf} \left(\frac{y-\bar{y}}{\sqrt{2}\sigma} \right) \right] \quad (5.7)$$

Equation (5.7) can be written in terms of the characteristic boundary layer parameters δ and δ^* , as shown below.

$$\gamma(y) = 0.5 \left[1 - \operatorname{erf} \left(\frac{\left\{ \frac{y}{\delta} \right\} \left\{ \frac{\delta}{\delta^*} \right\} - \frac{\bar{y}}{\delta^*}}{\sqrt{2} \sigma / \delta^*} \right) \right] \quad (5.8)$$

If the nondimensional parameters in Equation (5.8) are known, then this equation may be used to correct the distribution of various turbulence quantities for the effect of intermittency in a turbulent boundary layer. In lack of experimental data in a flow field like that encountered in the present investigation, the intermittency data published by Fiedler and Head [27] is used in conjunction with Equation (5.8). Fiedler and Head have given two separate correlations of the nondimensional parameters $\frac{\delta}{\delta^*}$, $\frac{\bar{y}}{\delta^*}$ and $\frac{\sigma}{\delta^*}$ as functions of the shape factor H , one for normally developing boundary layer with various pressure distributions and the second for flows recovering from upstream separation in a favourable pressure gradient. Their measurements indicate that as the shape factor decreases, the intermittency extends right through the boundary layer. Even though the shape factor H decreases downstream of reattachment, such an effect of H is not to be expected in the present investigation because the shape factor was found to decrease from a higher value to a lower value in a relatively short streamwise distance. Therefore, a typical value of 2.4 is chosen for H

in conjunction with the above nondimensional parameters. One is tempted to use the data obtained in the recovering boundary layer to evaluate the Equation (5.8) in the present flow situation. However, use of data obtained by Fiedler and Head in the reattached boundary layer gave large errors when intermittency corrections were applied. This may be because their experiments were conducted in the reattached boundary layer in a favourable pressure gradient, whereas in the present separated flow field there is sharp pressure recovery just upstream of reattachment and there is continued pressure rise after reattachment. Consequently, the nondimensional parameters $\frac{\delta}{\delta^*}$, $\frac{\bar{y}}{\delta^*}$ and $\frac{\sigma}{\delta^*}$ measured in a normally developing boundary layer were used to evaluate the Equation (5.8). The intermittency distribution through the boundary layer at a given streamwise position is then determined from

$$\gamma(y) = 0.5 \left[1 - \operatorname{erf} \left(5.24 \frac{y}{\delta} - 5.32 \right) \right] \quad (5.9)$$

Equation (5.9) is used for intermittency correction in the present investigation.

5.4 Test Program

The investigation consisted of measurements of turbulence intensities $\left(\frac{\sqrt{u'^2}}{U} \text{ and } \frac{\sqrt{v'^2}}{U} \right)$ and Reynolds shear stress $(-\rho \overline{u'v'})$ in turbulent boundary layers through the region of laminar separated flow field on an NACA 66₃-018 airfoil

section. These measurements were made in the region between the limits of transition and the position where the mean velocity field was found to attain equilibrium conditions. The investigation was made at a Reynolds number based on airfoil chord of 0.8×10^6 for angles of attack of 0° and 2° , respectively. Eddy viscosity was evaluated from the experimental data using measured Reynolds shear stresses and mean velocities.

The body diameter of the x probe prohibited the taking of measurements at any distance closer than 1.5 mm to the wall. Because of this limitation and the limitation on the size of the sensor available, it became necessary to make measurements in a boundary layer which is sufficiently large so that the ratio of length of the wire to boundary layer thickness is small enough to ensure sufficient data taken inside the boundary layer. At a Reynolds number of 0.8×10^6 , the boundary layer thickness δ was found to vary from 5 mm to 10 mm in the region of present interest. At Reynolds numbers higher than 0.8×10^6 , the boundary layer thickness was so small that it was not possible to take adequate data with a sufficient degree of accuracy.

5.5 Results and Discussion

5.5.1 Turbulence Intensity of of Streamwise Velocity

Figures (37) and (38) show the streamwise turbulence

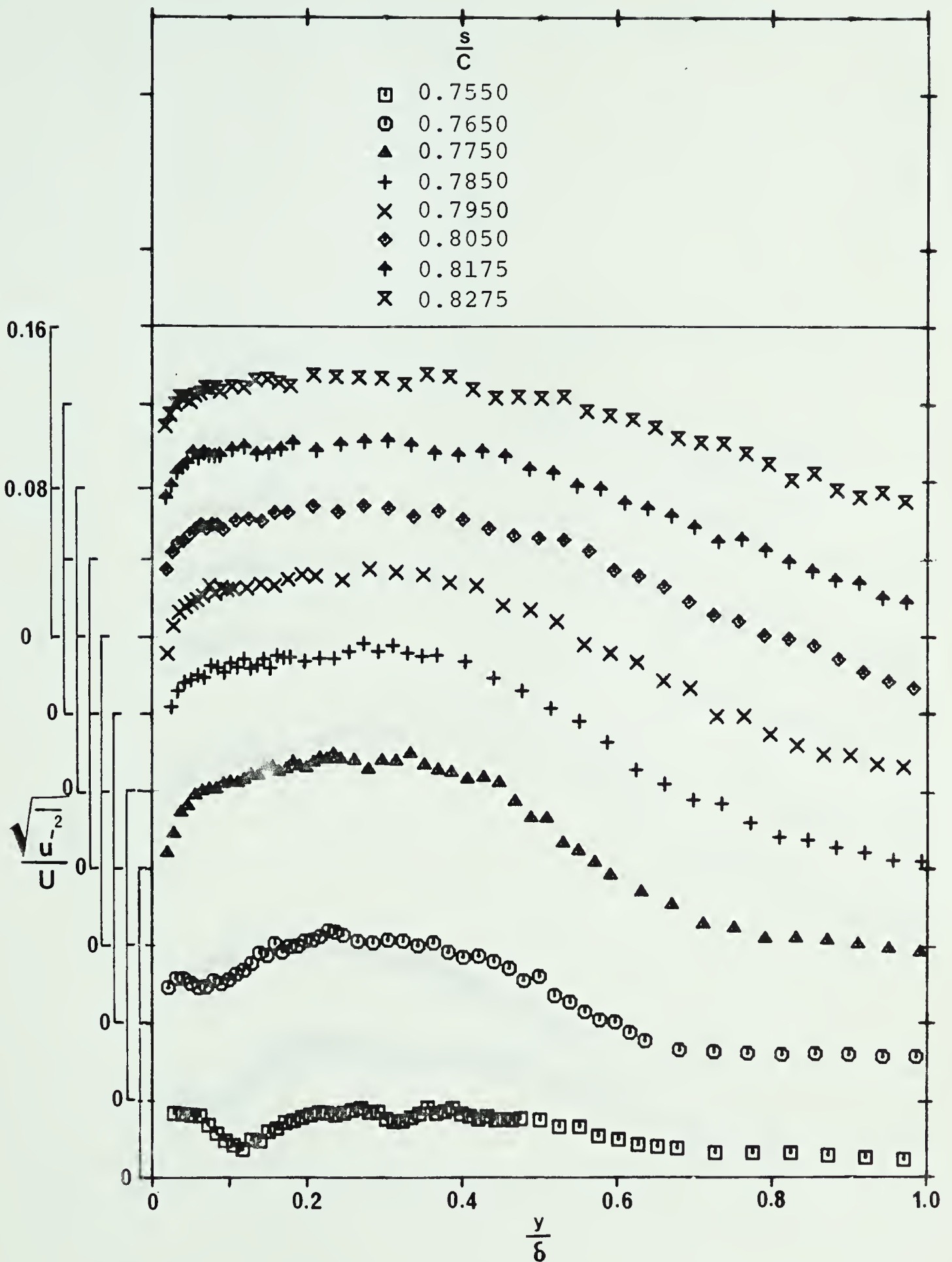


FIGURE 37--TURBULENCE INTENSITY OF STREAMWISE VELOCITY,
 $Re = 0.8 \times 10^6$, $\alpha = 0^\circ$

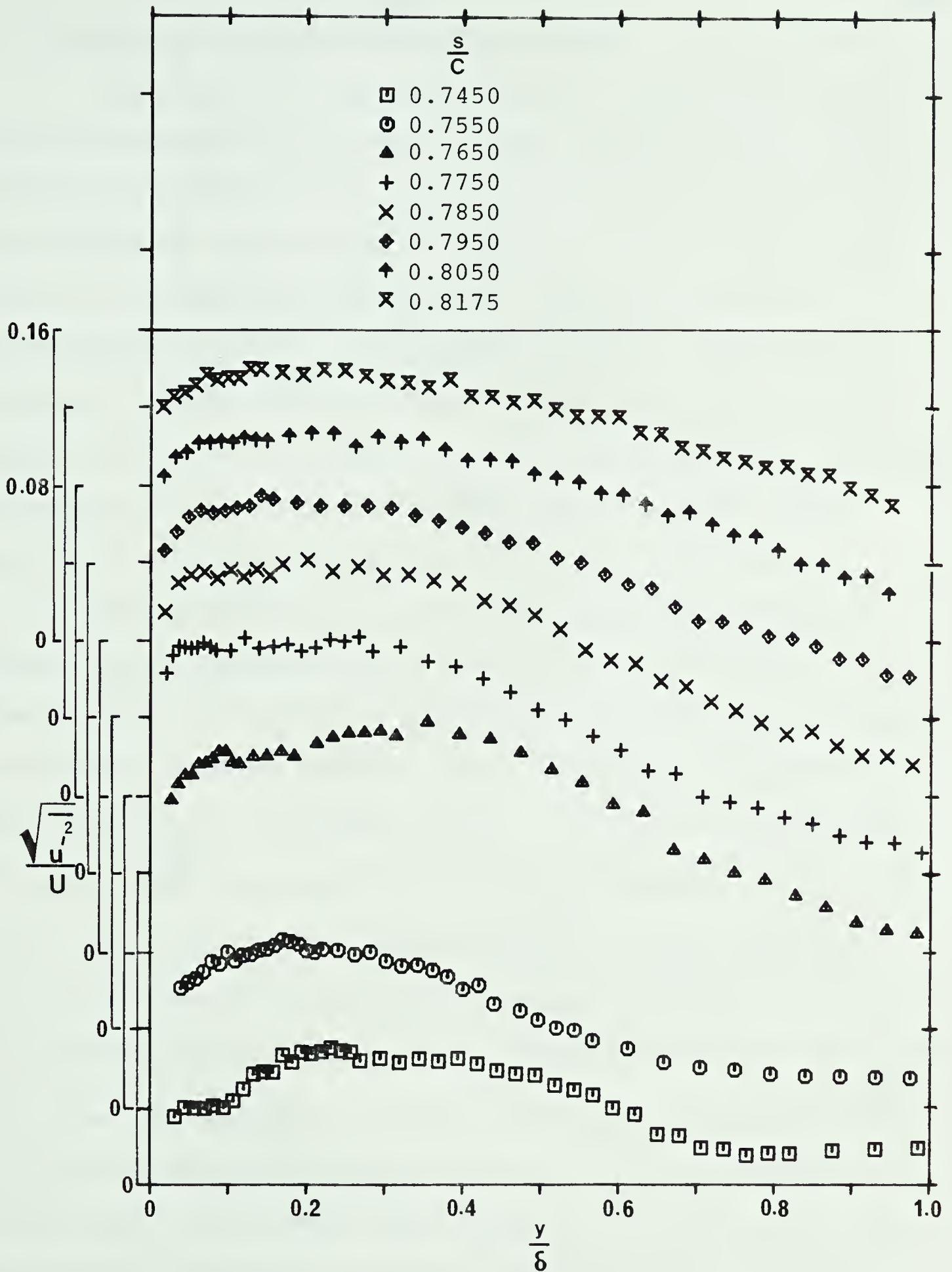


FIGURE 38--TURBULENCE INTENSITY OF STREAMWISE VELOCITY,
 $Re = 0.8 \times 10^6$, $\alpha = 2^\circ$

intensities plotted as $\sqrt{u'^2}/U$ versus y/δ .

The nature of the distribution of turbulence intensity is essentially the same for the two test cases. Transition to turbulent flow occurs in the separated shear layer at a value of approximately 0.755 for $\alpha = 0^\circ$. Similarly, for $\alpha = 2^\circ$ transition was found to occur at a value of approximately 0.745. At these positions, as indicated in Figures (37) and (38) the level of turbulence is relatively small. And also, at these stations, the streamwise turbulence intensity curve exhibits a minimum near the wall. This position of minimum turbulence intensity in the boundary layer may correspond to the location where the turbulence shear stress changes sign in the reverse flow region. As the downstream stations are approached the level of turbulence intensity increases rapidly until it attains a maximum value and then starts decreasing slowly. For $\alpha = 0^\circ$, the maximum value of $\sqrt{u'^2}/U$ is about 16% and this occurred at $s/C \approx 0.785$. For $\alpha = 2^\circ$, the maximum value of $\sqrt{u'^2}/U$ is also about 16% and this occurred at $s/C \approx 0.775$. These two stations along the airfoil surface are in the neighbourhood of the positions for flow reattachment. All the turbulence intensities, $\sqrt{\frac{u'^2}{U}}$, converge to nearly the same value as the flow progresses downstream. It is seen from Figures (37) and (38) that the streamwise turbulence intensity profiles appear to settle down to a nearly self-preserving form.

In the regions between the limits of transition and reattachment, the turbulence intensity appears to attain a maximum value roughly at $y/\delta = 0.2$. Since the flow is still separated in this region, the turbulence intensity gradually decreases as the wall is approached. For y/δ greater than approximately 0.2, the turbulence intensity first appears to remain constant and then decreases rapidly until it attains a nearly constant value across the main outerpart of the boundary layer. This indicates that the turbulence structure in the outer region of the boundary layer is not fully established

As the flow progresses downstream, the streamwise turbulence intensity spreads across the boundary layer, indicating that the turbulence structure is fully established. The turbulence intensity is almost constant in the central region of the boundary layer. In this downstream development region, a gradual reduction of turbulence intensity in close proximity of the wall is observed. As explained earlier, this is an effect of the drop in Reynolds shear stress toward the wall which results from the application of adverse pressure gradient.

5.5.2 Turbulence Intensity of Normal Velocity

The turbulence intensities of normal velocity component are shown plotted in Figures (39) and (40) as $\sqrt{v'^2}/U$ versus y/δ . A clear distinction is seen between the

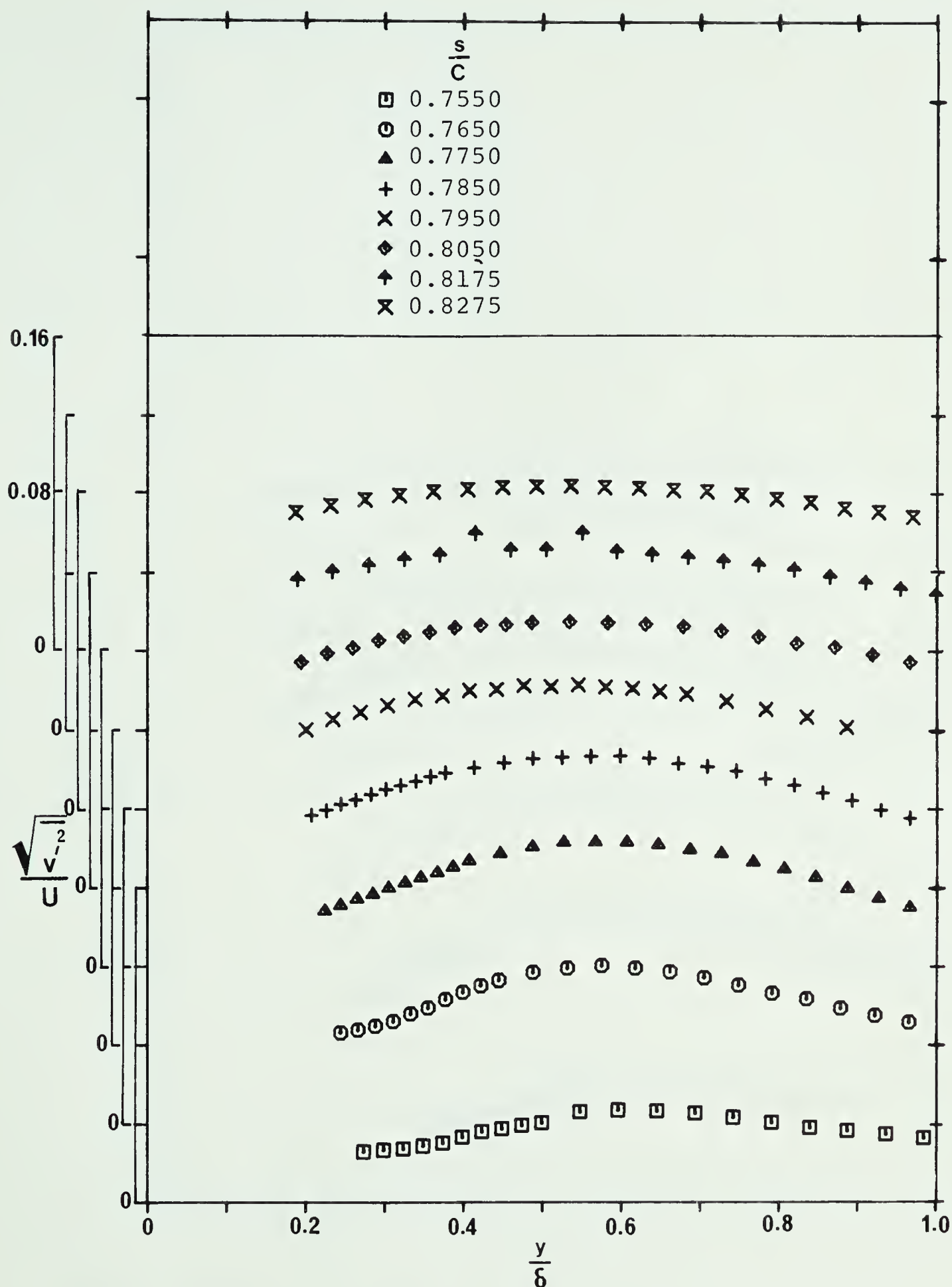


FIGURE 39--TURBULENCE INTENSITY OF NORMAL VELOCITY,
 $Re = 0.8 \times 10^6$, $\alpha = 0^\circ$

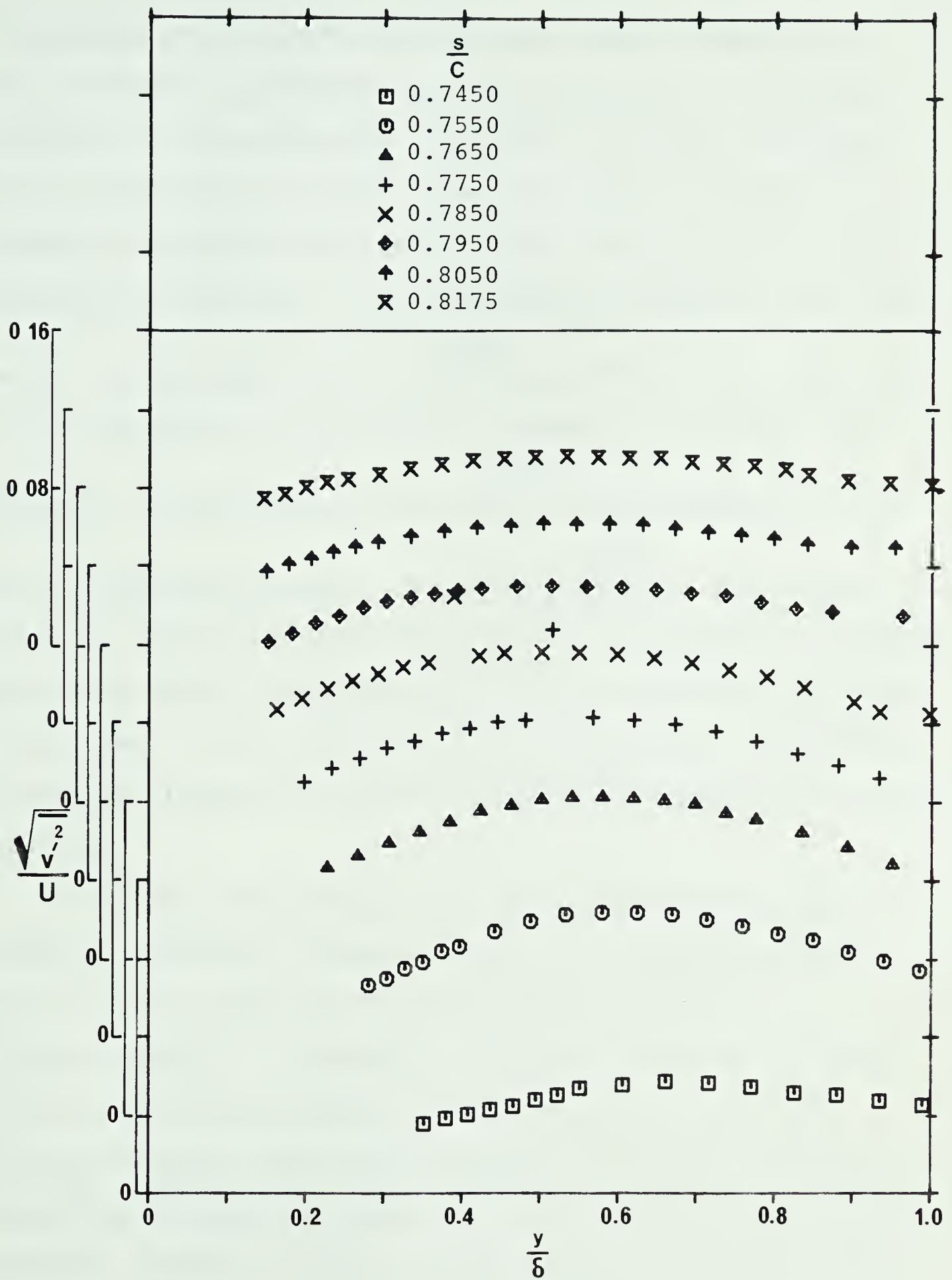


FIGURE 40--TURBULENCE INTENSITY OF NORMAL VELOCITY,
 $Re = 0.8 \times 10^6$, $\alpha = 2^\circ$

streamwise and transverse turbulence intensity profiles. The transverse turbulence intensity profiles are flatter compared to the streamwise turbulence intensity profiles. It is found that in general the magnitudes of transverse turbulence intensity are smaller than those of streamwise turbulence intensity. This anisotropy increases toward the wall. The maximum value of $\sqrt{v'^2}/U$ is about 12% as compared to 16% obtained for streamwise turbulence intensity. But, however, the maximum values of $\sqrt{v'^2}/U$ are attained at the same streamwise location as that for $\sqrt{u'^2}/U$. The normal velocity turbulence intensity profiles also appear to settle down to a nearly self-preserving form as the flow progresses downstream. It is interesting to note that the transverse turbulence intensity attains its maximum value well away from the wall.

Similar turbulence intensity measurements in a normally developing boundary layer on a smooth wall with zero pressure gradient are presented by Klebanoff in reference [28]. A comparison indicates that the turbulence level of the whole boundary layer measured in the flow recovery region, with adverse pressure gradient, is higher than that obtained by Klebanoff [28] in a region with zero pressure gradient. And the comparison also indicates that the level of turbulence intensity at distances well away from the wall is high. The higher magnitudes of turbulence

intensity in the whole region of the boundary layer are caused in part by the continued pressure rise and in part by the flow reattachment after upstream separation. The high level of turbulence intensity at distances well away from the wall are caused in part by the continued pressure rise and in part by the high level of upstream generated turbulence.

5.5.3 Distribution of Reynolds Shear Stress

Two-dimensional, steady incompressible turbulent boundary layer equation is written as [25]

$$u \frac{\partial u}{\partial s} + v \frac{\partial u}{\partial y} = - \frac{1}{\rho} \frac{\partial p}{\partial s} + \frac{1}{\rho} \frac{\partial \tau_{\ell}}{\partial y} + \frac{1}{\rho} \frac{\partial \tau_t}{\partial y} \quad (5.10)$$

where $\tau_{\ell} = \mu \frac{\partial u}{\partial y}$, viscous shear stress

$\tau_t = - \rho \overline{u'v'}$, turbulent shear stress or
Reynolds shear stress

In nondimensional form, the Reynolds shear stress can be written as

$$C_f = \frac{\tau_t}{\frac{1}{2} \rho U^2} = - \frac{\rho \overline{u'v'}}{\frac{1}{2} \rho U^2} = - \frac{2 \overline{u'v'}}{U^2} \quad (5.11)$$

The Reynolds shear stress distribution, in the non-dimensional form, is shown plotted in Figures (41) and (42). As seen from these figures, the turbulent shear stress in the reverse flow region is relatively very small. The non-dimensional Reynolds shear stress has a maximum value of

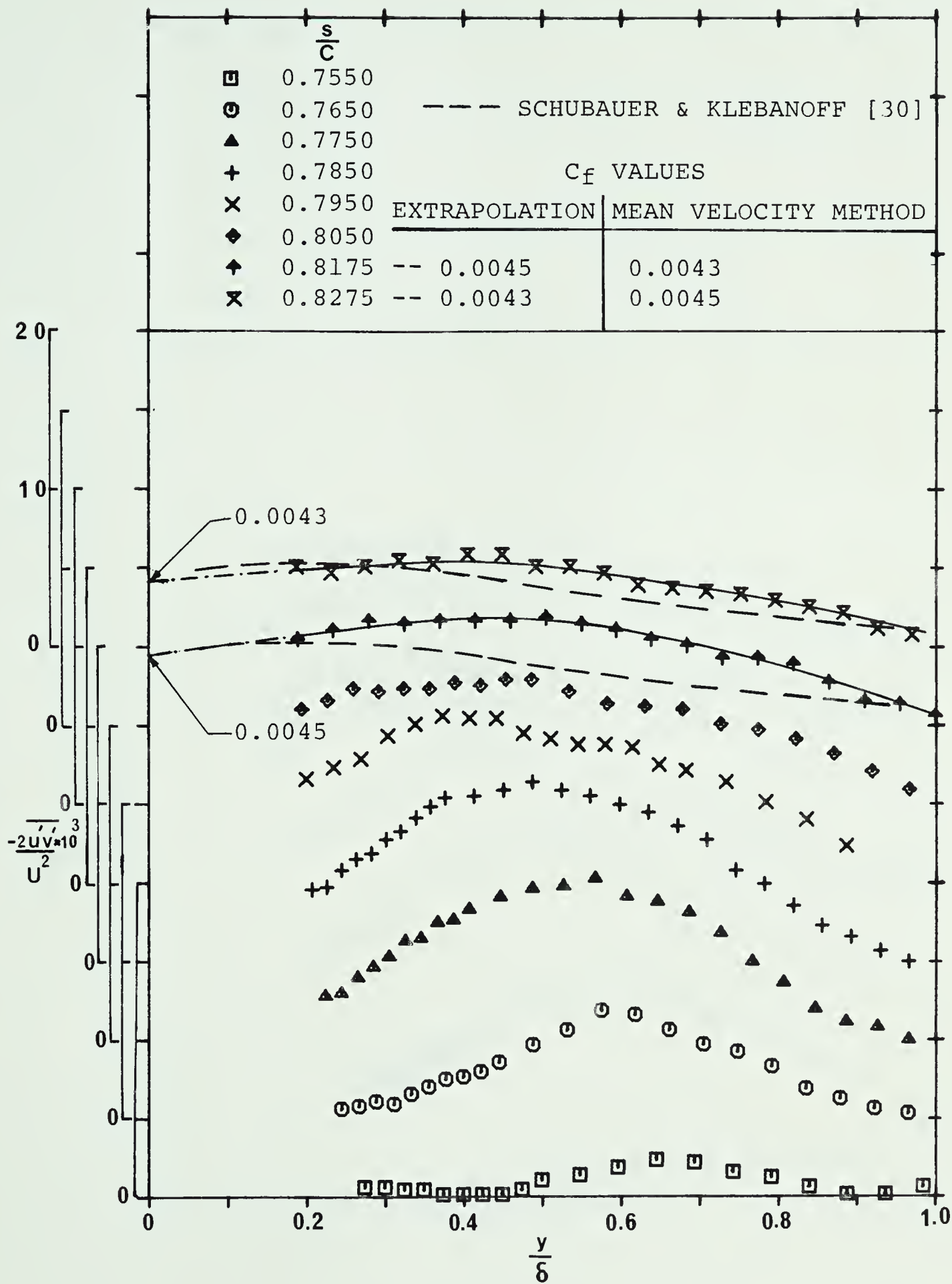


FIGURE 41--REYNOLDS SHEAR STRESS DISTRIBUTION,
 $Re = 0.8 \times 10^6$, $\alpha = 0^\circ$

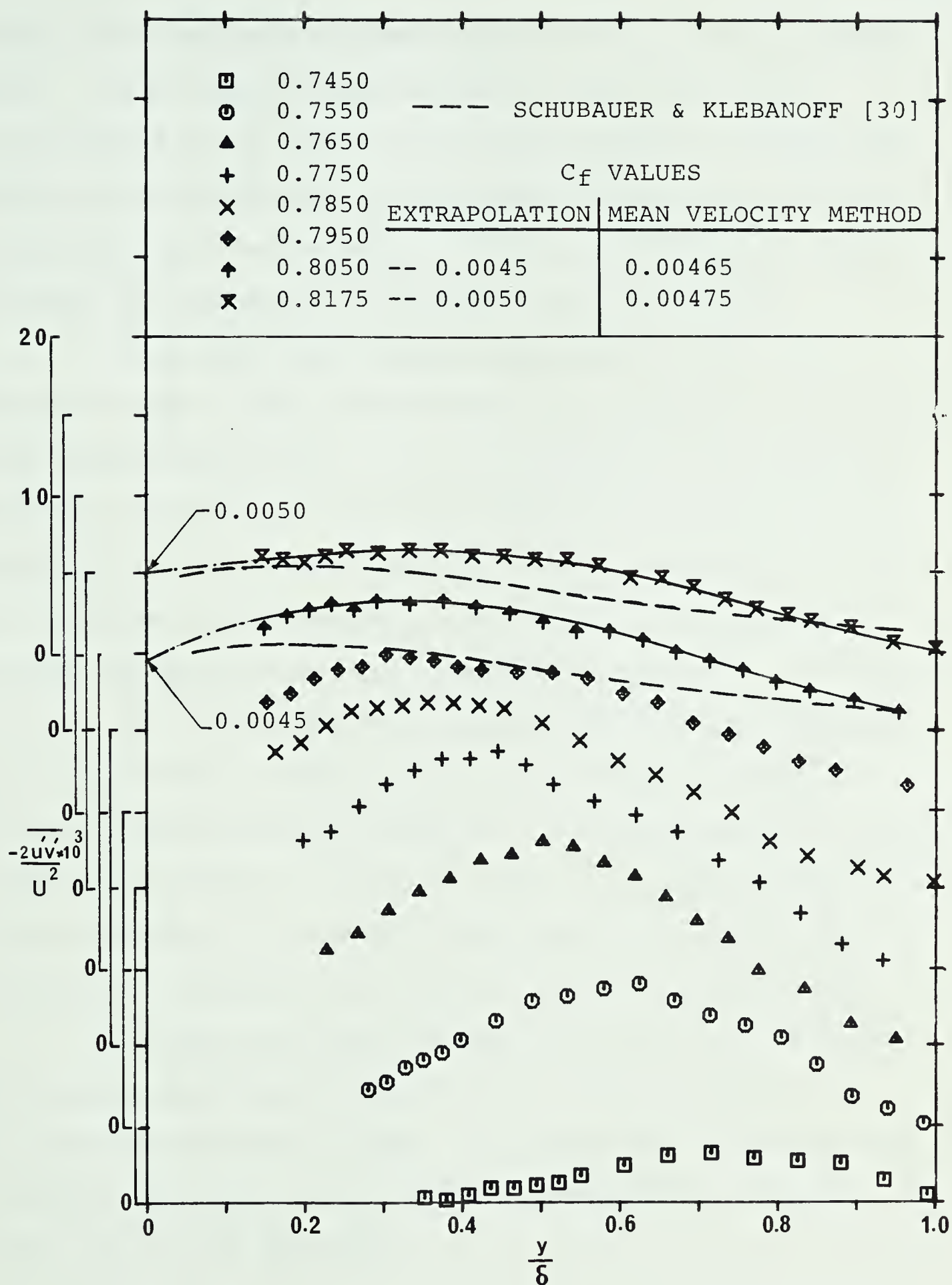


FIGURE 42--REYNOLDS SHEAR STRESS DISTRIBUTION,
 $Re = 0.8 \times 10^6$, $\alpha = 2^\circ$

about 0.012 occurring in the neighbourhood of flow reattachment. These higher values of shear stress near flow reattachment occur due to the intense turbulent mixing and sharp pressure recovery in the region between the limits of transition and reattachment. As the flow progresses downstream, the magnitude of the shear stress decreases.

It is seen from Figures (41) and (42) that the Reynolds shear stress curve attains its maximum at a distance well away from the wall. As was mentioned in the beginning, this is a manifestation of the effects of adverse pressure gradient. It is evident from the figures that the location of the shear stress maximum in the boundary layer moves toward the wall as the flow progresses downstream. This is in part due to the flow recovery from upstream disturbances and in part due to the decrease in the rate of pressure recovery after flow reattachment. It is interesting to note, comparing Figures (37) through (42), that the Reynolds shear stress maximum in a boundary layer occurs in between the maxima for streamwise and normal turbulence intensities.

The Reynolds shear stresses determine the magnitude of viscous shearing stresses in the laminar sublayer by forcing a high rate of shear. For some small distance from the wall, Equation (5.10) can be approximated as (since u and v are zero at the wall)

$$\frac{\partial \tau}{\partial y} \approx \frac{\partial p}{\partial s} \quad (5.12)$$

where τ is the total shear stress,

$$\tau = \tau_{\ell} + \tau_t$$

As the wall is approached, the turbulent shear stress falls to zero, as shown by the experimental data of Schubauer [29]. In the region where turbulent shear stress τ_t begins to decrease, the viscous shear stress τ_{ℓ} begins to increase in such a way that the total shear stress distribution is approximately determined by Equation (5.12). In other words, this Equation specifies the initial slope of the curves in Figures (41) and (42). Since Equation (5.12) gives the initial slope, it is an aid in finding the skin friction by the method of extrapolating the Reynolds shear stress distribution curves to $y/\delta = 0$. The value of skin friction coefficient C_f found in this way for profiles away from the position for flow reattachment, are given in Figures (41) and (42). In the same figures these values are compared with the values obtained from the mean velocity profiles following the method suggested by Clauser [24]. As would be expected there is close agreement between the skin friction coefficient values obtained by the two different methods. This is, perhaps, an indication of the accuracy of the measurements in the present investigation. It is evident from Figures (41) and (42) that the rate at which the Reynolds shear stress falls to zero decreases as the flow progresses downstream of reattachment. This suggests that the wall friction coefficient increases as the flow progresses

downstream of reattachment. Such an increase in C_f value was also found from the mean flow measurements.

Schubauer and Klebanoff [30] conducted an experimental investigation on a turbulent boundary layer near a smooth surface with pressure gradient sufficient to cause flow separation. A typical data curve of Schubauer and Klebanoff, measured at a station far upstream of separation, is shown plotted in Figures (41) and (42) by dotted lines. At s/C equal to approximately 0.8275 and 0.8175 for $\alpha = 0^\circ$ and $\alpha = 2^\circ$, respectively, there is good agreement between the two curves except for the central region of the boundary layer. Of course complete agreement is not to be expected since the two flow situations are different. However, the comparison demonstrates, qualitatively, how the turbulence velocity field recovers from upstream separation. Observation of Figures (41) and (42) indicates that the departure between the two data curves increases as the reattachment point is approached. Careful study of Reynolds shear stress distributions from Figures (41) and (42) suggests that the conditions near the wall are adjusted quite rapidly, while the outer portion of the boundary layer is not well adjusted to the upstream disturbances. As explained earlier, this is because the outer layer has a long memory.

At some distance downstream of flow reattachment, the Reynolds shear stress profiles are fully developed indicating that the turbulence structure is fully established

in this region. There is evidence from Figures (41) and (42) that the shear stress profiles tend to settle down to a nearly self-preserving form at approximately the same position on the airfoil surface where the mean velocity profiles exhibit similar shapes. However, the self-preservation in the shear stress profiles is not clearly pronounced.

5.5.4 Distribution of Eddy Viscosity

Adopting the Boussinesq concept of eddy viscosity, the Reynolds shear stress in Equation (5.10) can be written as

$$\tau_t = -\rho \overline{u'v'} = \rho \varepsilon \frac{\partial u}{\partial y}$$

$$\text{Therefore} \quad \varepsilon = \frac{\overline{-u'v'}}{\frac{\partial u}{\partial y}} \quad (5.13)$$

where ε is the kinematic eddy viscosity. Correcting the variables in Equation (5.13) for the effect of intermittency, ε can be written as

$$\varepsilon = \frac{\overline{-u'v'}}{\gamma} \frac{1}{\frac{\partial u_t}{\partial y}} \quad (5.14)$$

This eddy viscosity was evaluated from the experimental data using measured Reynolds stresses and mean velocities, with smooth curves fitted through the data to facilitate evaluation of derivatives. Mean velocities obtained by hot film

anemometer were employed in evaluating the eddy viscosity.

Figures (43) and (44) show the eddy viscosity distributions plotted in the nondimensional form as $\epsilon/(\delta*U)$ versus y/δ . In the reverse flow region, the nondimensional eddy viscosity appears to attain a maximum value with increasing distance from the wall and then approaches a linear variation with distance from the wall. In the region downstream of reattachment, the nondimensional eddy viscosity appears to attain a maximum value with increasing distance from the wall and then decreases slowly until it attains a nearly constant value across the main outerpart of the boundary layer. As the flow progresses downstream, the position of eddy viscosity maximum in the boundary layer moves from a value of $y/\delta \approx 0.65$ to $y/\delta \approx 0.4$, toward the wall. It is evident, after comparison with the data obtained by Klebanoff [28] on a smooth wall with zero pressure gradient, that the location of the maximum and the region with constant $\epsilon/(\delta*U)$ moved away from the wall in the present investigation.

It is seen from Figures (43) and (44) that the non-dimensional eddy viscosity $\epsilon/\delta*U$ is nearly constant across the main outer part of the boundary layer at all streamwise locations. The eddy viscosity in the outer part of the boundary layer can, therefore, be written as

$$\epsilon_o = K_2 (s^*) \delta * U \quad (5.15)$$

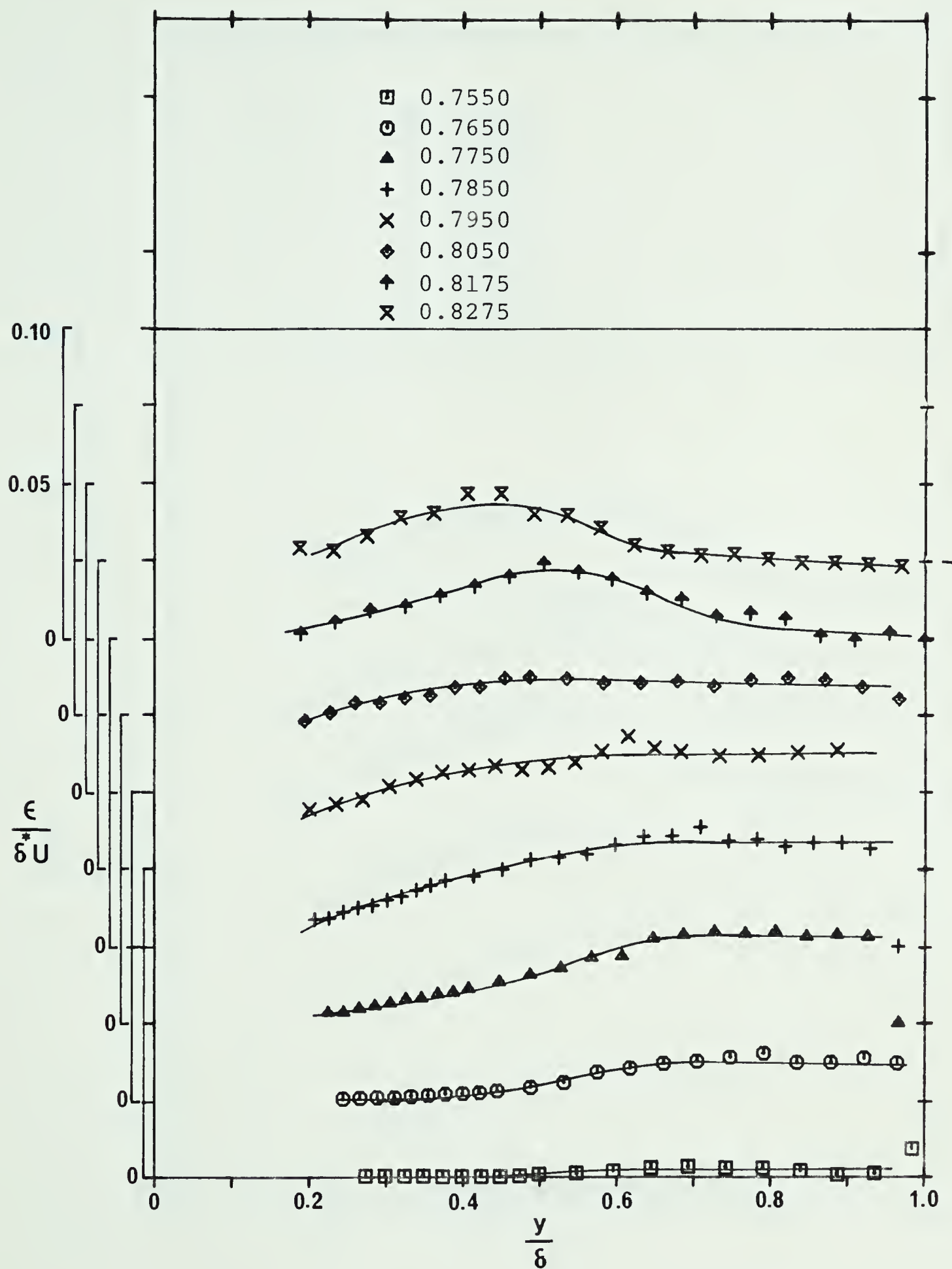


FIGURE 43--EDDY VISCOSITY DISTRIBUTION
 $Re = 0.8 \times 10^6$, $\alpha = 0^\circ$

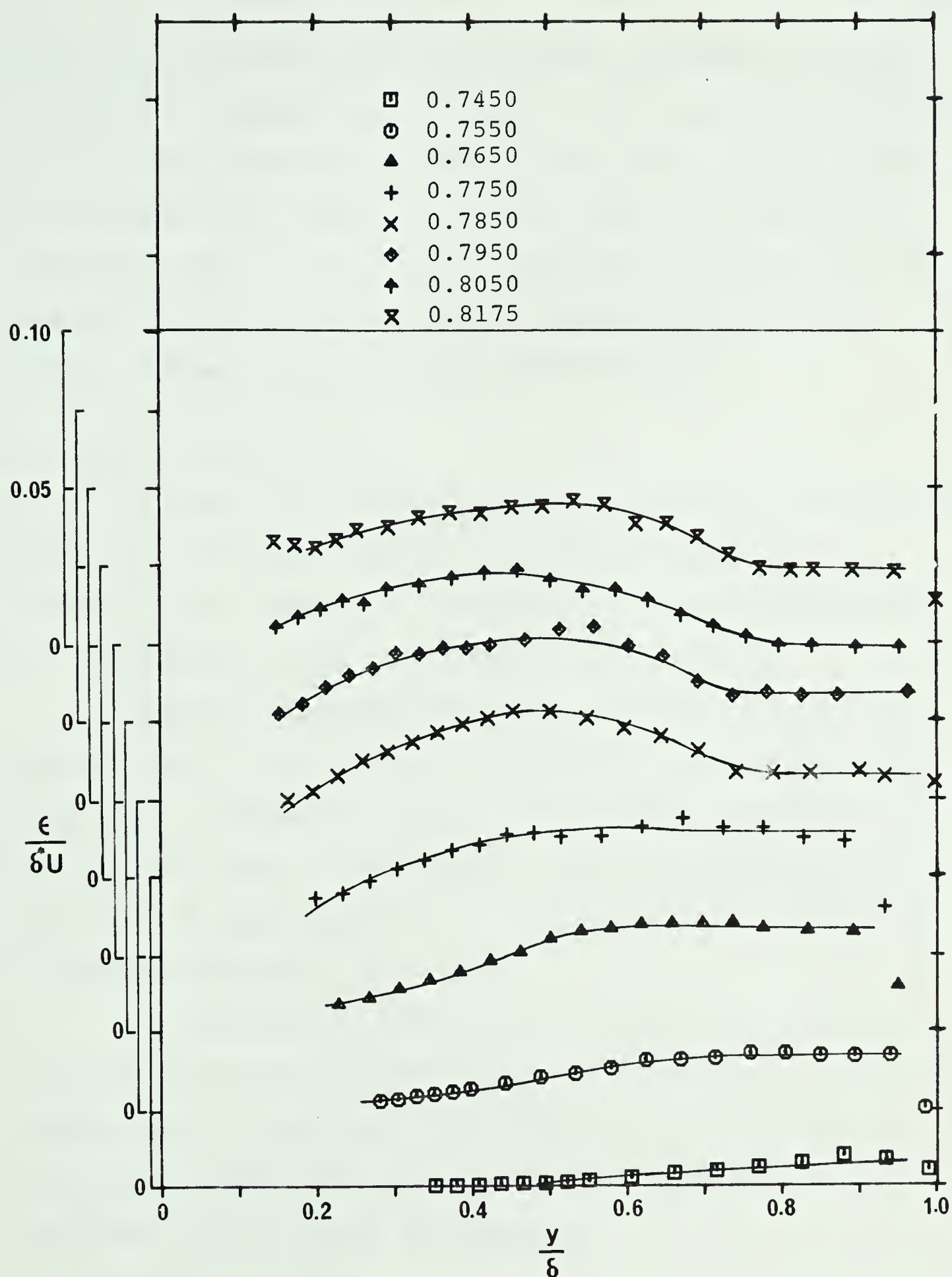


FIGURE 44--EDDY VISCOSITY DISTRIBUTION
 $Re = 0.8 \times 10^6$, $\alpha = 2^\circ$

where K_2 is a constant for a particular streamwise location. K_2 attains a maximum value of about 0.038 near flow reattachment and then decreases to about 0.023 near the region where the velocity field appears to settle down to a nearly self-preserving form. In a normally developing boundary layer K_2 does not depend on the streamwise location and it has a constant value of between 0.016 and 0.02 [25].

5.6 Eddy Viscosity Model

Figures (43) and (44) suggest that in the redeveloping region the turbulent boundary layer can be regarded as a composite layer made up of inner and outer regions depending on the behavior of eddy viscosity in those regions.

Separate expressions for eddy viscosity can be developed for use in each region. Therefore, a two-layer model which has two formulas, one for the inner region and another for the outer part of the boundary layer is developed here. This model is applicable only in the redeveloping region of the laminar separated flow field.

It was found in the previous section that the eddy viscosity in the outer part of the boundary layer is nearly constant and it is given by Equation (5.15). In order to use a single numerical constant for all streamwise locations, $K_2(s^*)$ can be expressed as

$$K_2(s^*) = K_3 f(s^*) \quad (5.16)$$

where K_3 is a numerical constant and $f(s^*)$ is a parameter. Since $f(s^*)$ depends on the behavior of the boundary layer at any streamwise location, it can be replaced by any one of the boundary layer parameters. The shape parameter H seems to be a reasonable choice. It is found that the value of H decreases from a higher value to a lower value as the flow progresses downstream of reattachment. Equation (5.15) can be rewritten as

$$\varepsilon_o = K_3 H \delta^* U \quad (5.17)$$

The value of the constant K_3 is determined from the data of mean flow and turbulent flow and it is about 0.0167.

Therefore, the expression for eddy viscosity in the outer layer, ε_o , is written as

$$\varepsilon_o = 0.0167 H \delta^* U \quad (5.18)$$

A convenient form is obtained by introducing non-dimensional variables in Equation (5.18). These variables

are defined as:

$$\Delta^* = \frac{\delta^*}{C}, \quad U^* = \frac{U}{U_\infty}, \quad \varepsilon_O^* = \frac{\varepsilon_O}{\nu} \quad (5.19)$$

If relations (5.19) are introduced into Equation (5.18) the following equation is obtained:

$$\varepsilon_O^* = 0.0167 H \Delta^* U^* Re \quad (5.20)$$

where Re is the Reynolds number based on the airfoil chord. Equation (5.20) is the proposed eddy viscosity expression in the outer layer.

5.6.2 Inner Layer

According to experiments with turbulent boundary layers, for example experiments of Klebanoff [28], eddy viscosity varies linearly with y in the inner region. However, such a variation cannot be verified with the present experiments due to lack of data close to the wall. But, at this stage it is reasonable to assume that such a variation exists in the flow field of present study. Then the variation of eddy viscosity in the inner layer can conveniently be described by Prandtl's mixing length theory, that is

$$\varepsilon_i = l^2 \left| \frac{\partial u}{\partial y} \right| \quad (5.21)$$

where l , the mixing length, is given by

$$l = K_1 y \quad (5.22)$$

K_1 is an empirical constant ($= 0.4$) known as Von Karman's constant. Equation (5.22) is to be modified to account for the viscous sublayer by using an empirical expression. The modification proposed by Van Driest [31] is used here and it is written as

$$l = K_1 y \left[1 - \exp \left(-\frac{y}{A} \right) \right] \quad (5.23)$$

where A is a damping constant defined as $26\nu(\tau_w/\rho)^{-1/2}$. This expression was obtained by relating the viscous sublayer to Stokes flow and it provides continuous velocity and shear distribution in the inner layer. Van Driest obtained Equation (5.23) for a flat plate flow with zero pressure gradient. Cebeci and Smith [32] modified the expression for the damping constant A to account for pressure gradient. The modification is obtained by defining A as $26\nu \left(\frac{\tau}{\rho} \right)^{-1/2}$ and then determining τ from the approximated Equation (5.12). From Equation (5.12) it follows that the shear stress close to the wall may be written as

$$\tau = \tau_w + \frac{\partial p}{\partial s} y \quad (5.24)$$

Then the constant A becomes

$$26\nu\left(\frac{\tau_w}{\rho} + \frac{dp}{ds} \frac{y}{\rho}\right)^{-\frac{1}{2}}$$

with these modifications the eddy viscosity expression (5.21) for the inner layer becomes

$$\epsilon_i = K_1^2 y^2 \left\{ 1 - \exp \left[-\frac{y}{26\nu} \left(\frac{\tau_w}{\rho} + \frac{dp}{ds} \frac{y}{\rho} \right)^{\frac{1}{2}} \right] \right\}^2 \left| \frac{\partial u}{\partial y} \right| \quad (5.25)$$

If relations

$$s^* = s/C, \quad y^* = y/C, \quad u^* = \frac{u}{U_\infty}, \quad U^* = \frac{U}{U_\infty}, \quad \epsilon_i^* = \frac{\epsilon_i}{\nu}$$

and $C_f = \frac{\tau_w}{\frac{1}{2}\rho U^2}$ are introduced into Equation (5.25) the

following dimensionless equation is obtained:

$$\epsilon_i^* = 0.16 \operatorname{Re} y^{*2} \left| \frac{\partial u^*}{\partial y^*} \right| \left\{ 1 - \exp \left[-\frac{\operatorname{Re} y^*}{26} \left(\frac{U^{*2}}{2} C_f - U^* \frac{dU^*}{ds^*} y^* \right)^{\frac{1}{2}} \right] \right\}^2 \quad (5.26)$$

Equation (5.26) is shown plotted in Figure (45) together with the present experimental data of the redeveloping region. In those figures full line represents Equation (5.26) and symbols represent experimental data. It appears from these figures that the available data near the wall tends to follow the line represented by Equation (5.26). This lends support to the assumption that eddy viscosity varies linearly with y in the inner region of the redeveloping boundary layer.

In the two-layer model proposed here, the outer layer eddy viscosity is given by Equation (5.20) and the inner

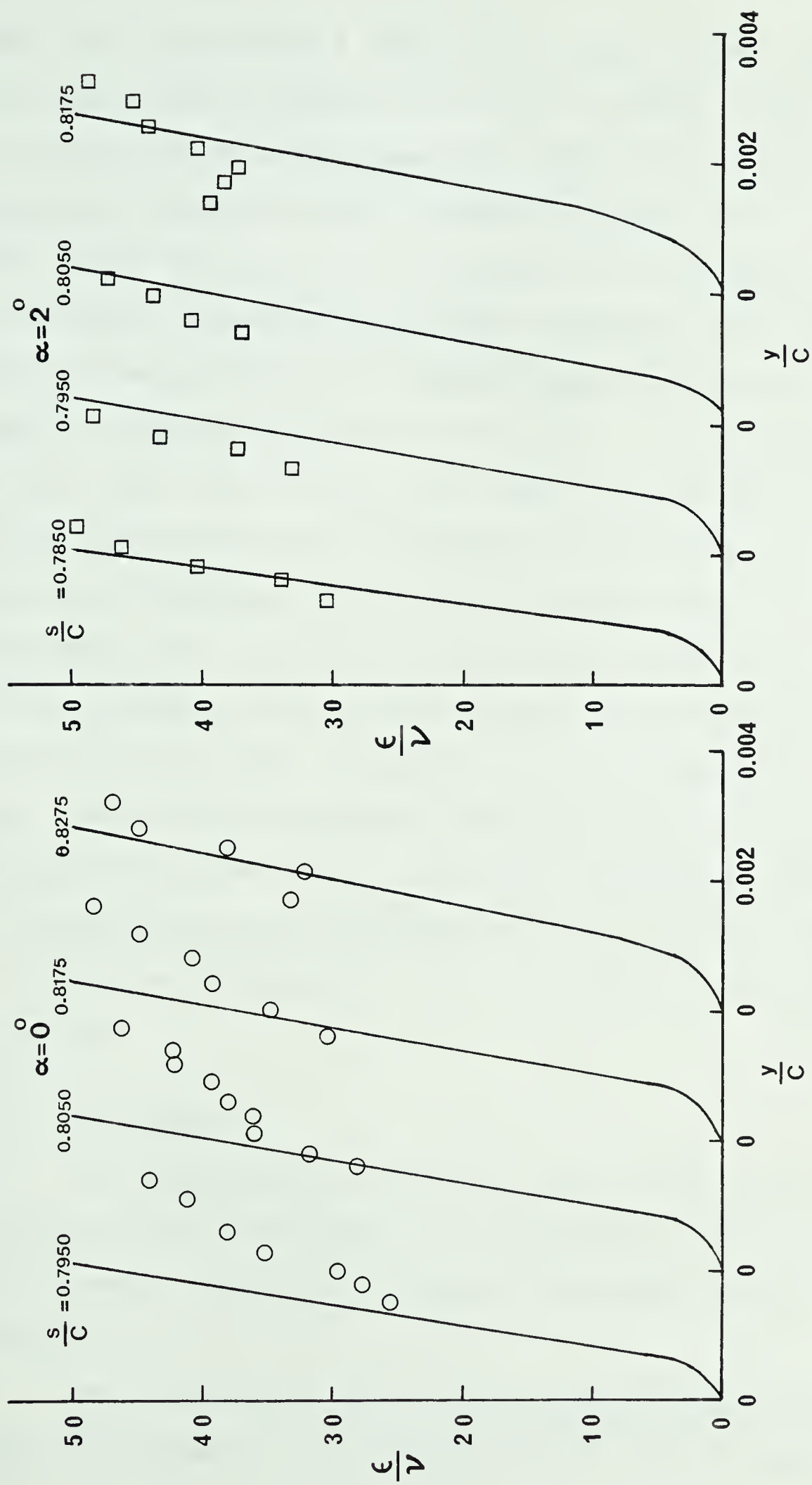


FIGURE 45--INNER LAYER EDDY VISCOSITY DISTRIBUTION, $Re = 0.8 \times 10^6$
— EQUATION (5.26); O, □ PRESENT MEASUREMENTS

layer eddy viscosity is given by Equation (5.26). The constraint used to define the inner and outer layers is the continuity of the eddy viscosity; from the wall outward, the expression for inner eddy viscosity applies until $\epsilon_i = \epsilon_o$. Even though the flow that was treated in the present study is different from the normal flow situations, the inner layer eddy viscosity expression obtained here is the same as that used in existing turbulence models [32]. As was explained earlier, the flow in the inner region is governed essentially by the local conditions and perhaps that is the reason for the validity of Equation (5.26) in the present flow. On the other hand, the flow in the outer region depends not only on the local conditions but also on the whole history of events in the flow upstream. Therefore, the expression for outer layer eddy viscosity obtained from the present data is different than that used in existing turbulence models. The turbulence model developed here will be used in Chapter VI to predict the boundary layer in a redeveloping region on an airfoil.

5.7 Conclusions

The magnitudes of Reynolds shear stress and turbulence intensities have a maximum in the immediate vicinity of flow reattachment, indicating an intense turbulent mixing in this region.

The turbulence level in the redevelopment region after reattachment is relatively higher than the turbulence

level in a region where the turbulent boundary layer is developing normally.

There is a high level of turbulence at distances well away from the wall.

The conditions in the inner region of the boundary layer are adjusted quite rapidly, while the outer region is not well adjusted and continues to show the effects of the upstream perturbation.

Self preservation of turbulence velocity field appears to attain at about the same streamwise location on the airfoil where the mean velocity field was found to attain equilibrium conditions.

The nondimensional eddy viscosity $\epsilon/\delta*U$ is nearly constant across the outer portion of the boundary layer.

The inner layer eddy viscosity can be determined from the expression proposed by Cebeci and Smith [32].

CHAPTER VI

ANALYSIS OF LAMINAR SEPARATED FLOW FIELD

6.1 Introduction

There are many excellent procedures available in the literature for the analysis of boundary layers on wing sections. However, there is presently no adequate theory to predict the flow characteristics in the case when a laminar separation bubble exists as a mechanism of transition from laminar to turbulent boundary layer flow. Short laminar bubbles are known to have little effect on either lift or drag, and the assumption that the bubble simply represents a transition point will allow the analysis to proceed. However, in the case of the midchord laminar separation bubbles that occur on laminar wing sections at a relatively low Reynolds number, the separated flow region has an appreciable effect on the turbulent boundary layer development and consequently affects the drag of the wing section. Development of a viscous flow analysis method which takes account of the flow field generated by a midchord bubble is the ultimate objective of the work reported here.

The composite physical nature of the laminar separated flow field is shown sketched in Figure (46). The primary difficulties in treating this problem analytically derive from the presence of reverse flow inside the bubble, the

interaction between the viscous and inviscid flow, the occurrence of transition from laminar to turbulent flow in the free shear layer, and the redevelopment of turbulent boundary layer just downstream of reattachment. Most of the previous work on transitional separation bubbles has been experimental. Analyses have been carried out using semi-empirical formulations for predicting what type of bubble (long or short) will occur in any given case, what will be the length of the bubble, and what effect the bubble will have on the stalling characteristics of an airfoil. Such semi-empirical theories have been reported by Owen and Klanfer [1], and Horton [9]. The small separation bubbles which form near the leading edge of airfoil prior to the onset of leading edge stall were analysed using an integral formulation by Crimi and Reeves [11]. The separation bubbles which form near the midchord of an airfoil were analysed numerically by Briley and McDonald [10]. However, as will be discussed later in this chapter, the previous modeling has not been adequate for analysis of the laminar separated flow field. The present modeling is based on the already existing work of others together with the observations of present experimental study.

A method of analysis for computing the laminar separated flow field with specified free stream velocity distributions is described here. The analysis assumes that the bubble is thin enough for the boundary layer concept to be

valid; and the interaction between the shear layer and inviscid free stream is limited to the bubble region. The analysis is based on finite difference solutions to the steady boundary layer equations. The boundary layer in the laminar region of the flow field is divided into two layers (shown in Figure (46)), along an assumed line of zero velocity, and solutions are computed by integrating the laminar boundary layer equations in each layer. The viscous-inviscid interaction is taken into account through an interaction between inviscid and boundary layer solutions such that the boundary conditions are matched. A correlation of local shear layer parameters at transition is used for determining the onset of transition in the separated laminar shear layer. The redeveloping turbulent boundary layer just downstream of reattachment is calculated by utilizing Boussinesq's eddy viscosity concept. The two layer eddy viscosity model that was developed in chapter V is used in this connection. The present numerical procedure is an outgrowth of the method developed in chapter II. Computed solutions for laminar separated flow fields are compared with the present experimental data and the experimental measurements of Bursnall and Loftin [4]. In general, the agreement is regarded to be reasonably good.

6.2 Physical Structure of Separated Flow Field

The experimental investigation of a laminar separated flow field covered the study of both the mean and turbulent characteristics of the flow, and was reported in detail in chapters IV and V. The experimental study corroborated the observations of other investigators in many respects; but also revealed some interesting characteristics that have not hitherto been available. Having in view the already existing work of others together with the observations of the present experimental study it is possible to present a composite physical picture of the laminar separated flow field. A schematic diagram of the flow field is shown in Figure (46).

The laminar boundary layer separates from the airfoil surface, transition occurs in the separated shear layer, and the resulting turbulence spreads and entrains the flow so that it reattaches to the surface. The region underneath the separated flow, between the points of separation and reattachment, and set into circulatory motion, is referred to as the recirculation region. The upper limit of this region is defined by the streamline (shown on Figure (46)) which leaves the surface at the laminar separation point and subsequently rejoins the surface at the reattachment point. Hence it is the dividing streamline between the circulatory flow and the exterior separated flow which passes downstream. The circulatory motion in the recirculation region apparently helps

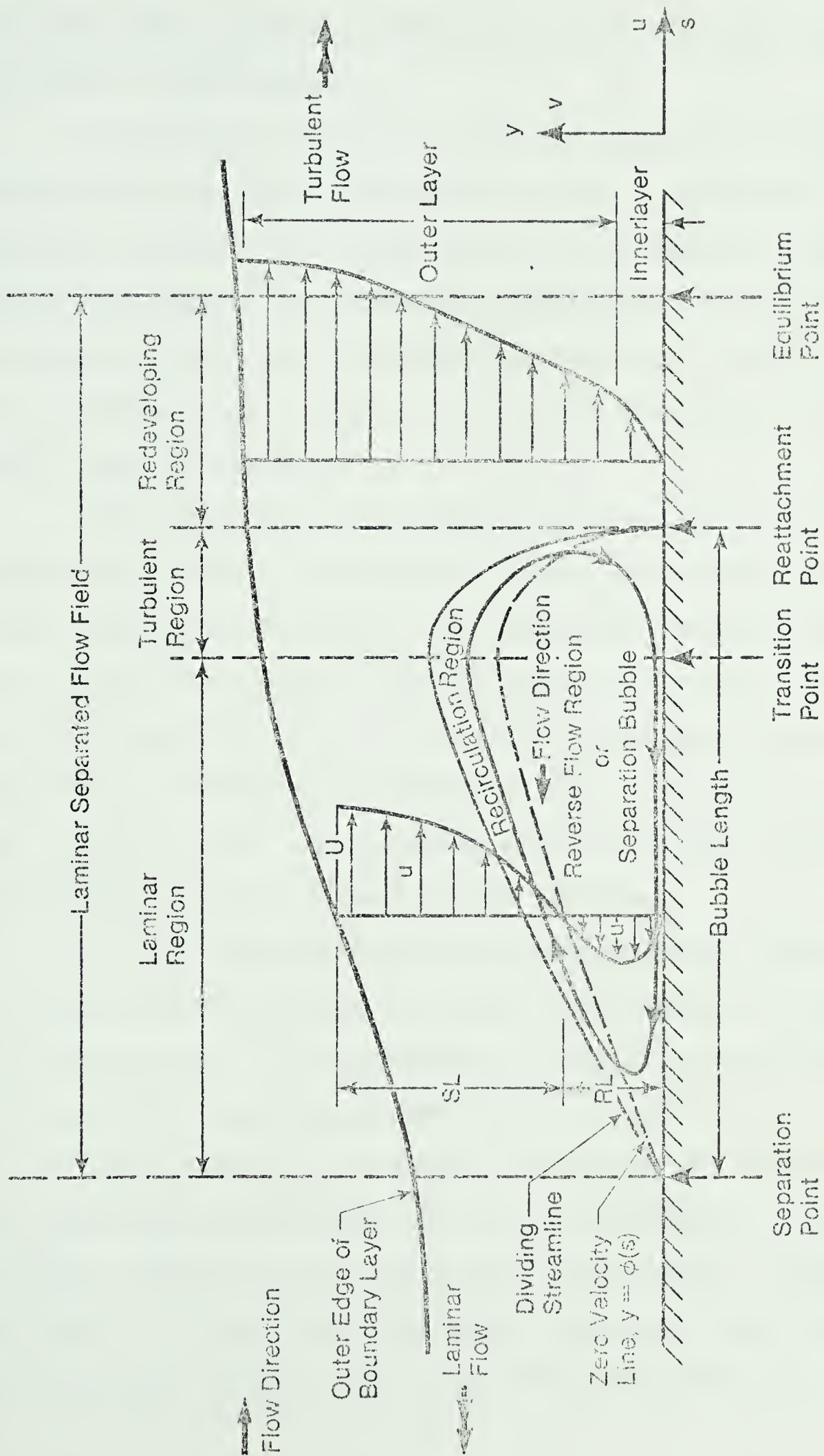


Figure 46. Composite Picture of Laminar Separated Flowfield

the entrainment process by which the turbulent shear layer reattaches to the surface.

The domain in which the flow is entirely reversed is referred to as the reverse flow region or, better, separation bubble. The upper limit of the bubble or the shape of the bubble is defined by the line of zero velocity. The length of the region between the limits of separation and reattachment is commonly taken to be the length of the laminar separation bubble.

After separation the width of the laminar shear layer spreads quite slowly, presumably because the stresses are all viscous and therefore small. The separated laminar shear layer is much less stable than an attached boundary layer and thus transition is triggered in the separated region. Transition to turbulence accelerates the expansion of the shear layer and then the intense turbulent mixing causes the flow finally to reattach to the surface.

At some streamwise position downstream of reattachment the redeveloping turbulent boundary layer reaches a nearly equilibrium state. This streamwise position is referred to as the equilibrium point (shown on Figure (46)).

Traditionally, the extent of the laminar separated flow field has been defined as the region between the points of laminar separation and turbulent reattachment. However, the study of the mean and turbulence velocity fields indicated that the region between the limits of reattachment point and

equilibrium point is also important while studying the behavior of laminar separation bubble. Therefore, it is proper to define the extent of the laminar separated flow field as the region between the limits of laminar separation point and the equilibrium point. As shown in Figure (46), the extent of the flow field is found to be characterized by three regions:

- (1) Laminar region: is the region between the points of separation and transition. The velocity profiles are characterized by negative velocities (reverse flow).
- (2) Turbulent region: is the region between the points of transition and reattachment. In this region turbulent mixing effects infiltrate the flow field. The velocity profiles are characterized by negative velocities (reverse flow).
- (3) Redeveloping region: is the region between the limits of reattachment point and equilibrium point. The flow starts recovering from upstream separation and at the equilibrium point the boundary layer almost becomes oblivious to the initial perturbation. Both the mean velocity profile and turbulence distribution profile at the equilibrium point are characterized by a self-preserving form.

6.3 Method of Analysis

In a general boundary layer analysis laminar flow calculations proceed from the leading edge to the point of turbulent transition, and the turbulent flow calculations proceed from the point of transition to the trailing edge of the airfoil. A method of analysis analogous to this approach could be used for predicting laminar separated flow field. However, the calculation procedure should account for the reverse flow, viscous-inviscid interaction transition to turbulent flow in the separated shear layer, and the redevelopment of turbulent boundary layer after reattachment.

6.3.1 Previous Methods

There have been only two previous attempts to compute a transitional separation bubble in detail. Crimi and Reeves [11] devised an integral procedure for analysis of the leading edge separation bubbles which accounts for viscous-inviscid interaction and transition to turbulent flow. In their formulation the velocity profiles for laminar or fully turbulent flow are characterized by a single parameter which is not related to the local pressure gradient. The family of similar solutions for reversed flow found by Stewartson [33] is employed for analyzing the free shear layer. The results of the analysis between separation and reattachment are in good agreement with the flow measurements reported by Gault [5]. However, direct application of Crimi and Reeves

procedure to the present study is not warranted for the following reasons. Since the bubbles that are treated in the present study are about ten times longer than the leading edge bubbles, the empirical results that are used in Crimi and Reeves analysis do not apply to the present flow. Secondly, it is not clear from their calculations whether such an integral formulation would be effective for analyzing the redevelopment flow just downstream of reattachment.

Briley and McDonald [10] developed a method for performing detailed computations of separation bubbles which occur near the midchord of an airfoil. Their method of analysis consists of solving the two dimensional time dependent boundary layer or Navier-Stokes equations using a finite difference method. The method of analysis uses the McDonald-Fish [34] turbulence model to predict the development of the time mean flow field as influenced by the free stream turbulence level. The turbulence model is based on the solution of an integral form of the turbulence kinetic energy equation. The agreement between computed velocity profiles and measured profiles is reasonably good, except near reattachment. Rapid flow variations just downstream of reattachment could not be predicted by their method. Velocity profiles and the position of transition computed by Briley-McDonald procedure are sensitive to the free-stream turbulence level even when that level of turbulence is relatively low ($< 0.2\%$). However, for a relatively low turbulence level ($< 0.25\%$) such an

effect of turbulence is not observed in the experiments [5,37].

6.3.2 Present Method

The present method of analysis consists of finite difference solutions to the steady boundary layer equations for the flow in the separated flow field. The analysis assumes that the bubble is thin enough for the boundary layer approximation to be valid. The effects of streamline and surface curvatures, and the associated normal pressure gradients are not included in the calculation method.

The calculations begin from a point just upstream of laminar separation. An initial velocity profile calculated from the upstream laminar boundary layer is necessary to start the solution. Such an initial profile is provided by the laminar boundary layer analysis that was developed in chapter II. In the laminar region of the separated field the boundary layer is divided into two layers, along an assumed line of zero velocity, and solutions are computed for each layer.

The interaction between the separated boundary layer and outer inviscid flow gives rise to a change in the interface boundary conditions. In other words, the presence of the bubble alters the velocity distribution outside the boundary layer that would otherwise be imposed on the bubble. In the present viscous-inviscid interaction model it is assumed that the interaction is limited to the region between the limits of separation and reattachment; and it is also assumed that the

interaction is due to the displacement of streamlines away from the wall.

A correlation of local shear layer parameters has been developed for determining transition to turbulent flow in the laminar shear layer. The correlation is based on an analogy between transition in separated shear layers and transition produced by two dimensional roughness elements.

Due to the lack of a turbulence model to describe the flow, the solutions in the turbulent region of the separated flow field (shown on Figure (46)) are not calculated here. In any case, numerical instabilities are found to exist in this region. A solution in the redeveloping region downstream of the reattachment point is initiated utilizing the velocity profile at transition to fully turbulent flow in the separated shear layer. Solutions of the equations of turbulent boundary layer in the redeveloping region are obtained using Boussinesq's eddy viscosity concept. The method employs the eddy viscosity model that was developed from the measurements of turbulence velocity field in this region.

6.4 Formulation of Governing Equations

6.4.1 Laminar Region

As shown in Figure (46), the boundary layer in the laminar region of the bubble is divided into two layers denoted by RL and SL respectively, where RL represents the layer

inside the domain of reverse flow while SL corresponds to the layer in the domain of laminar shear layer. The line $y = \phi(s)$ separates the two layers RL and SL and along this line $u = 0$. Thus, the original boundary layer problem is separated into two separate boundary layer problems in RL and SL which can be solved in each region with appropriate boundary conditions. As will be shown, a composite solution is obtained by matching the solution in SL with the solution in RL along the line $y = \phi(s)$.

The laminar boundary layer equations in their non-dimensional form can be written as (Equations 2.4, 2.5 and 2.6)

$$\frac{\partial u^*}{\partial s} + \frac{\partial v^*}{\partial y} = 0 \quad (6.1)$$

$$u^* \frac{\partial u^*}{\partial s} + v^* \frac{\partial u^*}{\partial y} = U^* \frac{dU^*}{ds} + \frac{1}{Re} \frac{\partial^2 u^*}{\partial y^2} \quad (6.2)$$

with the boundary conditions

$$y^* = 0: u^* = 0, v^* = 0 \quad (6.3)$$

$$y^* \rightarrow \infty: u^* \rightarrow U^*$$

Klemp and Acrivos [35] found that it is more convenient to rewrite Equations (6.1), (6.2) and (6.3) using Prandtl's transposition theorem which is described by Rosenhead [36].

According to this theorem, from any solution of the boundary layer Equations (6.1) and (6.2) further solutions can be derived by writing:

$$u^* = u^*(s^*, \xi) \quad (6.4)$$

where $\xi = y^* - \phi(s^*)$

The stream function is then

$$\psi^* = \psi^*(s^*, \xi)$$

and hence

$$V^* = v^*(s^*, \xi) - \phi'(s^*) u^*(s^*, \xi) \quad (6.5)$$

where V^* is the velocity associated with ξ .

Substitution of Equations (6.4) and (6.5) into Equations (6.1) and (6.2) yields

$$\frac{\partial u^*}{\partial s^*} + \frac{\partial V^*}{\partial \xi} = 0 \quad (6.6)$$

$$u^* \frac{\partial u^*}{\partial s^*} + V^* \frac{\partial u^*}{\partial \xi} = U^* \frac{dU^*}{ds^*} + \frac{1}{Re} \frac{\partial^2 u^*}{\partial \xi^2} \quad (6.7)$$

The boundary conditions for each region are, then

$$\left. \begin{array}{l} \xi = -\phi(s^*) : u^* = 0, V^* = 0 \\ \xi = 0 : u^* = 0 \end{array} \right] \text{ in RL} \quad (6.8)$$

$$\left. \begin{array}{l} \xi = 0 : u^* = 0, V^* = V_\phi^*(s^*) \\ \xi \rightarrow \infty : u^* \rightarrow U^* \end{array} \right] \text{ in SL} \quad (6.9)$$

$V_{\phi}^*(s^*)$ is the value of V^* along $y^* = \phi(s^*)$. The boundary layer problem of the laminar region in the transformed coordinates is shown in Figure (47).

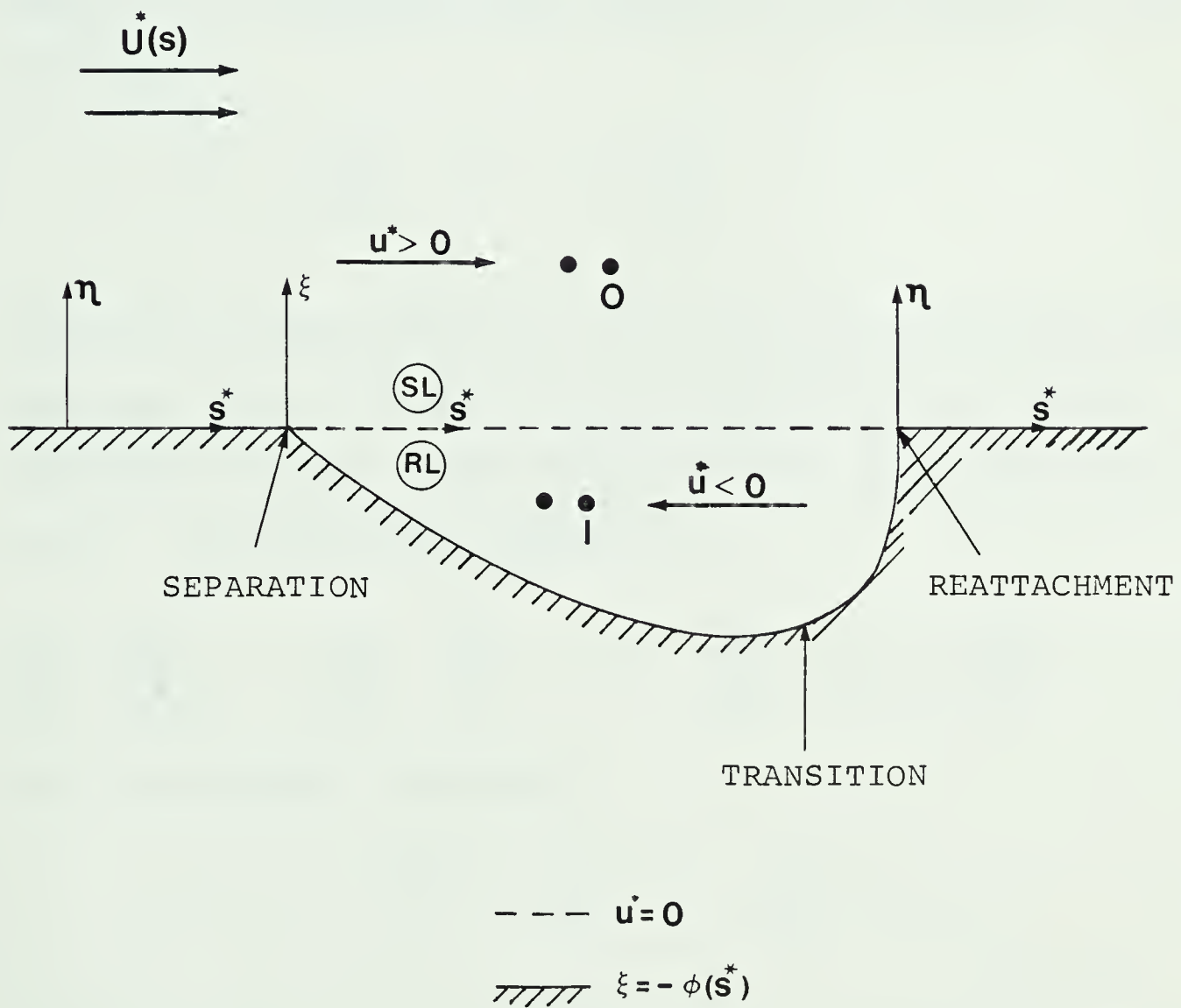


FIGURE 47--SCHEME OF COORDINATES

Equations (6.6) and (6.7) as such are difficult to solve. However, a far more convenient form is obtained by introducing two transformation variables, a dimensionless height η and a dimensionless stream function f , defined as:

$$\eta = \xi \sqrt{\frac{U^*}{s^*} \text{Re}}, \quad \psi^* = (s^*, \xi) = f(s^*, \eta) \sqrt{\frac{U^* s^*}{\text{Re}}} \quad (6.10)$$

where ψ^* is a dimensionless stream function defined by the relations:

$$u^* = \frac{\partial \psi^*}{\partial \xi}, \quad v^* = - \frac{\partial \psi^*}{\partial s^*} \quad (6.11)$$

Since the stream function ψ^* satisfies the continuity equation, Equations (6.6) and (6.7) can be combined into a single equation in terms of the stream function using the relations (6.11). The resulting equation is

$$\frac{\partial \psi^*}{\partial \xi} \frac{\partial^2 \psi^*}{\partial s^{*2} \partial \xi} - \frac{\partial \psi^*}{\partial s^*} \frac{\partial^2 \psi^*}{\partial \xi^2} = U^* \frac{dU^*}{ds^*} + \frac{1}{\text{Re}} \frac{\partial^3 \psi^*}{\partial \xi^3} \quad (6.12)$$

with the boundary conditions

$$\left. \begin{array}{l} \xi = -\phi(s^*) : \frac{\partial \psi^*}{\partial \xi} = 0, \quad \frac{\partial \psi^*}{\partial s^*} = 0 \\ \xi = 0 : \frac{\partial \psi^*}{\partial \xi} = 0 \end{array} \right] \text{ in RL} \quad (6.13)$$

$$\left. \begin{aligned} \xi = 0 & : \frac{\partial \psi^*}{\partial \xi} = 0; \quad \frac{\partial \psi^*}{\partial s^*} = \left. \frac{\partial \psi^*}{\partial s^*} \right|_{\phi} \\ \xi \rightarrow \infty & : \frac{\partial \psi^*}{\partial \xi} \rightarrow U^*(s^*) \end{aligned} \right] \text{ in SL} \quad (6.14)$$

If relations (6.10) are introduced into Equation (6.12) and if $\frac{\partial f}{\partial \eta}$ is represented by f' , etc., the following equation is obtained:

$$f''' + \frac{1+\beta}{2} f f'' + \beta (1 - f'^2) = s^* \left[f' \frac{\partial f'}{\partial s^*} - f'' \frac{\partial f}{\partial s^*} \right] \quad (6.15)$$

The term $\beta(s^*) = \frac{s^*}{U} \frac{dU^*}{ds}$ is a pressure gradient parameter and f' turns out to be the velocity ratio u/U . The boundary conditions are:

$$\left. \begin{aligned} \eta = -\phi(s^*) \sqrt{\frac{U^*}{s}} \text{ Re: } f = 0, f' = 0 \\ \eta = 0 : f' = 0 \end{aligned} \right] \text{ in RL} \quad (6.16)$$

$$\left. \begin{aligned} \eta = 0 : f = f(s^*, 0), f' = 0 \\ \eta \rightarrow \infty : f' \rightarrow 1 \end{aligned} \right] \text{ in SL} \quad (6.17)$$

Equation (6.15) is the governing equation in the laminar region with the boundary conditions (6.16) and (6.17) in the two separate layers RL and SL respectively. Equation (6.15) is a third order nonlinear partial differential equation which is more amenable to a numerical solution. The solution

of this equation subjected to the boundary conditions (6.16) and (6.17) will be described in later sections.

6.4.2 Shape of the Bubble

As explained earlier the shape of the bubble is defined by the line of zero velocity. As seen from Equations (6.16) and (6.17) this line of zero velocity, $y^* = \phi(s^*)$, is required for solving Equation (6.15) in the laminar region. On purely geometrical considerations, an attempt was made to find a curve which fits the bubble shapes in the laminar region that are given in references [4] and [5]. A curve that is given by the relation:

$$y^* = \frac{3 \times 10^4 s^{*1.5}}{(R\theta_s)^2} \quad (6.18)$$

was seen to provide a good approximation to the shapes given by reference data. This equation was used to determine the line of zero velocity in the laminar region of the separated flow field.

6.4.3 Length of the Bubble

Since the flow phenomena determining bubble separation are directly related to the behavior of the boundary layer, it appears appropriate to relate the length of the bubble to a Reynolds number typical of local conditions in the boundary layer. For this purpose the Reynolds number based on the momentum thickness and the velocity just outside the boundary layer, both measured at separation, appears to be a reasonable choice. Thus, a relation

of the form:

$$L_b = f\left(\frac{U\theta}{V}\right)_s = f(R\theta_s) \quad (6.19)$$

is postulated for determining the length of the bubble. The length of the bubble, L_b , is expressed as a percent of chord. Using the experimental data of Bursnall and Loftin [4], Gault [5], and the present study, Equation (6.19) was plotted in Figure (48). The curve drawn through the points is a plot of the simple relation:

$$L_b = \frac{75}{R\theta_s} \quad (6.20)$$

which is seen to provide good correlation with the data. This equation was used in the present calculations to locate the position of reattachment.

6.4.4 Transition Criterion

Transition from laminar to turbulent flow in a boundary layer depends on many variables including Reynolds number, free stream turbulence, pressure gradient, and surface roughness. Experimental pressure distributions indicate that the pressure gradients in the region between the limits of laminar separation and transition are not large. A.D. Young [37] indicated that the effect of free stream turbulence in causing an earlier transition in the separated shear layer is relatively small when the turbulence level is below 0.35%. The positions of transition determined by Gault [5] are in good agreement

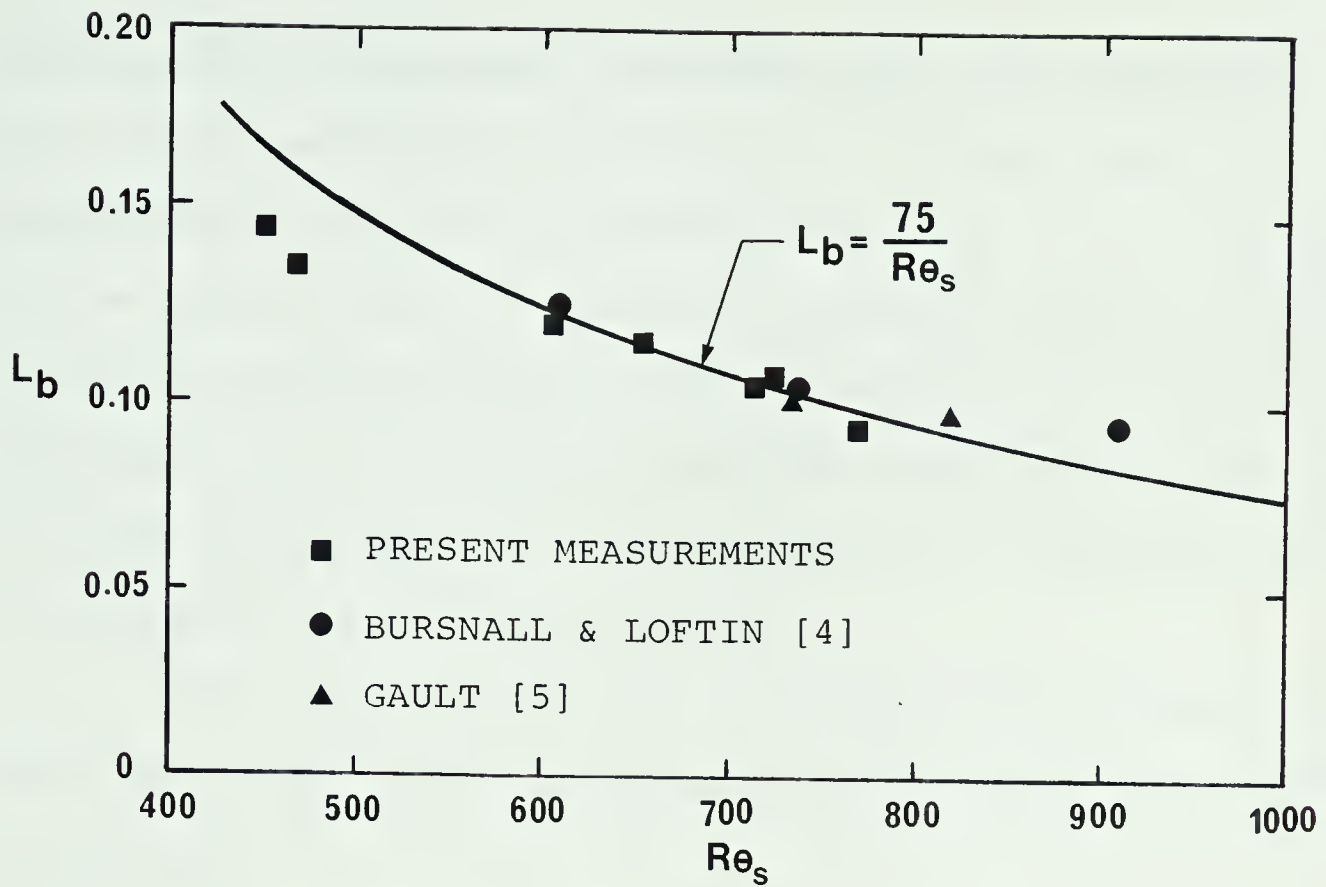


FIGURE 48--CORRELATION OF BUBBLE LENGTH

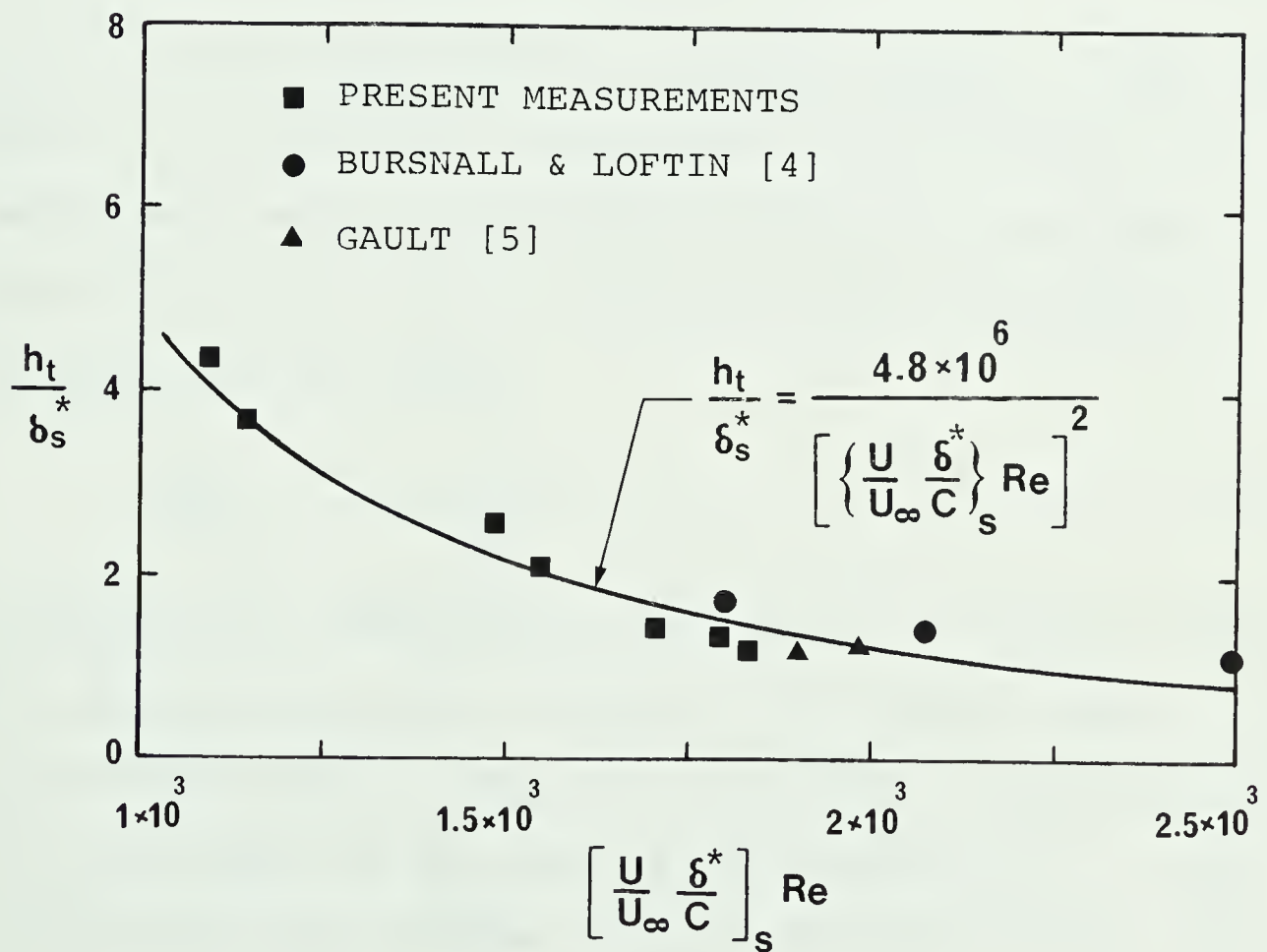


FIGURE 49--CORRELATION OF SHEAR LAYER PARAMETERS AT TRANSITION

with the data of Bursnall and Loftin [4] even though the free stream turbulence level for the reference data is a few hundredths of 1 percent in contrast to 0.15 to 0.20 percent for the data of Gault. Therefore, when the pressure gradients and free stream turbulence levels are small the mechanism for transition in a laminar separated flow field may be taken to be somewhat similar to the mechanism for transition caused by an element of surface roughness.

Tani and Hama [38] have reported that test data for transition produced by roughness elements could be correlated in the form:

$$\left(\frac{U\delta}{\nu}\right)_{\text{transition}} = f\left(\frac{k}{\delta}\right) \quad (6.21)$$

where k is the height of the roughness element. Crimi and Reeves [11] postulated a correlation for transition in a leading edge bubble which employs parameters analogous to those given in Equation (6.21). Based on their postulation, a correlation of the form:

$$\left(\frac{U\delta^*}{\nu}\right)_s = f\left(\frac{h_t}{\delta_s}\right) \quad (6.22)$$

is proposed for determining transition in a laminar separated flow field such as that treated in the present study. In this equation subscript s indicates conditions at separation and h_t is the height of the line of zero velocity ($y = \phi(s)$) at transition from laminar to fully turbulent flow. For

convenience, Equation (6.22) is written as:

$$\left(\frac{U}{U_\infty} \frac{\delta^*}{C} \right)_s \text{Re} = f \left(\frac{h_{t/C}}{\delta_s^*/C} \right) \quad (6.23)$$

Using the experimental data of Bursnall and Loftin [4], Gault [5], and the present study, Equation (6.23) is plotted in Figure (49). The curve drawn through the points is given by the relation

$$\left[\frac{h_{t/C}}{\delta_s^*/C} \right] = \frac{4.8 \times 10^6}{\left[\left(\frac{U}{U_\infty} \frac{\delta^*}{C} \right)_s \text{Re} \right]^2} \quad (6.24)$$

The excellent fit indicates the data are well correlated by the proposed relation. In the present calculations the position of transition to fully turbulent flow was determined by continuously evaluating $\frac{h/C}{\delta_s^*/C}$ in the laminar region and comparing its value to that of the right hand side of Equation (6.24).

6.4.5 Redeveloping Region

Steady, two-dimensional, incompressible turbulent boundary layer equations are written as [25]:

$$\frac{\partial u}{\partial s} + \frac{\partial v}{\partial y} = 0 \quad (6.25)$$

$$u \frac{\partial u}{\partial s} + v \frac{\partial u}{\partial y} = U \frac{dU}{ds} + \frac{\partial}{\partial y} \left[v \frac{\partial u}{\partial y} - \overline{u'v'} \right] \quad (6.26)$$

with boundary conditions

$$\begin{aligned} y = 0 & : u = 0, v = 0 \\ y \rightarrow \infty & : u \rightarrow U \end{aligned} \quad (6.27)$$

According to Boussinesq's eddy viscosity concept, the eddy viscosity ϵ , is defined as:

$$\epsilon = - \frac{\overline{u'v'}}{\frac{\partial u}{\partial y}}$$

or

$$\overline{-u'v'} = \epsilon \frac{\partial u}{\partial y} \quad (6.28)$$

Upon introducing this relation in Equation (6.26), the following Equation is obtained:

$$u \frac{\partial u}{\partial s} + v \frac{\partial u}{\partial y} = U \frac{dU}{ds} + v \frac{\partial^2 u}{\partial y^2} + \epsilon \frac{\partial^2 u}{\partial y^2} + \frac{\partial u}{\partial y} \frac{\partial \epsilon}{\partial y} \quad (6.29)$$

A convenient form is obtained by introducing nondimensional variables into the boundary layer equations. These non-dimensional variables are defined as:

$$\begin{aligned} s^* &= s/C, \quad y^* = \frac{y}{C}, \quad u^* = \frac{u}{U_\infty}, \quad v^* = \frac{v}{U_\infty} \\ U^* &= \frac{U}{U_\infty}, \quad \epsilon^* = \frac{\epsilon}{\nu} \end{aligned} \quad (6.30)$$

If relations (6.30) are introduced into Equations (6.25) and (6.29), the following equations are obtained:

$$\frac{\partial u^*}{\partial s^*} + \frac{\partial v^*}{\partial y^*} = 0 \quad (6.31)$$

$$\begin{aligned} u^* \frac{\partial u^*}{\partial s^*} + v^* \frac{\partial u^*}{\partial y^*} &= U^* \frac{dU^*}{ds^*} + \frac{1}{Re} \frac{\partial^2 u^*}{\partial y^{*2}} + \frac{1}{Re} \epsilon^* \frac{\partial^2 u^*}{\partial y^{*2}} \\ &+ \frac{1}{Re} \frac{\partial u^*}{\partial y^*} \frac{\partial \epsilon^*}{\partial y^*} \end{aligned} \quad (6.32)$$

with boundary conditions

$$\begin{aligned} y^* &= 0, \quad u^* = 0, \quad v^* = 0 \\ y^* &\rightarrow \infty, \quad u^* = U^* \end{aligned} \quad (6.33)$$

Following the procedure described in (2.2), the continuity and momentum equations can be combined into a single third order nonlinear partial differential equation in terms of the stream function f by means of the relations:

$$\begin{aligned} \psi^* &= \sqrt{\frac{U^* s^*}{Re}} f(s^*, \eta) \\ \eta &= y^* \sqrt{\frac{U^*}{s^*} Re} \end{aligned} \quad (6.34)$$

The resulting equation is

$$\begin{aligned} (1+\epsilon^*) f''' + \epsilon^* f'' + \frac{1+\beta}{2} f f'' + \beta (1-f'^2) &= \\ s^* \left(f' \frac{\partial f'}{\partial s^*} - f'' \frac{\partial f}{\partial s^*} \right) & \end{aligned} \quad (6.35)$$

with boundary conditions

$$\begin{aligned}\eta &= 0 & : & \quad f = 0, f' = 0 \\ \eta &\rightarrow \infty & : & \quad f' \rightarrow 1\end{aligned}\quad (6.36)$$

The term $\beta = \frac{s^*}{U^*} \frac{dU^*}{ds}$ is a pressure gradient parameter, and f' represents $\frac{\partial f}{\partial \eta}$, etc.

In the present approach the turbulent boundary layer is divided into inner and outer layers, and a separate formula for eddy viscosity is used in each layer. Based on the experimental evidence the two empirical formulas, one for the inner layer and another for the outer part of the boundary layer, were developed in chapter V. In the inner layer, the eddy viscosity based on Prandtl's mixing length theory is given by (5.26)

$$\epsilon_i^* = 0.16 \operatorname{Re} y^{*2} \left| \frac{\partial u^*}{\partial y^*} \right| \left\{ 1 - \exp \left[- \frac{\operatorname{Re} y^*}{26} \left(\frac{U^*}{2} C_f - U^* \frac{dU^*}{ds} y^* \right)^{\frac{1}{2}} \right] \right\}^2$$

or, in the transformed coordinates:

$$\epsilon_i^* = 0.16 \sqrt{U^* s^* \operatorname{Re}} \eta^2 \left| f'' \right| \left\{ 1 - \exp \left[- \frac{\eta}{26} (U^* s^* \operatorname{Re})^{\frac{1}{4}} \left(f'' - \beta \eta \right)^{\frac{1}{2}} \right] \right\}^2 \quad (6.37)$$

In the outer layer a constant eddy viscosity, ϵ_o^* , is used which is given by (5.20)

$$\epsilon_o^* = 0.0167 H \Delta^* U^* Re \quad (6.38)$$

The constraint used to define the inner and outer layers is the continuity of the eddy viscosity. From the wall outward the expression for inner layer eddy viscosity applies until $\epsilon_i^* = \epsilon_o^*$.

6.5 Viscous-Inviscid Interaction

Consistent with the assumption that the interaction is due to the vertical displacement of streamlines, the imposed condition that $u = 0$ on the line $y = \phi(s)$ allows for the interaction between the viscous and inviscid flows. Then the freestream velocity that satisfies the boundary conditions (6.16) and (6.17) with a properly chosen wall shear accounts for interaction. This treatment implies the need for iteration between inviscid and boundary layer solutions, in an effort to match boundary conditions. In the present approach this is done simply by adjusting the given pressure gradient parameter β and the guessed wall shear f_w'' , iteratively until convergence is realized in the solution. Then the new freestream velocity is determined from the converged pressure gradient parameter using the relation $\beta(s^*) = \frac{s^*}{U^*} \frac{dU^*}{ds}$. It was found from the calculations that the

singularity near separation is considerably weakened when interaction is allowed to influence the imposed velocity distribution.

There is substantial experimental evidence that the external velocity falls nearly linearly between the transition and reattachment points. Since the length of the bubble is known the external velocity distribution over the turbulent region of the separated flow field can then be determined easily.

6.6 Method of Solution

The partial differential equation of the boundary layer is approximated into an ordinary differential equation by replacing the streamwise partial derivatives by implicit two point finite differences while retaining the derivatives in a direction normal to the surface. Given the free stream velocity distribution, the method of solution of the resulting ordinary differential equation involves choosing a proper value of f_w'' and integrating the equation directly out to a suitably large value of η such that the boundary conditions are matched.

The finite difference method that was developed in chapter II was used to analyze the laminar boundary layer over the airfoil surface to provide initial conditions for the viscous flow analysis of the laminar separated flow field. The laminar boundary layer analysis was started at the front

stagnation point, and continued up to a point close to separation. The two analyses are connected by requiring continuity of velocity profiles.

Since the steady boundary layer equations are parabolic everywhere, the method of solution should be of the downstream marching type. In a region of reverse flow (shown in Figure (46)), this implies that the solution should proceed in the negative s direction from reattachment forward to separation point. However, in a flow such as that treated in the present study, the downstream conditions after separation are unknown a priori. For that reason, the solution of the boundary layer problem in the reverse flow region cannot be started from a point which is away from separation point in the positive s direction. On the other hand, the solution can be started right from the separation point because the width of RL is reduced to a point at separation.

In the present procedure, the finite difference scheme at any point I in the reverse flow region is constructed from two adjacent points, as shown in Figure (47). Integration of the approximated differential equation at I, with specified wall shear and free stream velocity, yields the flow pattern in RL. In the layer SL of forward flow, the solution of Equation (6.15) may start from the separation point utilizing the upstream flow information generated by laminar boundary layer analysis. The solutions in the layers SL and RL are connected by requiring continuity of f , f' and f'' at the

interface boundary i.e., at the line of zero velocity. The procedure of integrating column by column proceeds in the laminar region until transition to fully turbulent flow is located in the shear layer. In the laminar region interaction between inviscid and boundary layer solutions is necessary to match the boundary conditions. The pressure gradient parameter β and the wall shear f_w'' are adjusted iteratively until the boundary conditions are satisfied. The new free stream velocity is then determined from the converged value of β .

The velocity profile generated in the layer SL at transition is utilized to start a solution in the redevelopment region.

6.7 Numerical Procedure

6.7.1 Finite Difference Formulation

Laminar Region

Replacing the streamwise derivatives in Equation (6.15) by two-point finite difference formula (Equation (2.13)) at $s^* = s_{JJ}^*$, the following equation is obtained:

$$f''' + \frac{1+\beta}{2} f f'' + \beta (1-f'^2) = A_{11} f' \left[f' - f'_{JJ-1} \right] - A_{11} f'' \left[f - f_{JJ-1} \right] \quad (6.39)$$

Redeveloping Region

Replacing the streamwise derivatives in Equation (6.35) by two-point finite difference formula at $s^* = s_{JJ}^*$, the following equation is obtained:

$$\begin{aligned} (1+\epsilon^*)f''' + \epsilon^*f'' + \frac{1+\beta}{2}ff'' + \beta(1-f'^2) \\ = A_{11}f'\left[f' - f'_{JJ-1}\right] - A_{11}f''\left[f - f_{JJ-1}\right] \end{aligned} \quad (6.40)$$

Where $A_{11} = \frac{s_{JJ}^*}{s_{JJ}^* - s_{JJ-1}^*}$. Equations (6.39) and

(6.40) are ordinary differential equations in η with the known variable quantities f_{JJ-1} and f'_{JJ-1} at the upstream stations.

6.7.2 Satisfaction of Asymptotic Boundary Conditions

Since the present method is an outgrowth of the method described in chapter II, only a brief summary is given here, along with a description of the modifications introduced for the application to separated flow. In the laminar region, the pressure gradient parameter β and the wall shear f_w'' have to be adjusted iteratively until the boundary conditions are satisfied. The equations that are necessary to obtain corrections to β and f_w'' at each iteration are developed here.

In order to solve equation (6.15) it is required to find suitable values for β and f_w'' so that the boundary conditions (6.16) and (6.17) are satisfied. This is equivalent of finding solutions from the equations

$$f_\phi' [\beta, f''(0)] = 0 \quad (6.41)$$

$$f_e' [\beta, f''(0)] = 1 \quad (6.42)$$

$$f_e'' [\beta, f''(0)] = 0 \quad (6.43)$$

where f_ϕ' is the value of f' on the line of zero velocity, $y = \phi(s)$, f_e' is the value of f' at the edge of the boundary layer, and f_e'' is the value of f'' at the edge of the boundary layer.

Let $x = f''(0)$. A small change Δx in x changes f_ϕ' , f_e' and f_e'' by the amounts $\frac{\partial f_\phi'}{\partial x} \Delta x$, $\frac{\partial f_e'}{\partial x} \Delta x$, and $\frac{\partial f_e''}{\partial x} \Delta x$, respectively. Similarly small change $\Delta \beta$ in β changes f_ϕ' , f_e' and f_e'' by the amounts $\frac{\partial f_\phi'}{\partial \beta} \Delta \beta$, $\frac{\partial f_e'}{\partial \beta} \Delta \beta$, and $\frac{\partial f_e''}{\partial \beta} \Delta \beta$. Therefore, the necessary corrections Δx and $\Delta \beta$ can be found by solving the equations

$$f_{\phi x}' \Delta x + f_{\phi \beta}' \Delta \beta + f_\phi' = 0 \quad (6.44)$$

$$f'_{ex} \Delta x + f'_{e\beta} \Delta \beta + f'_e = 1 \quad (6.45)$$

$$\text{and } f''_{ex} \Delta x + f''_{e\beta} \Delta \beta + f''_e = 0 \quad (6.46)$$

where $f'_{\phi x} = \frac{\partial f'_\phi}{\partial x}$, $f'_{\phi \beta} = \frac{\partial f'_\phi}{\partial \beta}$, etc. Here, there are

two adjustable parameters Δx and $\Delta \beta$ but there are three equations to be satisfied. Therefore, a satisfactory procedure is to seek the least squares solution of Equations (6.44), (6.45), and (6.46). Let the discrepancies be

$$\delta_1 = f'_{\phi x} \Delta x + f'_{\phi \beta} \Delta \beta + f'_\phi$$

$$\delta_2 = f'_{ex} \Delta x + f'_{e\beta} \Delta \beta + f'_e - 1$$

$$\text{and } \delta_3 = f''_{ex} \Delta x + f''_{e\beta} \Delta \beta + f''_e$$

To minimize the sum of the squares of δ_1 , δ_2 , and δ_3 it is necessary to equate its first derivative with respect to Δx and $\Delta \beta$ to zero. This calculation yields expressions for Δx and $\Delta \beta$ which are written as:

$$\Delta x = \frac{\frac{f'_{ex} (1-f'_e) - f''_{ex} f'_e - f'_{\phi x} f'_\phi}{f'^2_{ex} + f'^2_{e\beta} + f'^2_{\phi x} + f'^2_{\phi \beta} + f''^2_{ex} + f''^2_{e\beta}}}{f'^2_{ex} + f'^2_{e\beta} + f'^2_{\phi x} + f'^2_{\phi \beta} + f''^2_{ex} + f''^2_{e\beta}} \quad (6.47)$$

$$\Delta\beta = \frac{f'_{e\beta} (1-f'_e) - f''_{e\beta} f'_e - f'_{\phi\beta} f'_\phi}{f'^2_{ex} + f'^2_{e\beta} + f'^2_{\phi x} + f'^2_{\phi\beta} + f''^2_{ex} + f''^2_{e\beta}} \quad (6.48)$$

The perturbation equations to evaluate the partial derivatives of f with respect to x and β are obtained by differentiating the terms of the original differential equation (6.39) with respect to x and β . The following perturbation equations are obtained:

$$\begin{aligned} & f''''_x + \frac{1+\beta}{2} [ff''_x + f''f_x] - 2\beta f'f'_x \\ &= A_{11}f'_x [f'-f'_{JJ-1}] + A_{11}f'f'_x - A_{11}f''_x [f-f_{JJ-1}] \\ & \quad - A_{11}f''f_x \end{aligned} \quad (6.49)$$

$$\begin{aligned} & f''''_\beta + \frac{1+\beta}{2} [ff''_\beta + f''f_\beta] - 2\beta f'f'_\beta + \frac{ff''}{2} - (f'^2-1) \\ &= A_{11}f'_\beta [f'-f'_{JJ-1}] + A_{11}f'f'_\beta - A_{11}f''_\beta [f-f_{JJ-1}] - A_{11}f''f_\beta \end{aligned} \quad (6.50)$$

with the initial conditions

$$\begin{aligned} \eta = 0 : f_x &= 0, f'_x = 0, f''_x = 1; \\ f_\beta &= 0, f'_\beta = 0, f''_\beta = 0 \end{aligned} \quad (6.51)$$

Corrections to the initial guesses of f''_w and β are obtained

by utilizing the Equations (6.47) to (6.51).

In the redeveloping region corrections to a first approximation in f_w'' can be obtained from the Equation (2.22) which was developed in chapter II. That equation is rewritten as

$$\Delta x = \frac{f_{ex}' (1-f_e') - f_{ex}'' f_e''}{f_{ex}'^2 + f_{ex}''^2} \quad (6.52)$$

The necessary perturbation equation is obtained by differentiating the terms in Equation (6.40) appropriately with respect to x . The perturbation equation is written as:

$$\begin{aligned} (1 + \epsilon^*) f_{xx}''' + \epsilon_x^* f_{xxx}'' + \epsilon^{*'} f_{xx}'' + \epsilon_x^{*'} f_{xx}' + \frac{1+\beta}{2} [f f_{xx}''' + f_x f_{xx}'''] \\ - 2\beta f' f_x' = A_{11} f_x' [f' - f_{JJ-1}'] + A_{11} f' f_x' - A_{11} f_{xx}'' [f - f_{JJ-1}] \\ - A_{11} f_{xx}'' f_x' \end{aligned} \quad (6.53)$$

with initial conditions

$$\eta = 0 : f_x = 0, f_x' = 0, f_{xx}' = 1 \quad (6.54)$$

The derivatives of ϵ_i^* are evaluated in Appendix 2.

6.7.3 Integration of the Ordinary Differential Equations

In order to integrate the boundary layer and perturbation differential equations it is necessary to rewrite them as systems of first order differential equations. This is

done by defining new variables as shown in Appendix 3. Integration of the differential equations was performed by a predictor-corrector type method that uses Adams-Moulton formulas [16]. The finite difference formulas contain a variable grid in the η -direction, which permits shorter steps close to the wall and longer steps away from the wall. The grid has the property that the ratio of lengths of any two adjacent intervals is a constant; that is, $\Delta\eta_J = G\Delta\eta_{J-1}$. For the type of flows that were considered by the present study, an initial η spacing $\Delta\eta_1 = 0.015$ and $G = 1.0015$ were found to be satisfactory for the range of transformed boundary layer thickness η_∞ between 8 and 20.

6.8 Results and Discussion

The results of analysis for transitional bubbles occurring on our NACA 66₃-018 airfoil are presented here for comparison with experiments. The necessary pressure distributions over the airfoil section were calculated using the computer program developed by Kennedy [39]. The first case was analysed for comparison with the present experimental measurements at a Reynolds number of 0.8×10^6 for 2° angle of attack. Velocity profiles computed at selected streamwise locations are shown compared with measurements in Figure (50). The agreement is considered to be reasonably good. However, it is to be noted that the hot film measurements cannot show the reverse flow region. The streamwise distribution of

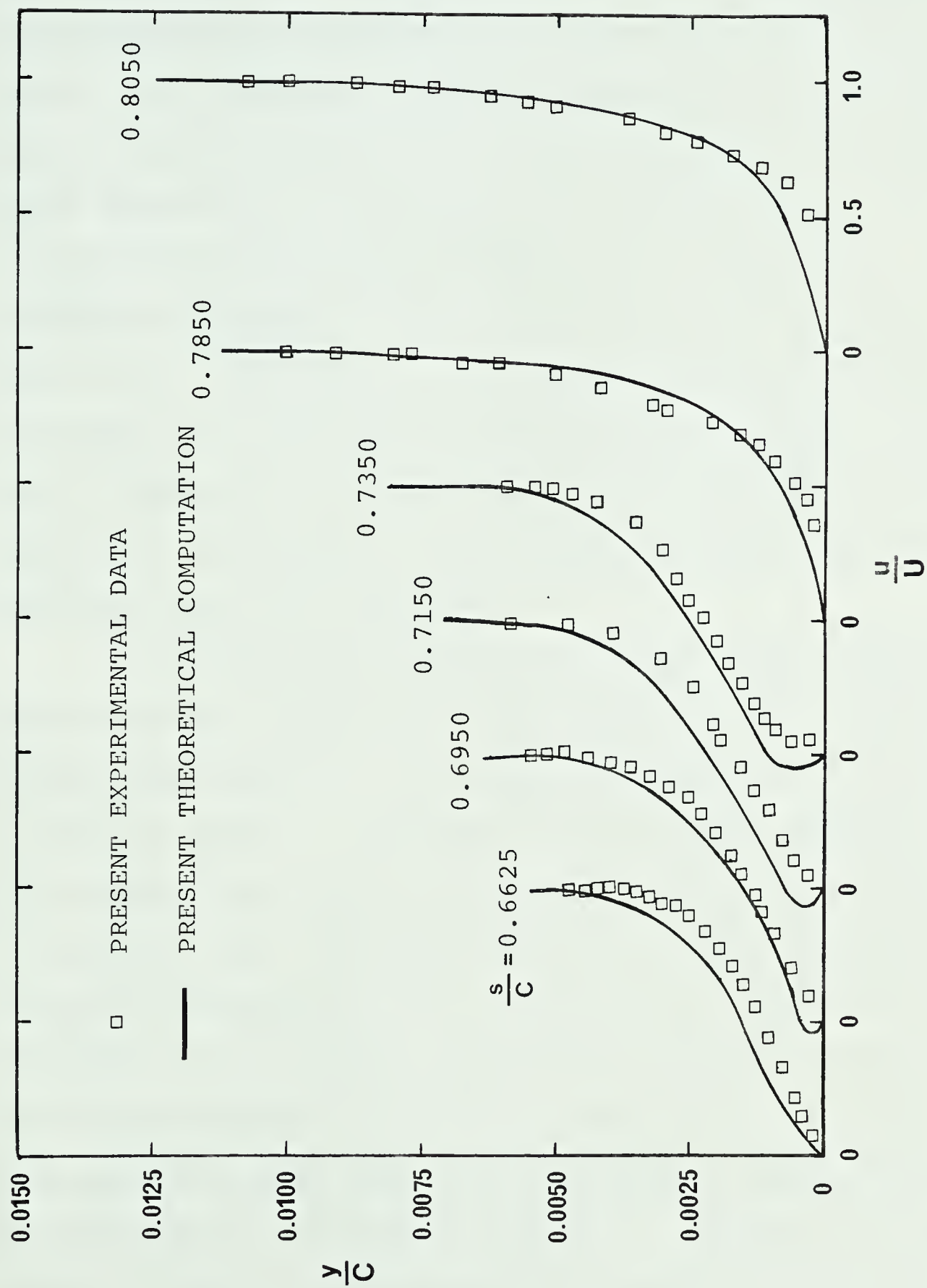


FIGURE 50--STREAMWISE VELOCITY DISTRIBUTION, NACA 66₃-018, $Re = 0.8 \times 10^6$, $\alpha = 2^\circ$

pressure coefficient C_p in the vicinity of the flow field is shown in Figure (51). The computed pressure distribution, which includes the correction for viscous-inviscid interaction, is in excellent agreement with experimental measurements. The distribution has a relatively constant pressure region downstream of separation, and rapidly returns to the specified pressure distribution near reattachment. The streamwise development of the shape factor $\frac{\delta^*}{\theta}$ is shown in Figure (52). The value of the shape factor seems to reach a maximum near transition and then decrease rapidly. It is seen by comparing the calculations with measurements that the location of transition to fully turbulent flow, and the bubble length are also well predicted.

To verify that the model is generally applicable, a second case was analysed for comparison with the data of Bursnall and Loftin [4] at a Reynolds number of 1.7×10^6 for 0° angle of attack. The results of the present analysis are also compared with similar calculations presented by Briley and McDonald [10]. Velocity profiles at selected streamwise locations are shown plotted in Figure (53). The profiles calculated by the present method show reasonable agreement with the measurements of Bursnall and Loftin. It is seen that the rapid flow variations just downstream of reattachment are well predicted by the present analysis. However, the calculations of Briley and McDonald do not predict such rapid flow variations. It may be noted that the computed velocity profiles

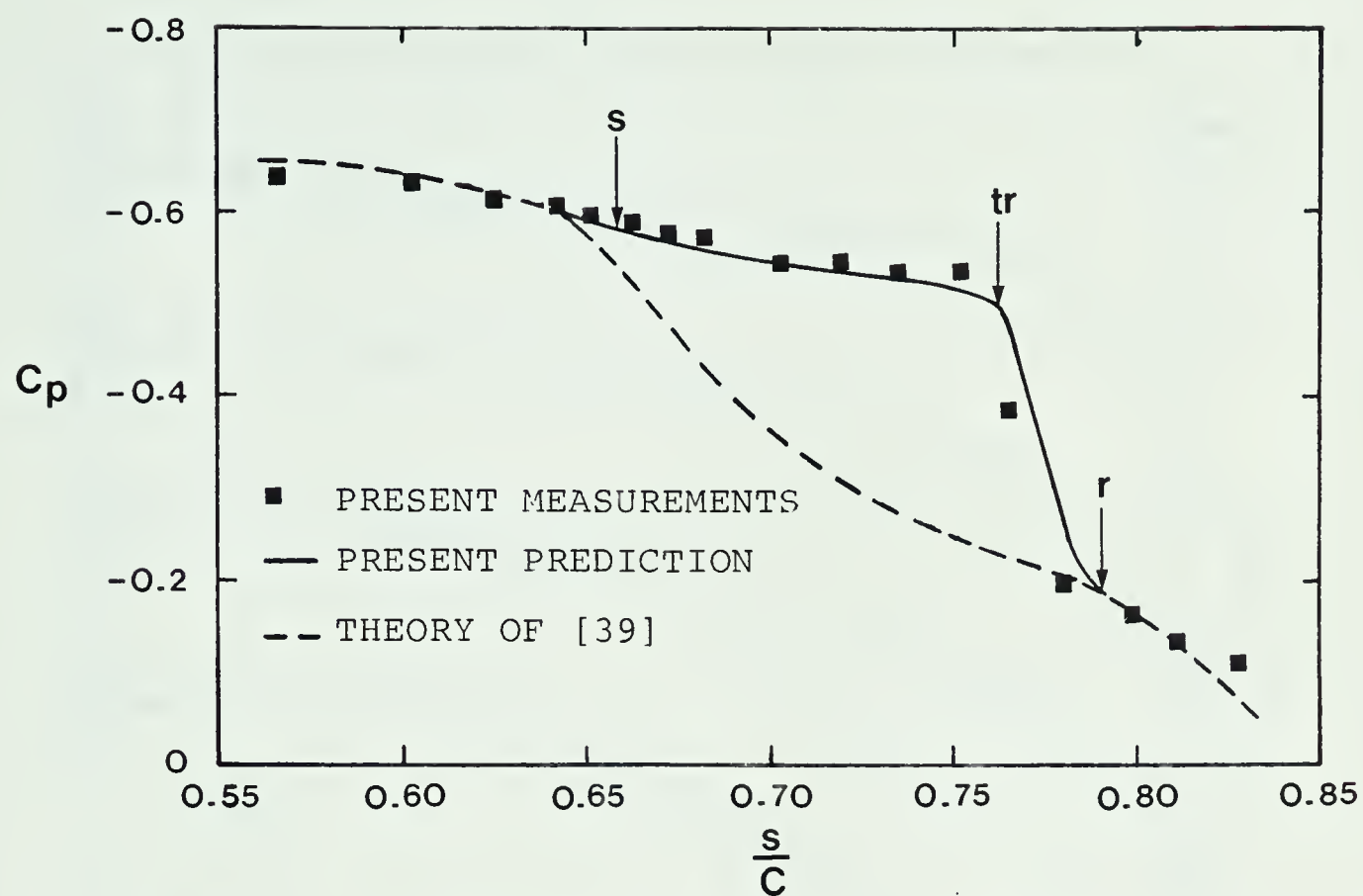
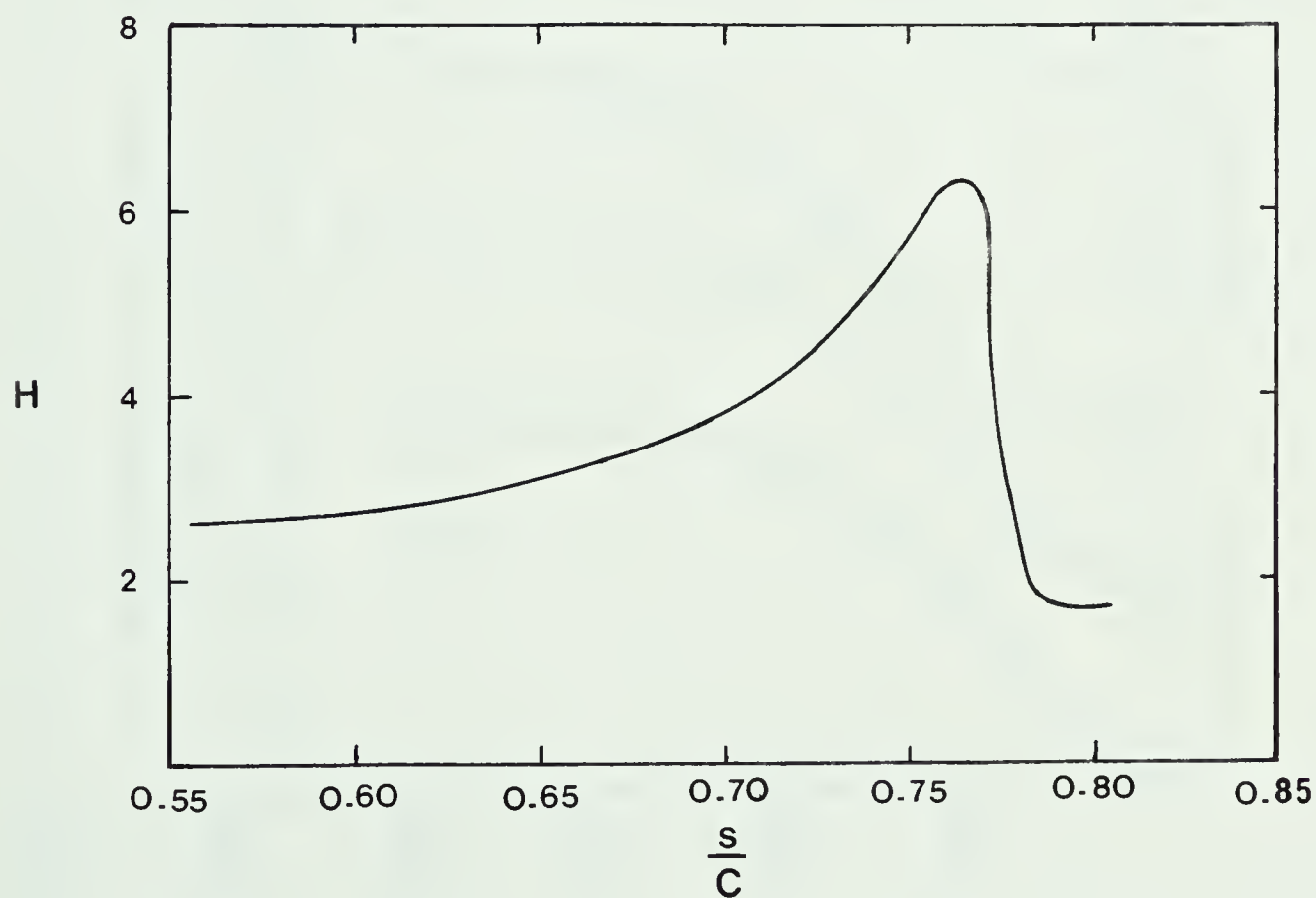


FIGURE 51--PRESSURE DISTRIBUTION

FIGURE 52--VARIATION OF SHAPE FACTOR H , NACA 66₃ - 018,
 $Re = 0.8 \times 10^6$, $\alpha = 2^\circ$

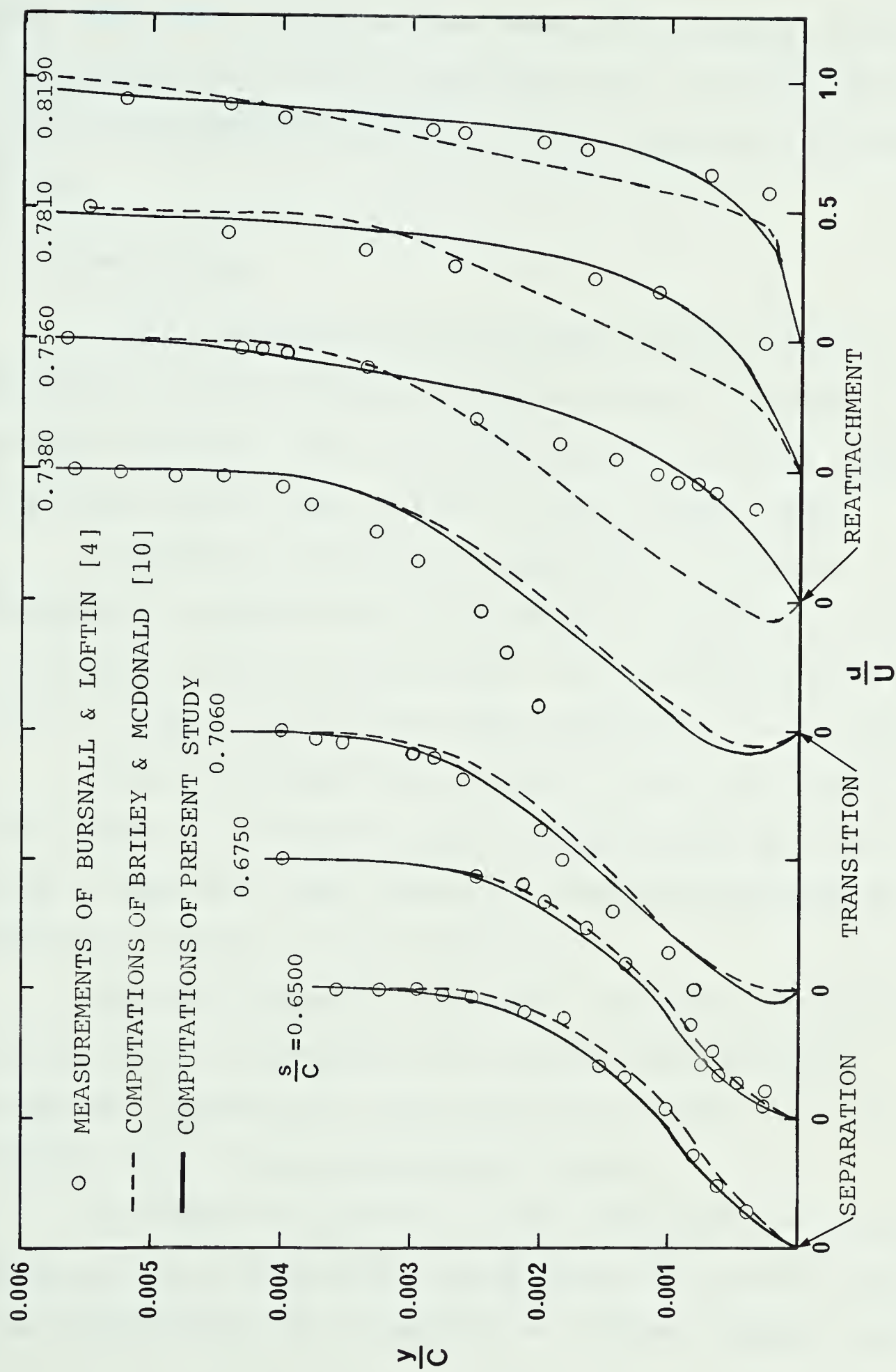


FIGURE 53--STREAMWISE VELOCITY DISTRIBUTION, NACA 66₃-018, $Re = 1.7 \times 10^6$, $\alpha = 0^\circ$

near transition correlate even though the present transition criteria does not include the freestream turbulence level while Briley-McDonald criteria employs freestream turbulence level.

6.9 Conclusions

From the results of the present study it can be concluded that the finite difference method of analysis developed here provides a good representation of a laminar separated flow field such as that treated in the present study.

Although a singularity occurs near separation, it is considerably weakened when interaction is allowed to influence the imposed velocity distribution. This implies that a solution ceases to apply only in the close proximity of separation point.

When the freestream turbulence level is relatively low, the transition correlation based on the analogy between transition in separated shear layer and transition produced by roughness elements is quite adequate.

The eddy viscosity model that is used in conjunction with the finite difference calculation method provides a convenient procedure for the prediction of the turbulent boundary layer in the redeveloping region.

It should be possible to use these tools to develop a viscous flow analysis method which takes into account the flow field generated by the separation of laminar boundary layer.

CHAPTER VII

PREDICTION OF BOUNDARY LAYER DEVELOPMENT IN THE PRESENCE OF SEPARATED FLOW

7.1 Introduction

While the presence of a laminar separation bubble will certainly effect the boundary layer characteristic on a wing section no methods of analysis are available at the present time to adequately predict the development of the boundary layer in the presence of a laminar separated flow field. Such a method of analysis is developed here, and the effects of separated flow on the boundary layer development are predicted.

The present method of analysis utilizes the procedure developed in Chapter VI for analysis of the separated flow field. The initial conditions to analyze the bubble are provided from an analysis of the upstream laminar boundary layer using the method developed in Chapter II. To reduce computing time the turbulent boundary layer downstream of separated flow field is calculated utilizing an integral method. The present method employs the velocity distribution developed by a converged equivalent airfoil section to predict the boundary layer development. Numerical predictions are presented for boundary layer development on the Wortmann FX 66-S-196 VI airfoil at angles of attack between -2 and 8 degrees with chordal Reynolds numbers of 0.5×10^6 and

1.5×10^6 . The results of the calculations are compared with wind tunnel measurements [42]. The calculated results are in good agreement with experiment.

7.2 Effects of Viscous Flow

The effect of viscosity are mainly confined to the boundary layer over the airfoil surface. The boundary has a tendency to displace the streamlines just outside this layer by a distance equal to the local displacement thickness. As a consequence of this, the pressure distribution is modified on the body as compared with inviscid flow. This is illustrated in Figure (54). In an inviscid fluid, the pressure distribution is such that the forward and backward



THE DISPLACEMENT THICKNESS (HATCHED AREA) REPRESENTS AN EFFECTIVE CHANGE TO THE SHAPE OF THE AIRFOIL.

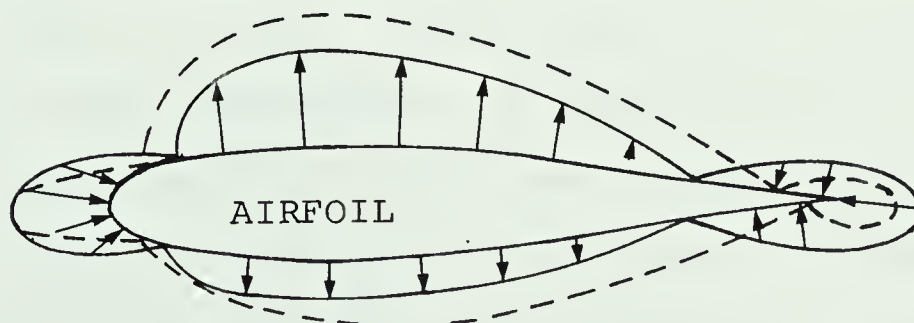


FIGURE 54--PRESSURE DISTRIBUTION ON AN AIRFOIL SECTION IN VISCOUS FLOW (DOTTED LINE) AND INVISCID FLOW (FULL LINE).

forces cancel out exactly for all shapes, giving zero overall drag. On the other hand, in a viscous fluid the pressure distribution is modified and the situation is such that the exact balance of the forces is upset, resulting in overall rearwards force. This force is the boundary layer normal pressure drag (or form drag). The surface traction at each point, which is a direct result of viscosity, has a component acting in the direction of the undisturbed stream. The total effect of these components (surface shearing stresses), taken over the whole of the body, is the skin friction drag.

The use of the boundary layer displacement thickness permits the determination of the displacement surface about which potential flow can be assumed to occur. The potential flow and viscous flow solutions can be matched by an iterative process which converges on what is termed an equivalent airfoil. This is the airfoil which, in potential flow, produces the pressure distribution of the section in viscous flow.

Thus it is necessary to analyze the boundary layer over the surface for the prediction of the actual performance of an airfoil section. This analysis will provide the boundary layer displacement thickness at any point on the surface, and the drag coefficient of the section.

There is substantial experimental evidence that the thickness of the boundary layer increases in the presence of the laminar separated flow field as compared to the flow without the separation bubble. Increase in drag is therefore

to be expected when the laminar boundary layer separates causing transitional bubbles to form near the midchord of the airfoil. Conventional prediction methods do not include the analysis of the laminar separated flow field, and therefore may not be able to predict this increase in drag. Transition to turbulent flow has a marked effect on the turbulent boundary layer development, and therefore transition in the shear layer has importance in determining the trailing edge stall caused by turbulent boundary layer separation ahead of trailing edge. When the laminar flow extends over the major part of the airfoil surface it is important to predict the location, if any, of the flow reattachment. Thus the mid-chord bubble plays an important part in limiting the performance of sections with long laminar roof top flows.

7.3 Method of Analysis

The present method of analysis is illustrated in Figure (55). The pressure distribution produced by the converged equivalent airfoil section is used in the present boundary layer analysis. The computer program developed by Kennedy [39] is utilized for constructing the equivalent airfoil section from the given input profile. This program determines the potential flow on any given section by using the surface singularity method described in reference [40]. The model of the viscous flow analysis method consists of

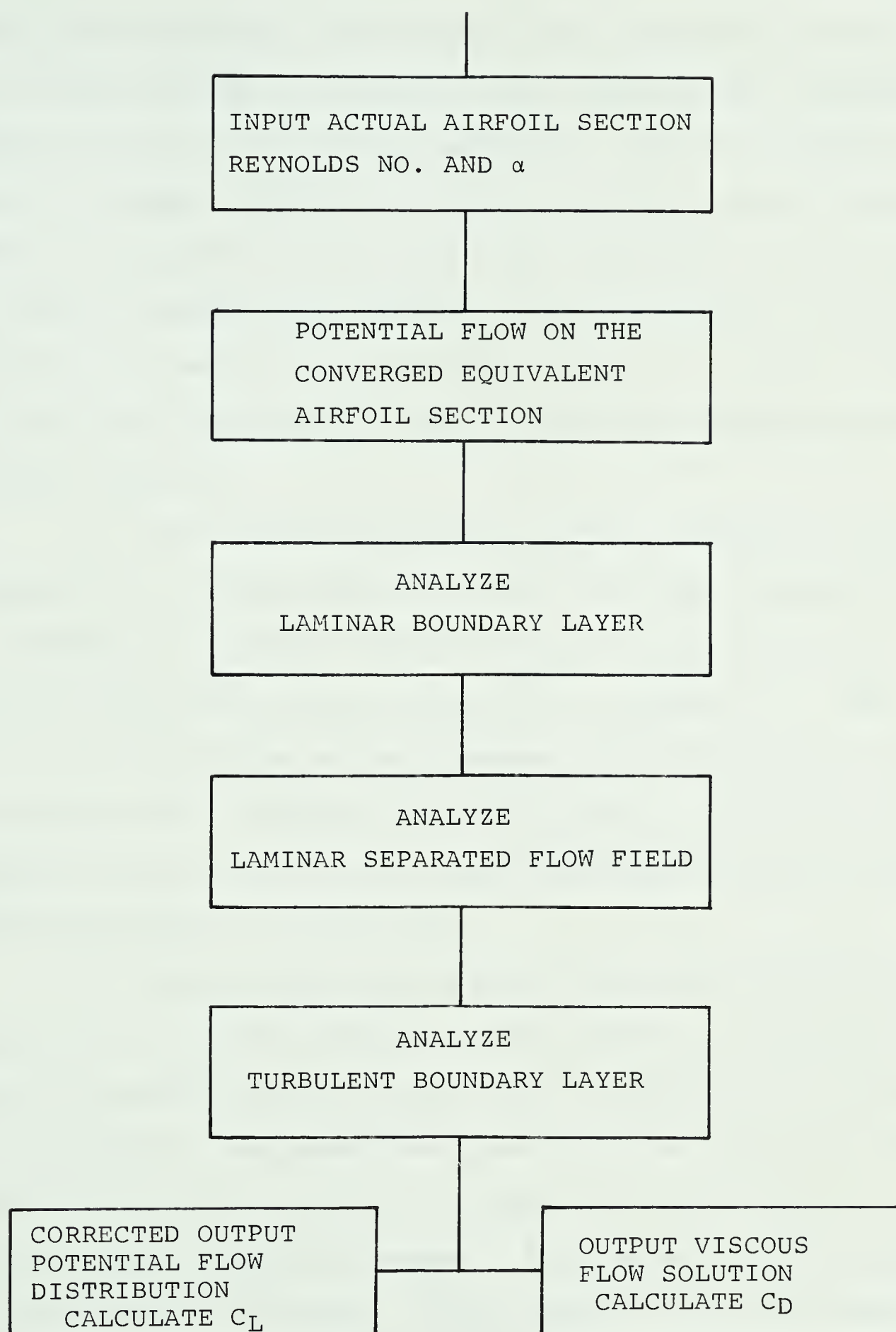


FIGURE 55--FLOW CHART OF VISCOUS FLOW PROCEDURE

taking the potential flow solution and iteratively correcting it for the effects of boundary layer displacement thickness using an equivalent airfoil technique. Kennedy's program uses an integral formulation for the boundary layer analysis based on velocities calculated from a potential flow analysis. In order to predict the boundary layer development in the presence of laminar separated flow field, it is only necessary to calculate the boundary layer on the converged equivalent airfoil section.

In the present procedure, initial conditions for the analysis of a laminar separated flow field are provided from an analysis of upstream laminar boundary layer using the finite difference analysis developed in Chapter II. The points of transition and reattachment and the pressure distribution over the bubble which includes the correction for viscous-inviscid interaction, are determined using the techniques developed in Chapter VI.

To reduce computing time the turbulent boundary layer downstream of laminar separated flow field was calculated using an integral method rather than a differential method. The analyses in the separated flow field and the downstream turbulent flow are connected by requiring continuity of momentum and energy thicknesses. The integral method based on the analysis of Felsch, Geropp and Walz [41] was programmed by Kennedy, and it is used in the present procedure for calculating the downstream turbulent boundary layer. The

profile drag coefficient of the section (sum of skin friction and form drag coefficients) is calculated from the semi-empirical relation of Squire and Young [14]. The drag coefficient due to one surface is given by

$$C_D = 2 \theta_{te} U_{te} \frac{[H_{te} + 5]/2}{U_{te}} \quad (7.1)$$

When the turbulent boundary layer separates ahead of trailing edge, the program uses the values of θ , U , and H obtained at the separation point to calculate the drag coefficient. The lift coefficient, C_L , is calculated by integrating the corrected pressures around the airfoil surface.

7.4 Calculations and Discussions of Results

The aerodynamic characteristics of the Wortmann FX 66-S-196 V1 airfoil section were investigated by Gooden [42] in a low-speed low-turbulence wind tunnel. The airfoil was tested in an angle of attack range from -6 to +20 degrees and Reynolds numbers between 0.5×10^6 and 2.0×10^6 . Large regions of laminar separated flow were found to exist near the midchord of this airfoil. In fact, one of the objectives of that investigation was to gain further knowledge on laminar separation bubbles in order to refine a viscous flow airfoil computer program. It is therefore in order, to predict the boundary layer development on that airfoil using the proposed method. Complete boundary layer calculations were performed at angles of attack between -2 and 8 degrees

with Reynolds numbers of 0.5×10^6 and 1.5×10^6 . Regions of turbulent separation ahead of the trailing edge, which influence the drag calculations, were predicted beyond this angle of attack range. For that reason, calculations were not performed beyond this angle of attack range. The results of the present analysis are compared here with experimental measurements of Gooden [42].

7.4.1 Pressure Distribution

The chordwise pressure distribution for a Reynolds number of 0.5×10^6 at 0° angle of attack is shown in Figure (56). The presence of a laminar separation bubble just behind the pressure minimum is clearly marked on the upper surface as well as on the lower surface. The predicted pressure distribution in the vicinity of the bubble, which includes the correction for viscous-inviscid interaction, is in reasonable agreement with experimental measurements. This pressure distribution has a relatively constant pressure region between separation and transition, and then rapidly returns to the specified inviscid pressure distribution near reattachment. The potential flow distribution on the converged equivalent airfoil, determined from [39], is in agreement with measurements except near the bubble region. In this case the bubble has negligible effect on the section lift coefficient.

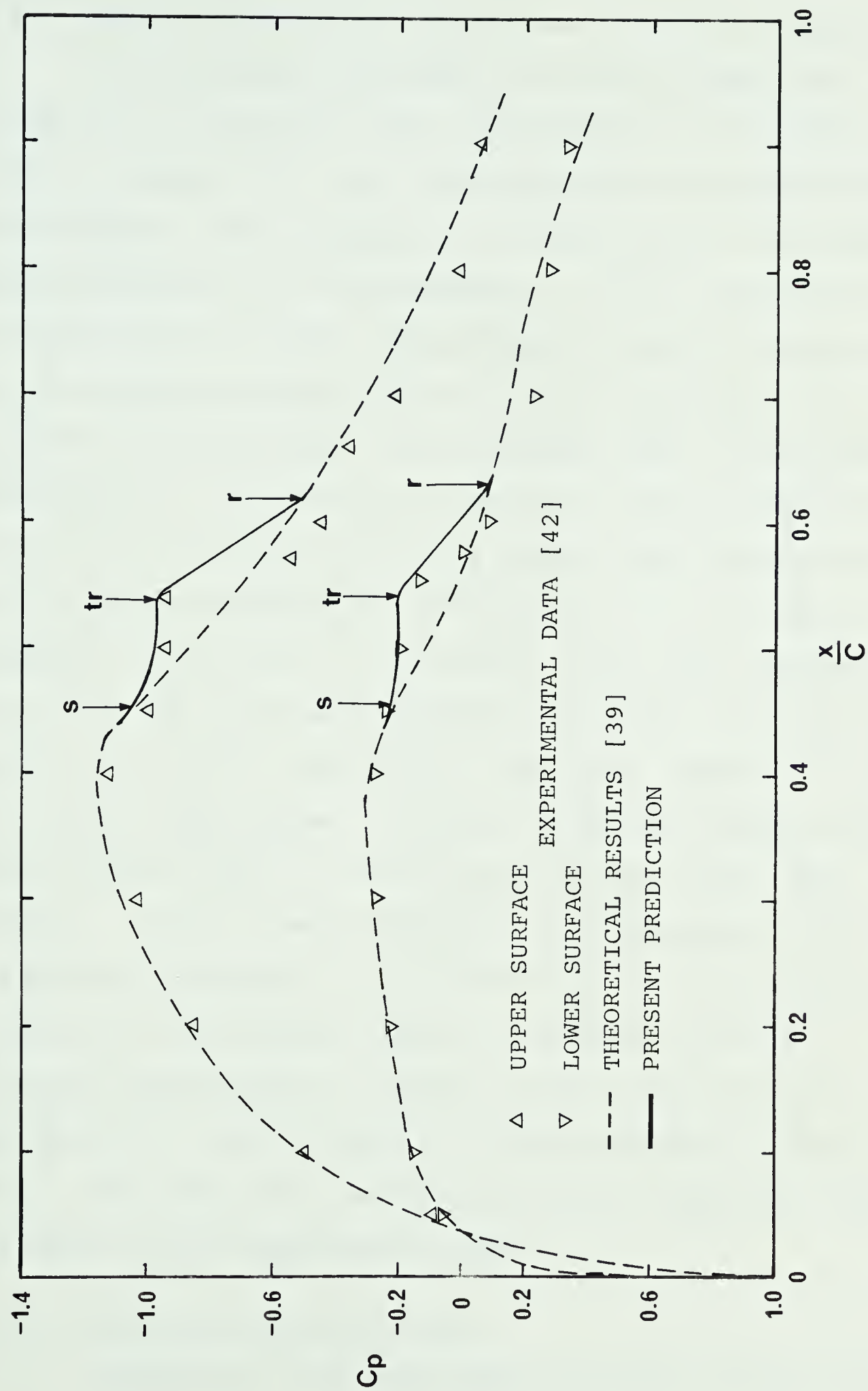


FIGURE 56--PRESSURE DISTRIBUTION, FX 66 - S - 196 VI, $Re = 0.5 \times 10^6$, $\alpha = 0^\circ$

7.4.2 Laminar Separation, Transition, and Reattachment

The predicted positions for laminar separation, transition to turbulent flow, and turbulent reattachment are shown in Figures (57)-(60) for comparison with experimental measurements. The agreement is probably within the experimental accuracy of the measurements. In the experimental investigation of Gooden, the position of laminar separation was determined by means of an oil-film technique, and the position of reattachment was determined from the pressure distribution; the position of transition was determined by means of a stethoscope and these results were supplemented with pressure distribution determinations and oil-flow patterns. The length of the bubble on the upper surface as well as on the lower surface amounts to about 7 percent chord at $Re = 1.5 \times 10^6$. Whereas, at a Reynolds number of 0.5×10^6 the bubble length amounts to about 15 percent chord on the upper surface with a slightly higher value on the lower surface. It may be mentioned that the experimental data presented in reference [42] for $Re = 0.5 \times 10^6$ indicates a tendency of the midchord bubble on the lower surface to increase considerably in length at angles of attack near maximum lift. Such a tendency is also observed in Figure (58). This might have caused the trailing edge stall that was shown in the experimental data.

7.4.3 Lift-Drag Characteristics

Figures (61) and (62) show the section profile drag

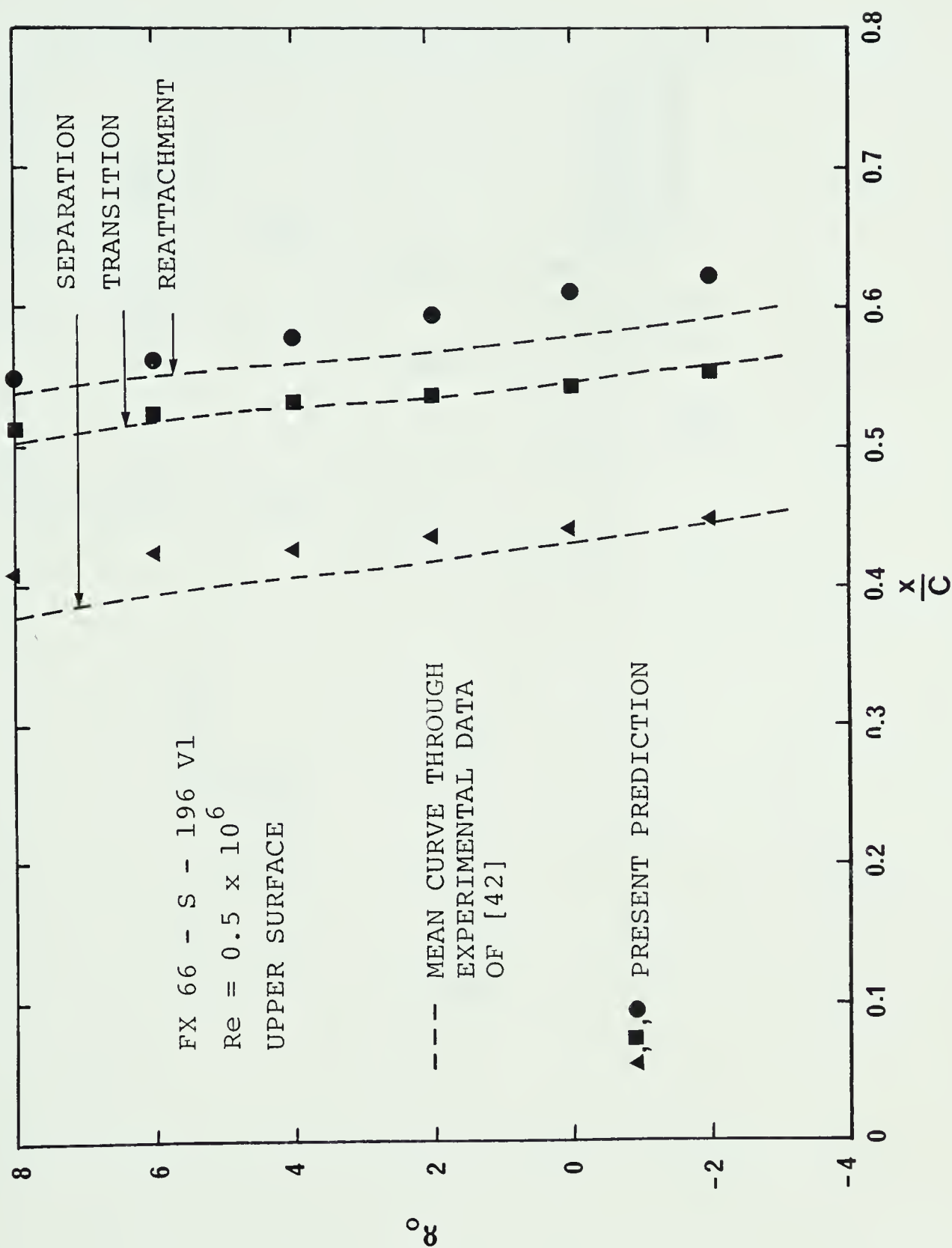


FIGURE 57--LAMINAR SEPARATION, TRANSITION AND REATTACHMENT

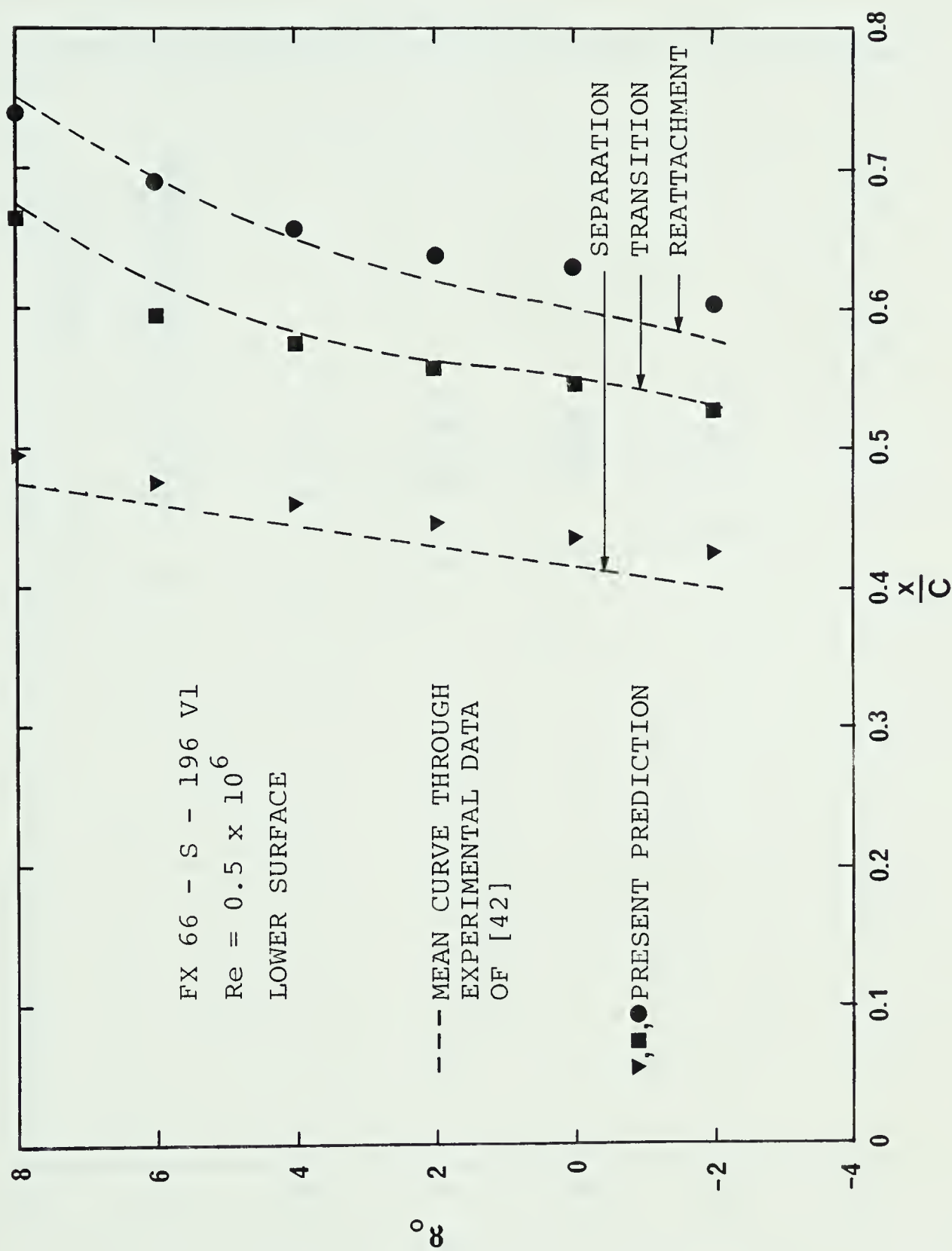


FIGURE 58--LAMINAR SEPARATION, TRANSITION AND REATTACHMENT

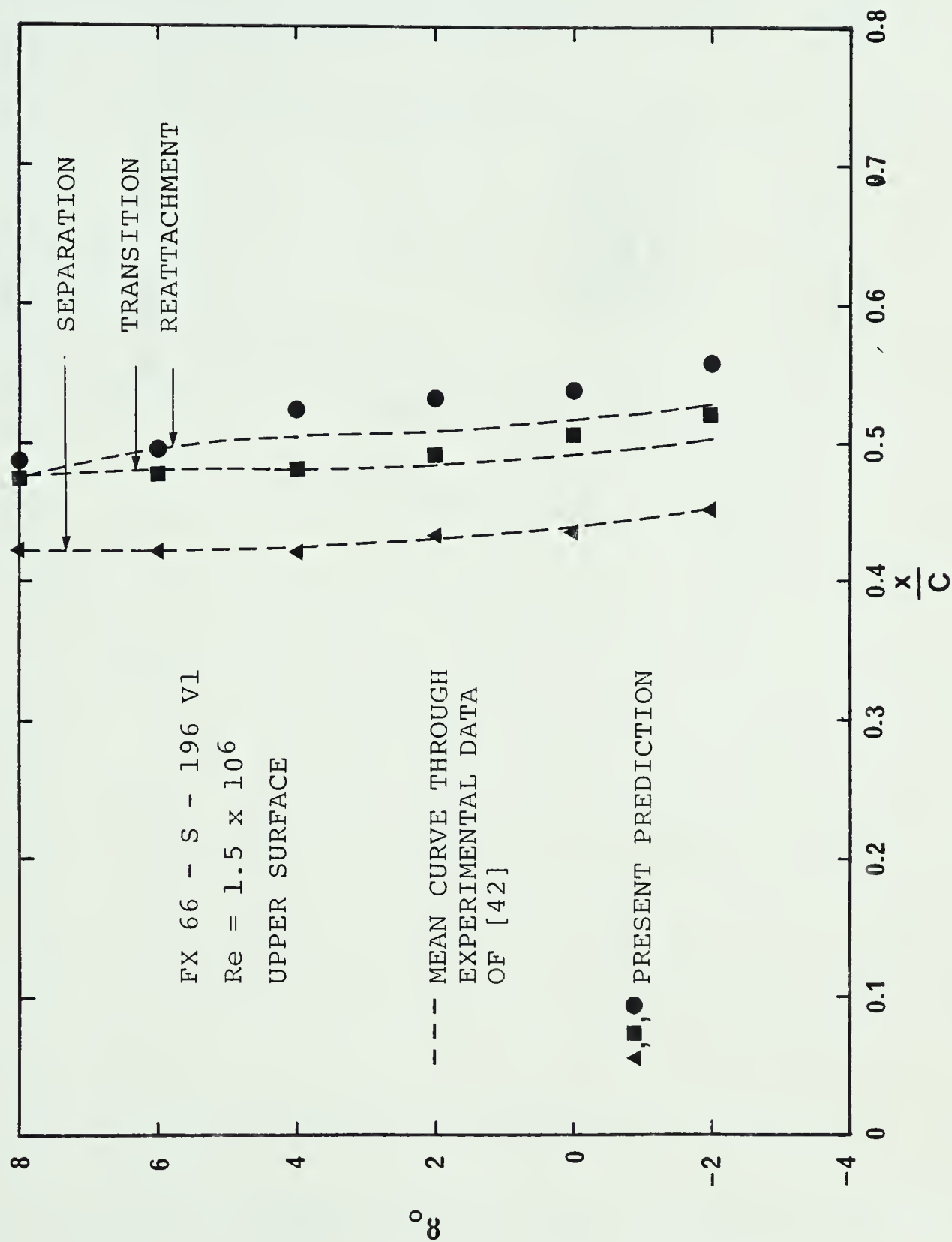


FIGURE 59--LAMINAR SEPARATION, TRANSITION AND REATTACHMENT

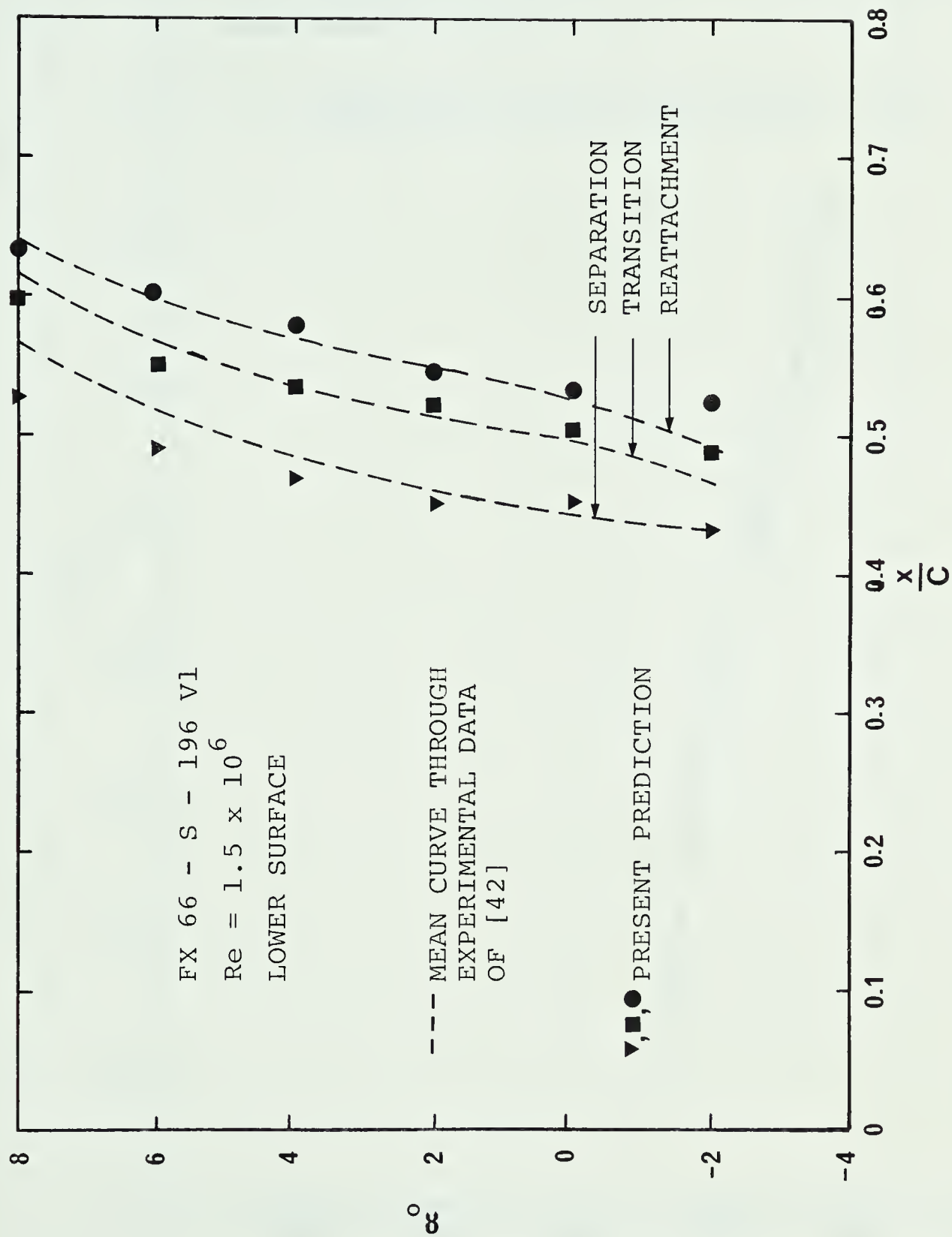


FIGURE 60--LAMINAR SEPARATION, TRANSITION AND REATTACHMENT

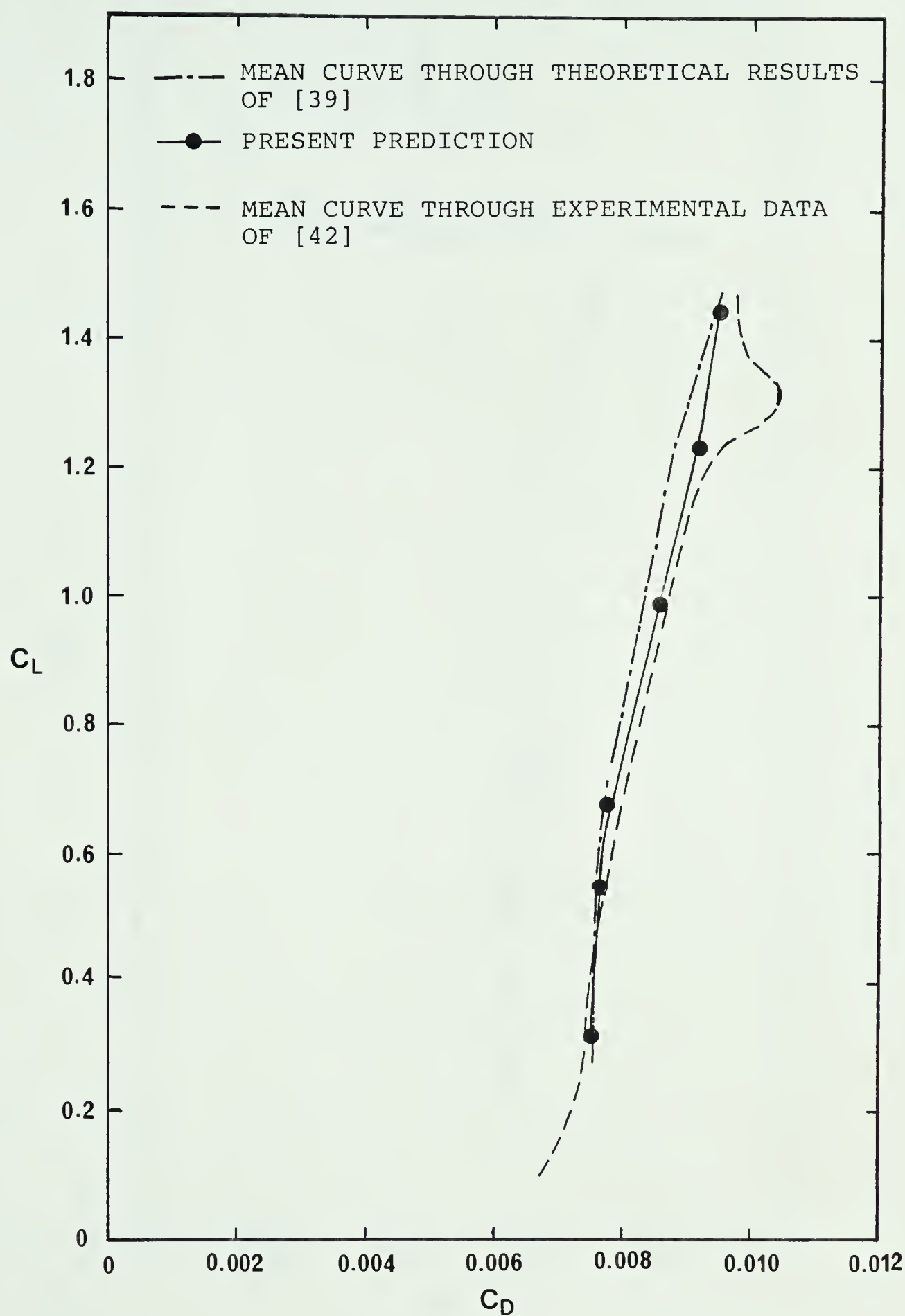


FIGURE 62--PROFILE DRAG POLAR, FX 66 - S - 196 VI,
 $Re = 1.5 \times 10^6$

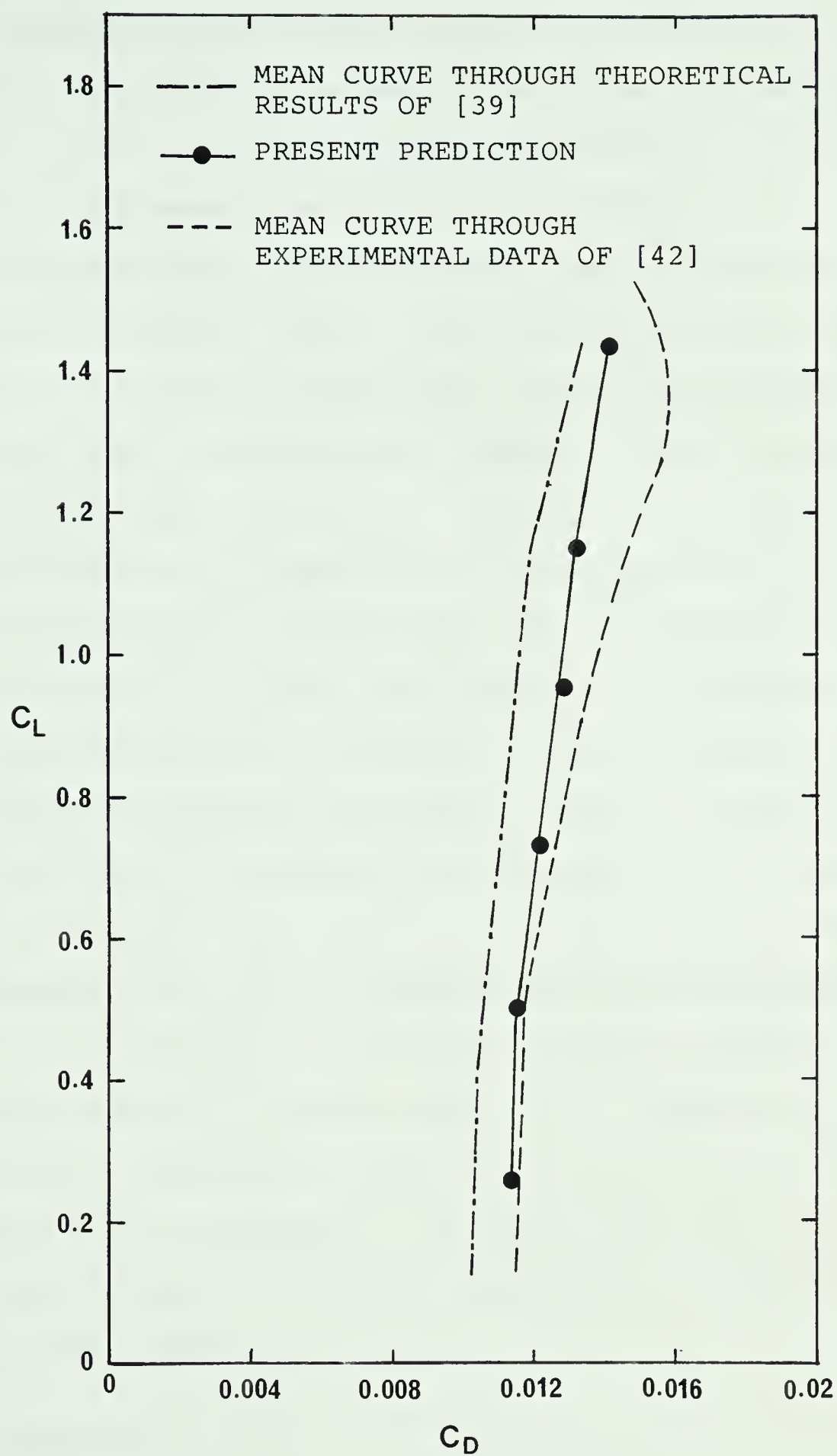


FIGURE 61--PROFILE DRAG POLAR, FX 66 - S - 196 VI,
 $Re = 0.5 \times 10^6$

characteristics. The values of the drag coefficient predicted by the present method are higher than those predicted by the method of [39]. This is clearly an indication of the effects of laminar separated flow field. The difference between the values of these drag coefficients is seen to decrease with increasing Reynolds number. This can perhaps be explained as follows. In the boundary layer calculation method devised by Kennedy [39], transition to turbulent flow is assumed to occur at the separation point. However, in the presence of a separation bubble transition to turbulent flow occurs at a position downstream of separation. As a consequence of this, higher values of boundary layer thickness are predicted for downstream development. However, at higher Reynolds numbers this predicted boundary layer may be similar to that which would otherwise be developed in the presence of a bubble.

At higher lift coefficients, the difference between the measured drag and the present prediction can be attributed mainly to the effects of predicted turbulent boundary layer separation ahead of trailing edge. In the absence of this trailing edge separation, present predictions are in good agreement with experiments. The predicted trend of the lift-drag curve is also in excellent qualitative agreement with the measured curve.

7.5 Conclusions

A procedure has been developed for predicting the boundary layer development in the presence of laminar

separated flow field near the midchord of the airfoil. The results of the analysis further verify the capabilities of the numerical method developed in Chapter VI for analyzing the separated flow field.

Predicted positions of laminar separation, transition and reattachment were found to be in good agreement, both qualitatively and quantitatively, with available experimental data. The computed pressure distribution in the vicinity of the bubble, which includes the viscous-inviscid interaction, is in reasonable agreement with measurements.

There is, in general, an increase in the predicted drag coefficient when the presence of laminar separated flow field is taken into account while calculating the boundary layer development. In the absence of trailing edge separation, the calculated drag coefficients show very close agreement with wind tunnel measurements.

CHAPTER VIII

CONCLUSIONS

A rapidly convergent method of solution of the laminar boundary layer equations using finite differences was developed. The iterative nature of the method makes it attractive for application in a situation where a large number of flows are to be analyzed. It was found that the present laminar boundary layer analysis method is suitable for establishing the accuracy and applicability of experimental methods.

The present experimental investigation was made of the boundary layer in the vicinity of laminar separated flow field on an NACA 66₃-018 airfoil section in the low speed wind tunnel of the University of Alberta. The investigation covered the study of both the mean and turbulent characteristics of the flow. The purpose of that investigation was to provide new information, to supplement the available data, and to provide further insight into the flow processes as the basis for an analytical approach.

The mean flow measurements corroborated the observations of other investigators in many respects; but also revealed some interesting new results. The physical structure of the separated flow field and the character of

the reattached turbulent boundary layer were described in the light of these new experimental observations. It is believed that the present study has gone further than the other investigations reported to date, especially with regard to the redeveloping region downstream of reattachment.

The results presented here describe the behavior of some of the turbulence characteristics that have not hitherto been available. Based on the experimental evidence, a two-layer eddy viscosity model was developed for the flow in the redeveloping region. The inner layer has an eddy viscosity based on Prandtl's mixing-length theory; and the outer layer has a constant eddy viscosity. Such a model proved to be adequate for analysis of the flow in the redeveloping region. It appeared that the mean and turbulence velocity fields nearly attain self-preservation at some distance downstream of reattachment.

In view of the already existing work of others together with the present data it was possible to develop a numerical method for analysis of the laminar separated flow field near the mid-chord of the airfoil. The method of analysis included the effects of reverse flow in the bubble, viscous-inviscid interaction, transition to turbulent flow in the shear layer, and the redevelopment of turbulent boundary layer after reattachment. The results of the analysis have a qualitative behavior similar to that observed in numerous experiments; and they are also in reasonable

quantitative agreement with available experimental data.

Traditional methods of analysis ignore the effects of the separation bubble while calculating the viscous flow over the airfoil surface. The ultimate objective of the present study was therefore to develop a procedure for predicting the boundary layer development in the presence of laminar separated flow field near the mid-chord of the airfoil. Such a procedure was developed here for the first time and it was shown to be productive in determining the effects of separated flow on the boundary layer characteristics and thus the lift-drag characteristics of the airfoil section. There was an indication that this procedure could be used for predicting the effect on trailing edge stall of the presence of a large midchord bubble.

REFERENCES

REFERENCES

- [1] Owen, P. R. and Klanfer, L., "On the Laminar Boundary Layer Separation from the Leading Edge of a Thin Aerofoil", RAE Rep. Aero. 2508, 1953.
- [2] Tani, I., "Low-speed Flows Involving Bubble Separation", Progress in Aeronautical Sciences, Vol. 5, 1964, pp. 70-103.
- [3] Ward, J. W., "The Behavior and Effects of Laminar Separation Bubbles on Aerofoils in Incompressible Flow", Journal of the Royal Aeronautical Society, Vol. 67, 1963, pp. 783-790.
- [4] Bursnall, W. J. and Loftin, L. K., "Experimental Investigation of Localized Regions of Laminar Boundary Layer Separation", NACA TN 2338, 1951.
- [5] Gault, D. E., "An Experimental Investigation of Regions of Separated Laminar Flow", NACA TN 3505, 1955.
- [6] Crabtree, L. F., "Effects of Leading Edge Separation on Thin Wings in Two-Dimensional Incompressible Flow", Journal of Aeronautical Sciences, Vol. 24, 1957, pp. 597-604.
- [7] Lochtenberg, B. H., "Transition in a Separated Laminar Boundary Layer", Journal of Aerospace Science, Vol. 27, No. 2, 1960.
- [8] Gaster, M., "The Structure and Behavior of Laminar Separation Bubbles", A.R.C., Report. 28-226, 1967.
- [9] Horton, H. P., "A Semi-Empirical Theory for the Growth and Bursting of Laminar Separation Bubbles", A.R.C., C. P. No. 1073, 1967.
- [10] Briley, W. R. and McDonald, H., "Numerical Prediction of Incompressible Separation Bubbles", Journal of Fluid Mechanics, Vol. 69, Pt. 4, 1975, pp. 631-656.
- [11] Crimi, P. and Reeves, B., "Analysis of Leading-Edge Separation Bubbles on Airfoils", AIAA Journal, Vol. 14, No. 11, 1976, pp. 1548-1555.

- [12] Hartree, D. R. and Womersley, J. R., "A Method for the Numerical or Mechanical Solution of Certain Types of Partial Differential Equations", Proc. Royal Society, A101, 1937, pp. 353-366.
- [13] Smith, A.M.O. and Clutter, D. W., "Solution of the Incompressible Laminar Boundary Layer Equations", AIAA Journal, Vol. 1, No. 9, 1963, pp. 2062-2071.
- [14] Schlichting, H., "Boundary-Layer Theory", McGraw-Hill Book Co., 1968.
- [15] Nachtsheim, P. R. and Swigert, P., "Satisfaction of Asymptotic Boundary Conditions in Numerical Solution of Systems of Nonlinear Equations of Boundary-Layer Type", NASA TN D-3004, 1965.
- [16] Hildebrand, F. B., "Introduction to Numerical Analysis", McGraw-Hill Book Co., 1956, pp. 199-236.
- [17] Smith, A.M.O. and Clutter, D. W., "Solution of the Incompressible Laminar Boundary Layer Equations", Douglas Aircraft Co., Report No. ES 40446, 1961.
- [18] Goldstein, S., "On Laminar Boundary-Layer Flow Near a Position of Separation", Quarterly Journal of Mech. Appl. Math., Vol. 1, 1948, pp. 43-69.
- [19] Hartree, D. R., "The Solution of the Equations of the Laminar Boundary Layer for Schubauer's Observed Pressure Distribution for An Elliptic Cylinder", R and M, No. 2427, 1939.
- [20] Marsden, D. J., "Wind Tunnel Tests of a Slotted Flapped Wing Section", Canadian Aeronautics and Space Journal, Vol. 24, 1978, pp. 83-91.
- [21] Garner, H. C., "Subsonic Wind Tunnel Wall Corrections", AGAR Dograph, No. 109, 1966.
- [22] Wilson, D. J., "An Experimental Investigation of the Mean Velocity, Temperature and Turbulence Fields in Plane and Curved Two-Dimensional Wall Jets: Coanda Effects", Ph.D. Thesis, University of Minnesota, 1970.
- [23] Rai, Shri Prakash, "An Investigation of Plane Turbulent Wall-Wakes", Ph.D. Thesis, University of Alberta, 1974.

- [24] Clauser, F. H., "Turbulent Boundary Layer in Adverse Pressure Gradients", Journal of the Aeronautical Sciences, Vol. 21, 1954, pp. 91-108.
- [25] Cebeci, T. and Smith, A.M.O., "Analysis of Turbulent Boundary Layers", Academi Press, 1974.
- [26] Corrsin, S., Kistler, A. L., "The Free-Stream Boundaries of Turbulent Flows", NACA TN No. 3133, 1954.
- [27] Fiedler, H. and Head, M. R., "Intermittency Measurements in The Turbulent Boundary Layer", Journal of Fluid Mechanics, Vol. 25, 1966, pp. 719-737.
- [28] Klebanoff, P. S., "Characteristics of Turbulence in a Boundary Layer with Zero Pressure Gradient", NACA TN No. 3178, 1954.
- [29] Schubauer, G. B., "Turbulent Processes as Observed in Boundary Layer and Pipe", Journal of Applied Physics, Vol. 25, 1954, p. 188.
- [30] Schubauer, G. B. and Klebanoff, P. S., "Investigation of Separation of the Turbulent Boundary Layers", NACA TN No. 2133, 1950.
- [31] Von Driest, E. R., "On Turbulent Flow Near a Wall", Journal of Aeronautical Sciences, Vol. 23, 1956, p. 1007.
- [32] Cebeci, T. and Smith, A.M.O., "A Finite-Difference Solution of the Incompressible Turbulent Boundary-Layer Equations By an Eddy-Viscosity Concept", AFOSR-IFP-Stanford Conference, Vol. 1, 1968, pp. 346-355.
- [33] Stewartson, K., "Further Solutions of the Falkner-Skan Equation", Proceedings of the Cambridge Philosophical Society, Vol. 50, 1954, pp. 454-465.
- [34] McDonald, H. and Fish, R. W., "Practical Calculations of Transitional Boundary Layers", International Journal of Heat and Mass Transfer, Vol. 16, 1973, p. 1729.
- [35] Klemp, J. B. and Acrivos, A., "A Method for Integrating the Boundary-Layer Equations Through a Region of Reverse Flow", Journal of Fluid Mechanics, Vol. 53, 1972, pp. 177-191.

- [36] Rosenhead, L., "Laminar Boundary Layers", Oxford University Press, 1963, p. 211.
- [37] Young, A. D., "Some Special Boundary Layer Problems", 20th Ludwig Prandtl Memorial Lecture, Copenhagen, 1977.
- [38] Tani, I. and Hama, F. R., "Some Experiments on the Effect of a Single Roughness Element on Boundary-Layer Transition", Journal of the Aeronautical Sciences, Vol. 20, No. 4, 1953, p. 289.
- [39] Kennedy, J. L., "The Design and Analysis of Airfoil Sections," Ph.D. Thesis, University of Alberta, 1977.
- [40] Kennedy, J. L. and Marsden, D. J., "Potential Flow Distributions on Multi Component Airfoil Sections", Canadian Aeronautics and Space Journal, Vol. 22, No. 5, 1976, pp. 243-256.
- [41] Felsch, K. O., Geropp, D. and Walz, A., "Method of Turbulence Boundary Layer Prediction," AFOSR-IFP- Stanford Conference, Vol. 1, 1968, pp. 170-176.
- [42] Gooden, J.H.M, "Experimental Low-Speed Aerodynamic Characteristics of the Wortmann FX 66-S-196 V1 Airfoil", Delft University of Technology, Department of Aerospace Engineering, July, 1978.

APPENDICES

APPENDIX 1

SYSTEM OF FIRST-ORDER EQUATIONS FOR INTEGRATING
LAMINAR BOUNDARY LAYER EQUATIONS

To integrate the boundary layer equation (2.16, 2.17) and perturbation equation (2.23, 2.24) a system of first-order differential equations is obtained by defining six new functions such that:

$$y(1) = f$$

$$y(2) = f'$$

$$y(3) = f''$$

$$y(4) = f'_x$$

$$y(5) = f''_x$$

and

$$y(6) = f'''_x$$

The derivatives of y_i are called F_i , and then:

$$F(1) = f' = y(2)$$

$$F(2) = f'' = y(3)$$

$$F(3) = f'''$$

$$F(4) = f'_x = y(5)$$

$$F(5) = f''_x = y(6)$$

$$F(6) = f'''_x$$

With this notation, the following system is obtained:

1. Two-point finite difference formulation:

$$F(1) = y(2)$$

$$F(2) = y(3)$$

$$F(3) = -\frac{(1+\beta)}{2} * y(1) * y(3) - \beta [1 - y(2) ** 2]$$

$$+ A_{11} * y(2) [y(2) - y(2)_{JJ-1}]$$

$$- A_{11} * y(3) [y(1) - y(1)_{JJ-1}]$$

$$F(4) = y(5)$$

$$F(5) = y(6)$$

$$F(6) = -\frac{(1+\beta)}{2} [y(1) * y(6) + y(3) * y(4)]$$

$$+ 2\beta * y(2) * y(5) + A_{11} * y(5) [y(2) - y(2)_{JJ-1}]$$

$$+ A_{11} * y(2) * y(5) - A_{11} * y(6) [y(1) - y(1)_{JJ-1}]$$

$$- A_{11} * y(3) * y(4)$$

with initial conditions:

$$y(1) = 0$$

$$y(2) = 0$$

$$y(3) = f'_w \quad (\text{initial guess})$$

$$y(4) = 0$$

$$y(5) = 0$$

$$y(6) = 1$$

2. Three-point finite difference formulation:

$$F(1) = y(2)$$

$$F(2) = y(3)$$

$$\begin{aligned} F(3) = & -\frac{(1+\beta)}{2} * y(1) * y(1) * y(3) - \beta [1 - y(2) ** 2] \\ & + y(2) [A_{22} * y(2) - A_{33} * y(2)_{JJ-1} + \\ & + A_{44} * y(2)_{JJ-2}] \\ & - y(3) [A_{22} * y(1) - A_{33} * y(1)_{JJ-1} + \\ & + A_{44} * y(1)_{JJ-2}] \end{aligned}$$

$$F(4) = y(5)$$

$$F(5) = y(6)$$

$$\begin{aligned} F(6) = & -\frac{(1+\beta)}{2} [y(1) * y(6) + y(3) * y(4)] \\ & + 2\beta * y(2) * y(5) + y(5) [A_{22} * y(2) - A_{33} * \\ & y(2)_{JJ-1} + A_{44} * y(2)_{JJ-2}] + A_{22} * y(2) * y(5) \\ & - y(6) [A_{22} * y(1) - A_{33} * y(1)_{JJ-1} + A_{44} * \\ & y(1)_{JJ-2}] - A_{22} * y(3) * y(4) \end{aligned}$$

with initial conditions:

$$y(1) = 0$$

$$y(2) = 0$$

$$y(3) = f'_w \quad (\text{initial guess})$$

$$y(4) = 0$$

$$y(5) = 0$$

$$y(6) = 1$$

APPENDIX 2

EVALUATION OF DERIVATIVES OF ϵ_i^* (Equation (6.37))

For convenience, the inner layer eddy viscosity expression (6.37) is rewritten here as:

$$\epsilon_i^* = 0.16 \sqrt{U^* s^* Re} \eta^2 \left| f'' \right| \left\{ 1 - \exp \left[- \frac{\eta}{26} (U^* s^* Re)^{\frac{1}{4}} (f_w'' - \beta \eta)^{\frac{1}{2}} \right] \right\}^2 \quad A2-1$$

$$\text{Let } A = \frac{\eta}{26} (U^* s^* Re)^{\frac{1}{4}} (f_w'' - \beta \eta)^{\frac{1}{2}} \quad A2-2$$

Differentiation of all the terms in Equation (A2-1) with respect to η yields:

$$\begin{aligned} \epsilon_i^* &= 0.16 \sqrt{U^* s^* Re} (1 - e^{-A})^2 \left[2\eta \left| f'' \right| + \eta^2 \left| f''' \right| \right] \\ &+ 2(0.16 \sqrt{U^* s^* Re} \eta^2 \left| f'' \right|) (1 - e^{-A}) \left(- \frac{d}{d\eta} (e^{-A}) \right) \end{aligned}$$

ie

$$\begin{aligned} \epsilon_i^{*'} &= 0.16 \sqrt{U^* s^* Re} (1 - e^{-A})^2 \left[2\eta \left| f'' \right| + \eta^2 \left| f''' \right| \right] \\ &+ 0.16 \sqrt{U^* s^* Re} 2e^{-A} (1 - e^{-A}) (U^* s^* Re)^{\frac{1}{4}} \eta^2 \left| f'' \right| \left[(f_w'' - \beta \eta)^{\frac{1}{2}} \right. \\ &\quad \left. - \frac{1}{2} (f_w'' - \beta \eta)^{-\frac{1}{2}} \beta \eta \right] \quad A2-3 \end{aligned}$$

Differentiating all the terms of the Equation (A2-1) with respect to x ($= f''(0)$), the following equation is obtained:

$$\begin{aligned} \varepsilon_{ix}^* = & 0.16 \sqrt{U^* s^* Re} \eta^2 (1-e^{-A}) \left[(1-e^{-A}) \left| f_x'' \right| \right. \\ & \left. + (U^* s^* Re)^{\frac{1}{4}} e^{-A} \frac{\eta}{26} \left| f'' \right| (f_w'' - \beta \eta)^{-\frac{1}{2}} \right] \end{aligned} \quad A2-4$$

Differentiation of all the terms of the Equation (A2-3) with respect to x ($= f''(0)$) yields:

$$\begin{aligned} \varepsilon_{ix}^{*'} = & 0.16 \sqrt{U^* s^* Re} \left\{ 2\eta \left| f'' \right| + \eta^2 \left| f''' \right| \right\} e^{-A} (1-e^{-A}) \\ & (U^* s^* Re)^{\frac{1}{4}} \frac{\eta}{26} (f_w'' - \beta \eta)^{-\frac{1}{2}} + 0.16 \sqrt{U^* s^* Re} \\ & (1-e^{-A})^2 \left\{ 2\eta \left| f_x'' \right| + \eta^2 \left| f_x''' \right| \right\} + 0.16 \sqrt{U^* s^* Re} \\ & (U^* s^* Re)^{\frac{1}{4}} \frac{\eta^2}{26} \left[e^{-A} (1-e^{-A}) \left| f'' \right| \left\{ (f_w'' - \beta \eta)^{-\frac{1}{2}} + \frac{1}{2} \right. \right. \\ & \left. \left. (f_w'' - \beta \eta)^{-\frac{3}{2}} - \beta \eta \right\} + (1-e^{-A}) \left| f'' \right| \left\{ (f_w'' - \beta \eta)^{\frac{1}{2}} - \frac{1}{2} \right. \right. \\ & \left. \left. (f_w'' - \beta \eta)^{-\frac{1}{2}} - \beta \eta \right\} \right\} - (U^* s^* Re)^{\frac{1}{4}} e^{-A} \frac{\eta}{26} (f_w'' - \beta \eta)^{-\frac{1}{2}} \left\{ \right. \\ & \left. + e^{-A} \left| f'' \right| \left\{ (f_w'' - \beta \eta)^{\frac{1}{2}} - \frac{1}{2} (f_w'' - \beta \eta)^{-\frac{1}{2}} - \beta \eta \right\} \right. \\ & \left. \left\{ (U^* s^* Re)^{\frac{1}{4}} e^{-A} \frac{\eta}{26} (f_w'' - \beta \eta)^{-\frac{1}{2}} \right\} \right. \\ & \left. + 2e^{-A} (1-e^{-A}) \left| f_x''' \right| \left\{ (f_w'' - \beta \eta)^{\frac{1}{2}} - \frac{1}{2} (f_w'' - \beta \eta)^{-\frac{1}{2}} - \beta \eta \right\} \right] \end{aligned} \quad A2-5$$

APPENDIX 3

SYSTEMS OF FIRST-ORDER EQUATIONS FOR INTEGRATING
THE DIFFERENTIAL EQUATIONS OF LAMINAL
SEPARATED FLOW FIELD

1. Laminar Region

In order to integrate the boundary layer equation (6.39) and perturbation equations (6.49 and 6.50) the following nine new variables are defined.

$$\begin{aligned}
 y(1) &= f \\
 y(2) &= f' \\
 y(3) &= f'' \\
 y(4) &= f_x \\
 y(5) &= f'_x \\
 y(6) &= f''_x \\
 y(7) &= f_\beta \\
 y(8) &= f'_\beta \\
 y(9) &= f''_\beta
 \end{aligned}$$

Then the derivative functions F_i are defined as follows:

$$\begin{aligned}
 F(1) &= f' = y(2) \\
 F(2) &= f'' = y(3) \\
 F(3) &= f'''
 \end{aligned}$$

$$\begin{aligned}
F(4) &= f'_x = y(5) \\
F(5) &= f''_x = y(6) \\
F(6) &= f'''_x \\
F(7) &= f'_\beta = y(8) \\
F(8) &= f''_\beta = y(9) \\
F(9) &= f'''_\beta
\end{aligned}$$

Using these variables, Equations (6.39), (6.49), and (6.50) can be written as a system of first-order equations to simulate the original equations on the computer. The resulting system is written as follows:

$$\begin{aligned}
F(1) &= y(2) \\
F(2) &= y(3) \\
F(3) &= 1 \frac{(1+\beta)}{2} * y(1) * y(3) - \beta [1 - y(2)**2] \\
&\quad + A_{11} * y(2) [y(2) - y(2)_{JJ-1}] \\
&\quad - A_{11} * y(3) [y(1) - y(1)_{JJ-1}] \\
F(4) &= y(5) \\
F(5) &= y(6) \\
F(6) &= - \frac{(1+\beta)}{2} [y(1) * y(6) + y(3) * y(4)] \\
&\quad + 2\beta * y(2) * y(5) + A_{11} * y(5) [y(2) - y(2)_{JJ-1}] \\
&\quad + A_{11} * y(2) * y(5) - A_{11} * y(6) [y(1) - y(1)_{JJ-1}] \\
&\quad - A_{11} * y(3) * y(4) \\
F(7) &= y(8)
\end{aligned}$$

$$\begin{aligned}
F(8) &= y(9) \\
F(9) &= -\frac{(1+\beta)}{2} [y(1) * y(9) + y(3) * y(7)] \\
&\quad - \frac{y(1) * y(3)}{2} + [y(2) ** 2 - 1] + 2\beta * y(2) * (8) \\
&\quad + A_{11} * y(2) * y(8) + A_{11} * y(8) [y(2) - y(2)_{JJ-1}] \\
&\quad - A_{11} * y(3) * y(7) - A_{11} * y(9) [y(1) - y(1)_{JJ-1}]
\end{aligned}$$

with initial conditions

$$\begin{aligned}
y(1) &= 0 \\
y(2) &= 0 \\
y(3) &= f_w'' \text{ (initial guess)} \\
y(4) &= 0 \\
y(5) &= 0 \\
y(6) &= 1 \\
y(7) &= 0 \\
y(8) &= 0 \\
y(9) &= 0
\end{aligned}$$

2. Redeveloping Region

Using the variables defined in Appendix 1, Equations (6.40) and (6.53) can be written as a system of first-order differential equations as shown below.

$$\begin{aligned}
F(1) &= y(2) \\
F(2) &= y(3) \\
F(3) &= \frac{1}{1+\epsilon} * \left\{ -\epsilon * y(3) - \frac{(1+\beta)}{2} * y(1) * y(3) - \right.
\end{aligned}$$

$$\begin{aligned}
& - \beta [1 - y(2) ** 2] \\
& + A_{11} * y(2) [y(2) - y(2)_{JJ-1}] \\
& - A_{11} * y(3) [y(1) - y(1)_{JJ-1}] \Big\} \\
F(4) &= y(5) \\
F(5) &= y(6) \\
F(6) &= \frac{1}{1+\epsilon^*} \Big\{ - \epsilon_x^* F(3) - \epsilon^{*'} * y(6) - \epsilon_x^{*'} * y(3) \\
& - \frac{(1+\beta)}{2} [y(1) * y(6) + y(4) * y(3)] + 2\beta * y(2) * y(5) \\
& + A_{11} * y(5) [y(2) - y(2)_{JJ-1}] + A_{11} * y(2) * y(5) \\
& - A_{11} * y(6) [y(1) - y(1)_{JJ-1}] - A_{11} * y(3) * y(4) \Big\}
\end{aligned}$$

with initial conditions

$$\begin{aligned}
y(1) &= 0 \\
y(2) &= 0 \\
y(3) &= f_w^{''} \text{ (initial guess)} \\
y(4) &= 0 \\
y(5) &= 0 \\
y(6) &= 1
\end{aligned}$$

B30244